

University of St Andrews



Full metadata for this thesis is available in
St Andrews Research Repository
at:

<http://research-repository.st-andrews.ac.uk/>

This thesis is protected by original copyright

STUDIES ON AN ELECTRONIC SIGNAL INTEGRATOR AND RECORDER DESIGNED FOR
USE IN ECOLOGICAL FIELD RESEARCH, WITH PARTICULAR REFERENCE TO
PHOTOSYNTHETICALLY ACTIVE RADIATION.

BY

THOMAS CHARLES HARDINGE GOING

A thesis presented to
The University of St. Andrews
(Dept. of Botany)
for the degree of
Doctor of Philosophy.

St. Andrews
September, 1981



Th 9866

ABSTRACT

The thesis reviews the requirements for radiometry in ecological studies, and the problems in designing successful apparatus for field use.

All common and historical methods of integrating solar radiant energy are examined in detail, including photochemical and photo-electrical methods. Electrochemical, electromagnetic and purely electronic means of integration are examined and compared.

Recording devices are considered, along with relationship between integration and recording and the contrasting benefits of continuous, discontinuous (sampling) and serial integration recording.

A new recording method in which serial irradiance integrals are recorded using a thermally sensitive paper tape is given, along with descriptions of the design with theoretical and practical aspects fully covered. A specially developed electronic integrator, based on a published design, and a newly developed range changer for use with the recorder are described, with consideration given to all aspects of design including temperature and power consumption. Testing procedures are discussed, including those for linearity, temperature stress and temperature coefficient. Laboratory and field trials are presented, with consideration given to ambient temperature, dimensional stability in the recording medium, the interpretation of irradiance records, and drift and constancy of the combined integrator and recorder. Calibration and thermal stress tests are presented, and comparisons are made of field trials alongside a Kipp and Zonen pyranometer.

The subsidiary use of the system to record temperature and low levels of irradiance are discussed. Appendices cover the choice of spectral response for sensors of photosynthetically active radiation, sensor design, batteries, solar power supplies, electrolytic capacitors and electromagnetic relays. An automated system for reading recordings is considered. Complete parts lists and electronic circuits are given, along with manufacturers names and addresses, and a comprehensive reference list. 273 references.

DECLARATION

I hereby declare that this thesis is based on my own readings and research, that it has been composed by myself, and that it has not been accepted in any application for a higher degree here or elsewhere. I also declare that I was duly admitted as a research student and candidate for the degree of Doctor of Philosophy of the University of St. Andrews under Ordinance General No. 12, Resolution of the University Court 1967, No. 1, and the relevant Regulations pertaining thereto.

Thomas Charles Hardinge Going
Candidate

CERTIFICATE

I certify that Thomas Charles Hardinge Going, B.Sc. (St. And) has devoted not less than nine terms to research work under my supervision and that he has fulfilled the conditions of the Ordinance, Resolution and Regulations above mentioned, and that he is qualified to submit the accompanying thesis in application for the Degree of Doctor of Philosophy.

Martin Gray Stanton
Supervisor

STATEMENT OF QUALIFICATIONS

First Matriculation as an undergraduate, St. Andrews, October 1970

Graduated, July 1975, with Honours in Botany

First Matriculation as a research student for the degree of Ph.D.

1st January, 1976

ACKNOWLEDGEMENTS

I am grateful for this opportunity to thank the many people who have helped me in my work - Professor D.H.N. Spence, F.R.S.E. for sparking my interest in this area of study; Dr. Barry Jupp and Mr. Harry Hodge for help with field work; Mr. Charles Roemm  l   and Mr Alec Reid for help in the laboratory, Mr. Christopher Eley for the circuit in Appendix 11; Mr. Andrew McMillan, Dr. Peter Welsh and Dr. James Going for reading parts of the text, and also the late Dr. Helen Blackler, Dr. David Weeks, Dr. Edward Drew, Mr. John Brown, Mrs. Doris Hunter, Dr. Christopher Walter, and the staff of Department of Physiology and Environmental Science at The Nottingham University School of Agriculture, Sutton Bonington.

I would like to thank Professor Rainer Goldsmith of the Department of Physiology, Chelsea College, University of London, for generously granting me leave of absence in the summer of 1978; and the staffs of the University Library, St. Andrews; Chelsea College Library; The Lyon Playfair Library, Imperial College; and those fascinating institutions, The Science Museum Library and the former Patent Office Library (now the Science Reference Library, Holborn Division)

I thank Professor John Allen, of the Department of Physics, St. Andrews for advice on silicon photodetectors, and Mrs. Susannah Roxburgh, my excellent typist. Much of the work was executed in the Gatty Marine Laboratory, by kind permission of the Director, Professor H.S. Laverack, F.R.S.E.

Last, but not least, I would like to thank my supervisor, Dr. Martin Stanton, whose help and constant encouragement over the years I have much appreciated.

For my
dear
and
indulgent
parents
with
my
thanks

Table of Contents

Reference	Page	
1	1	Biologically active solar radiation, and its measurement in ecology
1A1	1	Introduction
1A2	2	Thermometry, photometry and radiometry
1A2a	2	Thermometry
1A2b	3	Photometry
1A2c	4	Radiometry
1B	4	The impact of radiant flux on the biosphere
1C1	5	Practical radiometry - some problems and difficulties
1C2	6	Radiometer spectral response
1C3	6	Field environment
1C4	7	Further aspects of measuring and recording
1D	8	Conclusion to introductory sections
2	16	Integrators for use in radiometry - a review
2A	17	Principles of methods used in integrating instrument design
2B	20	Photochemical and physical effects
2B1	20	Displacement of liquid distilled through absorption of radiant flux
2B2	22	Photodecomposition of chemical substances
2C	24	Photoelectrical effects
2C1	24	Electrochemical methods
2C1a	24	Electrolytic generation of gas
2C1b	27	Electrolytic transfer of metal
2C1c	28	Electrolytic displacement of electrolyte zone
2C1d	29	Special variant I - metal transfer cell with electronic signalling of charge state
2C1e	32	Special variant II - solid electrolyte integrator
2C2	33	Electromagnetic methods
2C2a	33	The integrating motor
2C3	34	Electronic methods
2C3a	34	Capacitor charge - discharge methods
2C3b	40	The use of the capacitor in electronic integrators
2C3c	40	Examples of the use of capacitors in integrators
2C3d	44	Integrators for two purposes: digitization and averaging
2C4	44	Integrators for digitization
2C5	45	Integrators for averaging
2C5a	45	A common field data register - the electromagnetic counter
2C5b	46	Dynamic range
2C5c	46	Improving the dynamic range
2C5d	51	Detecting threshold voltages in the integrating capacitor
2C5e	52	Power consumption

3	54	Recorders for use in radiometry - a review
3A1	55	Introduction
3A2a	55	Which type of recorder
3A2b	56	Graph-charting recorders
3A2c	62	Number-registering recorders
3A2d	63	Digital recorders - ' data loggers '
4	65	A new design of recorder
4A	66	Introduction
4B	67	The new recorder
4C	69	Principle of the new recorder
4D	69	Advantages of the new recorder
4D1	69	Dynamic range, economy of paper and energising power
4D2	71	Provision for machine processing of the recordings
4D3	72	Simplicity of construction
4E	72	Practical considerations in the design of the new recorder
4E1	72	Time marking
4E2	74	Paper sources and types
4E3	75	Slitting the paper
4E4	76	Mechanical parts
4E5	78	Decoupling of parts of the mechanism
4E6	80	Effect of the recorder specification on the choice of integrator
4E7	82	Range-changing and the recorder
5	83	The design and development of the new integrator
5A	84	Background
5B	84	Specifications and circuits for integrators of Stanton (1973) and Going (this volume)
5C	88	The new integrator - Analysis of operation I
5C1	88	The recharge phase
5C2	88	The integration phase
5C3	91	Return to the recharge phase
5C4	92	Further detail
5C5	92	Solenoid driving circuit
5D	93	Analysis of operation II
5D1	94	The recharge phase
5D2	94	Recharge phase: 150 uF capacitor
5D3	95	Performance of Q8 - Q9
5D4	95	Performance of Q8 - Q9 (2)
5D5	96	Voltage conditions on integrating capacitor
5D6	96	Voltage conditions on integrating capacitor
5E	104	Analysis of operation III
5E1	104	Compensation for dead-time
5F	104	Aspects of performance
5F1	104	Temperature coefficients
5F2	106	Battery voltage
5F3	107	Ambient temperature
5F4	108	Sensitivity to impulsive interference

5G	108	Aspects of design and development
5G1	108	Introduction
5G2	109	Temperature stabilisation
5G3	110	Supply voltage stabilisation
5G4	114	Solenoid power : monostables with minimum quiescent current drain
5G5	114	Signal input circuitry
5H	119	Testing procedures for the integrator
5H1	119	Introduction
5H2	125	Tests for linearity
5H3	128	Testing for thermal failure
5H4	129	Testing the temperature coefficients
5H5	130	An abnormal state - the stalled integrator
5H6	132	Testing D10, Q8 and C6 for low leakage
6	134	The development of an auto-ranging circuit for use with the integrator-recorder combination
6A1	135	Background
6A2	135	The dynamics of radiometer auto-ranging
6A3	143	Introduction to and characteristics of the most recent auto-ranging unit
6B	144	Analysis of operation I
6B1	144	The comparator unit
6B2	146	The relay operating section
6C	147	Analysis of operation II
6C1	150	Output waveform of the comparator
6C2	150	The role of capacitors C4A and C9A
6C3	150	Check on thyristor gate drive current
6C4	152	Discharge - charge performance of C6A and C7A
6C5	152	Voltage waveforms on conducting relay
6D	152	Concluding notes to chapter 6
7	162	Equipment trials
7A	163	Laboratory trials
7A1	163	Effect of ambient temperature on thermal time marks
7A2	165	Dimensional stability of the recording paper
7A2a	165	Introduction
7A2b	166	Test method
7A3	167	Results
7B	171	The interpretation of tape irradiance records
7B1	171	Introduction
7B2	172	Operator error and the reading of tape records
7C	172	Recorder constancy
7C1	174	Statistical examination of recorder constancy
7D	177	Integrator calibration, drift of calibration, and temperature coefficient
7D1	177	Introduction
7D2	178	Integrator calibration and drift
7D3	181	Thermal stress test
7D4	185	Integrator temperature coefficient

7D5	186	Integrator response to fluctuating battery voltage
7D6	186	Conclusions
7E	191	Field trial results
7E1	191	Introduction
7E2	192	Results - 1: Long term : performance of the radiometer head and calibrations
7E3	194	Calibration of integrator with radiometer and radiometer head alone
7E4	195	Drift of the integrator calibration during the field trial
7E5	199	Results - 2: Short term : comparison of irr- adiance records (short term) from chart recorder and new recorder systems
7E6	199	Presentation of the irradiance graphs
7E7	200	Consideration of individual irradiance graphs
7E8	203	Discussion of the irradiance graphs
7E9	218	Results - 3 : Additional ways of using the new recording system
7E10	218	Twilight levels of irradiance
7E11	220	The recording of temperature
7F	222	Power and paper consumption in the recorder and integrator
8	226	Conclusion

Page	Fig. No.	Abbreviated Caption
11	1	Spectral Radiance E of the sun at mean earth sun separation.
11	2	The action spectrum for erythema and human photopic eye response.
12	3	Relative spectral luminous efficiency as a function of wavelength.
13	4	The spectral distribution of solar and terrestrial radiation
14	5	The electromagnetic spectrum
21	6	Spectral sensitivity of heliographic Ozalid paper no. 33NT
21	7	Two modifications of the Bellani pyranometer
26	8a	Details of the glasswork and electrodes of the siemens electrolytic meter
26	8b	Siemens - Schuckert electrolytic integrator
31	9	Cross-sectional drawing of a two-electrode timer cell
31	10	Voltage process of an electrolytic timer cell
31	11	Charge characteristics of a typical memoriode
37	12	Simple arrangement for using a capacitor in an integrating radiometer.
37	13	Characteristics of the integrating radiometer of Fig. 12.
38	14	EMF across the terminals of a capacitor subjected to discharge by a resistor.
42	15	Voltage waveforms on integrating capacitor
42	16	Output of integrator operating according to Fig. 15
43	17	Voltage waveforms on capacitor, and integrator output for varying input current
48	18	Positioning of dead-time (t_{dead}) correction resistance
48	19	Elimination of effect of t_{dead} at high integration cycle rates
50	20	Alternative voltage variation pattern on integration capacitor, to eliminate t_{dead}
56	21	Solar radiation for three cloudless days at Rothamsted, and for a day of broken cloud.
62a	22	A multi-range chart recorder using only mechanical processes
62a	23	Lambrecht windspeed recorder
68	24	Perspective view of the New Recorder
79	25	Diagram to show the position of decoupling springs in the New Recorder
81	26	This diagram is no longer extant.
86	27	Circuit of integrator of STANTON (1973)
87	28	Circuit " " " GOING (final version)
89	29	Going's integrator circuit - operational detail 1
90	30	" " " " " 2
97	31	" " " oscillogram of recharge phase 1
97	32	" " " " " 2

Page	Fig. No.	Abbreviated Caption	
98	33	Going's integrator circuit, oscillogram of recharge phase	3
98	34	" " " "	4
99	35	" " " "	5
100	36	" " " "	6
100	37	" " " "	7
101	38	" " " "	8
102	39	" " oscillogram of complete integration cycle	1
102	40	" " " "	2
103	41	" " " "	3
103	42	" " " "	4
105	43	" " " "	5
105	44	" " " "	6
111	45	" " circuit: detail, showing current drains	
113	46	Voltage stabiliser for integrator	
113	47	Graph of performance of voltage stabiliser	
115	48	Micropower monostable circuit - early circuit	
115	49	Basic monostable oscillator circuit	
116	50	Monostable with zero standby power consumption	
116	51	Refinement of circuit of Fig. 50	
120	52	Simplest basic integrating radiometer	
120	53	Development of Fig. 52	
120	54	Development of Fig. 53	
121	55	Characteristic curve for silicon diode	1
121	56	" " " " " "	2
121	57	Collector-base leakage currents in a silicon transistor	
122	58	transistor characteristic curve	1
122	59	" " " "	2
122	60	" " " "	3
123	61	Use of earthed-base transistor as a current limit	
124	62	Micropower voltage regulator	
127	64	Simple current source for integrator linearity tests	
126	65	Linearity of prototype integrator	
127	66	Test circuit for measuring semiconductor leakage	
135	67	Irradiance levels and natural biological responses	
138	68	Electronic damping network for auto-range change switch.	
138	69	Performance of Fig. 68	
139	70	Pseudo-diode characteristic response curve	
139	71	Circuit of pseudo-diode	
140	72	Auto range-change circuit performance	
141	73	Full circuit of auto range-change switch	
141	73a	Additional information to Fig 73	
142	74	Connection of signal-damping circuit to auto range-change switch	
148	75	Basic voltage comparator circuit	

Page	Fig. no.	Abbreviated caption
149	76	Further characteristics of Fig. 75
149	77	" " " 75
148	78	Performance of voltage threshold detector
154	79	Oscillograms of auto range-change circuit 1
154	80	" " " " " " 2
155	81	" " " " " " 3
156	82	" " " " " " 4
156	83	" " " " " " 5
157	84	" " " " " " 6
157	85	" " " " " " 7
157	86	" " " " " " 8
158	87	Suggested improved circuit for auto range change switch
159	88	Second suggested improved circuit for auto range change switch
160	89	The use of CMOS analogue switches in the integrator .
164	90	Effect of temperature on heat pen and recorder mechanism
169	91	Effect of humidity on recording paper tape 1
170	92	" " " " " " 2
176	93	New recorder : relationship between paper movement and solenoid counter mechanism operations.
179	94	Integrator test calibration - before thermal stress tests
180	95	Integrator drift and non-linearity in response to thermal stress
182	96	Time and temperature record for the thermal stress test
183	97	Thermal stress test results
188	98	Final circuit of integrator subjected to thermal stress test
189	99	Recorder hot-wire pen operating circuitry
190	100	Final circuit of range-changer subjected to thermal stress test
197	101	PhAR values: comparison between new recorder and reference system results
198	102	Distribution and size of errors from comparison test
199	103	Calendar showing distribution of recording errors
205-208	104-107	Pasted-out examples of recordings from the new recorder, both genuine and photocopies
209-217	108-116	Graphs of irradiance levels (PhAR) from Kipp solarimeter and from New system recorder
219	117-118	Twilight records (22.00 - 03.00 hours) from St. Andrews (May, 1977)
221	119-120	Temperature record from the new system recorder, and reading template
225	121	Radiometer receiver designed for use during the new recorder trials

Page no.	Table no.	Abbreviated caption
10	1	Check list of properties of recorders
15	2	Radiometric and photometric terms, symbols and units
19	3	Advantages and drawbacks of various signal integration systems
39	4	Leakage performance of selected commercially available capacitor dielectrics
85	5	Technical specifications for Stanton and Going integrators
112	6	Zener break-down voltage in base-emitter junctions
140	7	Temperature test results for new auto-range change unit
173	8	Error scores for subjects reading irradiance records
174	9	Statistical examination of recorder constancy
186	10	Integrator temperature coefficient
187	11	Coefficient of battery voltage supply
196	12	Integrator calibration factors before and after field trials
223	13	Analysis of power and paper consumption in the new recording system

Page	Appendix No.	Title
227	1	The choice of spectral response properties for sensors of photosynthetically active radiation - PhAR
234	2	Radiometric sensor design
239	3	Radiometric detectors
254	4	Batteries
262	5	Solar energy for the integrator and recorder
264	6	Electrolytic capacitors
265	7	Electromagnetic relays
266	8	An automated reader for tape records
269	9	Parts list and assembly drawings for the new recorder
277	10	A calibration aid : a constant current source
279	11	A crystal-controlled clock for the recorder
281	12	Selected manufacturers' names and addresses
285		References

PREFACE

There is a fairly wide range of instruments designed for field use by ecologists and others (MONTEITH 1972) but there is still a shortage of good cheap instrument designs which are suitable for prolonged unattended field use, and there are even fewer recorder designs which could economically be considered for construction in the ordinary university workshop.

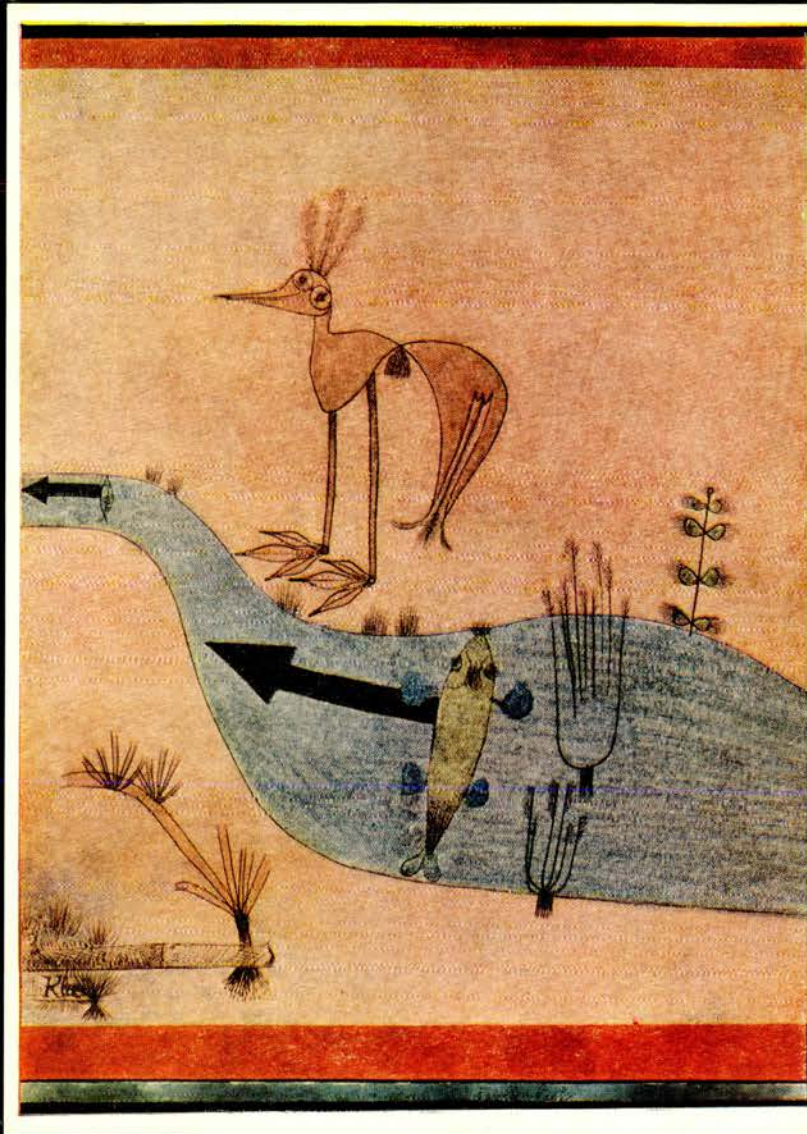
Lack of finance was an important factor in the conception and design of the recorder, integrator and ancillaries presented in this volume, as were the limited engineering skills of the author. Access to a lathe is, however, essential for the construction of the recorder.

Over the past six years, a major change in the range of electronic building bricks has occurred, to the benefit of the designer. Specialised miniature circuits of great complexity - silicon monolithic integrated circuits - are now widely and cheaply available, and even the much-flaunted microprocessor has begun to make its appearance. (See for example WEIHOFEN and WOHL 1981). These changes might make the circuits presented here, made only with discrete semiconductor elements, seem old fashioned, even obsolete. However, until quite recently, low static power consumption in the silicon integrated circuit was not considered an important design requirement, and those few "micropower" devices which were available were very expensive.

More importantly, it was hoped that the instruments produced would be amenable to construction outside the affluent west, and, just as important, that there should be a chance that the more humbly equipped electronic workshop should be able to effect repairs to the circuits, should that be necessary. One of the

transistors employed, the BC109 silicon planar type, has now been in production for approaching twenty years. Even so, the author was surprised recently to be asked to help with the apparently quite difficult task of procuring three such transistors for a department in a brand new university, costing many millions of pounds, in one of the third world countries.

No part of the equipment described here could not be assembled in a school workshop, and it is the author's hope that it might make part of a worthwhile school sixth-form project. In spite of this accent on simplicity, there is no technical barrier to machine processing of the recorded data from the system, so it could find its application in a very wide range of circumstances. It is the author's hope that it will do so.



Paul Klee 1879-1940

The artist as ecologist?
By the Troutstream

CHAPTER 1

BIOLOGICALLY ACTIVE SOLAR RADIATION, AND ITS MEASUREMENT IN ECOLOGY

1. BIOLOGICALLY ACTIVE SOLAR RADIATION, AND ITS MEASUREMENT IN ECOLOGY

1.A.1. Introduction

For as long as the memory of man has run, solar energy has been recognised as a driving force in all living processes. In spite of this, the evaluation and interpretation of quantitative information on natural irradiance remains an area of study with much conflict of opinion and aims, and with considerable problems of methodology and terminology. It is unfortunate that there have arisen several approaches to the study of solar irradiance, generated in the first instance by allowing the different ways the human organism perceives electro-magnetic radiation to impose artificial and essentially irrelevant boundaries.

The sun is a blackbody radiator at 6000°K emitting a wide continuous band of electromagnetic radiation in accordance with the laws of physics. This irradiance falls on the earth where the distribution of energy as a function of wavelength is modified by filtration through the atmosphere. The spectral distribution as perceived at sea-level on earth by unaided man has three regions: one causes the sensation of warmth, another of vision, and the third of discomfort to the skin - because of the erythemal effects of Ultra-Violet (uv) radiation, see Figs 2 and 3 . With instruments, the spectral irradiance distribution is found to form the discontinuous curves shown in Fig. 1 . Specific wavelength bands of the radiation are absorbed by chemical constituents of the atmosphere, principally water, carbon dioxide, and ozone; and scattering by air molecules (Rayleigh scattering) and aerosol particles (Mie scattering) account for further losses. The earth is in balance between incoming and outgoing radiation, and because of this the surface continues to remain at a stable blackbody temperature, which

happens to be suitable for the support of life. This average temperature, 287°K, is much warmer than the theoretical radiation balance temperature for a solid surface at the earth's distance from the sun, and this increased temperature is due to the transparency of air to incoming solar energy and its opacity to the outgoing terrestrial black-body radiation. See Fig. 4 , and BROOKS (1964); TRICKETT, MOULSLEY and EDWARDS (1957); and BARRY and CHORLEY (1968).

1.A.2 Thermometry, Photometry and Radiometry

Leaving aside the measurement of ultraviolet radiation, and ionising radiation of shorter wavelengths (not present in significant quantities at the terrestrial surface), there are two widely used systems of measurement relating to different spectral bands of electromagnetic radiation. One of these systems, Photometry, developed as a result of man's awareness of bodily sensitivity to a specific spectral region of the global influx of electromagnetic radiation. The other system, Radiometry, is absolute. These measurement systems are defined below, after a brief discussion of thermometry.

1.A.2a Thermometry

Thermometry is the measurement of temperature, or the molecular thermal agitation present in a body. A body which will absorb or emit radiant energy perfectly, regardless of wavelength, is called a Blackbody. The absolute temperature and the rate of emission of radiant energy from any blackbody are linked according to the Stefan-Boltzmann law, which states that the rate of emission of radiant energy from a blackbody is proportional to the fourth power of the absolute temperature. The radiant

energy emitted by a blackbody held at a certain absolute temperature is distributed over a range of wavelengths in the form of a lop-sided curve centering on a peak wavelength, λ_m . This curve is shown in Fig. 1 for a blackbody at 5900°K. The wavelength of the maximum, λ_m , shifts towards shorter wavelengths as the absolute temperature of the blackbody increases, in accordance with Wien's displacement law, which states that the product of absolute temperature, T, and the wavelength λ_m at which the maximum occurs is a constant.

However, most natural bodies do not behave as black-bodies, at least within the visible spectral range, and the relationships between temperature and radiant emittance and absorptance will be complex in any practical situation.

1.A.2b Photometry

Photometry measures the capacity of electromagnetic radiation to stimulate the eye of Homo Sapiens, and a given flux of energy into the eye is multiplied by a weighting factor in accordance with the wavelength of the said flux, so that, regardless of wavelength, equal photometric fluxes have a similar capacity to stimulate the eye, and are perceived as having much the same brightness. At 550 nm, the peak of eye sensitivity in scotopic vision (see Fig. 1), only 1/500th. of the radiant energy flux is required to give the same perceived sensation of photometric brightness as at 710 nm. Photometric units are strictly related to human perceived brightness, with the inherent action spectrum of the human eye that this implies. For this reason, it is usually inappropriate to use photometric units when measuring irradiance for correlation, for example, with plant responses. McCREE (1973) expresses the matter more forcefully,

"The art of making good light measurements seems to elude most plant scientists. As a matter of fact it eludes many physicists too. Perhaps we can all lay the blame on the lighting engineers who first introduced candles, grease spots, lumens, nits and other such fanciful notions into what had been a relatively clean science."

Photometric units are only appropriate when irradiance measurements are made for use in human vision studies. In most conditions of use, there is no known way of converting data expressed in photometric units to some radiometric equivalent, the exception being where the spectral quality of the irradiance being monitored is unchanging. In this case, readings taken with a photometer can be calibrated against radiometric evaluations, after which the data will be interconvertible from the one measurement system to the other.

1.A.2c Radiometry

Radiometry is the measurement of radiation in terms of energy, time and area, and necessarily a bandwidth is specified as well. The measures and units of radiometry and photometry are displayed and compared in Table 2 . ANDERSON, M.C. (1971) gives a clear account of radiometry, and is especially recommended.

1.B. The impact of radiant flux on the biosphere

The two main areas of effect of radiant energy are in the supply of energy to all life processes and in the modification of form, distribution and behaviour of living organisms. The primary uptake of solar energy in any ecosystem is by photosynthesis of sugars in plants and in micro-

organisms, and it is in photosynthetic studies that the main demands for quantification of incoming irradiance have so far arisen; however, the quantity and quality of irradiance also have major effects on species distribution and form. For example, the presence of critical ratios of irradiance within different spectral wavebands may effect major physical changes, such as occur through the mediation of phytochrome responses in plants. By such means dormancy and flowering are controlled in plants, as are migration, fertility and the metamorphosis of insect forms in the animal world, see DE WILDE (1962), SINCLAIR and LEMON (1973) MITRAKOS and SHROPSHIRE (1972).

1.C.1. Practical Radiometry - some problems and difficulties

Full sunlight has radiant flux density levels some six orders of magnitude higher than full moonlight, and yet changes of less than one magnitude at either end of this vast range may effect major biological changes. The high irradiance levels are of importance in photosynthesis, and throughout the biosphere generally, not least as a source of heat. Low levels can strongly influence animal and especially insect behaviour. WILLIAMS (1936) examined the Noctuidae in their apparent response to moonlight. CALLAHAN (1964) and MANLEY (1969) have both designed actinometers or photometers to deal with low-level irradiance; in Manley's case to facilitate studies on the insects Oncoptera spp. (pasture webworm) and plusia argentifera Guen (tobacco looper moth). See also BRADSHAW and PHILLIPS (1980).

Handling such a large range of irradiances is a difficult problem. One approach is to use a logarithmically-scaled radiometric recorder and detector, as is done by KAHN et al, (1975) who use a silicon detector. The silicon photodiode or photovoltaic generator will

often be the choice of radiometric detector, since it combines low cost with a wide dynamic range which can encompass all naturally occurring irradiance levels. An alternative is to use auto-ranging apparatus, as is done by BERRY and RANEY (1962) who use a recording galvanometer (which separately gives about one order of magnitude), with a series of five switchable shunts, which gives a total range of five orders of magnitude - quite adequate for many studies. According to KAHN (1975) a dynamic range of 2-3 orders of magnitude is needed for primary production studies, but for photomorphogenesis research a wider range is likely to be necessary.

1.C.2. Radiometer spectral response

The spectral response characteristic chosen for a radiometer is often governed by the question of inter-establishment and inter-national comparability of data, and needs for comparability and for specificity to particular biological studies often conflict. For example, the customary spectral response in use world-wide by Meteorological authorities takes in the infra-red as well as what is usually considered to be Photosynthetically Active Radiation (PhAR), and for photosynthetic studies a correction factor of 0.50 is often applied to IR-inclusive radiometric data to convert them for photosynthetic use. See WESTLAKE (1965) and SZEICZ (1974). This matter is given further attention in Appendix 1. see also STANHILL and FUCHS (1977) and McCREE (1981)

1.C.3. Field environment

The major factor in the design of apparatus for field use is field environment and unfavourable conditions of climate and poor accessibility

will often occur, constraining the designer a great deal. Sometimes comparative (as opposed to absolute) radiometry is the final objective of research, as for example in turbidity studies in limnology. WEINBERG (1974) describes an apparatus for such studies with two radiometric detectors and an electronic circuit which gives a presentation of the irradiance of one detector (subsurface) as a percentage of the surface irradiance. The most common restricting factors are the need for reliable unattended operation and great robustness; and the difficulty of providing adequate supplies of electricity and recording medium.

1.C.4. Further aspects of measuring and recording

In studies involving continuous recording of irradiance, the type of recording needed will depend on the aspect of the variation considered to be important. If the observer is interested in peak rate-of-change of radiant flux, then a totalising printer giving daily solar irradiance values will not satisfy the requirement, which can only be met by a chart record from a fast response recorder. Sometimes hourly or daily totals of irradiance are the target result, in which case a printed readout is more satisfactory than a chart record which usually involves planimetry to reveal the needed statistics.

If irradiance data are to be subjected to mathematical operations it is important to consider the data-handling capacity of the computer and memories which are later to handle it. Digital processing of analogue signals relies on the fact that it is possible to analyse the waveform of a varying unknown by sampling it at intervals; common sense dictates that the more frequent the fluctuations in the unknown

the more often will samples have to be taken if the fluctuations of the unknown are to be fully characterised. BYRNE (1970) quoting SHANNON (1949) states that a variable having Fourier frequency components up to f can be completely reconstructed if it is sampled at intervals of $t = (2f)^{-1}$. For example, a signal known to have frequency components no higher than one cycle per minute can theoretically be completely reconstructed from samples taken at half minute intervals.

To sum up: recording devices can operate in three basic ways:

- I Totalisation - or integration of an irradiance signal for a specified time
- II Continuous recording of instantaneous values on a chart or other recording medium
- III Regular (discontinuous) sampling of instantaneous values on a chart or other recording medium

1.D Conclusion to introductory sections

There have been many studies of irradiance, made under diverse conditions. Limitations in money, time and in quality of apparatus as well as the nature of this field of research mean that few of these works are complete, or universally applicable. These facts, and the pressing need for greater understanding of the ways in which man unbalances and harms his surroundings, together with man's apparently endless thirst for energy combine to suggest that there will continue to be a demand for apparatus to help foster research into naturally occurring irradiance. The papers by BROOKS (1964);

TRICKETT, MOULSLEY and EDWARDS (1957), GAASTRA (1968), SZEICZ (1974), WESTLAKE (1965), STRICKLAND (1958), VOLLENWEIDER (1969) and ANDERSON (1971) are excellent introductions to the subject. see also CAMPBELL, (1981), McCREE (1981), BJORKMANN (1981) CALDWELL (1981), and JEFFREY (1981) all in LANGE (1981)

- I Totalisation - or integration of an irradiance signal for a specified time
- II Continuous recording of instantaneous values on a chart or other recording medium
- III Regular (discontinuous) sampling of instantaneous values on a chart or other recording medium

Table 1 - Checklist of properties of recorder, based on the divisions I, II and III above

	I	II	III
Average values recorded?	Yes	(Yes)	(Yes)
Total values recorded?	Yes	(Yes)	(Yes)
Peak values recorded?	No	Yes	Yes
Versatility	3	2	1
Cheapness	1	3=	3=
Simplicity	1	2	3

1 = best

2 = intermediate

3 = worst

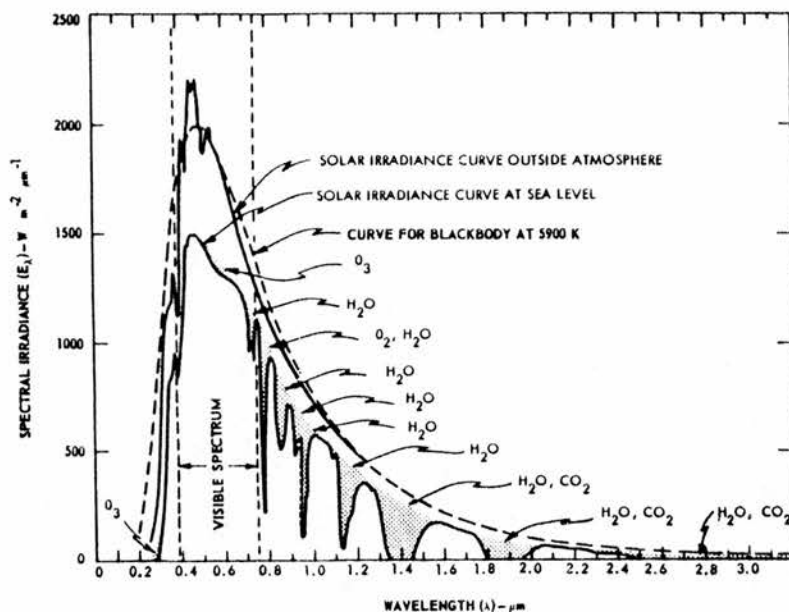


Fig. 1 Spectral radiance E_{λ} of the sun at mean earth-sun separation. Shaded areas indicate absorption at sea level due to the atmospheric constituents shown from RCA (1974)

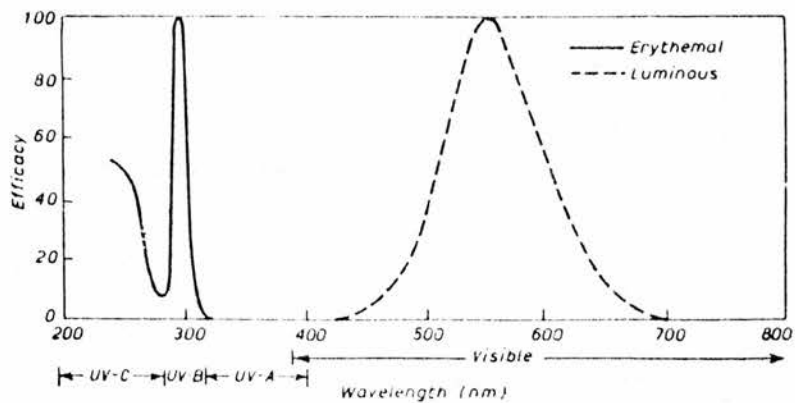


Fig. 2 The action spectrum for erythema and human photopic eye response

from RUFF (1970)

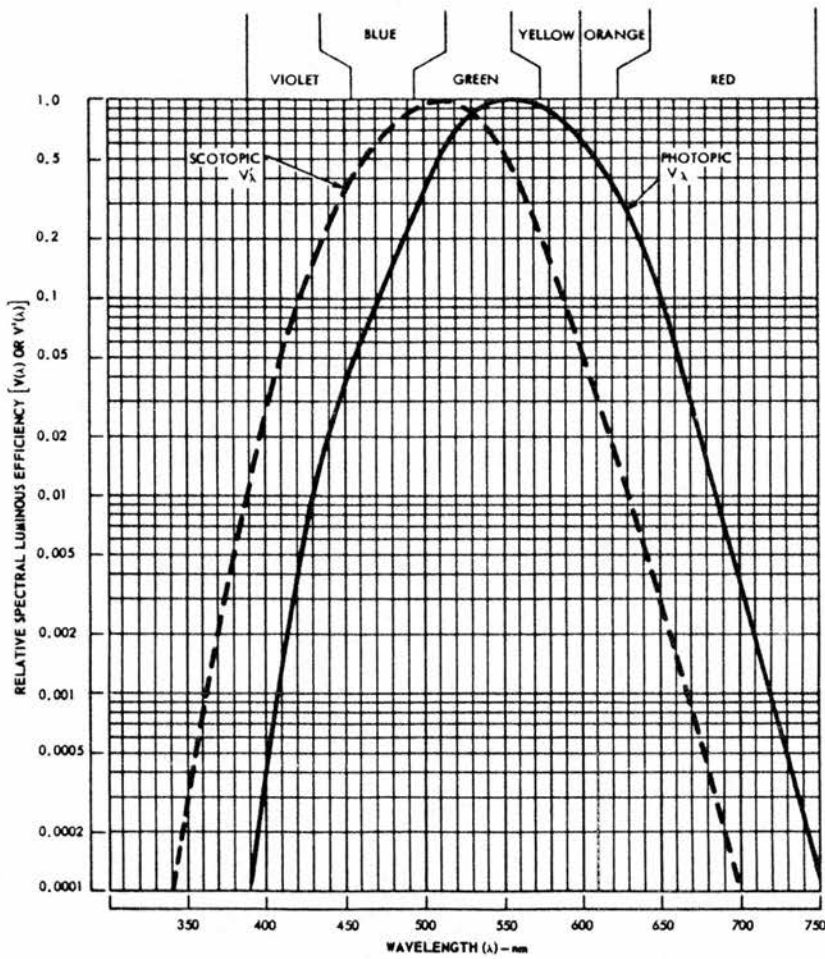


Fig. 3 *Relative spectral luminous efficiency as a function of wavelength. The relative response of the human eye to radiation of a given wavelength.*

from RCA (1974)

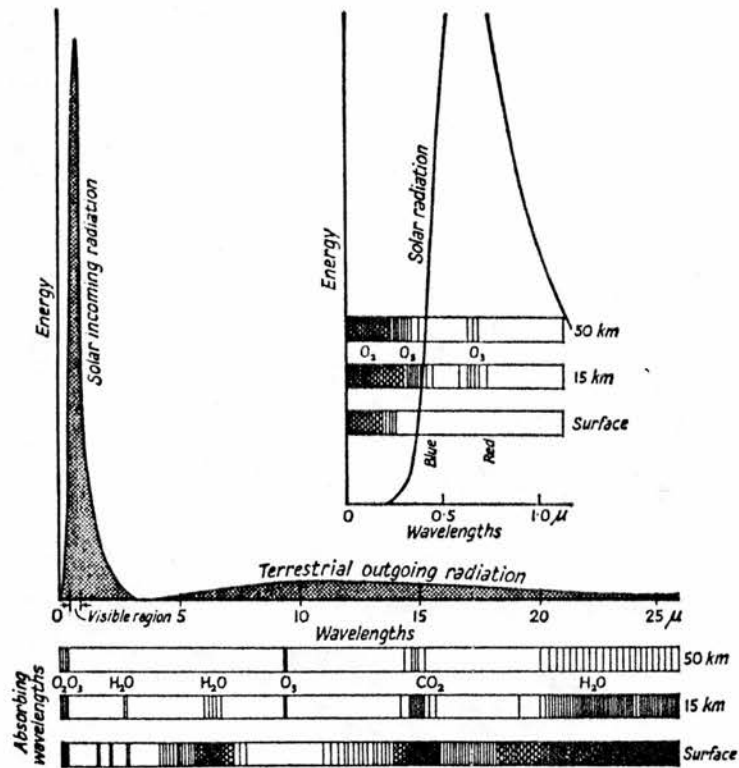


Fig. 4

The spectral distribution of solar and terrestrial radiation, showing the striking difference between them. The shaded strips indicate the wavelengths in which the atmosphere absorbs radiation at the surface, 15 km and 50 km. These show that much of the absorption involves the outgoing terrestrial radiation by the lowest layers of the atmosphere (from Dobson, 1963).

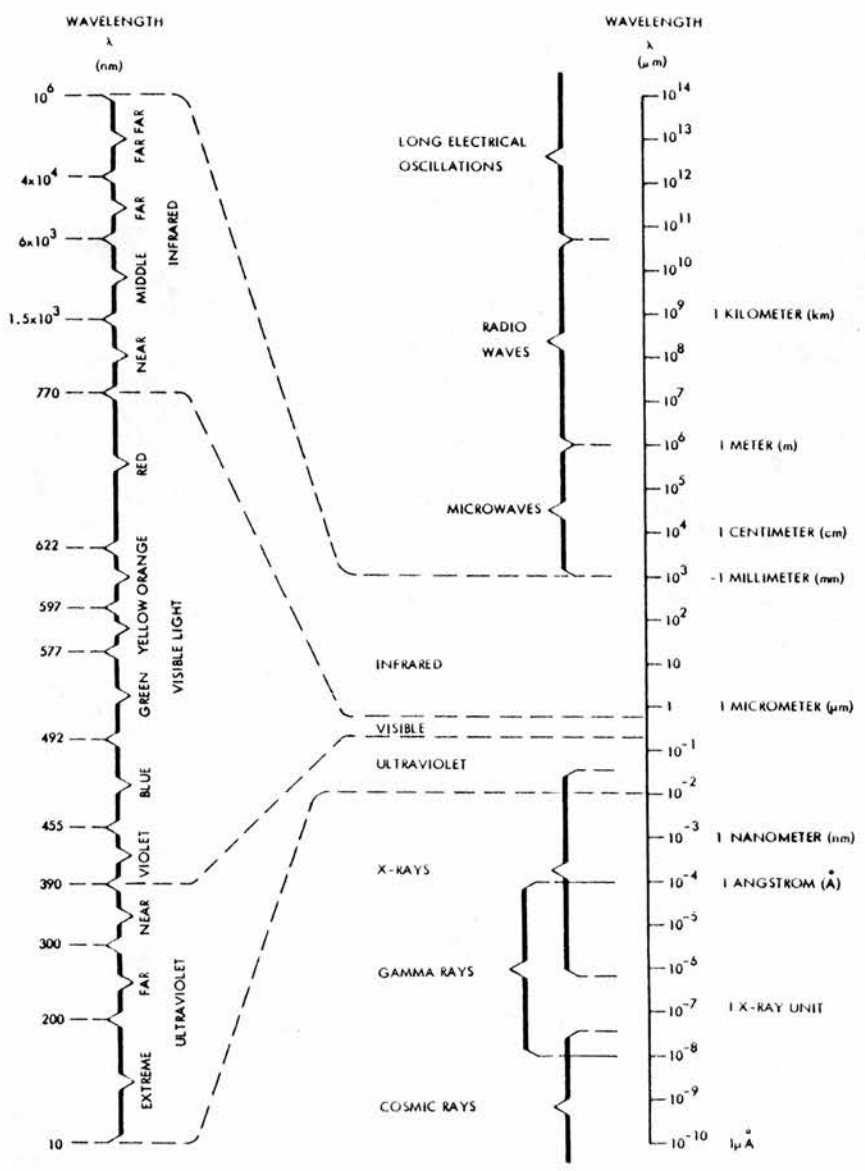


Fig. 5 Electromagnetic spectrum.

from RCA (1974)

Table 2 Radiometric and photometric terms, symbols, and units

radiometric		photometric		Concise definition	
Radiant energy	Q_e	J, W s	Luminous energy, light	Q	Im s Energy in the form of electromagnetic waves
Radiator, source, lamp			Luminator, source, lamp		Device converting a certain form of energy into the radiant one (into the light)
Radiation			Lumination		Process of generation of radiant (luminous) energy
Radiant emittance	$M_e = \frac{\Phi_e}{dS_e}$	$J m^{-2} s^{-1}; W m^{-2}$	Luminous emittance	$M = \frac{\Phi}{dS_e}$	Radiant (luminous) flux emitted per unit area of radiating body
Radiant flux	$\Phi_e = \frac{Q_e}{dt}$	$J s^{-1}; W$	Luminous flux	$\Phi = \frac{Q}{dt}$	Rate of propagation of radiant energy (light)
Radiant flux density	$F_e = \frac{\Phi_e}{dS \cos \alpha}$	$J m^{-2} s^{-1}; W m^{-2}$	Luminous flux density	$F = \frac{\Phi}{dS \cos \alpha}$	Radiant (luminous) flux passing through a plane of unit area
Radiant flux intensity	$I_e = \frac{\Phi_e}{d\omega}$	$J sr^{-1} s^{-1}; W sr^{-1}$	Luminous flux intensity	$I = \frac{\Phi}{d\omega}$	Radiant (luminous) flux emitted by a point-like source into a unit solid angle
Radiance	$L_e = \frac{\Phi_e}{d\omega(dS \cos \alpha)}$	$J m^{-2} s^{-1} sr^{-1}; W m^{-2} sr^{-1}$	Luminance ¹ Brightness ¹	$L = \frac{\Phi}{d\omega(dS \cos \alpha)}$	Radiant (luminous) flux intensity per unit area in direction of emission
Irradiance	$E_e = \frac{\Phi_e}{dS}$	$J m^{-2} s^{-1}; W m^{-2}$	Illuminance	$E = \frac{\Phi}{dS}$	Radiant (luminous) flux intercepted per unit area
Irradiation			Illumination		Emission of radiant (luminous) flux, which is incident on the surface of some body
Radiant exposure	$H_e = \frac{Q_e}{dS}$	$J m^{-2}; W s m^{-2}$	Light exposure	$H = \frac{Q}{dS}$	Amount of radiant energy (light) intercepted per unit area during a certain period

1. Terms used for the characterization of light sources.

CHAPTER 2

INTEGRATORS FOR USE IN RADIOMETRY - A REVIEW

2. INTEGRATORS FOR USE IN RADIOMETRY - A REVIEW

As has been stated in the introductory chapter, the totalisation, or integration of an irradiance signal is one of the main methods of handling such data.

$$E = \int_{t_1}^{t_2} E_{inst.}(t)dt$$

E = integral of irradiance recorded between times t_1 and t_2
 $E_{inst.}(t)$ = instantaneous irradiance values

2.A. Principles of methods used in Integrating Instrument Design

* Photochemical and Physical Effects

- 1- Displacement of liquid distilled through absorption of radiation
- 2- Photo-induced decomposition of chemical substances.

Both these methods have been and continue to be used, they are very cheap in initial outlay, but that is their only real advantage.

* Photoelectrical Effects

The conversion of radiant flux - photons - into an electron flux offers the most versatile framework for the development of radiometers. The first main principle is the Seebeck effect (1826) strictly a thermo-electric, and not a photoelectric, effect, which exploits the voltage which develops in response to the temperature differences between two identical junctions of dissimilar metals connected in opposition. If these so-called hot and cold junctions are thermally coupled to plates of differing absorptance and

reflectance, there opens up the possibility of using the Seebeck effect in radiometry.

The other is the Photoelectric Effect , in which photons interact with the electrons in the surface layer of the photo-detector, releasing them from their normal atomic orbits. Once released, into space in the vacuum photocell or the junction region of a semiconductor photodiode, the electrons may be channelled into suitable external electronic circuitry. Measurement of irradiant photon flux (radiometry), after conversion to an equivalent electron flux, becomes a problem of coulometry. Most integrators work either by charge storage and conversion, or in using the energy available if the charge is driven by a certain driving force or voltage, and these methods are listed below before being given detailed consideration.

1- Electrochemical Methods

- a) Electrolytic generation of gas
- b) Electrolytic transfer of metal
- c) Electrolytic displacement of electrolyte zone
- d) Special Variant I - metal transfer cell with electronic signalling of charge state.
- e) Special variant II - the solid-electrolyte integrator

2- Electromagnetic Method

- a) Integrating motor with gear train and number-wheels

3- Electronic Method

- a) Capacitor charge-discharge methods

The general advantages and drawbacks of these methods are tabulated in Table 3 , before detailed discussion.

	Physical Distillation	Photo-chemical Decomposition	Electro -gas	Electro -metal	Curtis meter	Bisset Berman	Memoriode	Integrating Motor	Electronic systems
Method	A	A	B	B	B	B	B	B	B
Criterion	1	2	1a	1b	1c	1d	1e	2a	3a
Self powered?	yes	yes	yes	yes	yes	yes	yes	yes	NO
Reliable?		NO	yes	yes	yes	yes	yes	NO	yes
Low initial cost?	yes	yes	yes	yes	yes	yes	yes	yes	yes
Threshold and starting problems?	YES		no	no	YES	YES	YES	YES	no
Linearity?	fair	fair	fair	fair	fair	fair	good	BAD	fair-good*
Moving parts?	no	no	no	no	no	no	no	YES	no
Harmed by running off scale?	no	no	MAYBE	no	YES	?	?	no	no*
Limitations in spectral response	YES	YES	n.a.	n.a.	n.a.	n.a.	n.a.	n.a.	n.a.

Key: n.a. = not applicable
 * = if correctly designed
 ? = not known

Table 3

Advantages and drawbacks of various signal integration methods

2.B. Photochemical and physical effects

2.B.1. Displacement of liquid distilled through absorption of Radiant Flux

The first practical embodiment of this idea was suggested as long ago as 1836 by Bellani, and is generally known as the Bellani, or Gunn-Bellani radiation integrator or distillometer. The principle lies in the fact that the latent heat of evaporation of a liquid is a physical constant, therefore, (ignoring the question of specific heat by assuming no net temperature increase), a certain energy input into a volume of liquid should generate vapour in proportion. If the vapour quantity can then be measured, it should reflect the energy put into the system. In the Bellani distillometer, radiation is absorbed by a blackened surface inside a sealed glass sphere. The upper space is connected by a tube to a long sealed calibrated glass stem, which in use is sunken into a well in the ground. Heat generated in the black surface causes an increase in vapour pressure above the liquid nearby, and the lower vapour pressure in the cool region of the stem causes net transfer of vapour down the stem, where it condenses. The volume of liquid gathering in the calibrated stem then shows the integral of radiant energy absorbed by the system. According to the liquid selected the properties of the distillometers will vary; water can be used, but carbon tetrachloride, for example, is more sensitive, having a specific heat of 0.2 and a latent heat of 52 cal. g^{-1} which is one tenth that of water. TRICKETT, MOULSLEY and EDWARDS (1957).

Gunn-Bellani integrators are cheap and are relatively widely used. PEREIRA (1959) found that his results were highly correlated with those from a Kipp Solarimeter, as likewise they were when compared

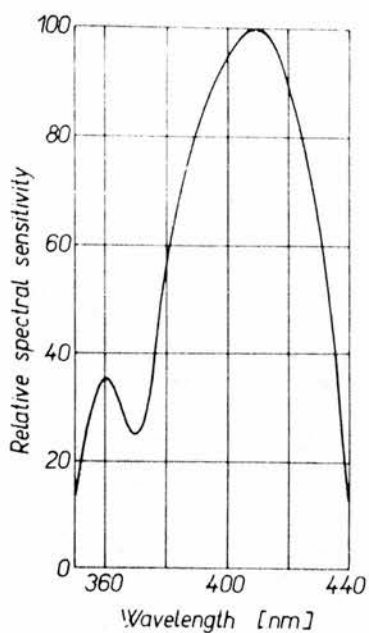


Fig. 6 Spectral sensitivity of heliographic *Ouzalid* paper No. 33 NT (from Friend 1961).

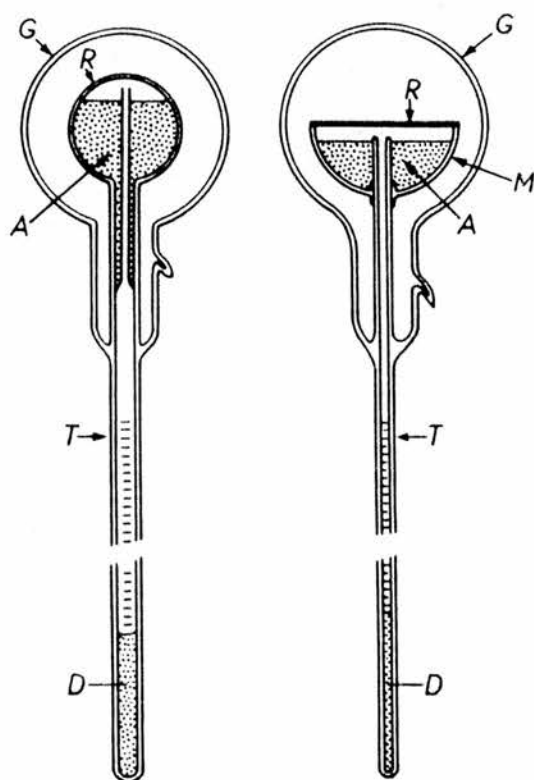


Fig. 7 Two modifications of the Bellani pyranometer. Left: all-glass model with a spherical receiver fitted with a non-selective absorbing layer (designed by The Physical and Meteorological Observatory, Davos); right: combined model of glass and metal with a flat receiver (design by National Institute of Agricultural Engineering, Silsoe, U.K.). *G*: outer glass vessel; *R*: receiver; *M*: metal-plated mirror surface (with flat receiver); *A*: alcohol filling; *T*: calibrated tube; *D*: distilled liquid (from Courvoisier & Wierzejewski 1954; Trickett, Mouldsley & Edwards 1957).

with the Eppley pyrhelimeter in measurements made in summer at 42° lat. in the USA, SHAW and McCOMB (1959). MONTEITH and SZEICZ (1960) have suggested that the good correlations found by Pereira are due partly to the relative independence of soil temperature and season, and partly to the small seasonal changes in relationship of radiation received by the spherical and horizontal surfaces of the instruments when they are used near the equator. However, generally these integrators are not very satisfactory, and should be used with caution at lower irradiances. See also COURVOISIER and WIERZEJEWSKI (1954).

2.B.2. Photodecomposition of chemical substances

Photons impinging on molecules may, if of appropriate wavelengths bring about chemical changes. It is possible to use this effect in radiometry if the photochemical reaction triggered is irreversible, and is not affected by other factors such as temperature or spontaneous decomposition of the reagents

All these systems have the disadvantage of having action spectra which can barely be considered to cover the plant-active and visible spectral regions. The main peaks are in the ultraviolet, and in the words of DREW (1972), 'their use in anything other than direct sunlight is therefore limited, and they are no use whatsoever under conditions where the ultraviolet is preferentially absorbed, as in the underwater environment.'

examples of such systems are:

Peak Sensitivity	Principle	Reported By
350nm	Photochemical transformation of anthracene in benzene	DORE (1958)
410nm	Photosensitised Ozalid paper	FRIEND (1961)
280-450nm	Photodecomposition of oxalic acid in presence of uranyl ions	ANDERSON and ROBERTSON (1925)

The uranyl oxalate system was investigated by LEIGHTON and FORBES (1930) and has been used in plant studies by HEINECKE (1963). MAGGS and ALEXANDER (1970) have exhaustively analysed the usefulness of the method and used it to study irradiance in an orchard. For radiant flux receivers, they used celluloid ping pong balls containing 12ml. of active solution, and found them satisfactory, showing good linearity, low heat-induced decomposition, low sensitivity to infra-red, and a low rate of self-decomposition in storage after exposure. They also found that for their particular study the limited spectral response adequately sampled the radiant environment with which they were concerned.

If the radiant flux to be integrated were to strike a surface of high absorptance, as in the Gunn-Bellani distillometer, it might be theoretically possible to use a chemical temperature-time integral indicating change such as the inversion of glucose from the α to β form, analysing the changes polarimetrically BERTHET (1964), but such a system is likely to be highly non-linear, and nobody, so far as is known, has tried to use it.

Finally, it is worth noting that the incremental increase in weight in Impatiens parviflora is linearly related to Irradiance up to levels of ca. $80 \text{ kJ.M}^2 \text{ day}$, HUGHES (1965)

2.C. Photoelectrical effects

2.C.1. Electrochemical methods

All the methods described below rely for the success of their operation on Faraday's Law of Electrolysis:

$$M = zIt \quad (1)$$

where M = mass of element liberated

z = a constant for each element: the Electrochemical equivalent

I = current

t = time of passage of current.

The Electrochemical equivalent is the mass (in grams) of element liberated by 1 coulomb of charge. For certain systems, 'mass of element liberated' can equal 'mass of element dissolved' on reversal of the current flow, this being an important factor in operation. Faraday in 1840 developed the first coulometers, which liberated H_2 and O_2 for subsequent measurement, BOGENSCHÜTZ (1974).

2.C.1.a. Electrolytic generation of Gas

In the original form of the coulometer the combined gases H_2 and O_2 resulting from electrolysis were collected in a gas burette where the volume could be measured, and if necessary corrected to NTP. This was not very satisfactory, and apart from the danger of explosion of the gas meter, the electrolyte needed occasional replenishment. A far more successful refinement (due to HOLDEN (1905)) is the Siemens-Schuckert meter which was at one time widely

used in continental Europe for domestic electricity measurement. The commercial realisation is a sealed system with an easily read manometer tube and scale housed in an outer shell which tips downwards on a hinge for the purpose of resetting. Hydrogen released at the cathode bubbles up into the manometer tube, and the oxygen is generated at the anode which is in a chamber separated from the cathode. When the meter is reset by inversion, the hydrogen bubble passes round to the anode cavity, where the oxygen is in fact never released since the hydrogen round the anode gauze is oxidised back to water by the nascent oxygen at the platinum anode, which acts as catalyst for the reaction.

This type of integrator was first used by GORCZYNSKI (1936) in direct connection with a thermopile. TRICKETT and MOULSLEY (1956) exploited it to measure the output of photocells and TRICKETT, MOULSLEY and EDWARDS (1957) preferred it to the integrating motor, (see below) but they noted that the back EMF generated in the integrator spoils the linearity when it is used directly with a thermopile. They solved this problem by using a magnetic amplifier. MONTEITH and SZEICZ (1962), responding to a demand from the World Meteorological Organisation for the production of equipment of low cost, but acceptable ease of handling and accuracy, reassessed the non-linearity problem. They cancelled the back-EMF (a procedure sometimes known as 'bucking') with a variable electrical potential from a variable resistance and dry cell, and found that this modification secured results which compared well with those from a Kipp solarimeter with its attendant magnetic amplifier and integrating motor.

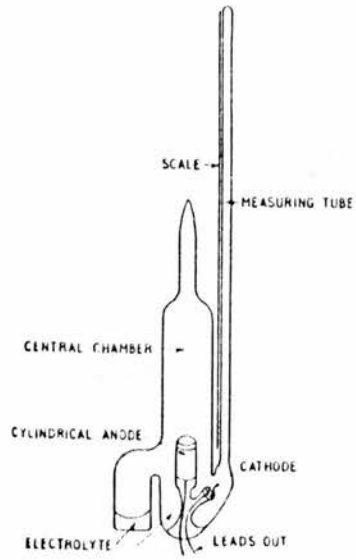


FIG. 8 a
DETAILS OF GLASS WORK AND ELECTRODES OF THE SIEMENS
METER

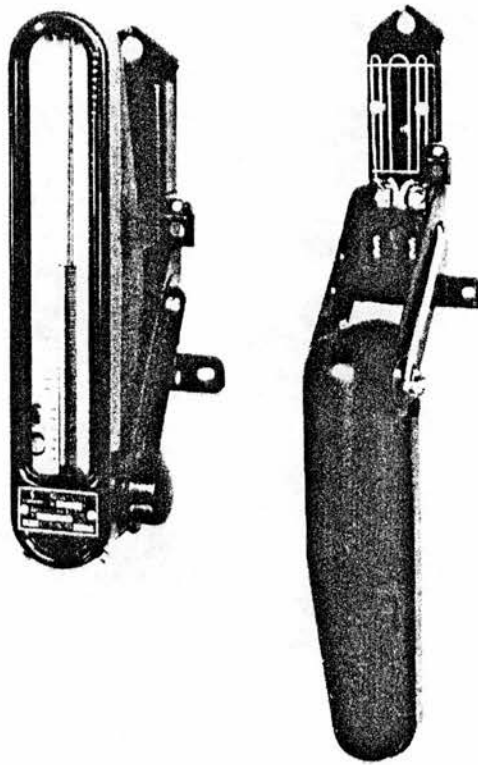


Fig. 8 b *Siemens-Schuckert* electrolytic integrator. Left; instrument in operational position; right; instrument turned upside down for filling the tube.

2.C.1b. Electrolytic transfer of metal

Some of the earliest coulometers depended on the electrolytic transfer of metals, for example silver and copper, from anode to cathode in a suitable electrolyte. LUCKOW (1865) used silver nitrate in 10% aqueous solution with a silver anode and a platinum cathode. JACKSON and SLATER (1967) developed copper coulometers for use in an integrating photometer for outdoor use, and these were used in a study of apple tree canopies by JACKSON (1970). BOGENSCHÜTZ (1974) gives a formula for a suitable electrolyte for use in a copper coulometer as being:

copper sulphate	$\text{CuSO}_4 \cdot 5\text{H}_2\text{O}$	200g. litre ⁻¹
sulphuric acid S.G.1.84	H_2SO_4	20g. litre ⁻¹
ethanol	$\text{C}_6\text{H}_5\text{OH}$	20g. litre ⁻¹

This electrolyte performs best at temperatures of 14-40°C and at cathode current densities of a 5mA.cm⁻².

It is not stated why the ethanol is present in the electrolyte, but organic molecules tend to **enhance** the deposition properties of electroplated metals. It is a problem with some of the simpler coulometer patterns that the metal deposited at the cathode is friable and readily shed falsifying subsequent weight-gain measurements. The coulometer cathodes have to be oven dried after use and weighed before and after, and they are therefore tedious to use, and do not reveal any results when on the field site. In spite of this they continue to be used because they have negligible cost and are amenable to local construction.

Unlike the Siemens hydrogen gas coulometer, there is with these coulometers no need to correct for troublesome back-EMF; when anode and cathode are of like material in a solution of ions of the same

material this EMF is very low, and copper is the best metal, generating only 10mV. TRICKETT, MOULSLEY and EDWARDS (1957). A disadvantage with copper deposition, however, is that current efficiency is never 100%, since there is a disproportionate formation of cuprous ions in the anode region according to the formula $\text{Cu} + \text{Cu}^{++} \rightleftharpoons 2\text{Cu}^+$. KORTUM (1957 in BOGENSCHUTZ 1974). Similar integrators have been used by MACFADYEN (1956), MADFADYEN and HEALEY (1965), (silver metal coulometers) and HANSEN and HAGEMANN (1967) (Copper metal coulometer).

2.C.1c. Electrolytic displacement of Electrolyte zone

This principle is a variant of 2.C.1b above. Mercury is the metal cross-plated, and this lends itself to visual self-indication. Each electrode is in the form of a thin cylinder of uniform area of cross section. This is assured since the electrodes are constrained by the walls of a fine-bore capillary tube. Between the electrodes is a short strip of electrolyte, and by cross-plating of mercury the cathode grows forward, the anode foreshortens and the electrolyte "bubble" moves. The coulometer can be calibrated in mA hours.mm⁻¹ or even directly in irradiance units. The originator of this pattern is LEHFELDT (1902) but it is in the last twenty years that a small highly sensitive version called a Curtis meter or Merchron has become available. This commercial form of the device will readily integrate microampere currents, typically showing a sensitivity of 2.5mm (mAHour)⁻¹. Normally, the device is scaled in each direction, and a switch is used to reverse the direction of current flow whenever the scale reading has been used up. If the current is allowed to drive the electrolyte blob until all mercury has dissolved

from the anode column, the meter will be destroyed by electrolytic migration of the end-contact metal, and the capillary will become blocked. This means that radiometers based on these integrators have to be used with caution if there is any possibility of this happening. McKEE (1963) was one of the first to use mercury coulometers for irradiance studies, recording the currents from selenium and silicon photodetectors. HUGHES and LINCOLN (1969) used them with a thermopile solarimeter and transistorised amplifier; CAIN (1969) a cadmium sulphide photocell, and DREW (1972) a selenium cell and coulometer mounted in a subaquatic housing made of perspex. MACFADYEN and WEBB (1968) found the consistency of the Curtis mercury coulometer to be within 1% between individuals in a batch.

Apart from the susceptibility to damage, these integrators are the simplest and most accurate form of electrolytic integrator, and for that reason they have been used by several investigators.

2.C.1d. Special Variant I - Metal transfer cell with electronic signalling of charge state

As described in Section 2.C.1b coulometers relying on the transfer of metal normally have to be 'read' by a weighing process. TRICKETT, MOULSLEY and EDWARDS (1957) were among the first to exploit the possibility of estimating integrated charge by timing the process of deplating under constant-current condition. If a constant current is fed in reverse into a silver coulometer; and the electrolytic process is 100% efficient, then:

$$\text{(forward)} \int_0^{t_1} i_1(t) dt = \int_0^{t_2} i_2(t) dt \quad (\text{reverse})$$

if i_2 is fixed, then:

$$t_2 \propto \int_0^{t_1} i_1(t) dt$$

What is required is an indication when the silver deposited on the cathode in integration has been exactly removed on reversal, and this indication can readily be obtained if the cathode is for example, carbon or platinum. During the 'read' cycle the former cathode of silver plated carbon becomes anode, and the potential across the cell rises sharply after all the silver has been removed and the evolution of oxygen begins. This sudden voltage change can be used to trip the deplating operation at its finish. TRICKETT, MOULSLEY and EDWARDS (1957) used a copper coulometer with a platinum base electrode for the cathode, and a circuit with a transistor and relay to supply stabilised constant deplating current and detect the endpoint. Their apparatus was emphasised to be experimental, and was found to have rather a high internal impedance and too high a back-EMF for direct connection to a thermopile radiometer.

Commercial versions of these integrators have appeared in greatly refined form, using silver as the operating material, and electrolytes designed for use at temperatures of -50 to $+80^\circ\text{C}$ for example, silver phosphate (Ag_3PO_4) in concentrated phosphoric acid, or other silver salts in such solvent media as n-butyronitrile, acetonitrile and tetrahydrofuran. A typical end-point curve for an integrator of this type is shown in Fig. 10 with two electrolyte systems, and Fig. 9 shows a cross-section of a commercial example (Bisset-Berman Inc. Los Angeles) BOGENSCHÜTZ (1974) RAUCH et al., (1966), in BOGENSCHÜTZ (1974)

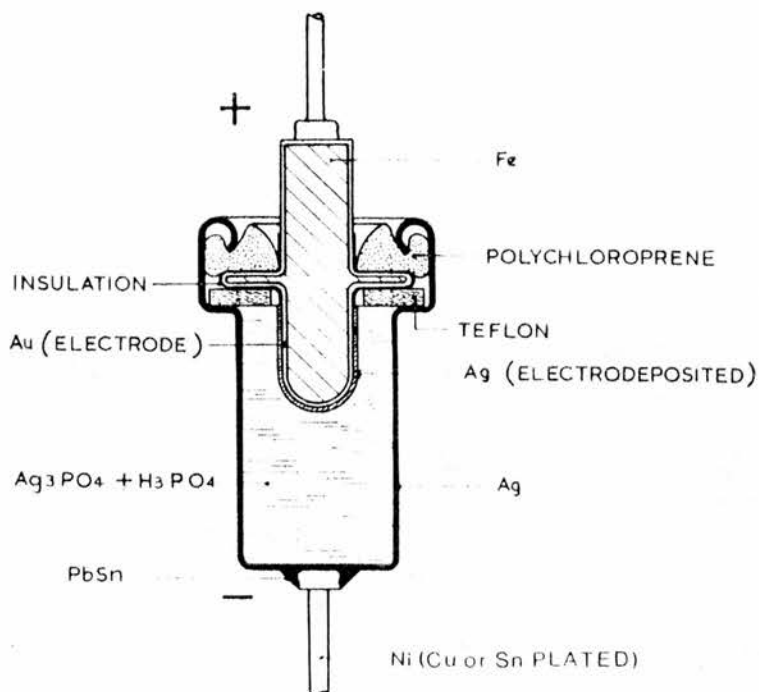


Fig. 9 Cross sectional drawing of a two-electrode timer cell

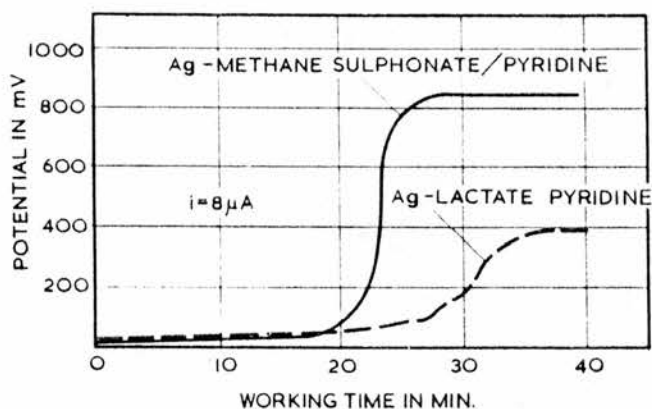


Fig. 10 Voltage process of an electrolytic timer cell

from Bogenschutz (1974)

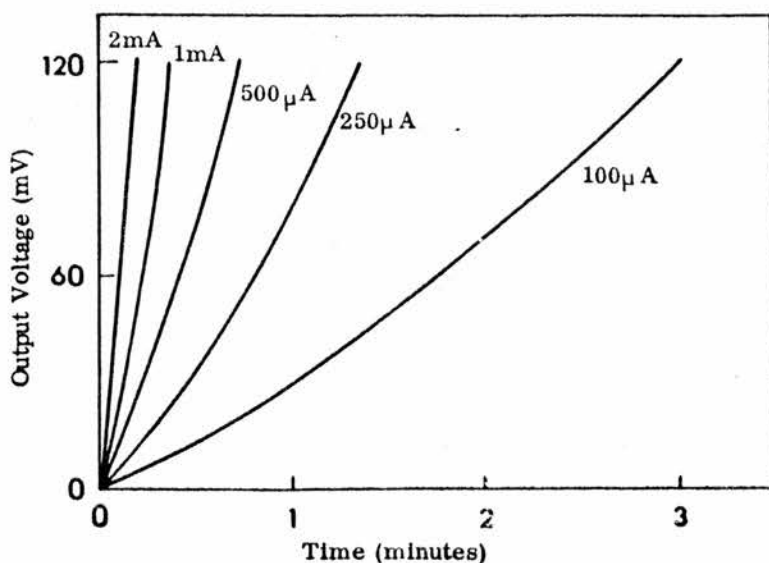


Fig. 11 Charge characteristics of a typical memoriode

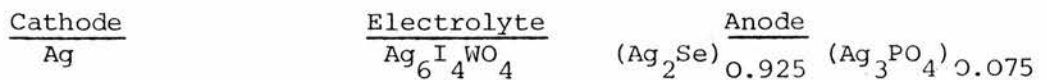
from Ikeda (1975 - 8)

For a description of the use of these devices, see PLATT, LARSEN and VINE (1970) and HUMPHREY and WOLFF (1967) who have designed a small temperature-integrator to be worn on human subjects. This device is commercially available.

A related device is the solion integrator (Texas Research and Electronic Corp.) which depends on a Redox reaction. See MARTIN and COX (1962).

2.C.1e. Special Variant II - Solid electrolyte integrator

Recently there has become commercially available an integrator based on improvements in the field of solid electrolytes. Ions are not normally mobile in solid materials, but since 1950 new complex materials have appeared which show high ionic mobility at room temperature. IKEDA and TADA (1976) describe a device made with the following electrode system:



In operation, a changing silver ion concentration at the anode caused by the passage of current in the forward direction causes a voltage to develop across the cell in accordance with the formula:

$$E_{\text{anode}} = \frac{RT}{F} \ln a_{\text{Ag}} + E'$$

where: E = electric potential at anode, E' = a reference level
 a_{Ag} = activity of silver, R = gas constant
 F = Faraday constant, T = absolute temperature

An empirical formula has been found to apply to these devices, being

$$E_{\text{anode}} \propto \int_0^t i_{\text{in}} dt \quad \text{for all practical purposes}$$

E_{anode} , and the total cell voltage is almost linearly related to the

charge stored as is shown in Fig. 5, (IKEDA 1975-8) The EMF developed is held for lengthy periods of time, showing less than 0.3% change in 48 hours after cessation of input. This can be considered the memory phase of operation, and at any time during charge or memory phase the integrated charge can be directly read without affecting integration by means of a high impedance voltmeter ($>100M\Omega$). Whilst integration is proceeding there is a slight overvoltage effect, but this can be almost eliminated in the three terminal version of the cell in which there is an extra reading electrode independent from the main anode terminal. The normal operating range is from 0 - 100 mV, and for this range there are three sizes of coulometer at present available: 1, 5, and 50 μ A hours. After reading, the integrator is reset to zero by the reverse passage of current, which should not be high enough to take less than 5 seconds to complete resetting.

The effect of temperature is slight, and cycle life tests show that even 10^5 reversals have little effect on the performance. The Memoriode, as the commercial device is known, is not expensive, and seems likely to render most other electrochemical systems obsolete for practical use. The memoriode is made by the Japanese firm SANYO. See also IKEDA (1975-8) , and VALVERDE (1981)

2.C.2. Electromagnetic methods

2.C.2a. The Integrating motor

This device is no longer often used since almost any of the more recent designs of electronic integrator perform better on a cost-for-cost

basis. It was however of great importance before the advent of the transistor.

The integrating motor is a special type which has a rotor speed proportional to input voltage over the range 6 - 8mV to 1500mV. A special magnetic circuit is employed to give these properties and a low loss system of gears and number wheels gives the output a numerical value. It was customary to use the motor with a magnetic amplifier to raise the output voltage from the thermopile radiometer above the starting threshold of the motor and to provide a suitable load impedance for the thermopile.

It was found that with time the slope of the V in / rotor speed characteristic changed due to increasing friction and that the starting threshold voltage would also change, necessitating return to the makers (Electromethods Ltd.) for overhaul, TRICKETT, MOULSLEY and EDWARDS (1957); BLACKWELL (1954) and UCHIJIMA (1968).

A much more robust approach to the problem of the sensitive integrating motor is to use a large bank of solar cells and a domestic DC electricity meter, but this is not very satisfactory, the starting current of these meters being quite high. A commercial instrument suitable for general purposes is available from Rauchfuss Instruments and Staff F ty. See also WHILLIER and TOUT (1965).

2.C.3. Electronic Methods

2.C.3a Capacitor charge-discharge methods

The essential feature of all electronic integrators, in common with the previously described electrochemical types, is the charge-store.

Such a store is called a capacitor, and appropriately perhaps, at one time the unit of capacity was the 'jar'. The important characteristic of a capacitor is that

$$Q \propto V$$

Where: Q = the charge within the capacitor

V = the voltage across the terminals of the capacitor

Introducing a constant of proportionality, C , it is found that

$$Q = CV$$

The constant C is called the capacitance of a conductor, and is the amount of charge in coulombs required to raise its potential by one unit. The MKS unit of capacity is the Coulomb.volt⁻¹ or FARAD. If a conductor has a capacitance of 1 Farad, its potential will be raised by 1 volt when given a charge of 1 coulomb (ie. 1 amp-second).

From Fig.11 it will be seen that the memoriode described in section B 1-e could also be considered as a capacitor. The 'capacity' of these, specified there as ampere-hourage to produce 0.1 Volt increase in potential on the terminals of the cells, gives effective values of:

1 μ A. h	360 μ F
5 "	1800 "
50 "	18000 "

Theoretically, then, the simplest way of using a capacitor as a radiant flux integrator is to use it in the same way as the memoriode. Changing the subject of the formula, we find:

$$V = \frac{Q}{C}$$

and with $C = \text{const.}$

$$V \propto Q$$

therefore, the simplest working arrangement might be as in Fig. 12 and Fig. 13 in which a photodiode, fed with constant radiant flux and driven by a suitable external EMF charges a capacitor, C_{intg} . The voltage, $V_{C_{\text{intg}}}$ rises linearly with time until it reaches the same value as the external EMF, V_{bat} .

It is instructive to compare the memoriode and its equivalent capacitor further. For the memoriode, an input of $50 \mu\text{A.Hr.}$ raises the output potential by 0.1 volt, which corresponds to the behaviour of a perfect capacitor of $18,000 \mu\text{F}$. That is a very large value, but if a 10V output potential swing could be realised across the capacitor, this would correspond to $180 \mu\text{F}$ - and there would seem to be no reason to use the relatively expensive memoriode for practical use. Unfortunately, reality is different, and all real-life capacitors have a built-in resistance in parallel with the capacitance, which causes leakage of charge. The time course of change of voltage on the terminals of a capacitor subjected to discharge by a resistor is shown in Fig. 14. The time taken for a given capacitor-resistance combination to discharge from V to $0.37V$ is called the time-constant of the combination, and is given by the formula:

$$T = RC$$

where: T = Time-constant in seconds

R = Resistance in Megohms

C = Capacitance in Microfarads

The leakage resistance, per unit of capacitance, is constant for, and dependant on the inherent defects in the commercial dielectric chosen for the construction of the capacitor. It follows that for any given dielectric the goodness of the resulting capacitor may be expressed by a (self-) time-constant, and typical values expressed thus are in Table 4.

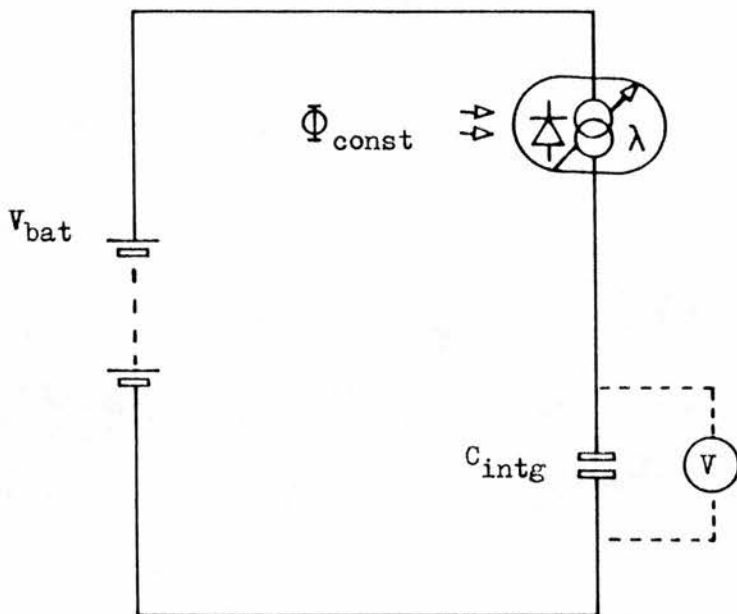


Fig. 12 Simplest possible arrangement for using a capacitor, C_{intg} in an integrating radiometer

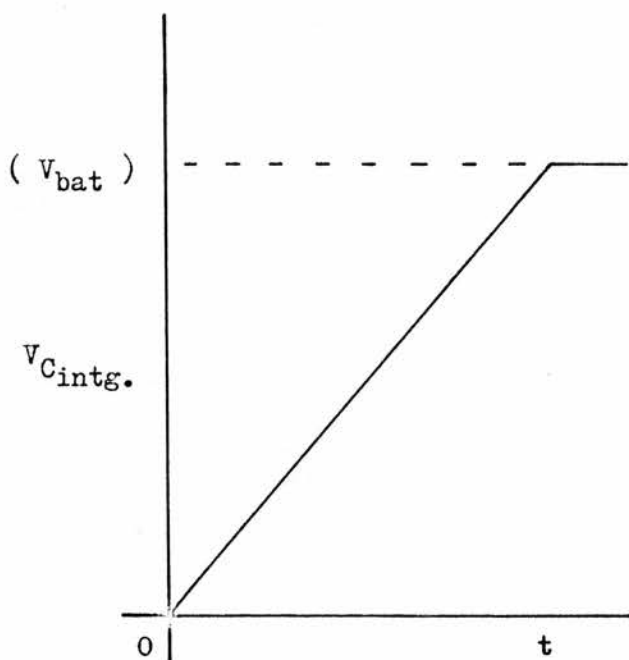


Fig. 13 $\frac{dV}{dt}$ graph for C_{intg} . voltage. Radiant flux (Φ) into face of photodiode constant.

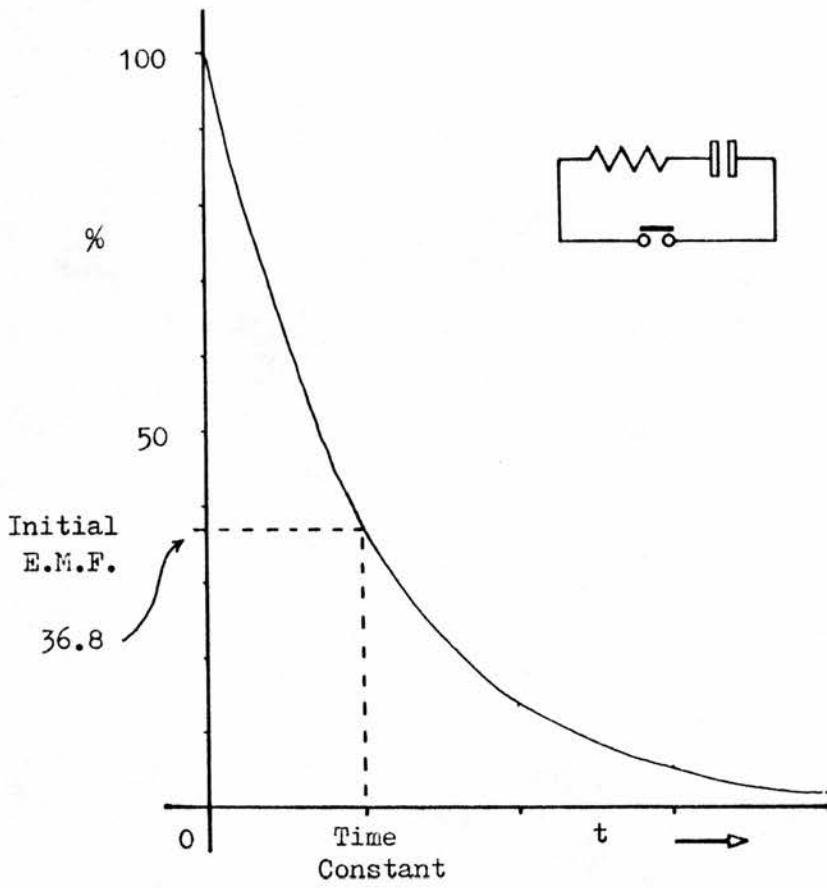


Fig. 14 E.M.F. across the terminals of a capacitor subjected to discharge by a resistance

Table 4

Leakage performance of selected commercially available capacitor dielectrics

Dielectric	Time-const. (for 63% loss of initial charge)		Volume of typical 100 μ F 63V capacitor Cubic Centimetres
	Seconds	Hours	
polystyrene	250,000	70	5,000
polyethylene terephthalate	30,000	8	45
polycarbonate	30,000	8	
cellulose acetate	15,000	4	
tantalum pentoxide	1,700	0.5	2.5
aluminium oxide	68	0.015	1.9

The high capacitance/volume ratio of Ta and Al electrolytic capacitors is explained by the high dielectric constant and operating field voltage applied to the oxide dielectrics. For aluminium oxide the field strength can be 8 megavolt.Cm⁻¹, an extraordinarily high value

Capacitors with the lowest leakage have the largest volumes, and the necessary sizes and costs, coupled with the poor charge-storage properties as witnessed by the time-constant figures, mean that capacitors are never used directly in the manner of the memoriode. It is fair to say that the time-constants given for the dielectrics are worst-case values, and frequently the true figure will be an order of magnitude better. MACHATTIE (1971) records a time-constant value of 400 days for a polystyrene capacitor. The question of the performance of capacitors is a most important one and is considered further in Appendix 6.

2. C.3b The use of the capacitor in electronic integrators

As shown above in section 2.C.3a, capacitors have the disadvantage on account of leakage of being poorly fitted for storing integrated charge. The leakage properties cannot be improved, but if the capacitor can activate another circuit as soon as it has received a known charge, instead of being required to hold that charge, then a whole range of electronic integrating circuits based on the capacitor becomes possible. These circuits are considered in the following sections.

2.C.3c Examples of the use of capacitors in integrators

In practice, a fixed capacitor is charged through a range of voltage, ΔV , the value of which is fixed by the choice of upper V_2 and lower V_1 cut-off values. When the capacitance in the circuit has been charged to the upper potential, V_2 , the passing of this voltage

threshold triggers the removal of charge until the lower threshold, V_1 , is reached; simultaneously with this, and, dependent on the rate of recycling, a pulse signal is taken to an auxiliary circuit, which may for example be an electromagnetic counter.

Whilst the capacitor is being discharged, it is not receptive to further incoming charge, so this period is called dead-time, t_{dead} - see Fig 15 which shows the course of these events. Whereas Fig 15 shows the sawtooth of constant periodicity which results when the incoming I_{intg} is constant, Fig 17 a, b, and c show the variations which result when I_{intg} is fluctuating. The output of the integrator (Fig. 17c) is a pulse train, and the frequency of the output signal spikes at any one time is proportional to the mean value of the charge flux being integrated - as established over the time interval between previous spikes, $t_{\text{integrate}}$. (see Fig. 15) This frequency (f_{inst}) is $\frac{1}{t_{\text{integrate}}}$ for this integration cycle.

For a given I_{intg} , if a smaller value of C_{intg} is chosen, the frequency of the pulse train will be higher. The higher the frequency of the pulse train for any constant charge flux (current) being integrated, the higher is the resolution with which the integrated signal reflects the original signal. As mentioned before - page 7 para 3 - too many data values may be an embarrassment for an investigator, whose computers and data stores will not handle the data, and for whom the majority of the data values may be redundant.

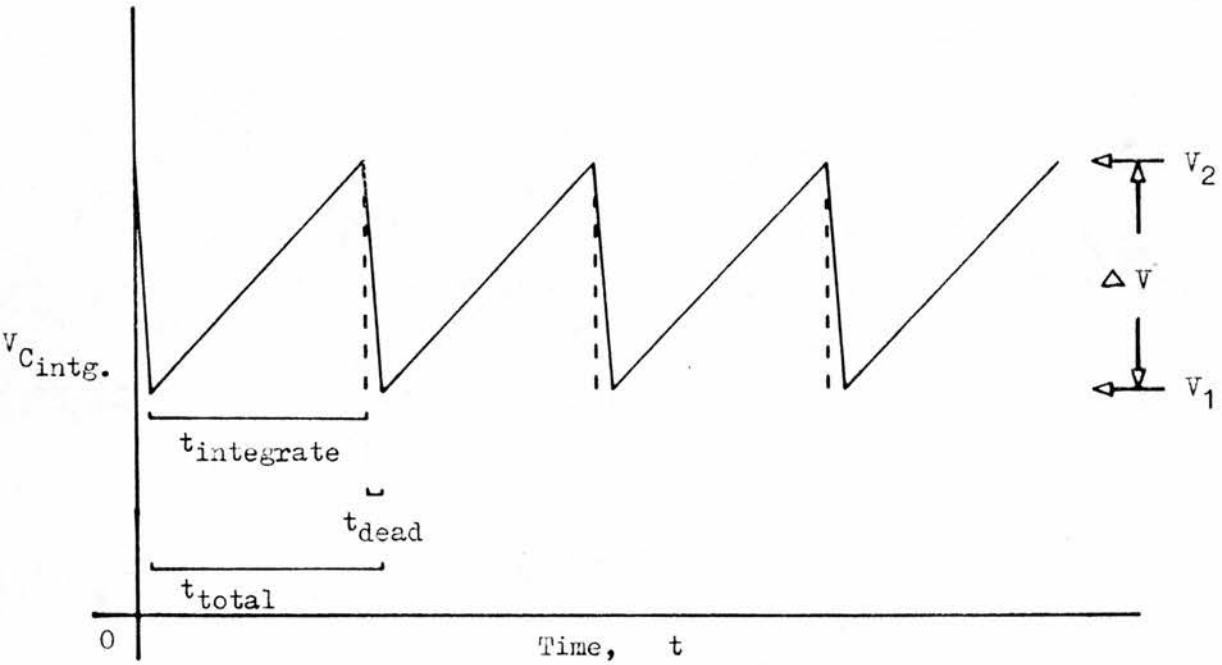


Fig. 15 Voltage waveforms on $C_{intg.}$, constant $I_{intg.}$ to capacitor. Dead-time t_{dead} is shown in relation to $t_{integrate}$ and t_{total} - the cycle time under these constant conditions.

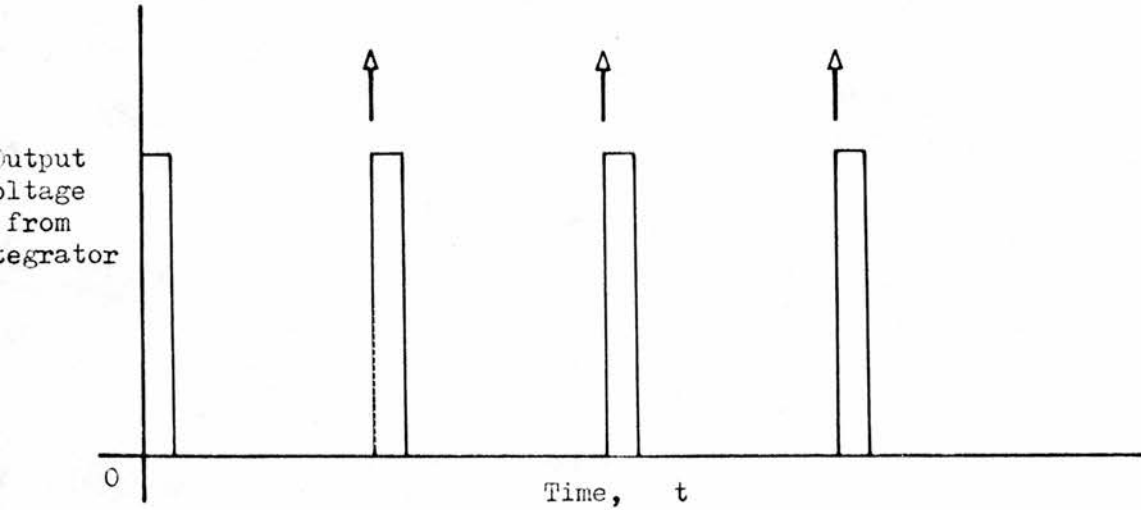


Fig. 16 Output of integrator: pulses triggered by the start of the discharging phase of the integration cycle

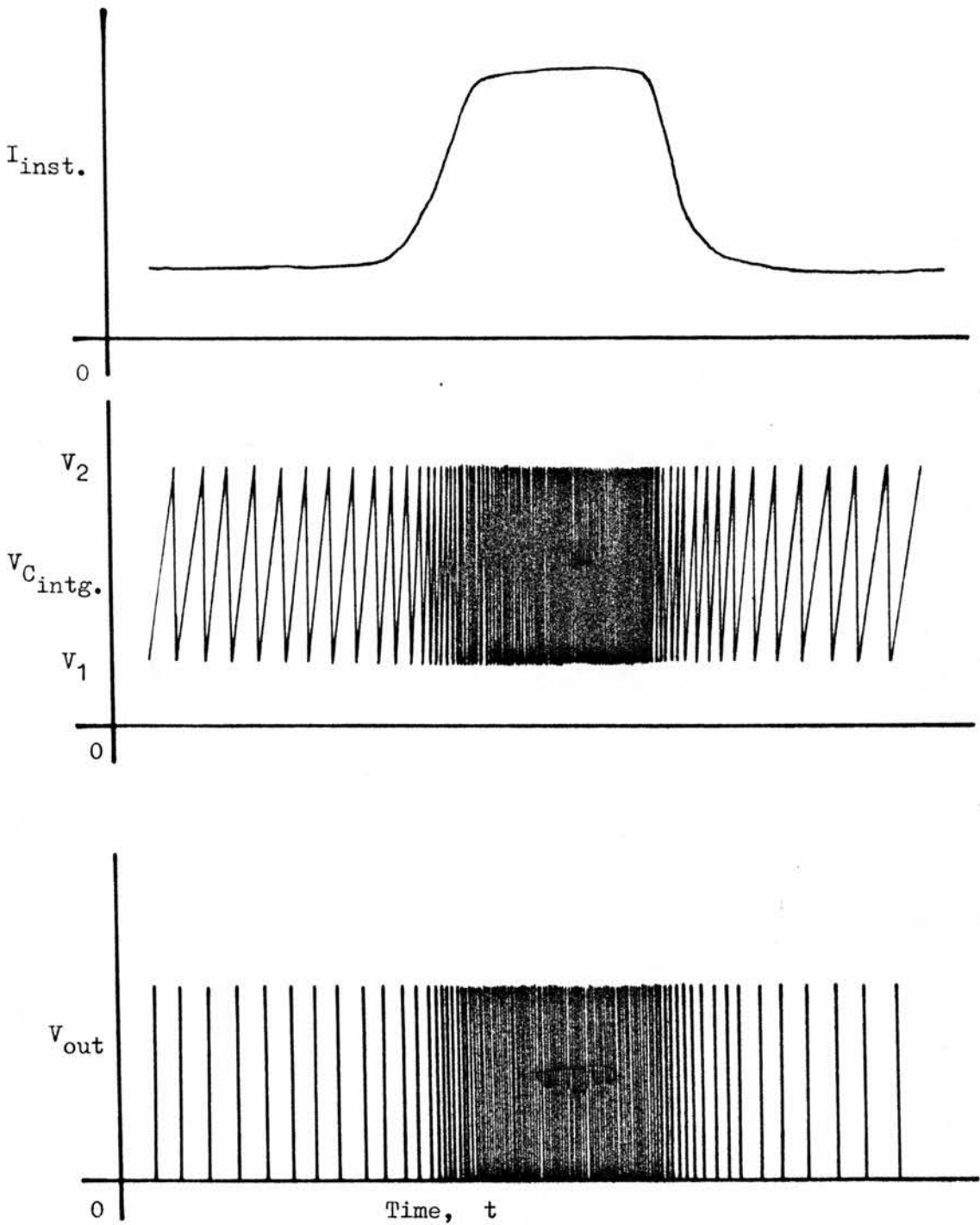


Fig. 17 a) Time graphed against a changing instantaneous input current to an integrator capacitor operating over a fixed voltage range ΔV between V_1 and V_2 (see text)

b) Waveform of voltage present on integrating capacitor

c) Pulse train output from the complete integrator

2.C.3d Integrators for two purposes: digitisation and averaging

At this point, it will be found that the users of integrators diverge in their requirements; one group seeks integrators for averaging, with output frequencies of 1 pulse per hour up to a maximum of 10 per second; the second, frequencies from perhaps 10 per second (10 Hz) to 10 KHz, for digitisation.

2.C.4 Integrators for digitisation

The conversion of an analogue signal into a pulse train with a certain frequency is a means whereby a **varying** analogue signal may be converted to a DIGITAL equivalent. Analogue signals - say, the handful of micro-amps from a radiometer - are readily subject to spurious interfering losses and additions in transmission and handling caused by electrical leakage. This especially often occurs with long runs of cable, leaky joints and connectors used under humid conditions and in industrial plant. Amplification of the analogue signal is often no answer to the problem, since the same percentage of the amplified signal may continue to be lost through leakage. In contrast, a low impedance digital signal may be passed over long distances, and a very large proportion of electricity in the signal can be lost whilst complete fidelity to the original signal is retained. If the frequency pattern of the signal can be detected after amplification, then no loss of data has occurred.

When integration as a means of DIGITISATION is used, a high maximum frequency may be required if the signal being digitised has in it high frequency components (as explained in page 8 further aspects of measuring and recording .)

Digitisation is also the main means of preparing an analogue signal for radio-telemetry, which is an important tool wherever the laying of cables between pieces of apparatus is undesirable.

2.C.5 Integrators for averaging

2.C.5a A common field data register - the electromagnetic counter

In radiometry for field use, a general and international tradition has developed over the last forty years of designing integrators round a simple, robust and reliable internationally available device called the Post-Office pattern electromagnetic counter. This device is solenoid-operated and displays four or five digits in a small window at the front, and a typical example is shown in Plate. 8 Many authors, including the following, have used the Post-Office type, or similar versions, in their ecological field studies.

MIDDLETON 1953

KUBIN and HLADEK 1963

THURTELL and TANNER 1964

KERR, THURTELL and TANNER 1967

BRACH, MACK and ST. AMOUR 1969

KING 1972

STANTON 1973

BUCKLEY 1976

MCLAUGHLIN and ALLAN 1976

TANG, McNAUGHTON and BLACK 1976

This electromagnetic counter consumes no current in remembering the number on display and takes only a short high-power pulse - typically 1-2 watts for $t = 40$ ms - to advance the digits. The maximum speed of operation is about 10 counting operations per second, at which rate the usual scale of 0 - 99999 lasts a little longer than one day. At the rate of 1 count per second, the display

can record for a reasonable 10 days, and it is quite simple to calibrate a whole radiometer-integrator-counter so that x units of total irradiance correspond with y counts on the display. More recently the Liquid Crystal Display Counter has shown signs of displacing the electromagnetic counter. See SAFFELL, CAMPBELL and CAMPBELL (1979).

2.C.5b Dynamic Range

The ideal integrator is wholly linear over the entire range of irradiances occurring in the field of experiment. For the reasons indicated in sections 2.C.3 , the reality will be different, with increasing departure from linearity at low and high irradiances, and their respective pulse-rates. The self-leakage of the integrator capacitor spoils linearity to a progressively greater extent with decreasing input currents, and at high count-rates the dead-time (t_{dead}) becomes a progressively greater percentage of the total integrating cycle time t_{tot} .

For these reasons integrators will have a DYNAMIC RANGE, over which the linearity will not depart by more than an acceptable amount from the theoretical straight-line characteristic. This is often about 2 decades of input fluctuation.

2.C.5c Improving the dynamic range

By various subterfuges this performance can be increased considerably. The best quality integrating capacitor should always be used, but after this the residual effect of leakage can be carefully

balanced out by a counter-current (KØIE 1954). t_{dead} can be compensated by increasing the basic sensitivity of the integrator at high input currents. THURTELL and TANNER (1964) and GOING (this volume). This can be arranged by lowering the value of V_2 (in Fig. 15) thus lowering ΔV which will increase the pulse repetition frequency for a given I_{intg} . Both THURTELL and TANNER and GOING lower ΔV by inserting a resistance in series with the integrating capacitor (see Fig. 18) which induces a voltage drop (Ohms' law) proportional to the current flowing.

In obeying Ohms' law, the depression of V_2 shown in Fig. 19, caused by the passage of I_{intg} through R_1 , introduces the needed increase in sensitivity to compensate for the t_{dead} effect.

It may seem surprising that with a comparatively low integrator pulse rate of 10 Hz, dead time should pose a problem, but an appreciable time for discharging C_{intg} may be necessary if the capacity is high, because of the inevitable resistance of the discharge path. For simplicity and low electricity consumption and cost it has often been necessary to use the time constant of the $R_{\text{discharge path}} - C_{\text{intg}}$ combination to control the length of the driving pulse for the electromagnetic counter, and this being rarely less than 40 milliseconds, represents 40% dead time at ten pulses per second, and a 40 % low pulse figure for the integral of I_{intg}

Fig 18 Positioning of dead-time (t_{dead}) correction resistance

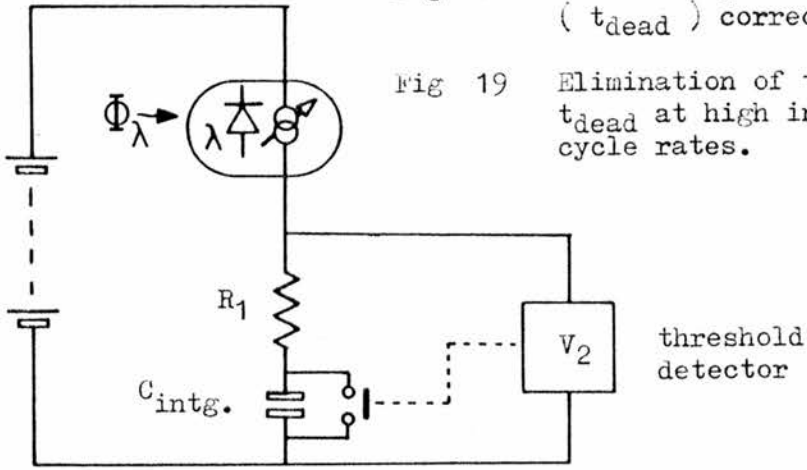
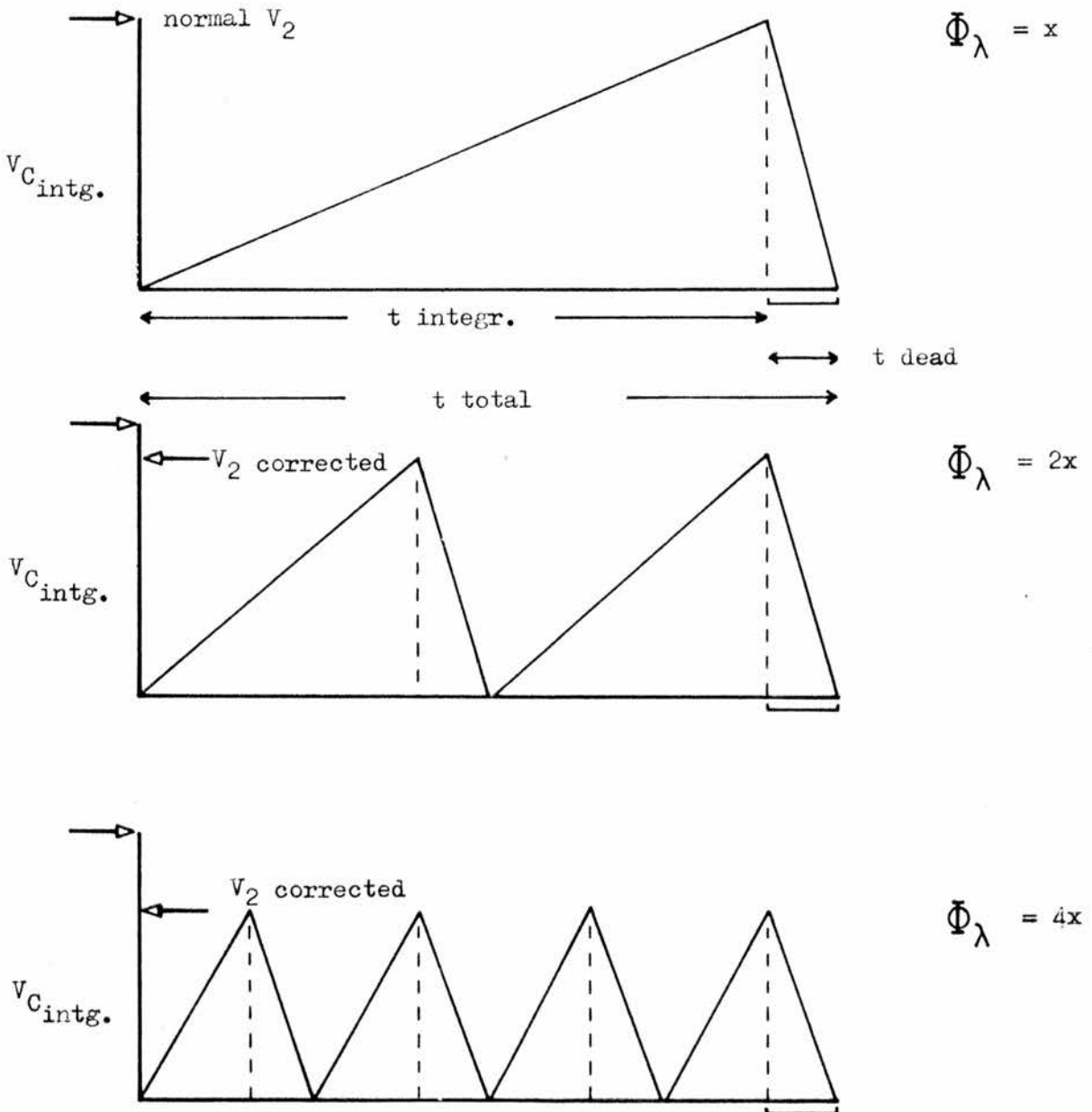


Fig 19 Elimination of the effect of t_{dead} at high integration cycle rates. see text



See Postscript, p. 303 for an analytical solution for the value of R_1 , by Dr. M. G. Stanton.

being handled. It must be pointed out that t_{dead} still exists even when it has been corrected for; under slow changing input conditions this is no problem, but if there is a periodicity in the input signals, beat phenomena could occur, leading to erroneously high or low estimations.

More recently it has become possible to divorce the $t_{\text{discharge}}$ period from its role in defining the pulse length to be fed to the electromagnetic integrator, and when this happens, $t_{\text{discharge}}$ hence t_{dead} can be shortened until it is of little significance. This approach is used by BRACH, MACK and ST. AMOUR (1969) and KING (1972).

An unusual variant which eliminates t_{dead} altogether is used by MOBLEY (1962) whose circuit, whenever the upper C_{intg} threshold voltage V_2 is reached, causes the removal of a fixed quantity of charge from C_{intg} , and this process of course does not interfere with the continuing integration of the incoming signal current. However, this approach uses far more complex electronic circuitry than is usually warranted.

Another interesting arrangement is to reverse the direction of integrating current when the threshold voltages V_1 and V_2 for C_{intg} are reached. This produces a triangular waveform for a constant I_{intg} as in Fig 20. The advantages of this method are that t_{dead} is again eliminated, as the discharge phase of the integration cycle is now used to continue integrating, giving symmetrical operation, and THURTELL and TANNER (1964), who introduced the method, did so also to nullify the effect of temperature

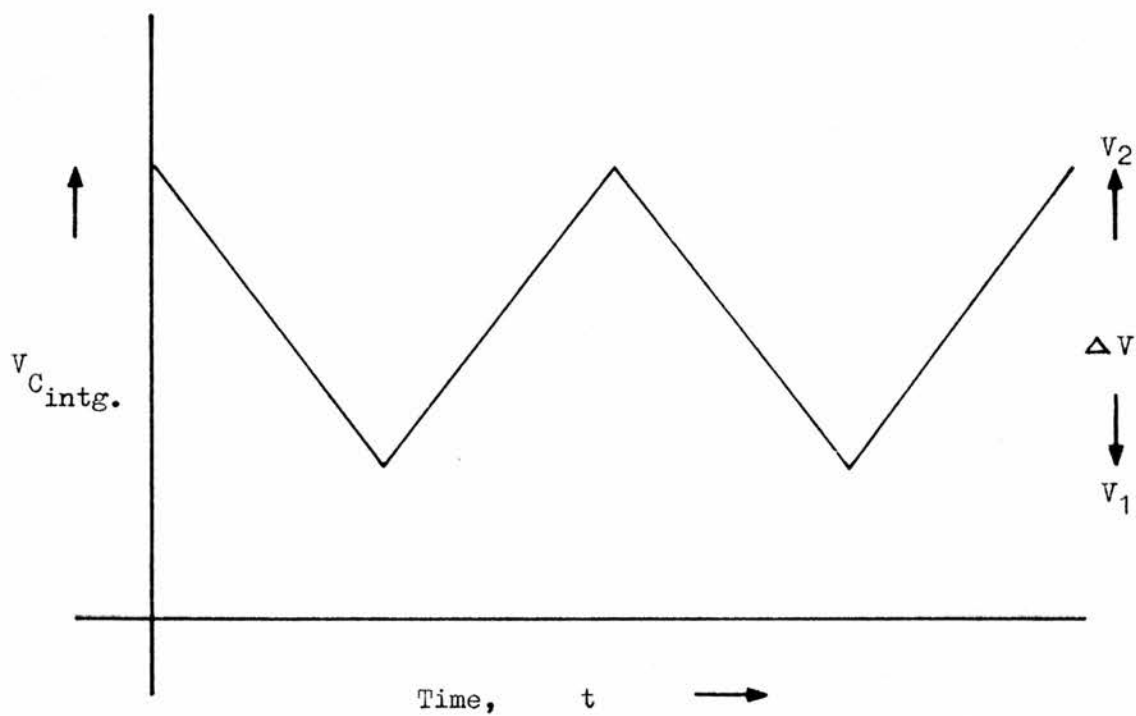


Fig. 20 Reversal of $I_{\text{intg.}}$ whenever threshold voltages V_2 ; V_1 are reached. Note the absence of dead-time, t_{dead} .

induced changes in offset voltage and drift in the operational amplifier circuit which they used. In their case, t_{dead} was not quite removed, since the threshold detection and input reversing were done with relays; it was for this reason that they introduced the resistance in series with the integrating capacitor, as discussed on page 47. More recently, CAMPBELL (1974) TANG, McNAUGHTON and BLACK (1976) and FRITSCHEN (1977) have used the same principles except that t_{dead} compensation is no longer called for, the signal-polarity reversal now being carried out with high-speed solid state devices - CMOS bilateral switches.

2.C.5d Detecting threshold voltages in C_{intg}

The detection of the threshold voltages on C_{intg} has always been central to the design of integrators, and although a large survey of the field is not appropriate it is worth listing the control devices which have figured in the literature, with their dates.

1. Cold-cathode gas filled relays

RENSCHLER 1941 and 1943
 SPRAGUE and WILLIAMS 1941
 SOMERS and HAMNER 1950
 BLACKMAN, BLACK and MARTIN 1953
 MIDDLETON 1953
 TRICKETT and MOULSLEY 1956
 COOPER, HILBORN and HEPPLER 1958
 BELL, CHMORA and KORNILEV 1959
 TUKLEY, FLUCK and MARSH 1960
 KUBIN and HLADEK 1963

2. Thermionic valves

TAYLOR 1941
 KØIE 1954
 ALLAN and McCREE 1955

3. Unijunction transistors (analogous to 1)

THURTELL and TANNER 1964

KERR, THURTELL and TANNER 1967

WEAVING 1967

BRACH, MACK and ST. AMOUR 1969

KING 1974

4. Thyristors (PNPN transistors)

McLAUGHLIN and ALLAN 1976

5. Operational Amplifiers

THURTELL and TANNER 1964

CAMPBELL 1974

TANG, McNAUGHTON and BLACK 1976

FRITSCHEN 1977

6. Other: Field-effect transistors

STANTON 1973

2.C.5e Power consumption

For many years, the old pattern of integrator based on the Cold-cathode gas filled relay, as originally introduced by ANDERSON (1930) and RENTSCHLER was the most widely used, as the power consumption was only about $1\mu\text{A}$ at 135V (135 μ Watts) a figure easily supplied by dry batteries, which could last for more than 2-3 months in continuous field use. KUBIN and HLADEK (1963) were the last to improve the design, which in their version showed a dynamic range of 1:100 for 5% deviation from linear response.

Where power consumption increased, it was usually the cost of producing a circuit with superior properties in linearity, temperature coefficient, and versatility. The unijunction transistor is the modern solid-state analogue of the cold-cathode

gas-filled relay (thyatron) and has also been fairly widely used. The operational amplifier was for a long time unsuited for battery operated equipment, since it drew large standby currents; however the so-called micro-power operational amplifier and low-power complementary metal oxide semiconductor integrated circuits have in the last five years almost completely changed the pattern of electronic design and freed the designer in many ways.

The declining standby consumptions of integrators over the years can be seen from these figures.

THURTELL & TANNER (1964)	135mA @ 12V = 1.6 Watts
TANG, MCNAUGHTON & BLACK (1966)	2mA @ $\pm 6V$ = 0.024 Watts
CAMPBELL (1974)	0.5mA @ $\pm 4.5V$ = 0.0045 Watts

The integrator of TANG, MCNAUGHTON and BLACK is a modern version of the original circuit of THURTELL and TANNER.

CHAPTER 3

RECORDERS FOR USE IN RADIOMETRY - A REVIEW

3. RECORDERS FOR USE IN RADIOMETRY - A REVIEW

3.A.1. Introduction

So far, integrators which record a cumulative total irradiance have been described. Their use could be considered as recording, but in the next section recorders will be taken to mean devices which produce, by whatever means, a more detailed measurement of the relationship of time with the variation of irradiance, or other input signal. The type of recorder used will depend on many conflicting factors, as in the case of the integrators, but initial and running costs, the length of time of unattended operation, and the use to be made of the data are the main considerations.

3.A.2a Which type of recorder?

The graph-charting recorder is the device which usually springs to mind when recording is mentioned. This is natural, because the record is visually appealing and instantly informative. Fig 21a shows an irradiance record graph for a cloudless summer day; Fig 21b however, shows that of a day of alternating cloud and sunshine. One frequent requirement, as explained in earlier sections, is to be able to establish integrals of radiant flux. These can be obtained, by simple means, from graphs like Fig 21a but not from Fig 21b. It is fairly common practice to run both an integrator and a chart recorder from one radiometric detector, so that records of both the daily totals of irradiance

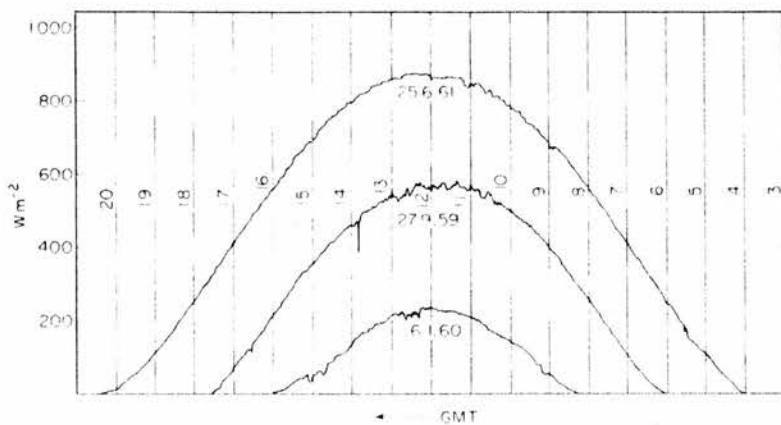


Fig. 21a

Solar radiation on three cloudless days at Rothamsted (52°N, 0°W). During the middle of the day, the record tends to fluctuate more than in the morning and evening, suggesting a diurnal change in the amount of dust in the lower atmosphere, at least in summer and autumn. Three recorder charts were superimposed to facilitate this comparison.

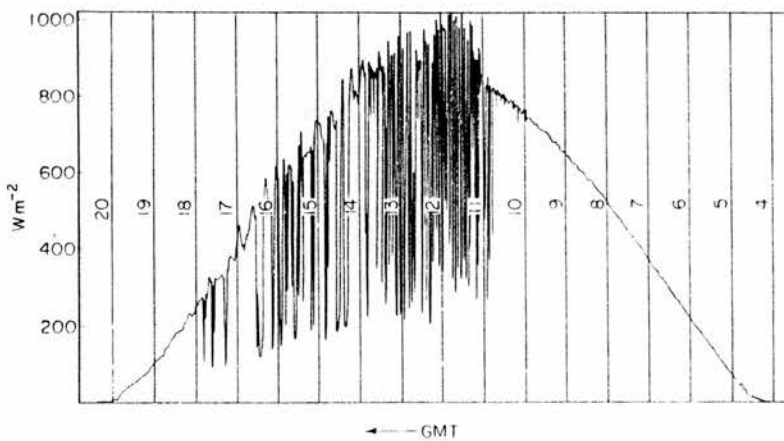


Fig. 21b

Solar radiation on a day of broken cloud (11 June 1969) at Rothamsted (52°N, 0°W) taken directly from recorder charts. Note very high values of irradiance immediately before and after occlusion of the sun by cloud and the regular succession of minimum values when the sun is completely obscured.

and the distribution patterns are available. However, it is possible to compromise by using a number-registering counter to divide the day into short sections. The resulting figures may then be graphed or summed at a later date, according to requirements.

If a great deal of data has to be handled in a mathematical manner visual records such as these become inappropriate, and machine-readable data recording forms become necessary. With most of these the recording is invisible, and often takes the form of digitally-encoded magnetic tape or, less often latterly, punched reels of paper tape.

- * Graph-charting recorders
- * Number-registering recorders
- * Digital recorders - 'data loggers'

3.A.2b Graph-charting recorders

With the exception of the special Campbell-Stokes recorders, these recorders all depend on a constantly or regularly moving sheet of paper, calibrated in time intervals on the x axis, with the y value directly plotted by some means on the y axis. The length of time for which they will operate is dependant only on power supply, the length of paper which can be handled and the speed of chart movement. The simplest of these devices is the Robitsch-Fuess bimetallic actinograph (ROBITSCH 1915 and 1932 in PALM 1959) which strongly resembles the traditional barograph. A calibrated paper sleeve is fitted on to a drum, which revolves by clockwork once in twenty four hours. This gives the x-axis movement, and on the y-axis an inked pen traverses the paper according to the bending of a blackened bimetallic element which is situated

above the recording drum and underneath a suitable weatherproof transparent dome. The coupling between the element and the drum is via a system of mechanical linkages. This recording actinometer is well tried and relatively inexpensive, and is therefore quite widely used. McCOMB and IYAMABO (1968).

Most other chart recorders use electricity for both paper and pen movement, although the paper drive can of course be clock-work. One of the earliest designs was the 'Spannungsregistrierapparat' of Siemens and Halske (1880) described by HEIDEN (1969), see Plate. 6 In this recorder a solenoid and ratchet system slowly fed paper forward from a reel, at the rate of three discrete steps a minute; at the same time the voltage being recorded was led to an electromagnet which was arranged to attract an iron stylus suspended above the paper with its major axis aligned along the axis of paper travel. A varying voltage changed the attraction of the magnet to the stylus, which would accordingly swing across the width of the paper as the voltage rose or fell, and in the time lapses between paper movement another mechanism caused the stylus momentarily to pierce the paper, perpetuating a record of the stylus position. The recording produced was primitive by modern standards, but well enough served the original purpose, which was to check the grosser fluctuations of the electricity supply.

By 1888, with the advent of the Weston movement, electromagnetic galvanometers had reached a state of development where good sensitivity, linearity of scale and accuracy could be expected, but the delicacy of such instruments precludes the possibility of causing the pointer arm to be used directly to carry a pen. CALLENDAR (1897) (in DUNSHEATH (1962)) evaded the problem by inventing

the first self-balancing potentiometric recorder. In this a motor, thread and pulley system moves an ink-filled pen over whatever distance of travel is necessary to produce a null voltage reading on a slide-wire wheatstone bridge attached to the same pulley system. When the minimum potential difference between input signal and wheatstone sliding contact is detected, the motor driving the system switches off, and the position of the pen corresponds to the input voltage. Any further fluctuations in the input voltage cause a re-energising of the motor and movement of the pen and slider to seek the null point again. The potentiometric recorder has a linear scale and records continuously.

The cheaper alternative to the potentiometric recorder, and allegedly devised as such by Sir Horace Darwin in 1905, DARWIN (1905) and DUNSHEATH (1962), is the chopper bar, thread, or Cambridge recorder. In fact, pace DUNSHEATH, RAPS (1897) working for the German firm SIEMENS AND HALSKE, should be credited with prior invention of the thread recorder, RAPS (1897). See also HEIDEN (1969).

In both cases, the principle of operation is the same. A large galvanometer with a long pointer is used, and the pointer has a measure of freedom to move in the vertical as well as in the horizontal plane. A paper chart is wound along the major axis of the pointer, which normally floats above it. At intervals a bar descends forcing the galvanometer pointer on to the paper against an anvil. Under the galvanometer needle runs an inked thread and this is forced by the galvanometer pointer into contact

with the paper, thus marking it. The recording is made up of a series of spot readings, and these are so closely spaced that for many purposes the recorded trace can be considered continuous.

Both these types of recorder are in use today for recording incoming radiant flux. The Cambridge thread recorder is the most widely used type; it has the advantage over the potentiometric recorder of not requiring any electronic circuitry because of which electric propulsion of the paper is frequently dispensed with, clockwork being used instead, often with a thermopile self-generating radiometer, eliminating altogether the need for batteries or mains electricity. Maintenance can then consist of monthly visits to wind the clockwork and change the paper chart. GORCZYNSKI (1936) was the first to use in this fashion a Moll-Gorczyński thermopile radiometer with a Cambridge Thread Recorder, and the combination is still used after more than 50 years, BINDLOSS (1976). In the field, a small modern economical chopper bar recorder widely used is that made by the American firm RUSTRAK, and it can even be employed underwater in a fairly confined enclosure. CHAPMAN et al., (1976). These recorders have also been used by BARNEY (1972), HUNTINGTON and JOHNSTONE (1973) and BERRY and RANEY (1968).

Most of these commercial recorders will not run for long enough for studies in difficult terrains where people may not be available to maintain them. SUMNER (1959) describes a recorder using pinpricks (as in the Siemens recorder of 1880). His recorder runs for up to one year without attention, using 3 ins. of paper a day from 100 ft. reels. Most actions in this recorder, including the winding of the Kienzle clock movement, are controlled by solenoids

fed from a 1.5 volt cell, and an auxiliary time check is provided by the sun, which, via a lens and slit arrangement causes a burn mark to appear on the record at apparent noon. The commercially produced Sumner recorder is available from RAUCHFUSS INSTRUMENT and STAFF PTY.

As was mentioned on page 5 the big problem with irradiance records is the need for very large dynamic ranges. The difficulty with all chart recorders has been finding ways of securing wide dynamic range and good resolution at the same time. With normal linear-axis chart records, the resolution is rarely better than $\frac{1}{10}$ of the width of the chart, this limitation being caused by a combination of finite width of the recorded trace, backlash and dead-time (due to frictional limitations of the mechanics), and lateral wandering in the position of the paper. The modern approach to the problem is to use either log/linear chart paper with a linear-to-logarithmic electronic converter placed in the path of the signal (JUNG 1980); to use an amplifier/attenuator network to modify the signal when its value approaches the limits of the recorder BERRY and RANEY (1968); or to 'buck' the signal to zero whenever it has risen close to the maximum input level HILLMAN (1976). For the sake of completeness, the ingenious pre-electronic method adopted by ASKANIA AG. using only mechanical processes is shown in Fig 22, from PALM (1959). This design was part of a water-level monitor.

There is one chart recorder which has the unique property of not having any (terrestrial) moving parts. This is the CAMPBELL-STOKES sunshine recorder, and the sweep of the sun across the sky is used to define its own trace by scorching a curved chart placed behind a focussing globe. This device is the simplest radiant flux recorder

there is, and was adopted by the World Meteorological Organisation in 1964 as interim reference recorder (CASELLA leaflet 934/6 (-)). The interpretation of Campbell-Stokes charts is a skilled task, and they can reveal more information than is apparent to the untrained eye.

3.A.2c Number-registering recorders

KØIE (1952) was one of the first to use a printing recorder in irradiance studies. His device, an integrator and electromagnetic counter, prints the reading from the counter on successive lines on a roll of paper. An electronic clock actuates the printing process at regular intervals, and the date and time are printed next to each integrator measurement. Subtraction of an integrator reading from its previous neighbour gives the integral for any particular time period. This device is manufactured by, among others, SODECO, and a full system with suitable accessories is available from the firm LINTRONIC.

The need in field work to break the total recording period into shorter sections caused two teams of workers to devise means of channelling the output of an irradiance or other sensor to, in succession, a battery of post-office pattern electromagnetic counters, COKER and COKER (1972), and CZOPEK et al., (1965). Both used Post-office pattern uniselectors to route the output pulses in accordance with instructions from a clock. In the first case, six succeeding 1-day totals were recorded; in the second 24 one-hourly sub-totals, and in each case the totals were read off the dials at the end of the recording period. If this was not done, the results were summed with those for the next period, and thus lost. To avoid this it is possible to photograph the counter dials at the end of each cycle. If there are

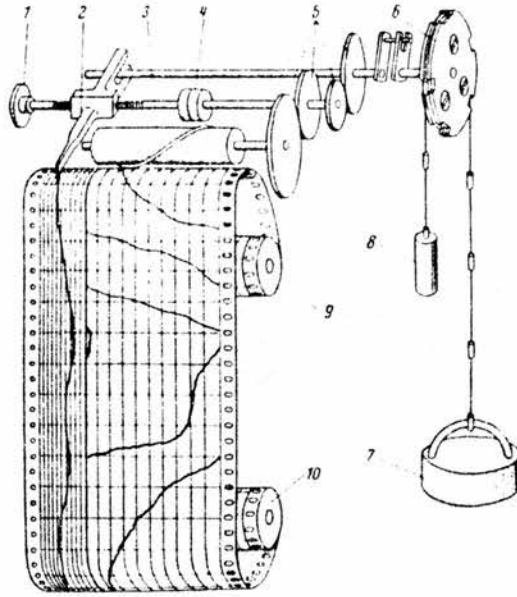


Fig. 22

An ingenious multi-range chart recorder using only mechanical parts - originally from a water-level recording system made by the firm Askania
from Palm (1959)

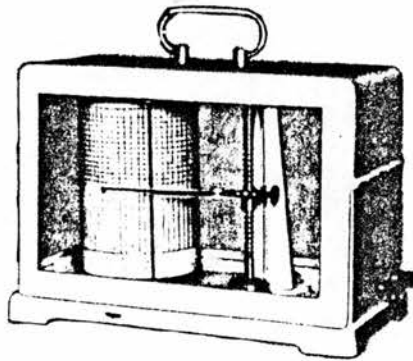


Fig. 23

Lambrecht windspeed recorder, see page 67. A possible candidate considered for use as an irradiance recorder, in a modified form.

from Palm (1959)

twenty-four counters recording hourly counts the camera could run for more than one month on a thirty six frame film, producing more than 800 individual recordings. This approach has been used commercially by C.W. THORNTHWAITE ASSOCIATES (USA).

3.A.2d Digital recorders - 'data loggers'

For large surveys, involving the recording and mathematical analysis of more than one variable, it is almost a necessity to use digital recording techniques from the beginning. The expense of the apparatus is usually much higher than in the case of the chart recorders and number printing counters, but not necessarily so if the recorder is intended to handle comparatively simple data. It is outside the scope of this review to consider the variety of apparatus and techniques available, since these, and the costs of available options, are changing fast. SUTTON and RORISON (1970) and (1972) and CERNUSCA (1968) have both used a d-MAC limpet logger (d-MAC Ltd., Glasgow). CERNUSCA used punched paper tape, as was perhaps more commonly used in the 1960's than now, but a typical field digital event recorder that uses paper tape is produced by RAUCHFUSS INSTRUMENTS AND STAFF PTY. MONTEITH (1972). A typical modern data logger for field use, which has, for example, been used at the Scottish Horticultural Research Establishment at Mylnefield, is the RAPCO portable data logging system. This sequentially scans the outputs of 10 or 20 sensors at regular intervals, is battery operated and can work for up to three months in the field without attention. The cost was £2,500 (1976 prices) excluding ancillary apparatus. BYRNE (1970) draws attention to some of the points which have to be considered if the correct use is to be

made of data recorders. EEUA Handbook No. 28 - 'the Specification and Selection of Data Logging Equipment', 1968, gives advice on the selection of data processing equipment, and includes a useful glossary.

It is likely than an increasing role will be played in data recording by all-solid-state devices, the recorders containing not one moving part. The first of these recorders is on the market and is called the 'SOLICORDER' (AMBULATORY MONITORING, INC.). This instrument uses a 16,000 bit memory, which is sufficient for recording in digital format 2048 8-bit data words. Each 8-bit word can represent in binary notation a number between 0 and 256, giving a maximum dynamic range of 256:1, and over one week of measurement at 10 readings per hour. See also BAHARESTANI et al., (1979) for a circuit of a solid-state recorder.

A list of manufacturers of equipment is given in the Appendices.

CHAPTER 4

A NEW DESIGN OF RECORDER

4. A NEW DESIGN OF RECORDER

4.A. Introduction

As will be apparent from the previous chapter, the researcher in need of field equipment has a diverse range available, but no one scheme is free of compromises - in fact, the common needs of accuracy, long periods between service visits, wide dynamic range, data processor compatibility and low cost are generally mutually exclusive.

The author was faced in 1972 with the problem of evaluating underwater photosynthetically active radiation (PhAR) at the low lying Loch Leven in Fife, a fairly shallow, eutrophic loch filling a glacially scoured hollow. SMITH (1973). The study operated on a small budget, and the central items of equipment were the integrator designed and constructed by STANTON (1973), who kindly made available a unit, and, for reference purposes, the Kipp and Zonen radiometer operated at Kinross by the Institute of Terrestrial Ecology, as part of their contribution to an International Biological Programme study of Loch Leven, BINDLOSS, (1976). It soon became apparent that without some kind of recorder, the observations that could be made would be too limited in scope to enable scientific conclusions to be drawn. There was insufficient money to afford a Sodeco printing counter. Since the Stanton integrator was a fixed part of the programme (a secondary brief was to evaluate it) investigations were made into the possibility of designing a recorder to operate in tandem with it. For any study intended to be of manageable proportions the recording of consecutive short-term averages was considered to offer data having the greatest overall value, particularly where, as with radiant flux, the frequency and range of fluctuations is considerable.

Funds necessitated that any recorder chosen to interface with the integrator could be constructed with limited workshop facilities. The most promising device for this was a proposed variant of the windspeed recorder made by the German firm Lambrecht (PALM 1959). This has a clockwork operated drum, revolving at a suitable speed, geared to a vertical feed-screw which causes the resting position of a drum pen to be steadily lowered down the face of the drum, describing a helix on the paper. Also attached to the pen is an electromagnet which when energised (in the original instrument by the geared-down rotating vanes of an anemometer) causes the pen to deflect for an instant, marking a 'blip' on the paper. The paper from the drum, when flattened out, reveals a series of gently inclined near-horizontal lines, with vertical strokes at intervals indicating each rotation of the anemometer. The x-axis of the chart is calibrated in time of day, and the y-axis (assuming one revolution of the drum per day) can be marked with a date beside the start of each line. In fact, the original windspeed recorder made 24 revolutions per day, but the principle remains the same. With the aid of a good 8-day clock movement the approach might have yielded a usable instrument, but the alternative idea described below caused this one to be abandoned. See Fig 23.

4.B The new recorder

The reader is recommended to study Plates 7, 8, 9 and 10 which show photographs of the new recorder from side, top, in perspective and in part detail. Fig 24, which is an annotated sketch of Plate 9 illustrates some points specifically mentioned in the text.

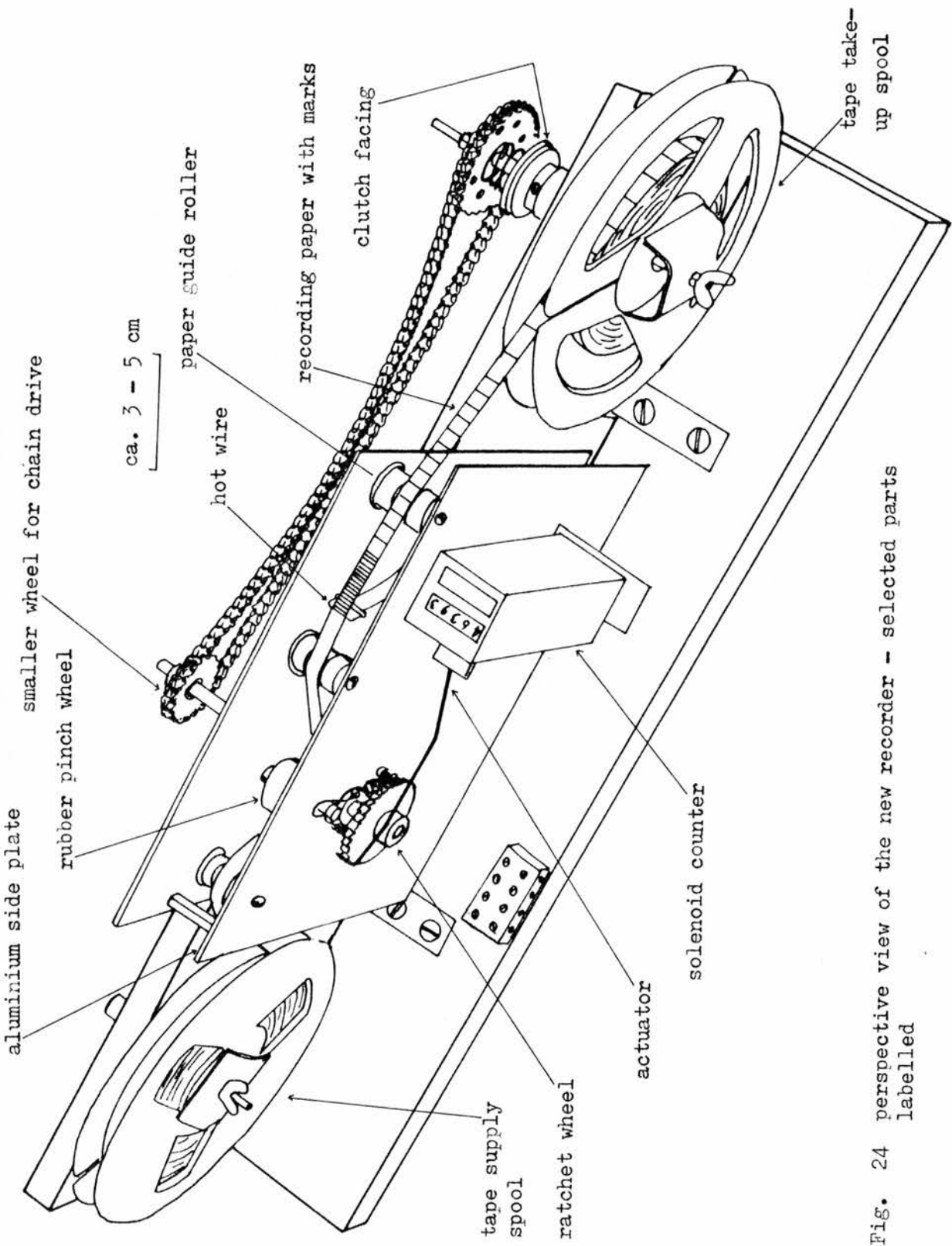


Fig. 24 perspective view of the new recorder - selected parts labelled

4.C Principle of the new recorder

The principle of the new recorder is very simple, and represents a natural extension of the capabilities of the combination of an integrator and a post-office-pattern electromagnetic counter. An extensive literature search has, however, failed to reveal any previous description.

The moving actuator in the electromagnetic counter is extended by a simple lever, so that in addition to rotating the number wheels of the counter a ratchet wheel is turned through a small angle β° with every impulse fed through from the integrator. This ratchet wheel is mounted on a spindle, concentrically with a capstan which it drives, and upon which bears a roller system; the diameter of the capstan is such that the angular movement β° of the ratchet is converted to a lengthwise motion in a piece of paper tape by winding the tape through, wringer fashion. All that remains necessary is to mark-off lengths of tape at appropriate time-intervals, so that each consecutive length of tape will then have a length proportional to the integral of the input signal received over the chosen time-period.

4.D Advantages of the new recorder

4.D.1 Dynamic range, economy of paper and energising power

The dynamic range of the new recorder is much greater than that of the conventional chart recorder, but it is difficult to specify the range in a way that is unequivocal. In any time period, the smallest count that can be registered clearly is one count, and since the information is digital, there is no 'percent of full-scale deflection'

error of the kind which is a disadvantage of analogue pen recorded graphs. The highest count is limited by the time taken for the completion of the counting cycle, which in the prototype was of the order of 100 milliseconds: 60 mS for the 'on' part of the counting cycle, and 40 mS to allow the return spring on the counter to operate. Based on a convenient time-period of 0.1 hour (six minutes) and the assumptions that the lowest total count is to be 1, and that the highest, at 10 counts per second, is 3,600 counts, the dynamic range might be interpreted as being 3,600 : 1. Further, at low count-rates the data is rendered less useful because of the resolution problem (discussed on page 61) and at high count-rates the consumption of paper may be unacceptable.

The new recorder is unique, therefore, in that the amount of paper taken by the recorder is in theory linearly proportional to the signal presented to the integrator and recorder. In the prototype, the recording medium is a thin paper strip, ca. 5 mm. wide, stored in 135 m reels on magnetic-tape spools. Perhaps the most appropriate way to think of a roll of recording tape is as a store of data-points which may be used at the operators' discretion. Two examples, considered further in the later chapter 7 are the radiation records shown in Figs 91 and 92 . In the first, February 10th, 1975, the electromagnetic counter showed a total of 983 counts recorded, and in the second, for February 16th, 1975, 291 counts. These graphs could be considered as mosaics, and the one containing about 1000 points below the curve from an aesthetic point of view, clearly offers a quite reasonable detailed picture of the day's total irradiance record, whilst that recording about 300 points does not. If the mean consumption of 'data points' is 1000 per day, and a 'data point' occupies 1mm. of tape, as in the prototype recorder,

then the 135 metre spool employed in the recorder will last for about $4\frac{1}{2}$ months at 1m per day - an impressive figure. To place this figure in perspective, however, 5 metres were used to record a cloudless August day, shown in Fig 93 (cf. Fig 21). Clearly the nature of the input signal, the dynamic range, the resolution, and the length of duty which one reel of recording must provide interact with each other, but experience has shown the system to be particularly valuable where the ratio of maximum short-term peak signal level to average value is high - as in the recording of natural radiant flux.

Directly related to the foregoing are economies of consumption in both paper recording medium and power. Natural radiant flux is particularly suited to measurement by this recorder. By night, the paper and electricity consumptions fall to almost zero. By comparison, the conventional graph-plotting recorder is at a disadvantage, since the recording paper not only should have at all times the maximum width (y-axis) needed to cope with peak input values, but also should usually have to continue motion even in darkness. The waste paper is all the paper above the recorded curve, and will almost always exceed one half of the total used.

4.D.2 Provision for machine-processing of recordings

One of the most important factors in the choice of modern data recorders is, as discussed earlier on pages 7 and 63 , the need for machine compatibility. The cost of employing personnel to convert large quantities of data from one form to another is too great, in financial and psychological terms, to be acceptable. In this new recorder the possibility for direct optical scanning of recorded tapes

exists, and the dimensions of the tape and spool sizes chosen for the prototype instrument are fully compatible with current tape-transport mechanisms. An outline scheme for an interface unit for computer and chart-recorder use is shown in Appendix 8.

4.D.3 Simplicity of construction

The mechanical construction is as simple as the appearance in Plate 9 suggests. The moving parts are machined to a moderate standard of finish and dimensional accuracy, and only the radius of the capstan was machined to a tolerance of closer than ± 0.25 thousandths of an inch. Full drawings and part and materials lists are given as appendix 9.

4.E Practical considerations in the design of the prototype new recorder

4.E.1 Time-marking

A thermal system is used to mark off the paper. The possibilities of using pin-pricks (SUMNER 1959) or inking pens (as in many other recorders) were rejected because of the added complication of moving parts and the inherent problems associated with ink. Several thermal papers are available, which respond to the application of moderate heat by developing a contrasting colour. These are considered further in paragraph 4.E.2, Pages 74 and 75. The mark is applied by a length of wire (see Plate 8) shaped like a croquet hoop, which rests on the undersurface of the paper. In this way the delicate pen is shielded from damage, and more importantly, there is no possibility of the hot wire becoming stuck through fusing into the waxen surface

used in some types of thermosensitive paper. The definition lost through the travel of heat through the paper base appears to be negligible.

At first sight, a large problem with the new recorder is that in the absence of an input to the recorder, no movement of the paper occurs, and if this happens, superimposition of time-marks occurs, leading to the loss of absolute time-keeping properties in the recorder. This problem may be solved by cross-connecting the clock to the electronic drive circuitry which feeds the electromagnetic counter. In this way all time marks are separated by a small length of tape and when the length of tape between time marks is estimated, allowance for this extra length is made by subtraction.

At the time the recorder was first constructed, crystal-controlled high accuracy clocks were expensive and bulky. For this reason, the clock consisted of a replicate integrator, loaded with a dummy input signal which was preset to give the required time interval between marking pulses.

If the chosen integrator used with the recorder has a pronounced temperature coefficient, and the clock is a duplicate integrator with the same coefficient, it will be found that the coefficients balance each other but become represented as deviation in the absolute time-keeping on the recorded tape - a 10% loss of sensitivity in the integrator is balanced by a 10% lengthening in the integration-period. Whether a distortion of time-keeping properties or of sensitivity in the integrator is the greater evil is for the individual user to evaluate, but with care and modern design temperature coefficients should not present problems anyway.

At first sight, the use of heat to mark the paper might not seem to be the most power-efficient solution, even if the lack of moving

parts is attractive. However, as is shown on page 168 the efficiency is quite favourable.

4.E.2 Paper sources and types

Heat-sensitive papers consist of a plain paper base treated with either a coating containing a chemical which irreversibly changes colour at a temperature near 150°C - called by the manufacturer 'Heat Sensitive Thermal' types, or, alternatively, with a twin-layer structure, comprised of a lower black layer overlain by an opaque white wax layer which melts at a low temperature to reveal the black layer - the 'Heat Sensitive Mechanical' types.

In initial tests, the heat-sensitive mechanical paper was used, but it is an unsatisfactory product in certain ways; it is sensitive to pressure (scratches) water and hydrocarbons (oil, etc.) all of which damage the wax surface. In addition the paper tends to be thicker than is ideal, thereby limiting the length which can be stored on a spool. The paper feels 'coated' and waxy and is somewhat inflexible. The heat sensitive thermal paper is much better in all respects, and it is even difficult to tell which is the coated side, except in good illumination.

Like many organochemical dyes, the developed colour of the heat sensitive thermal paper slowly fades in natural light, but storage of unused and developed paper in a dark place in a temperate climate seems to cause no visible degradation after two years. If it is intended to make photocopies of the records, blue or green papers should be avoided since they may give faint copies.

The papers used in tests of the prototype recorder were Cambridge Cardiograph 539-525, and Sensitised Coatings Ltd.,

Heat Sensitive Thermal. Under some conditions it might be necessary to coat paper in the laboratory. In Britain this is not worth doing, and the best thermo-sensitive papers appear to have some complex materials in the coatings, such as metallic soaps, diazo and phenolic compounds. MOSHER and DAVIS (1968) outline some of the features of these papers, and for a full bibliography of thermographic papers see ROTH and WEINER (1965). For the chemistry of the heat sensitive thermal paper, see B.Pat. 1,438 765 (Wiggins

4.E.3 Slitting the paper

(Teape Ltd. 1972

The desired width of the paper is the same as magnetic tape, which is given by MOIR (1961) as being $6.25 \text{ mm} \pm 0.05 \text{ mm}$ (British Standard BS 1568). So far a slitting machine has not been devised; initially using a $2\frac{1}{2}$ inch wide reel of tape, slitting was done with a chisel mounted on the tool-carrier of a lathe, the paper roll rotated in the chuck, and the slit paper was wound off the parent roll into a cardboard box for subsequent spooling. Later on, using the Heat Sensitive Thermal paper, the $8\frac{1}{2}$ inch master roll was cut into lengths of 5 yard x 45 mm., and these were drawn by hand through a rank of inclined razor blades, clamped between plywood spacers in the jaws of a vise. This method is quite effective, but it must be pointed out that the process is dangerous and probably should not be used in premises covered by the Health and Safety at Work Act.

Splices are easily executed. The two tapes to be joined are superimposed and cut obliquely with a pair of scissors. The fresh ends are then butted together and a piece of cellulose acetate adhesive office tape (not sellotape or other cellulose tape) is placed obliquely across the join. The edges of the join are carefully trimmed

to complete the splice. It is good (standard studio) practise to use oblique cuts and splices; these show no tendency to unstick when running over guides with a small radius of curvature, and do not jolt when passing between capstan and pinch wheel. If they are available, the most satisfactory splicing facilities are provided by the "Emitape" solid aluminium type of editing block and Eveready safety razor blade.

4.E.4 Mechanical parts

The materials for the prototype recorder were with few exceptions either made from scrap or standard laboratory items. Rollers, sleeve bearings, the capstan and some spindles were lathe-turned from mild steel rod, and as a result they have proved slightly prone to rust. The clutch drive uses "Meccano" chain and wheels obtained from a toyshop, and the clutch itself has cardboard for one clutch surface, and mild steel for the other. The tension in the clutch assembly is adjusted by means of a compression spring, which is initially set for adequate torque when the take-up spool is full of paper. The sides are duralumin plate, 0.1 inch thick, and were drilled as a pair so that all holes are correctly aligned with their opposite numbers. They are spaced apart by 3/4 inch tapped pillars, and by the spindles of the rollers.

The hot wire of the pen is made from 34 SWG Eureka wire, soldered to some shorter copper wires. The pen is mounted on strips of clock spring, and to maintain the greatest freedom of movement in the vertical plane, the current lead-in wires are either copper foil strips or finely braided 'pig-tails'. The hot wire is fixed with Araldite; although this is not a heat-resisting material, it seems not to matter because of the intermittant nature of the heating. The pen, however,

is not strong enough to withstand accidental continuous energising, and under fault conditions can burn out. If this happens the paper tape is cut through by the heat, and any flame tends to be extinguished by the recoil of the tape ends, which are normally under tension; nevertheless, all sensible precautions against fire should be taken. It is ineffective to protect the pen with a fuse, because the melting time would be little quicker than that of the pen. If dry cells are used for pen power, short circuits are limited by cell internal resistance, but if an accumulator is used, fusing to protect the wiring is essential.

The solenoid coil of the standard electromagnetic counter has to be re-wound unless it has been specially designed for 12 volt use. The usual voltage for those on the surplus market is 48, the standard telephone voltage; if the coil is for this voltage it will be found simplest to cut the old wire off the bobbin with a sharp knife, unless the wire is in good condition and there is compelling reason to keep it, for it will be very fine and difficult to handle. The replacement winding has the maximum number of turns consistent with filling the winding area and securing the nominal resistance desired, viz. 12 ohms, and 22-24 SWG wire will probably be found suitable. In the present case, the solenoid was re-wound empirically with some material which was to hand, until the correct resistance was obtained.

The pinch wheel is of rubber composition, about 1.5 cm. wide, formed on a sintered bronze bearing sleeve, and came from an old Grundig tape recorder, although most other makes would have proved suitable. It was found to be too hard to grip the tape evenly with a light downward pressure, so it was faced with a ridged layer of soft silicone rubber, applied as an uncured paste (Dow Corning RTV silicone rubber). This operation was carried out in a lathe.

The actuator consists of a bent piano-wire extension fixed to the main soft-iron actuator in the body of the electromagnetic counter, where it is held with a small plate and two 8BA bolts. This can be clearly seen from Plate 8 . The ratchet wheel was cut from a sheet of 0.1 inch brass, and thirty-six teeth were filed in the periphery at 10° spacings. With each operation of the electromagnetic counter the ratchet wheel turns through 10° , and this is converted by the capstan which has a circumference of 3.60 cm. into a movement of 1.0 mm. The diameter of the capstan should, however, be undersize in radius by the thickness of the paper tape, if the movement is to be exactly 1.0 mm.

4.E.5 Decoupling of parts of the mechanism

It is important that the motion of the supply and take up spools be decoupled mechanically from the motion of the tape through the capstan and pinch roller, if tape movement is to follow the capstan faithfully. The electrical pulse to the electromagnetic counter is a square waveform, but the motion of the actuator could not follow this; if it did, the acceleration involved would probably damage the actuator and break the tape. The peak acceleration with which the actuator operates is, even so, quite high, and for this reason two springs are installed, one on each side of the capstan assembly, and these take in enough tape to supply the capstan with 'low-impedance' tape on the supply side, and to maintain the tape tension on the output side of the capstan. The position of these two springs is shown in Fig 25 but the supply decoupling spring, only, is present and to be seen in the view of the recording channel given in

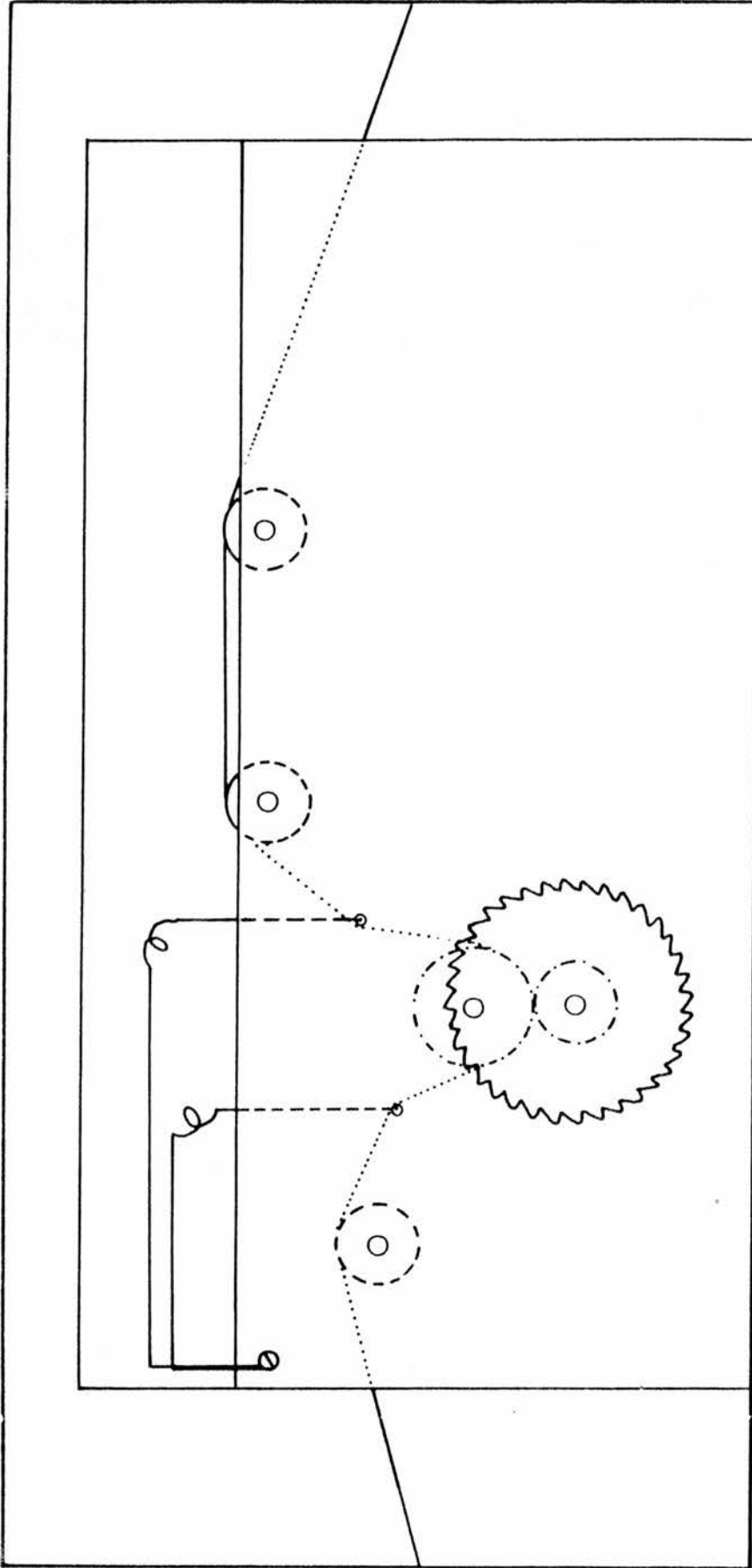


Fig. 25 Diagrammatic representation of the positioning of the decoupling springs, and the path followed by the recording tape in the prototype recorder see page 78

plate 10. The third Spring, which decouples the clutch assembly, serves the secondary function of setting the force which controls the friction in the clutch slip-plates. This spring can clearly be seen in Fig . 4 in Appendix 9 .

As a result of the presence of these springs, there is (except in the vicinity of the capstan) a reduction in the peak velocity of the tape, and also the acceleration, and there is a time delay between the peak speed of tape passage at the capstan and the ensuing motions of tape from the supply spool and on to the take-up spool.

Without these springs the performance of the recorder would be much poorer, and the energy storing properties of the mass-spring systems contributes considerably to the power economy of the recorder. For a theoretical discussion of mechanical decoupling, see, for example McKNIGHT (1964).

4.E.6 Effect of the recorder specification on the choice of integrator

Given the wide effective dynamic range of the recorder, an integrator which can match this range is desirable. It seemed not unreasonable to attempt an improvement in the linearity of the STANTON, 1973, integrator, until the range of 1 count in 0.1 hours to several counts per second could be encompassed with no greater deviation from linear response than ca. 2%.

4.E.7 Range-changing and the recorder

If it is desired to use an integrator with more than one sensitivity range, it is perfectly possible to split the hot-wire time marker laterally into sections, energised in different combinations according to the integrator range in use. In this way the time-mark will be divided into specific numbers and lateral positions of segments which can encode the range-setting of the integrator into the recording in such a way as to remain compatible with either visual or machine readability.

CHAPTER 5

THE DESIGN AND DEVELOPMENT OF THE NEW INTEGRATOR

5 THE DESIGN AND DEVELOPMENT OF THE NEW INTEGRATOR

5.A Background

Between 1971 and 1972, Stanton developed a simple integrator, intended to operate with Cadmium sulphide photoresistive detectors. STANTON (1973). Stanton kindly supplied the author with an example of the integrator to allow an evaluation of its performance, and tests were performed between 1973 and 1975 in connection with an honours project during undergraduate studies. Various irregularities of performance became apparent during these tests and as a result, certain changes were made to the circuit. Between 1976 and 1977, these changes were followed by redesign of the circuit in more fundamental ways, to match the performance of the integrator more closely to the needs of the new recorder.

The design philosophy underlying the choice of circuit materials was that only simple semiconductor devices should be used, in order that there should be less difficulty in construction and component replacement worldwide than if the newer, less freely available integrated circuits were employed.

Additionally, low power consumption was considered a prerequisite; the very few early operational amplifier integrated circuits which met this requirement were prohibitively expensive.

5.B Specifications and circuits for integrators of STANTON (1973) and GOING (this volume)

Figs. 27 and 28 show the published circuit of STANTON (1973) and the final circuit of GOING, to be described below. Table 5

Table 5

Technical specifications for Going and Stanton integrators

<u>Variable</u>	<u>Stanton (1973)</u>	<u>Going</u>
Operating voltage	9 V	9 - 15 V
Quiescent battery drain (A)	ca. 0.5 mA	49 μ A at +65°C 59 μ A at -8°C
Voltage coefficient (B)	high - to be run from stable battery	+0.28% V ⁻¹ (C) (E) +0.06% V ⁻¹ (D) (E)
Operating dynamic range	100 : 1 (F)	10,000 : 1 (G)
Range of operating temperature	0-35°C	-25 to +65°C
Temperature coefficient (H)	-0.5% °C ⁻¹	-0.13 to -0.06% °C ⁻¹ (I)

Notes

- (A) Battery voltage - 12 volts, nominal
- (B) Effect of fluctuating supply voltage
- (C) Battery voltage = 9 - 12 volts
- (D) Battery voltage = 12 - 15 volts
- (E) Worst case, as percentage of count rate
- (F) For unspecified deviation from linearity
- (G) For +2.3, -3.2% deviation from expected over range 2.5 mA to 250 nA.
- (H) Expressed as percentage of count rate
- (I) Poorer figure for T_{amb} -8° to +14°C; better for T_{amb} +14.5° to +65°C

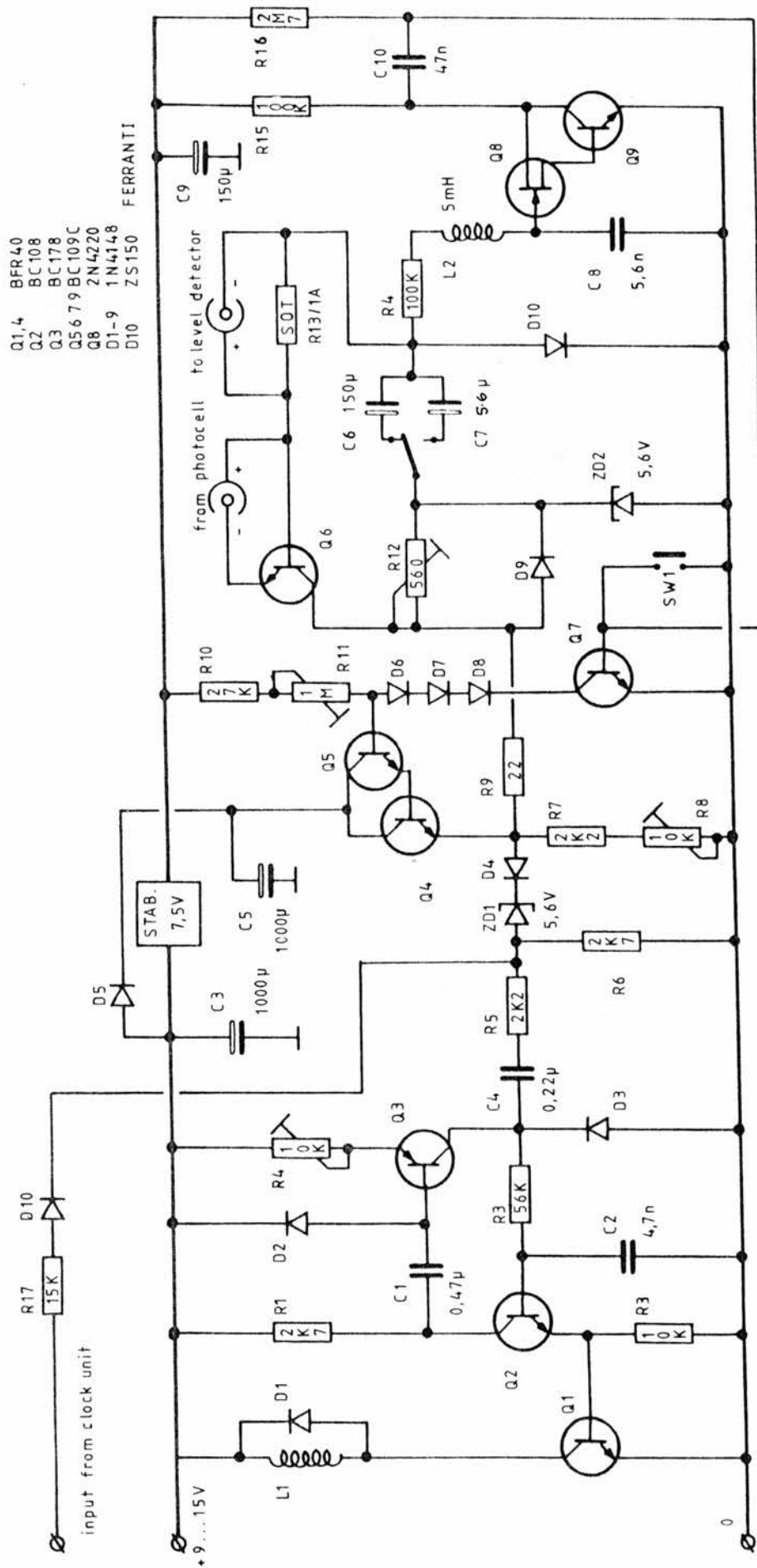


FIG 28 Final circuit of the new integrator

shows the technical specifications of both integrators.

5.C The new integrator - Analysis of operation I

The following description and component references relate to Fig 28 which shows the most recent circuit to be evolved; and to Figs 29 and 30 which illustrate by means of coloured connections various electrical conditions present in the circuit during different phases of the integration cycle. It will be assumed that the cycle begins with the recharge phase.

5.C.1 The recharge phase - see Figs 28 and 29

In the recharge phase, current flows unimpeded through D5, Q4, Q5, R9 and D9 into C6 which charges up, via D10, relative to ground. For the moment assume that Q7 suddenly begins to conduct, depriving Q4 and Q5 of the base current which had been driving them, which instead flows through D6-8 via Q7 to ground. At this stage, C6 is charged up to a voltage above ground, set by ZD2, less about 0.5 volt dropped by D10 in the charging process.

5.C.2 The integration phase - see Figs 28 and 30

At the end of the recharge phase C6 has been pre-loaded with a fixed charge. This leaks away via R12, Q6 and R13/1A in direct proportion to the current to be integrated, this current simply being fed, with correct polarity, through the base-emitter junction of Q6. Q6 is a constant current generator, a transistor operating

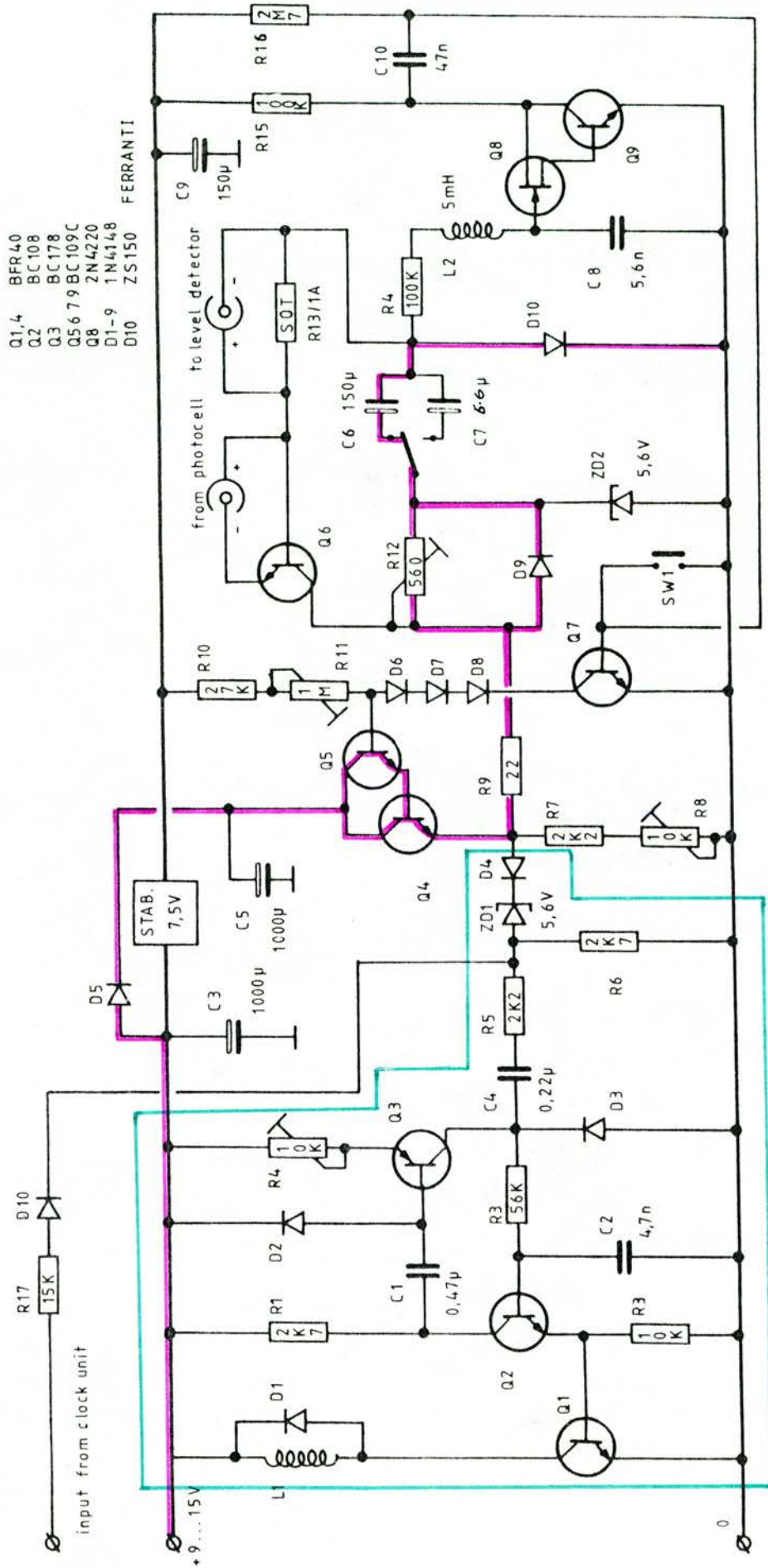


FIG 29 Red line shows current through integrator capacitor C6 during the recharge phase of the integration cycle. Blue box shows zero static consumption monostable. See section 5.C.5, p. 92

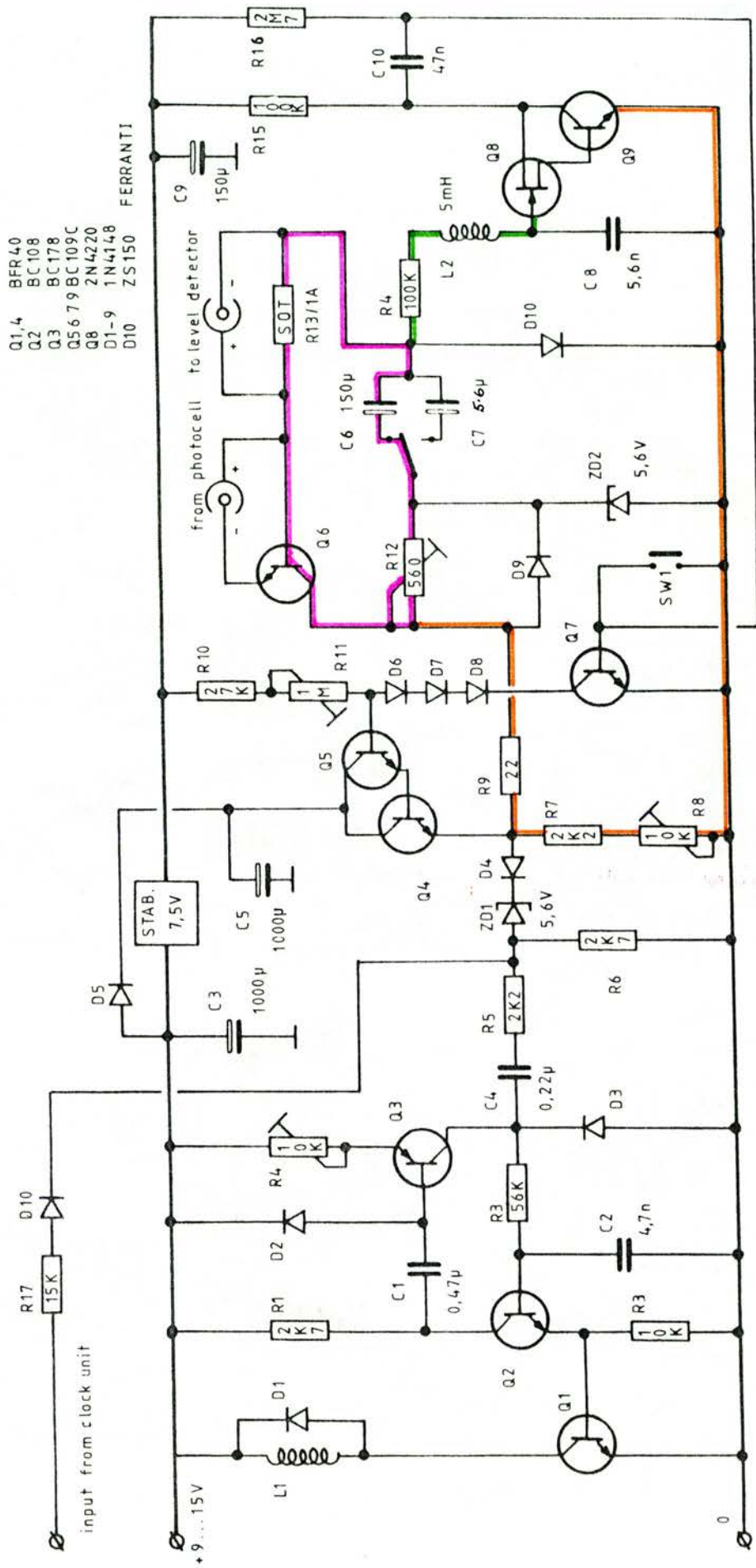


FIG 30 Integrator operation in 'integrate' phase of cycle. Discharge current path shown in red; green and orange lines depict route through which the Q8-Q9 combination detects the voltage across C6

in the earthed base mode. Meanwhile, the voltage on the capacitor C6 is being monitored by Q8, Q9 by way of the path outlined in green and orange.

5.C.3 Return to the recharge phase - see Figs. 28 and 29

When the negative voltage present on the gate of Q8 (ie. the voltage left on C6) becomes too low, Q8 and Q9 begin to conduct, causing the R15-end of C10 to be electrically connected to ground. This therefore means that Q7 suddenly begins to have its base reverse biased since it happens that whilst Q8 and Q9 were off, C10 had charged up to rail voltage through R15 via the be junction of Q7. With the R15 end of C10 now connected to ground, the other end (and hence the base of Q7 and the lower end of R16) must find itself negative with respect to ground. Since Q7 must now be off, the circuit is back to the situation in paragraph 5.C.1, the Recharge phase, where Q4 and Q5 are switched on again.

In fact, the process is regenerative, since the tendency of Q7 to begin to switch off results in the tendency for Q4 and Q5 to begin the recharging of C6, which in turn leads to a rapid change in the voltage on Q8 gate to become positive, re-inforcing the trend for Q7 to turn off even further. The change of state takes only microseconds to occur, once a critical phase is reached and positive feedback commences. The recharge phase is brought to a sudden, equally predictable end when the R16 end of C10 is no longer negatively biased, because of the recharge current flowing through R16. Q7 begins to conduct again, and regeneration causes the recharge phase to end very abruptly.

5.C.4 Further detail

The time-constant of R16-C10 determines the length of the recharge cycle, which has to be long enough for C6 to recharge to the upper threshold set by ZD2. The peak recharging current is limited to a value safe for Q4 by R9 so the process can take some tens of milliseconds for large values of C6.

During the recharge cycle, the D4 anode is made very positive, and this positive excursion sets off the solenoid driving circuit (Blue box in Fig 29). In fact, Q4 and Q5 are never completely off; R7 and R8 set a slight current through them. This slight current flow (ca. $25\mu\text{A}$) is necessary to keep the circuit 'alive', and it remains self-balancing with respect to thermal properties of the semiconductor junctions. This allows the circuit to operate in a satisfactory way over a wide range of ambient temperatures. See page 109 for further explanation.

5.C.5 Solenoid driving circuit - see Figs 28 and 29 Blue box

When the solenoid is not energised, Q1, Q2 and Q3 are all off, conserving electrical energy. If a steeply rising voltage waveform appears at D4 anode, this is communicated to the base of Q2 via ZD1, R5, C4 and R3. Q2 turns on, drawing a current through C1, which tends to turn on Q3. Q3 is, however, coupled back to Q2, thus tending to turn it on further. Q2 and Q3 therefore both turn full on in regenerative manner until C1 becomes charged up, when the circuit abruptly switches off, also in a regenerative fashion, as

follows. As Q2 switches off, the R1-end of C1 becomes connected via R1 to the positive rail, and the charge in C1 biases Q3 off, which in turn hastens the switching off of Q2. C1 discharges via D2 and R1; C4 discharges via R5, R6 and D3, and the circuit is reset in readiness to be triggered again after a few milliseconds. The 'on' cycle time is set by R4, and depends on the time-constant C1-R4. Current from Q2 feeds Q1, the driver of the solenoid, which has sufficient gain to operate in saturation. The circuit around Q1, Q2 and Q3 is a refinement of one due to FURUICHI and SASAKI (1968). Their original circuit is shown in Fig 50.

5.D Analysis of operation - II

Figs. 31 to 42 reproduce photographs of stored oscilloscope traces showing waveforms obtained from selected points in the circuit, Fig 28 , and serve to illustrate the description of the circuit given in Analysis of operation I. The letters in the top right hand corners of each graph relate to the connections of the positive and negative probes of the oscilloscope and are given on the circuit, Fig 28a. The vertical sensitivities and timebase calibrations are marked on the individual graphs, which were selected to illustrate the effects on a number of key waveforms of normal and low battery voltage, and two widely differing sizes of integration capacitor, C6.

The oscillographs were obtained using a Tektronix 546B oscilloscope with 3A3 amplifier module. The circuit loading of the input probe was $1M\Omega$ input resistance with parallel capacitance of 47pF, and except where stated, is of sufficiently high impedance not to have affected the operation of the integrator. The

A minimum battery voltage of 9 remains satisfactory.

5.D.3. Figs. 36 and 37

Probe posn. J-X

These show the performance of Q8-Q9, which monitor the lower voltage level on C6, and initiate the recharge cycle. Both waveforms are very similar, and show a threshold voltage of 6.27V at which regenerative action commences. Although there is a considerable difference in size of integrating current and C6 value, the dv/dt value remains similar, hence there is little difference in threshold voltage and in the shape of the waveforms. Note that the standing DC potential on Q8-Q9, shown as being Ca. 6.8V, is somewhat lower than in reality, because of loading effects of the oscilloscope probe, ($1M\Omega$ resistance).

5.D.4 Fig. 38

Probe posn. J-X

In contrast to Fig 37 the current being integrated is reduced tenfold, and with it the dv/dt value on C6. The effect of this is to lower the voltage at J at which regeneration begins, since it is the point J, and not the absolute voltage, which determines when regeneration begins. However, in this instance, the Q8-Q9 pair, instead of having an 'on-off' snap action, pass through a range of negative gate bias voltage over which an amplifying function can occur, as evidenced by the 50 HZ ripple to be seen on Fig 38 . Unfortunately, the gain of the Q8-Q9 pair is very high at this point, and 50 HZ electromagnetic pick-up or very small spikes of interference voltage presenting

themselves at the gate will cause premature triggering of the integrator, degrading the performance. For this reason, L2 and C8 (Fig. 28) are inserted to decouple the gate to AC voltages, and in practical realisations of the circuit adequate screening is essential. The loading of the oscilloscope again affects the DC voltage level at J .

5.D.5 Figs. 39 and 40

Probe posn. H-X

These show the dv/dt conditions on the integrating capacitor such as were present for Figs 36 and 37 . Since the I_{in} discharge was in each case constant, the slope of the discharge section is linear, and the dv/dt value constant. This is a fundamental feature of a capacitor in discharge. The positive portion of the graphs shows the voltage drop present on D10, during recharge and the high initial charging current is responsible for the cusp, most clearly visible in Fig. 40.

5.D.6 Figs. 41 and 42

Probe posn. E-H

In these figures is shown the voltage across C6 for two different values of C6 and I_{int} . It is an unusual feature of this integrator that the capacitor is pre-loaded with a fixed charge, which is then lost in accordance with the integral of the incoming unknown signal to be integrated. Most other circuits use the capacitor in the reverse mode, allowing it to charge in accordance with the increasing integral, until the stored charge reaches a threshold maximum, after which rapid discharge occurs.

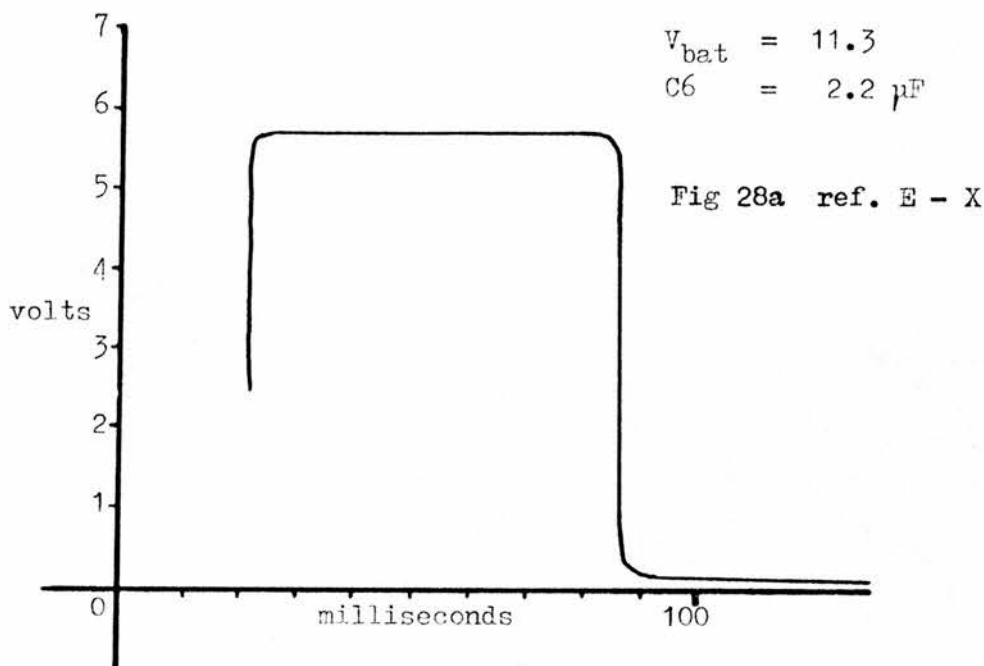


Fig. 31 Recharge Phase - small value of C6

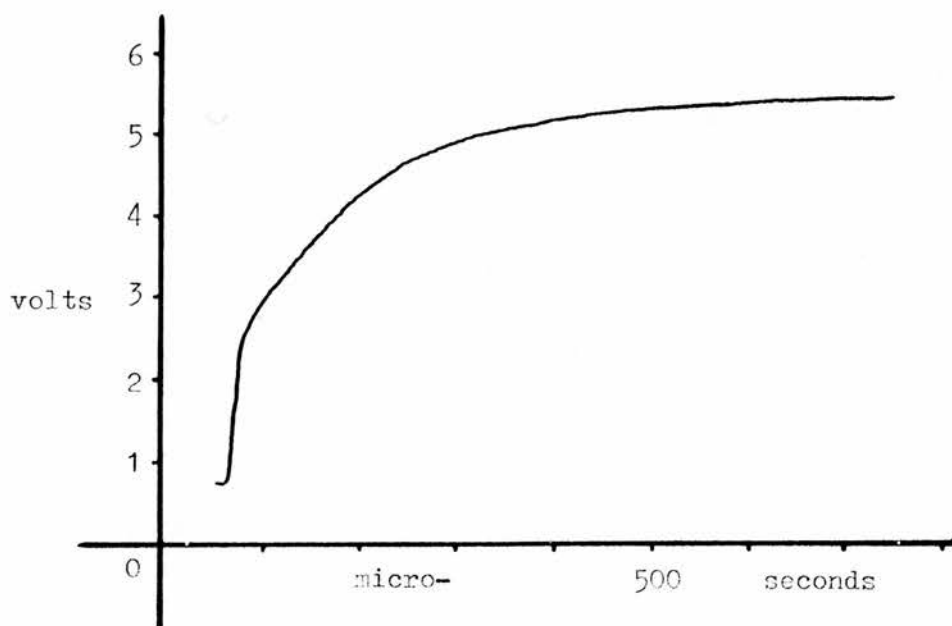


Fig. 32 Recharge Phase - as for Fig. 31 but expanded timebase

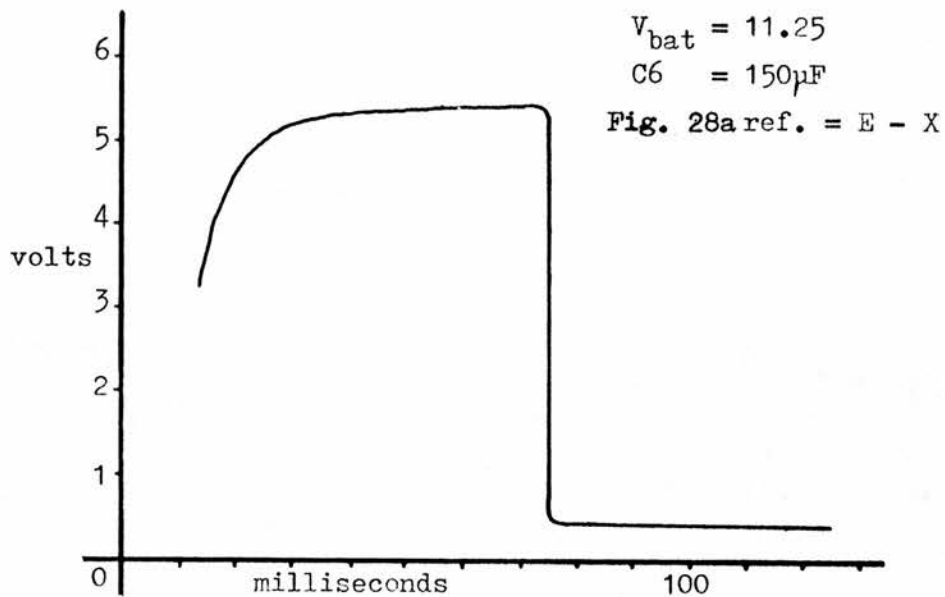


Fig. 33 : Recharge Phase - normal battery voltage

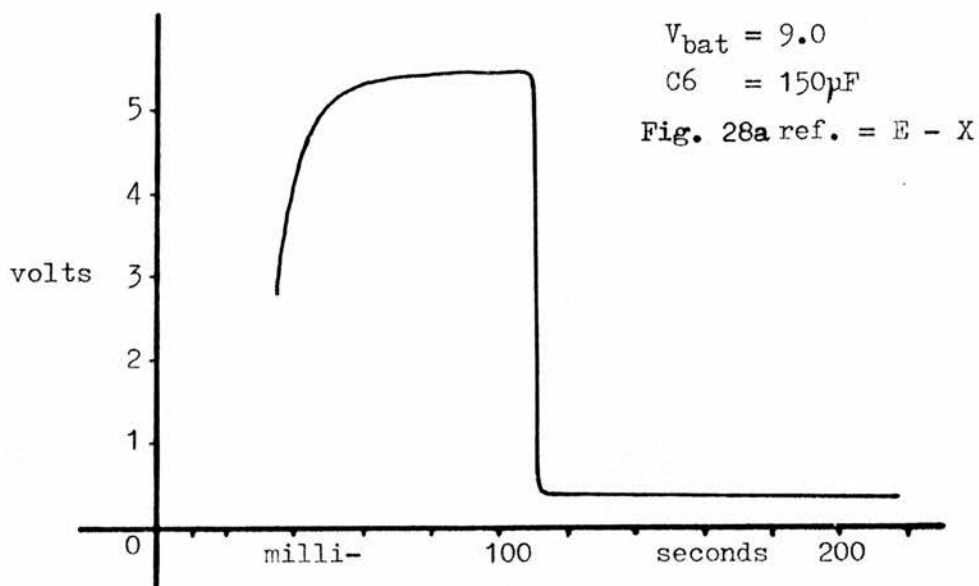


Fig. 34 : Recharge Phase - low battery voltage, large C6
i.e. worst operating conditions

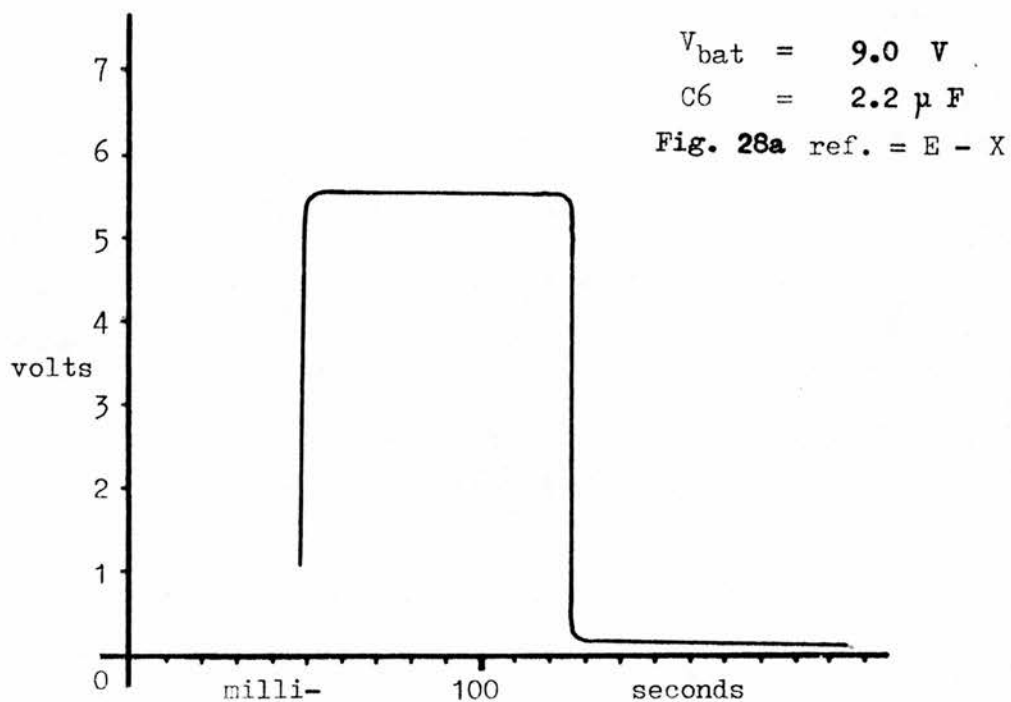


Fig. 35 Recharge Phase - low battery voltage, cf. Fig 34

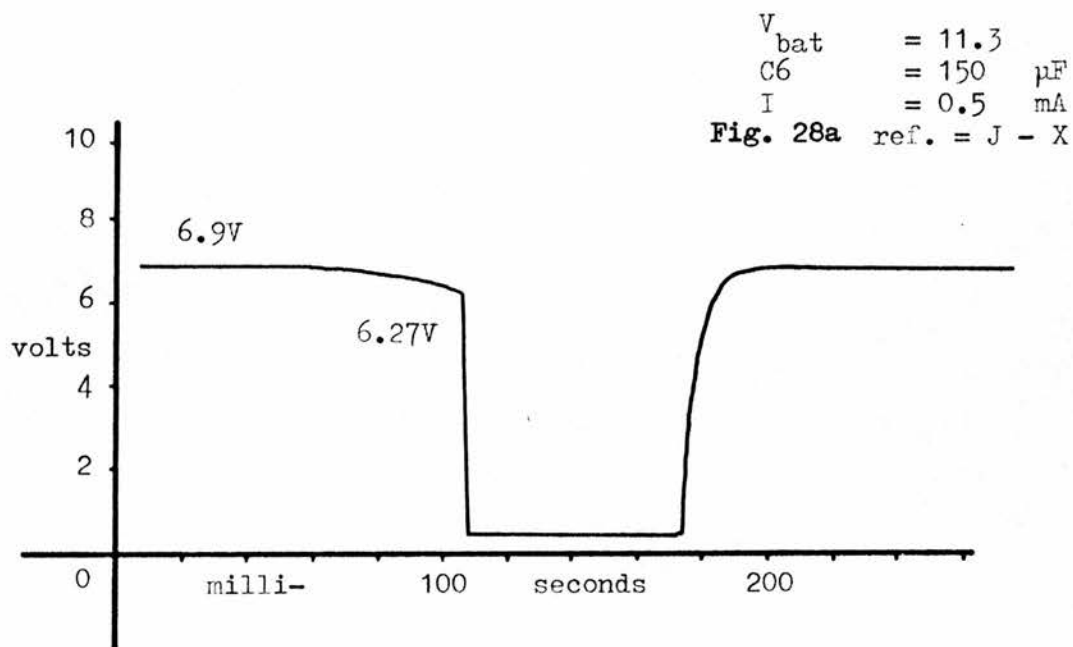


Fig. 36 Recharge Phase - Voltage on drain of Q8
 dV/dT on C6 = $3.4 \text{ V} \cdot \text{s}^{-1}$

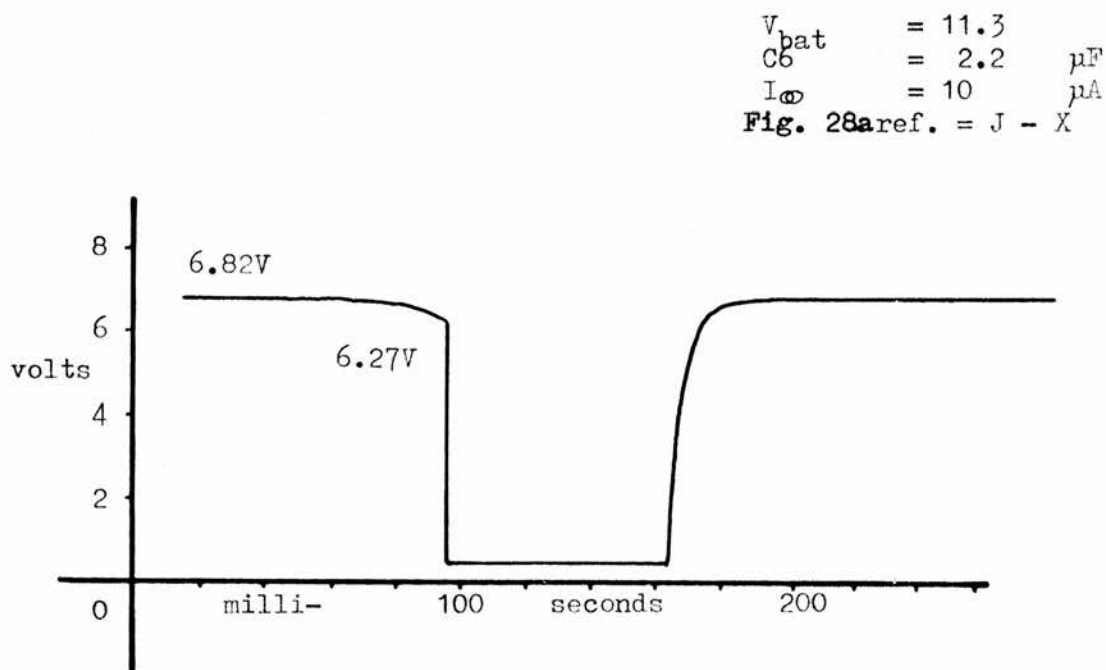


Fig. 37 Recharge Phase - Voltage on drain of Q8
 dV/dT on C6 = $6.1 \text{ V} \cdot \text{s}^{-1}$

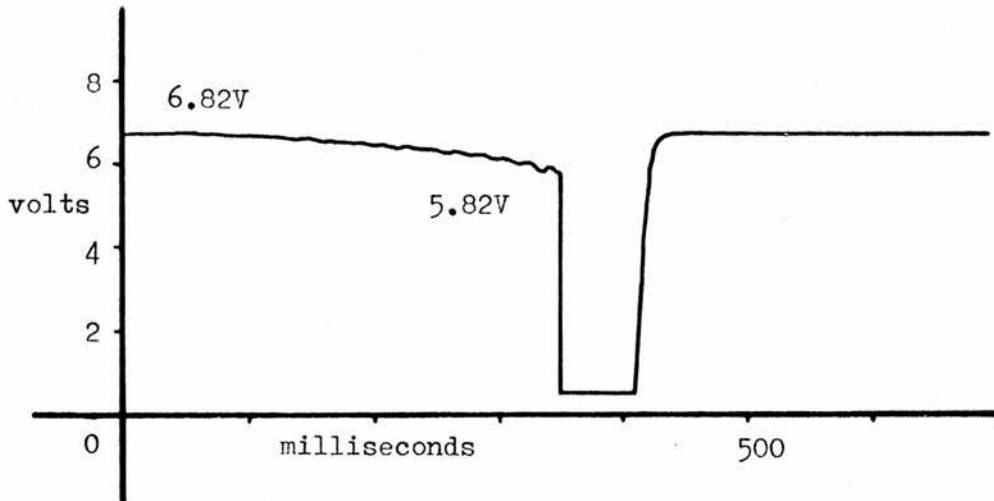


Fig. 38 Recharge Phase - Voltage on drain of Q8
 dV/dT on C6 = $0.6 \text{ V} \cdot \text{s}^{-1}$. Note
 50 HZ ripple voltage present on Q8 drain.

V_{bat} = 11.3
 $C6$ = 2.2 μF
 I_{∞} = 1.0 μA
Fig. 28a ref. = J - X

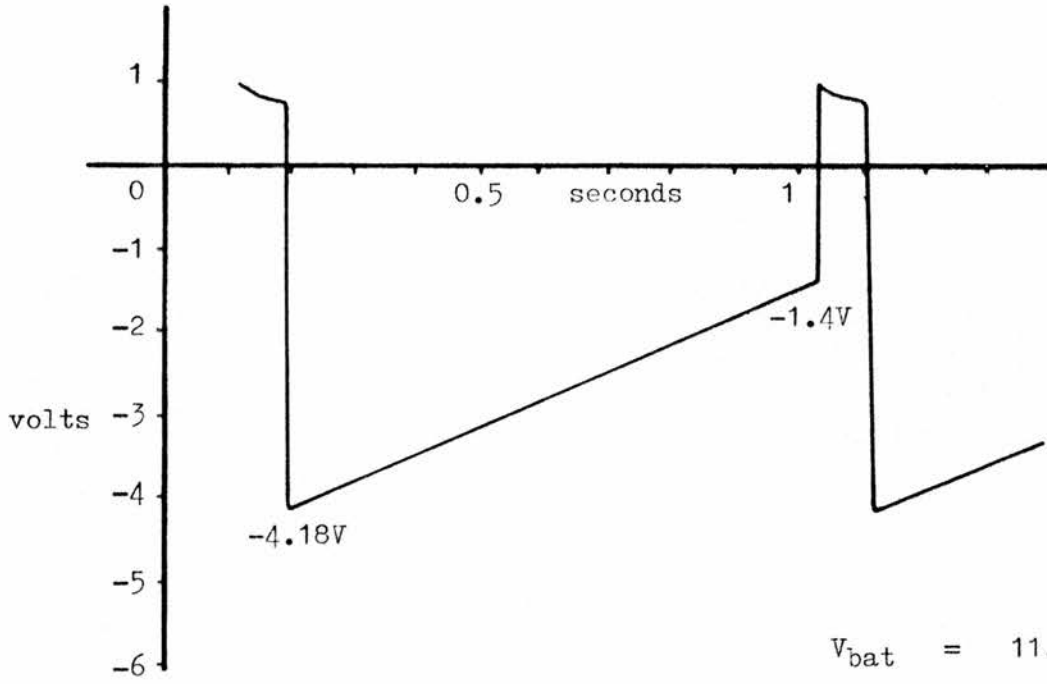


Fig. 39 Complete cycle -
voltage on gate of Q8

$V_{bat} = 11.3$
 $C6 = 150 \mu F$
 $I_{\omega} = 1.5 \text{ mA}$
 Fig. 28a ref. = H - X

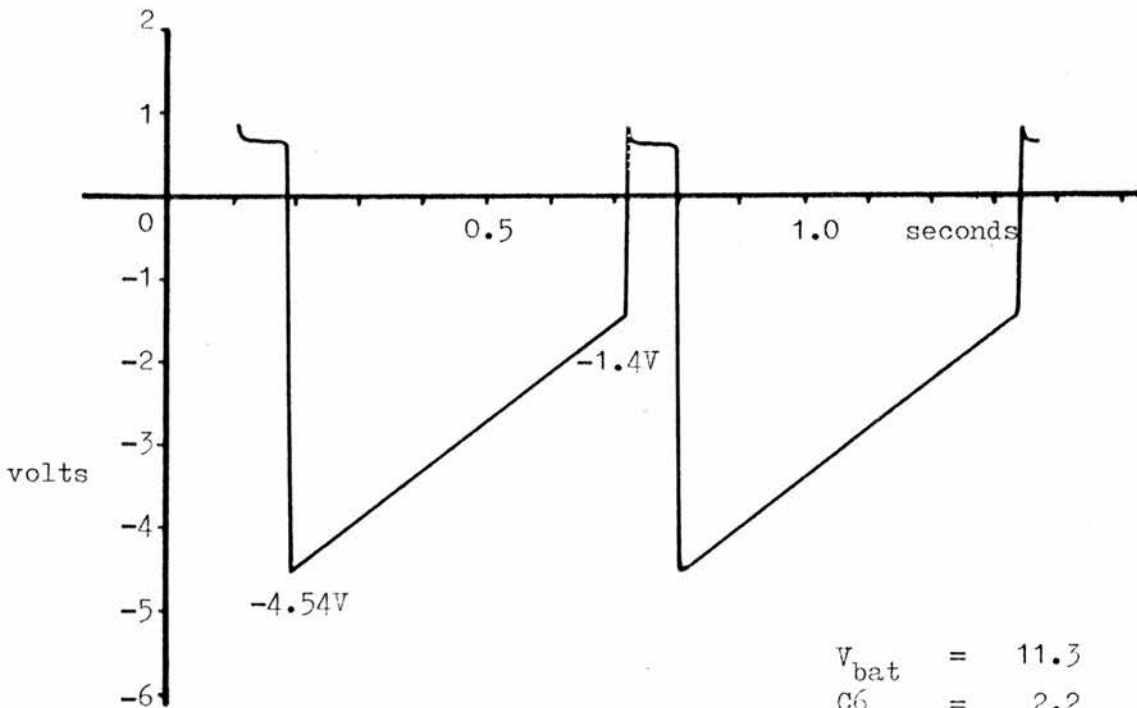


Fig. 40 Complete cycle -
voltage on gate of Q8

$V_{bat} = 11.3$
 $C6 = 2.2 \mu F$
 $I_{\omega} = 10 \mu A$
 Fig. 28a ref. = II - X

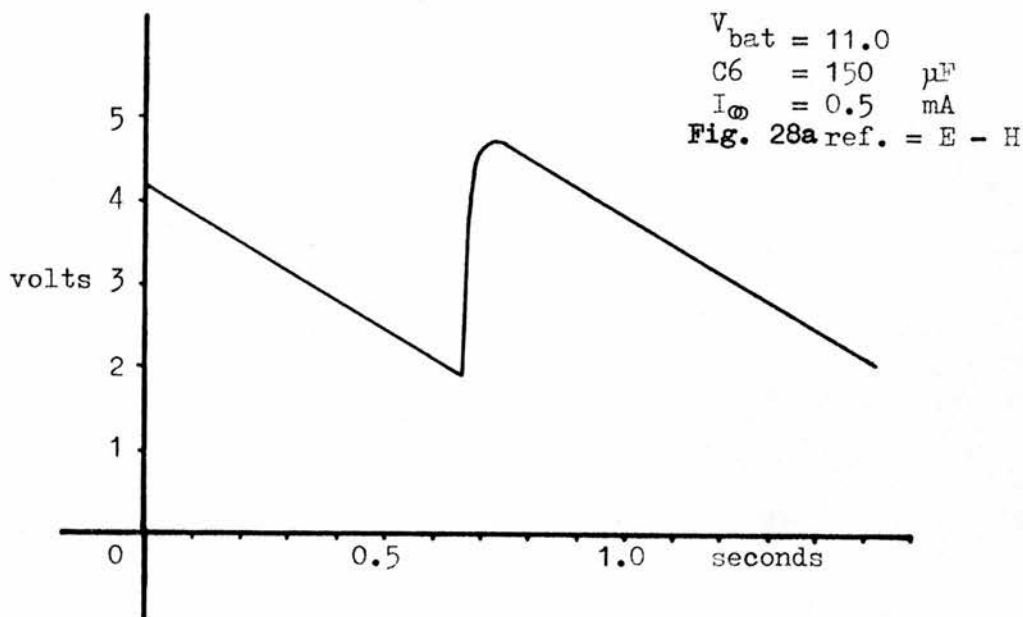


Fig. 41 Complete cycle of charge - discharge voltage present at C6. $dV/dT = 3.4 \text{ V} \cdot \text{s}^{-1}$

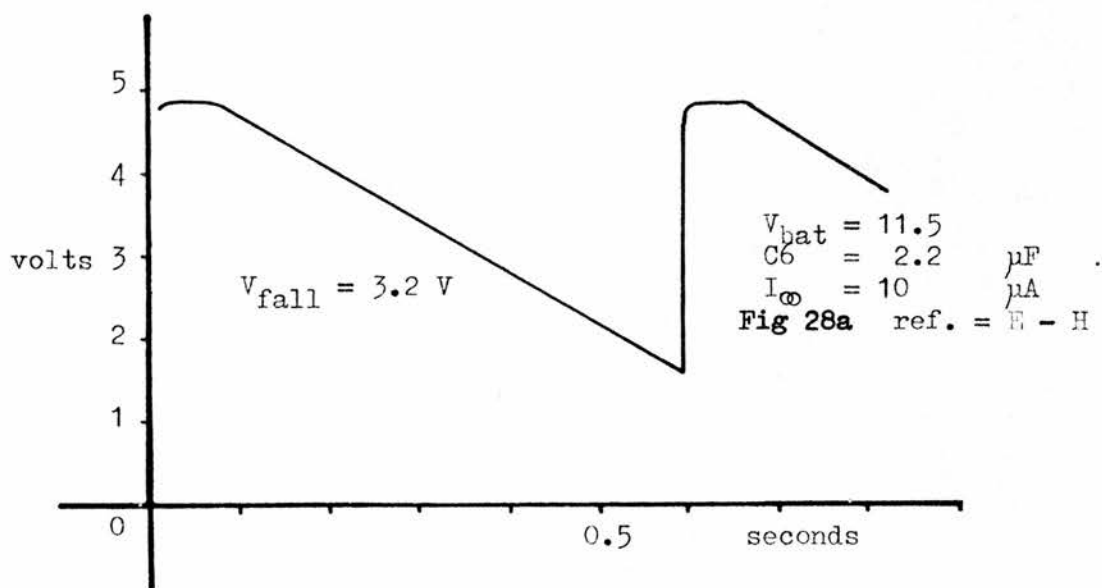


Fig. 42 Complete cycle of charge - discharge voltage present at C6. $dV/dT = 6.1 \text{ V} \cdot \text{s}^{-1}$

5.E Analysis of operation - III

5.E.1 Compensation for dead-time

As was discussed in greater detail in the first section on integrators (see page 46 para. 3) 'dead-time', or that part of the integration cycle when the integration capacitor is being reset, causes increasingly serious underestimation of the signal being integrated as the pulse rate increases. This is clearly shown by Fig 43 in which signal currents, themselves exact multiples of the lowest current, 0.5 mA, fail to produce cycle trains with times thus related. If the cycle time for 0.5 mA, 1.07 seconds, is assumed to be correct, then cycle times for 1.0 and 2.0 mA are, respectively, 6% and 18% too slow by comparison. The cure for this condition is explained on Page 47 and a single pre-set resistance, R12 in Fig 28 effects the necessary correction. A diode, D9 ensures that R12 is effectively short-circuited during the recharge phase. Fig. 44 shows corrected superimposed graphs as for Fig 43, except that here the dead-time effect has been all but eliminated, giving the integrator a much improved performance. The correct value for R 12 is found by experiment.

5.F Aspects of performance

5.F.1 Temperature co-efficients

The worst temperature co-efficient of the final circuit is good. The values were estimated with the integrator supplied

$V_{bat} = 11.25$

$C6 = 150 \mu F$

Fig. 28a ref. = E - H

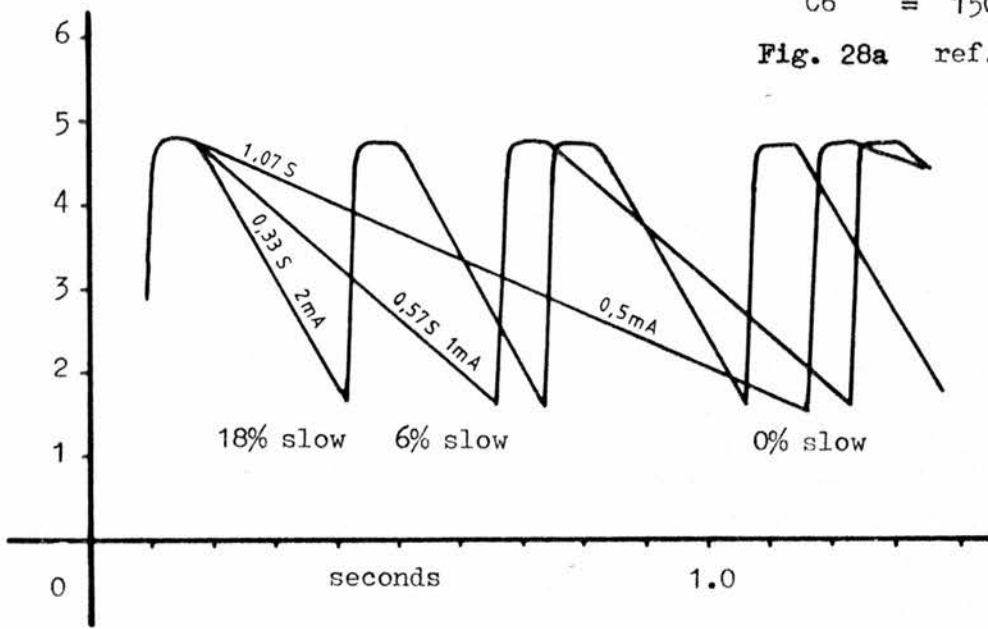


Fig. 43 Complete charge - discharge cycles, dead-time not compensated for. Test currents 2, 1, and 0.5 mA.

$V_{bat} = 11.25$

$C6 = 150 \mu F$

Fig. 28a ref. = E - H

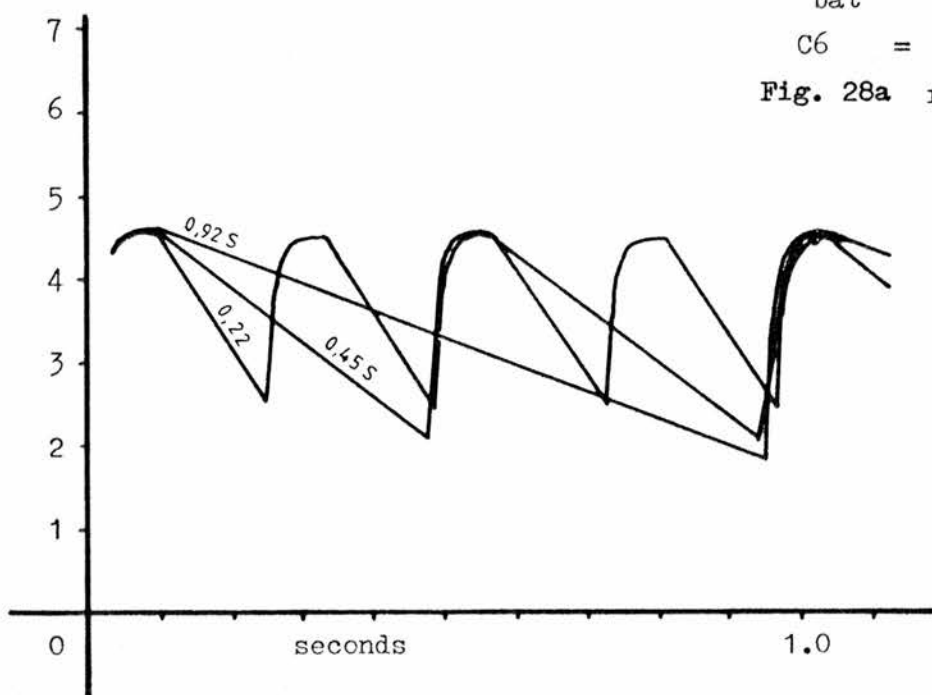


Fig. 44 As above, but with substantially correct dead-time compensation.

with the nominal battery voltage 12V (11.6V), and operated at three values of integrated current, 10, 100, and 500 μ A, with $C_6 = 150 \mu$ F. The co-efficients were checked over two temperature bands:

1. -8°C to $+14.5^{\circ}\text{C}$ ($\Delta t = 22.5^{\circ}\text{C}$)
2. 14.5°C to 65°C ($\Delta t = 50.5^{\circ}\text{C}$)

when the results were:

Temperature Band	-8°C to $+14^{\circ}\text{C}$	14°C to 65°C
I test 10 μ A	-0.103%*	-0.058%
100 μ A	-0.129%	-0.052%
500 μ A	-0.084%	-0.057%

*All values expressed as percent change in count rate at 14.5°C per degree centigrade rise in temperature.

The worst case value is, as may be seen -0.13% which is likely to be insignificant in most experimental conditions. In practice, the source of the input signal will possess its own temperature coefficient, which may react with that of the integrator to produce a better or worse final value. See also page 129

5.F.2 Battery voltage

The integrator has been designed to operate from a battery source of wide voltage variability with the least possible effect on performance. This is essential, since in any field programme, many things can go wrong, and batteries, especially Leclanché types, very often do not have reliably known capacities. Sufficient 'over-capacity' must often be allowed, especially where meteorological apparatus is to be left in remote sites.

The Voltage co-efficient was measured over two bands of battery voltage:

1. 9V to 12V ($\Delta V = 3V$)
2. 12V to 15V ($\Delta V = 3V$)

when the results were:

Voltage Band	9 to 12V	12 to 15V
I test $10\mu A$	+0.163%*	+0.059%
$100\mu A$	+0.277%	+0.049%
$500\mu A$	+0.238%	+0.014%

$C6 = 150\mu F$

*Expressed as percent change in count rate per volt rise referred to count rate at 12 volts. All measured at room temperature $16^{\circ}C$

As might be expected, greater effects are noticeable towards the lower limit of battery voltage. It is possible that the 9-12V band incorporates a considerably worse value occurring within the range 9-10V, disguised by being amalgamated with the values occurring between 10 and 12 volts. The capacitor C3 (Fig 28) serves to buffer the battery against the demands made by L1, the electromagnetic counter, and C3 must have adequate size (as verified by an oscilloscope) to decouple L1 from the battery. In turn, the other parts of the circuit are decoupled from both battery and electromagnetic counter by D5 - C5 and the combination of C9 and the stabiliser block.

5.F.3 Ambient temperature

The integrator has been designed with the extremes of temperature within a temperate region in mind; and it has been shown

to work from -25°C to $+65^{\circ}\text{C}$. It is likely that the integrator will continue working at lower temperatures, the limits being set by those components which contain liquid electrolytes, viz. batteries and electrolytic capacitors. With careful selection, it is probable that the circuit would work in arctic conditions, and if the circuit housing is suitably shaded, it should rarely be necessary to exceed the upper tested limit of 65°C . See also Appendices 4 and 6, Batteries and Capacitors.

5.F.4 Sensitivity to impulsive interference

In the development of the integrator, the electronic circuitry was constructed on a 'breadboard' system, with fairly long interconnections between some parts of the circuit. The laboratory was situated in the centre of a busy building, and it was found that, as stated in section 5.D.4. and Fig 38, interference from electrical switching transients generated in the building could cause spurious triggering.

When the circuitry is constructed in final form, and installed in a metal case, the problem is eased, but nevertheless the L2 - C8 combination (Fig. 28) serves to decouple the gate of Q8 from interference pulses.

5.G Aspects of design and development

5.G.1 Introduction

In this section, various aspects of design which required special consideration are presented. It is not intended to

be exhaustive, but merely to draw attention to certain difficulties, and alternative methods of achieving similar results.

5.G.2 Temperature stabilisation

In any transistorised circuit intended for operation over a wide range of ambient temperatures, care has to be taken that currents drawn cannot exceed specified safe maxima, and that transistor gains, which fall at low temperatures, are always adequate to maintain correct operation. In practice, temperature compensation in the form of self-balancing circuit arrangements is usually necessary if a circuit is to be exposed to the full natural range of ambient temperatures. In addition to transistor gain, collector-to-emitter and base-to-emitter voltages (V_{ce} and V_{be}) and diode leakage currents are all strongly temperature dependent.

From the temperature point of view, the critical parts of the integrator are those centred on Q4/5, D6-8 and Q7. The simplified circuit, with the currents which flow, is shown in Fig 45 . In setting the values for R11 and R8 (nomenclature remains the same as in Fig 28), the current through R11 is set to $25\mu A$, as is the current through R8. The β value for Q4/5 is ca. 36,000 (600^2) at room temperature, and will range according to temperature from ca. 9,000 (300^2) to 64,000 (800^2). Q4 and Q5 form a voltage follower circuit, and $V_{D-X} = V_{C-X} - (V_{be}^{Q4} + V_{be}^{Q5})$. Because of the very high gain of Q4-Q5, the $\frac{25}{\beta}$ factor is very small, and ranges from 0.39 to 2.7nA (nanoampere) with temperature change from $-25^{\circ}C$ to $60^{\circ}C$. This current is itself insignificant in comparison with $25\mu A$, hence the current through the two arms of the circuit in Fig 45 vary but slightly with wide ranging ambient temperature. Diodes D6-8 form a constant voltage drop which makes

sure that V_{C-X} is always sufficient to bias transistors Q4 and Q5 'on' and the temperature co-efficients of V_{be} of Q4 and Q5, and of forward conduction voltage on D6-8 with V_{ce} Q7, are well enough matched to keep the circuit operating over the necessary wide range of temperatures. The total standby current consumption of the integrator is $59\mu A$ at $-8^{\circ}C$ and $49\mu A$ at $65^{\circ}C$ (sic).

5.G.3 Supply voltage stabilisation

An early part of the improvement programme for the original integrator of STANTON (1973) was voltage stabilisation to render supply voltage variation immaterial. The first step was to fix a voltage ceiling for the charging potential supplied to the integrating capacitor, C6. This was easily accomplished by R9 and ZD2.

Unfortunately, the use of all ordinary zener diodes for stabilising steady DC supplies to other parts of the circuit was ruled out, since these normally require a continuous current flow of at least 1 mA before the potential across the semiconductor junction stabilises. However, it is possible to use the base-emitter junction of a silicon planar transistor as a stable voltage reference; the resulting 'zener diode' has an exceedingly sharp characteristic in comparison with the ordinary commercial zener diode. As WILLIAMS (1967), who draws attention to the fact, states, this technique "has some of the characteristics of a state secret - many people know something about it, but those who know most, say least."

The properties of some NPN and PNP planar silicon transistors were therefore evaluated. As the overall quality of the NPN transistors was suspect, those results have been discounted, but the

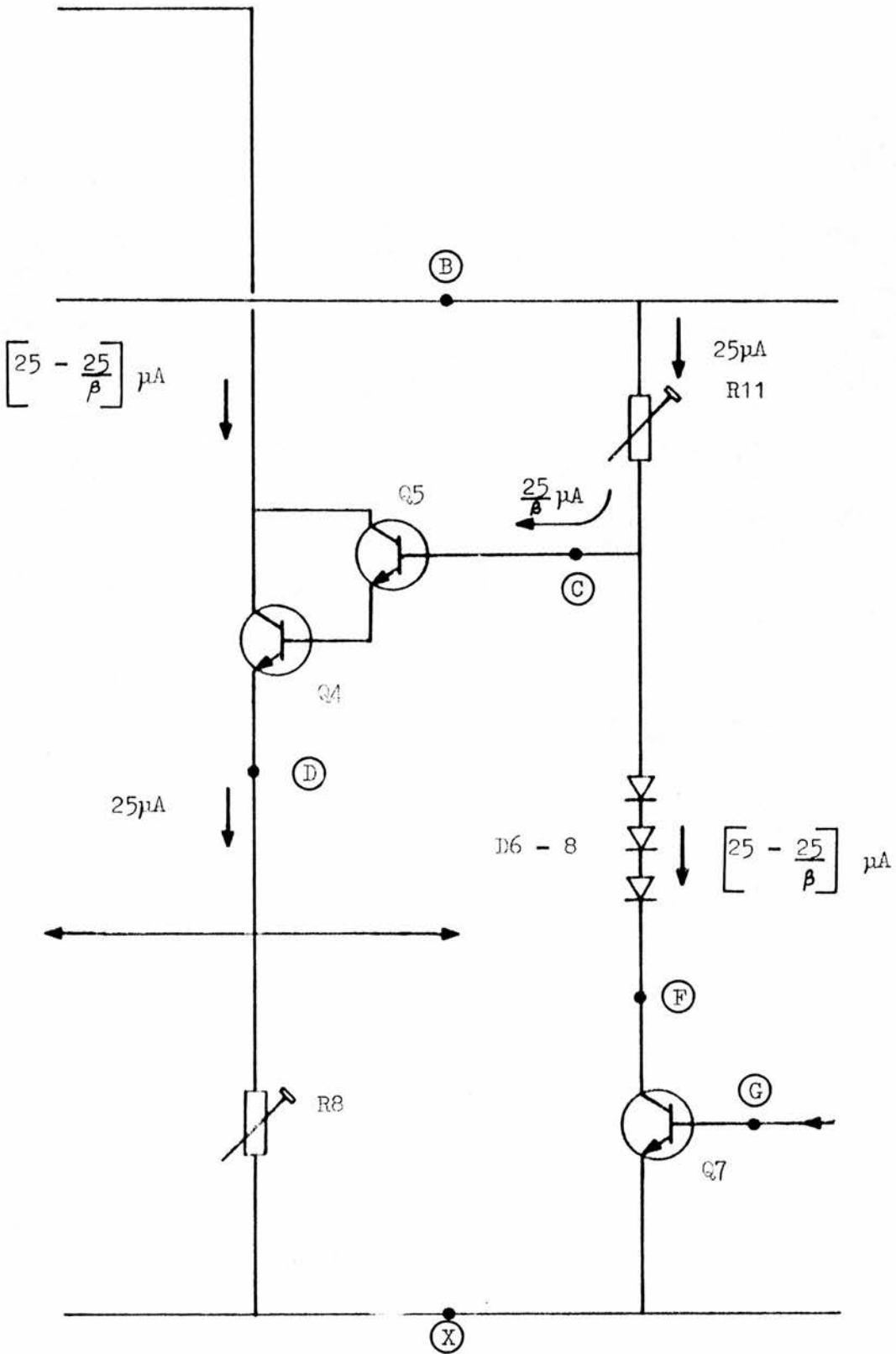


Fig. 45 Simplified circuit of part of the integrator, showing currents. Component references as in main circuit diagram, Fig. 28

PNP transistors, of the BC212 family, gave the following measurements:

Table 6 Zener breakdown characteristics of Base-Emitter junctions in the BC212 family of PNP Silicon Planar Transistors

*Sample size	23
*Mean breakdown voltage	6.67V
*Standard deviation	0.65V
*Test current	10 μ A
*Percentage of sample showing $\leq 2\%$ change in Zener voltage for I between 1 and 100 μ A	91 %
*Percentage of sample showing less than 1% change in zener voltage for I between 1 and 100 μ A.	48 %

In general, for small signal transistors, the breakdown voltage will be ≤ 14 volts, and any having a value of between 5.5 and 7 volts will be suitable in the following circuit. FERRANTI (1974) give performance figures for another transistor, the BCW10, which has a mean zener voltage of 8.5V, and MacHATTIE (1971) gives a value of 5.7V for the 2N3563. Since, once used in the zener breakdown mode, transistors may show degraded noise and gain characteristics, tested examples should be segregated from laboratory stocks. See also PREIS (1969).

The final circuit for the stabiliser is shown in Fig 46 . Static consumption is low, and, regulation adequate. Fig.47 shows performance curves for three values of load current. The circuit continues to work satisfactorily at -25°C . More recently, MAXWELL (1977), has used an integrated transistor array and field effect transistor to produce a superior micropower voltage regulator, the circuit of which is given in Fig. 62 . Quiescent current is only $4\mu\text{A}$. This circuit has not, however, been evaluated for use with the integrator. See also REHAK (1980).

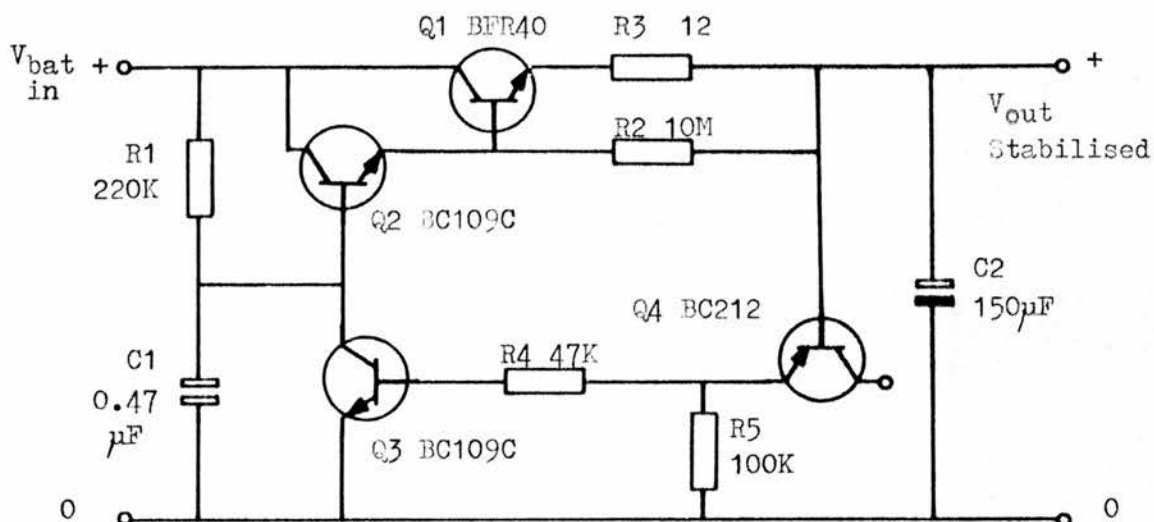


Fig. 46 Circuit of stabiliser for integrator - " Stab 7.5 " in Fig. 28

Zener Voltage: 6.9V
Room temp. 24°C

Static consumption:

V_{bat} :	9.0V	6.3 μA
	12.0V	14 μA
	15.0V	22 μA

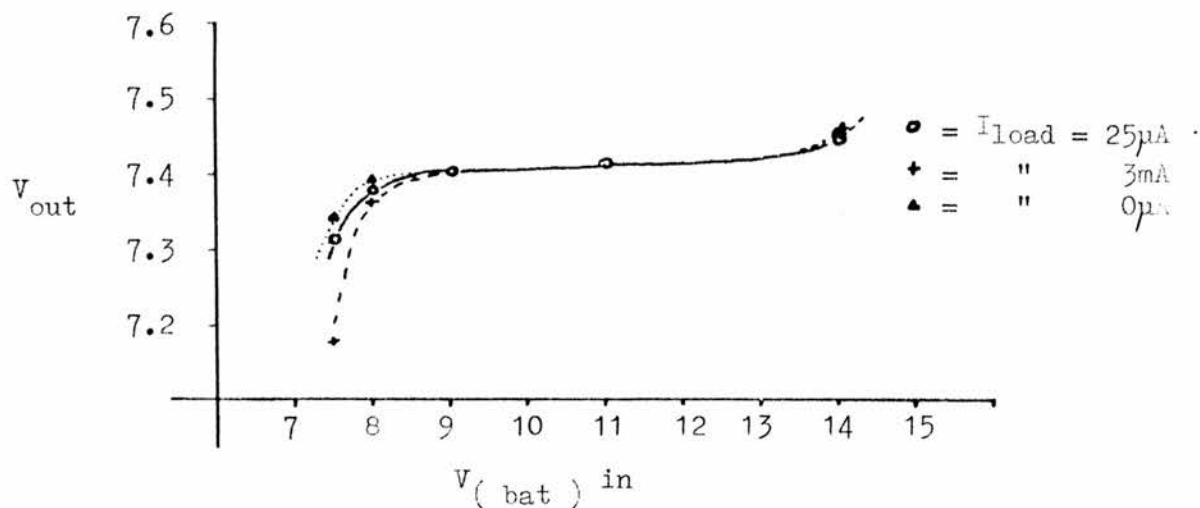


Fig. 47 Performance of circuit shown above

5.G.4 Solenoid power: monostables with minimum quiescent current drain

The requirement for the solenoid, L1 in Fig 28 is that it should be supplied with electricity from for example, a monostable oscillator which supplies full power for just sufficiently long for the solenoid to complete its mechanical movement. In the original integrator of Stanton Fig 27 , the length of pulse supplied to the solenoid was the same as the recycle time of the integrator, and was of an unalterable duration matched to the needs of the electromagnetic counter which Stanton used. The advantage of this arrangement was the simplicity of the resulting circuit.

However, in the interests of reducing the power consumption of the total integrator and recording system, it is advantageous to have an adjustable pulse length from the solenoid driver, which can then be trimmed to suit operating conditions at will, and independantly of the duration of the recharge part of the integrator cycle.

Two circuits were evolved to fulfil this need. The first consisted of taking the conventional monostable flip-flop circuit of Fig 49 and developing it for operation at micropower consumption levels and at -25°C . This circuit, fully developed, gave way however to the intrinsically superior circuit shown in Fig 50 . This second circuit, originated by FURUICHI and SASAKI (1968) has the advantages of having zero power consumption in the normal static state, and of using fewer components. The basic circuit is shown in Fig 50 , the final circuit below it in Fig 51 .

5.G.5 Signal input circuitry

The original, and simplest method of coupling a photodiode,

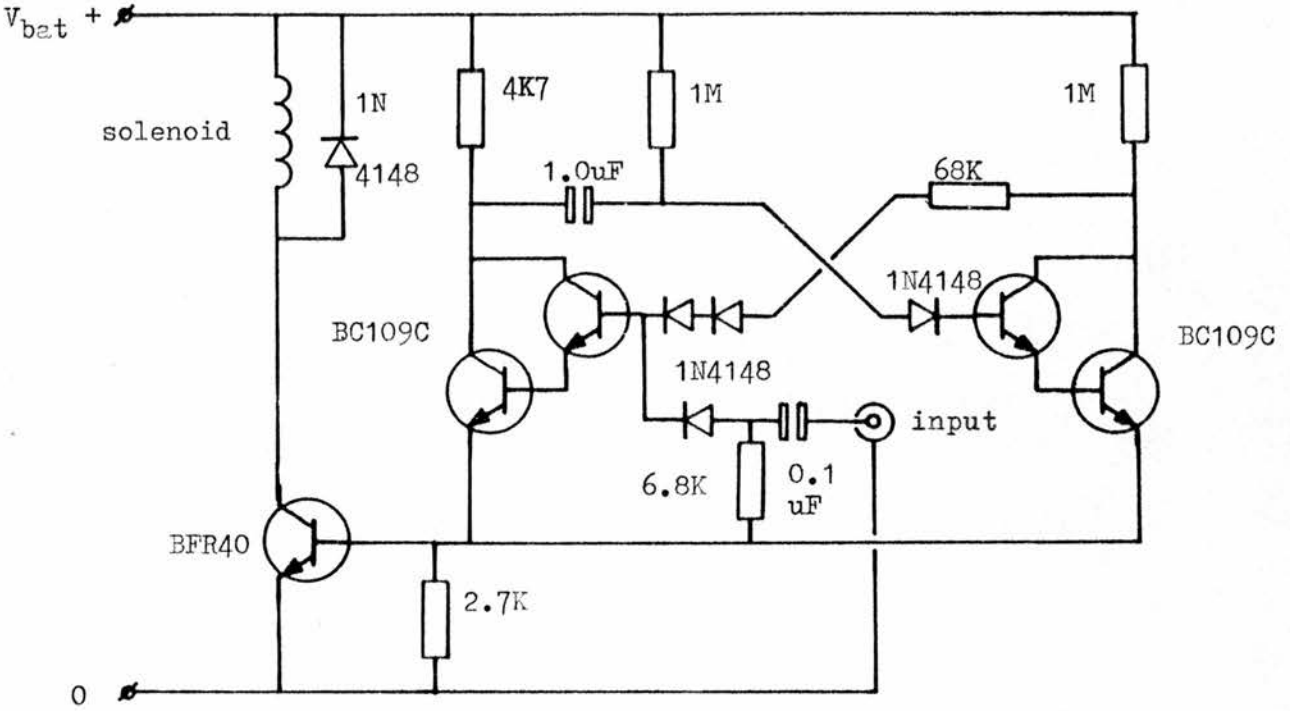


Fig. 48 Micropower monostable oscillator - original circuit

Current Consumption:

@ V supply

8.5V	15 μ A
11.5V	21 μ A
14.5V	27 μ A

Pulse Length:

@ -25 C	860mS
+12 C	850mS

@ 12°C Room temperature

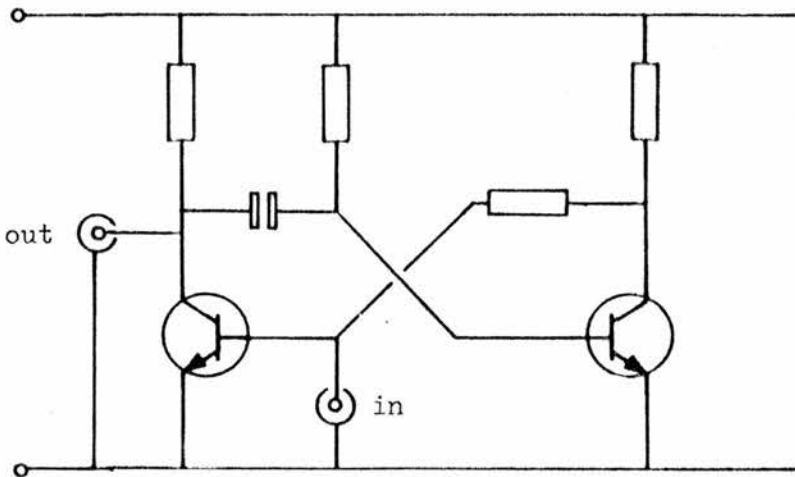


Fig. 49 Basic monostable oscillator circuit

the current source for which the integrator has been designed, to the integrating capacitor, C6 (Fig 28) is to place it directly across the terminals of the capacitor, observing photodiode polarity, as in Fig 52 . This simple method is satisfactory provided the reverse bias voltage which the photodiode can withstand is not less than the peak voltage to which C6 charges. This is not the case with many of the higher quality photodiodes available today, (see appendix 3) nor with the photogenerative cells of the silicon 'solar cell' or selenium type.

Fortunately, there is a simple solution available, the NPN (or PNP) silicon planar transistor, operated in Common Base mode. Figs. 58, 59 and 60 show the input, output, and transfer characteristics obtainable in this mode of operation. It will be appreciated from these that the transistor may be used as a constant current generator, directly controlled by the photocell, as in Fig 53 . From the input characteristic (Fig 58) it will be apparent that the photodiode-driving cell combination 'looks into' a load which is a forward biased junction across which there naturally never develops a voltage much higher than 0.6V.

Photodiodes with low reverse breakdown voltages can thus be driven with a single 1.4 volt cell, possibly in series with a silicon diode to drop the voltage to give ca. 0.8V. bias on the photodiode itself.

The output characteristics in Fig 59 show that the collector-base junction of the transistor makes a near ideal 'current sink', capable of discharging the capacitor C6 totally, should other circuit conditions permit it. The breakdown voltage of this junction is far above that to which it is exposed in the circuit of the integrator, and the minimum voltage which triggers the recharging process lies between 1 and 2 volts, according to the individual properties of

Q8-Q9 (Fig 28).

The forward current transfer ratio of the transistor is very nearly unity, as is apparent from Fig 60, and only begins to depart from this ideal condition when leakage current, I_{cbo} in standard nomenclature, assumes a significant part of the total current flowing. Fortunately, with modern transistors, such as the ubiquitous BC109C used in the circuit, this current is very low indeed, as is shown by Fig 57 SIEMENS (1979). It could be reduced still further by the use of a high-voltage planar transistor, for example the BF 259.

If, for the sake of argument, the lower (triggering) voltage on C6 is 2.5 volts, it is then permissible to insert any desired load into the return path between the base of the transistor and the minus side of the capacitor, provided that the voltage across this load never exceeds 2.5 volts at the maximum current ever to be correctly integrated. Fig. 54 shows two useful possibilities. The first provides for measurement of instantaneous current flowing in the integrating circuit. Provided that a low-resistance multimeter is plugged into the appropriate socket, the voltage across the two diodes will be insufficient to make them conduct, and the meter will give a true, unshunted, reading. (The forward conduction characteristic of a typical silicon diode is shown in Fig. 56). Upon disconnection of the meter, the forward conduction voltage of the diodes, ca. 1.2V, will be exceeded, and the integrator current will continue to flow uninterrupted, and unmodified.

The second possibility was referred to in section 2: that of using more than one value of C6, and hence sensitivity, in the integrator. The resistor R_{det} develops a voltage across its ends

in proportion to the integrator current flowing, and this voltage can be used to trigger appropriate range-changing circuitry, as is further discussed in section 6.

A third possibility which has also been tested, is the insertion of a second constant current generator, as shown in Fig. 61, which can act as an 'electronic end-stop' blocking the passage of any current above a predetermined level, set in the base-emitter arm of the circuit. Experimentally, this circuit was set to a 'stop' value of $100\mu\text{A}$, and Fig 63 shows a graph of the performance.

5.H Testing procedures for the integrator

5.H.1 Introduction

A piece of scientific equipment is only as good as the tests which it has passed, and if it has not been tested, it is scientifically speaking useless, even if it should later prove to work perfectly. It is important, therefore, that a testing routine should be constructed which can readily be implemented before, after and during a scientific research programme. Some tests, such as those on combined effects of temperature and supply voltage extremes probably need only to be done before initial acceptance of a piece of equipment, but others - calibration of the integrator input-output characteristic - for example, should be done regularly, particularly if there is any suspicion of dirt or water having entered the housing.

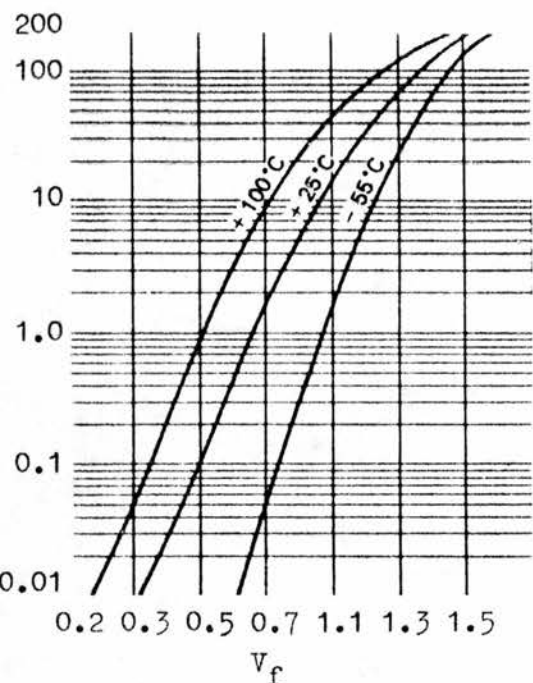


Fig. 55 Effect of temperature on forward voltage drop in one typical sample of the 1N4148 diode

(TEXAS INST.

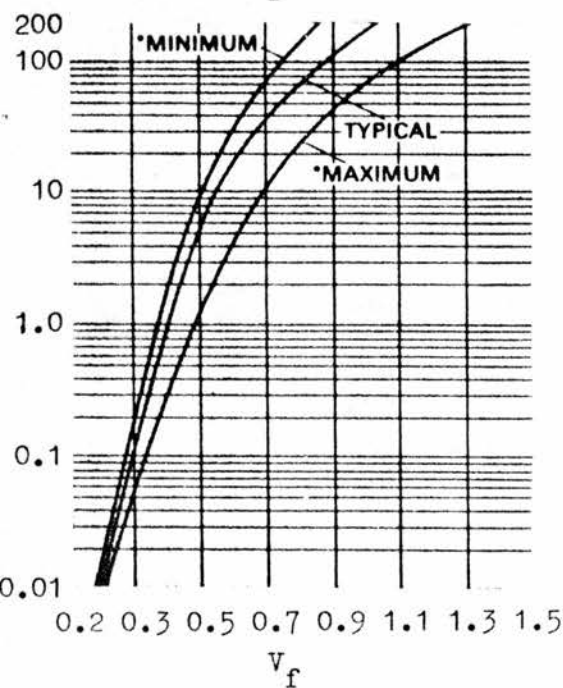


Fig. 56 Variability in forward voltage drop across a typical small-signal silicon diode - the 1N4148

(TEXAS INST.

Collector base cutoff current versus temperature $I_{CB0} = f(T_{amb})$ for maximum permissible reverse voltage BC 107, BC 108, BC 109

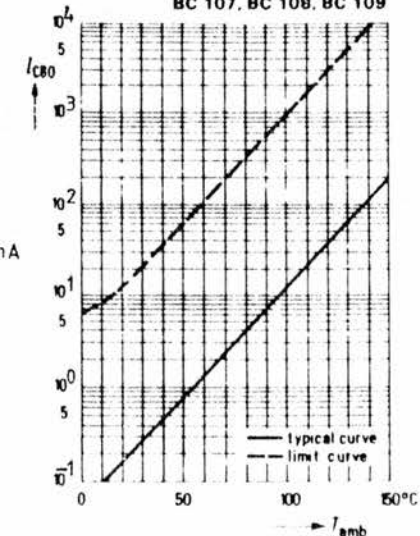


Fig. 57 I_{cbo} , the leakage current flowing from collector to base with the emitter left open circuit, showing the very low values typically found in the ordinary silicon planar transistor.

(SIEMENS

Reproduced from AN INTRODUCTION TO SEMICONDUCTORS by K.J. Close and J. Yarwood by permission from Heinemann Educational Books Ltd.

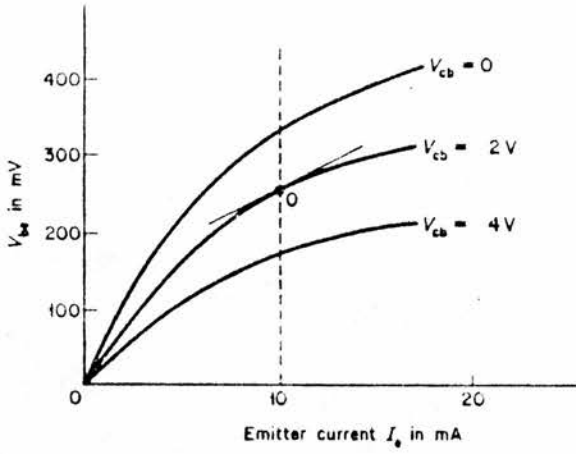


Figure 58 Typical input characteristics of a n-p-n transistor in common-base connection

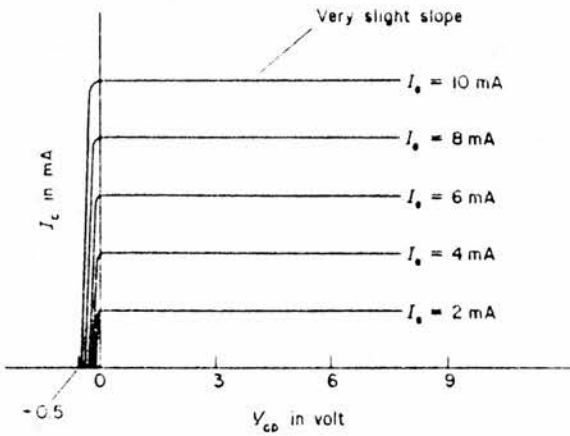


Figure 59 Typical output characteristics of a n-p-n transistor in common-base connection

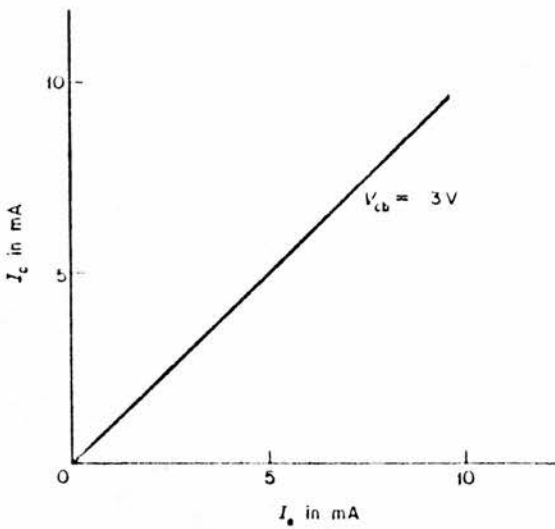


Figure 60 Typical current transfer characteristic for a n-p-n transistor in common-base connection

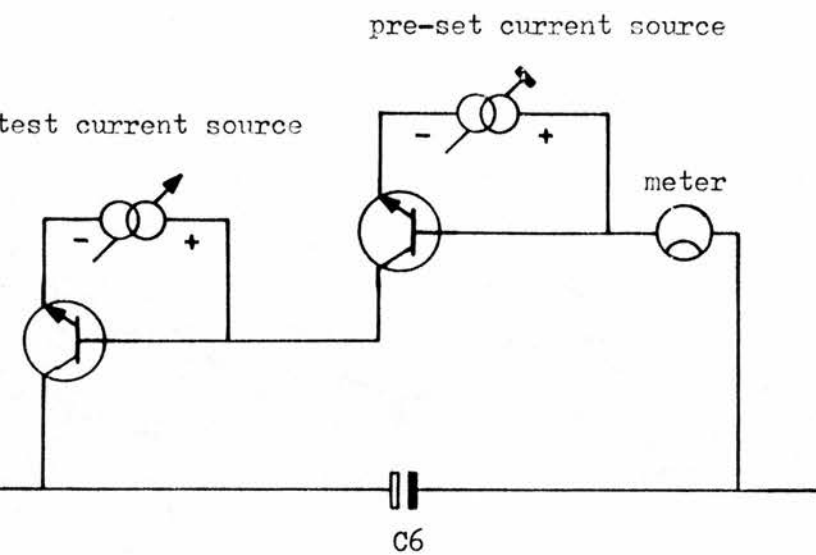
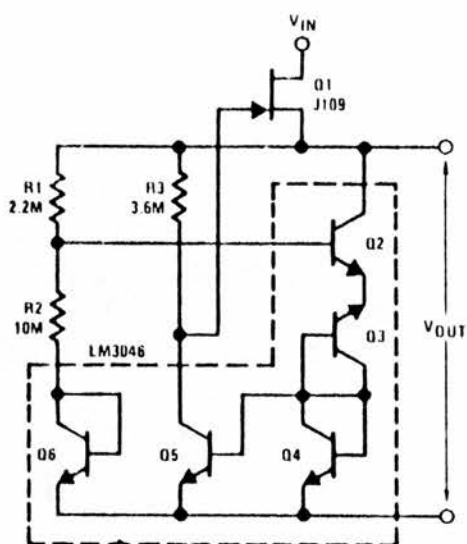


Fig. 61 The use of a second, earthed-base transistor as a pre-set "end-stop" current limiter

pp.118 - 9 for an explanation of the circuit.



Output Voltage

$$V_{OUT} = V_{BE} \left(2 + \frac{R1}{R2} \right) + BV_{EB} \left(1 + \frac{R1}{R2} \right)$$

Drift

$$\frac{\Delta V_{OUT}}{\Delta T} = \frac{\Delta V_{BE}}{\Delta T} \left(2 + \frac{R1}{R2} \right) + \frac{\Delta BV_{EB}}{\Delta T} \left(1 + \frac{R1}{R2} \right)$$

Quiescent Current $\approx 4 \mu A$

Micropower Regulator

Fig. 62 Micropower voltage regulator

(NATIONAL SEMICONDUCTOR

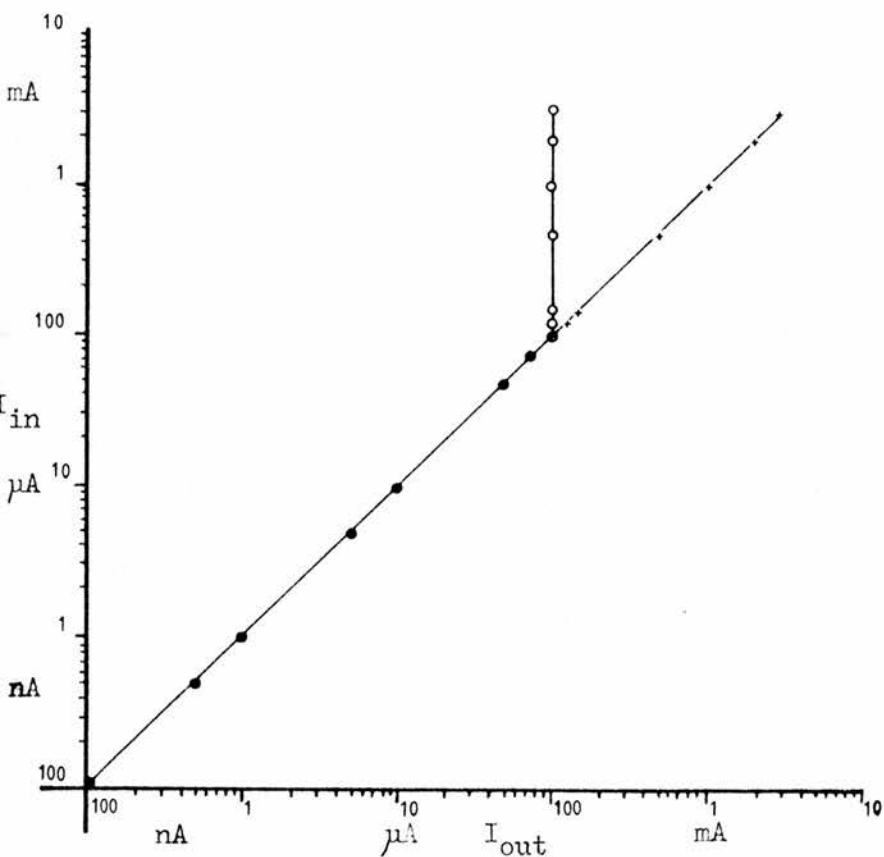


Fig. 63 Graph of typical performance of " electronic end-stop " pre-set to operate at 100 μA . Circles - with end-stop operating
Crosses - with end-stop by-passed. See p. 119

For advice on the good design of meteorological instruments, THALLER (1970) can be recommended.

5.H.2 Tests for linearity

In a procedure to test the linearity of the circuit, the simple arrangement in Fig 64 was adopted as a source of current to the integrator. In this circuit a stable voltage source - V - and the 1K multiturn potentiometer R1 serve as a voltage source variable down to 0V. For any voltage selected, R2 - R5 will pass a current, monitored by the meter, into the input of the integrator, ie. to Q6 junction (Fig 28). The calibration graph, showing time between output pulses of the integrator, against input current, is shown in Fig 65, and was prepared using this simple current source in conjunction with an Electronic Avo multimeter model EAll3. The circuit shown in appendix 10 is for a superior current source which dispenses with the need for a meter, since the current is selected on a 10 - turn Beckman Helipot dial, giving resolution down to better than 1% F.S.D. over each range selected.

Deviation from absolute calibration might be caused by drift in the value of C6, or changes in those parts of the integrator circuit which detect the voltage thresholds on C6. Poor linearity at high currents will probably be due to the mis-setting of R12 (Fig 28), the dead-time compensation resistance, or, at low currents, leakage paths caused by moisture, dirt, or both affecting C6, C8, Q6, Q8 or D10, (Fig 28), or else to poor internal leakage properties of these components, the testing of which is considered in section 5.H.6.

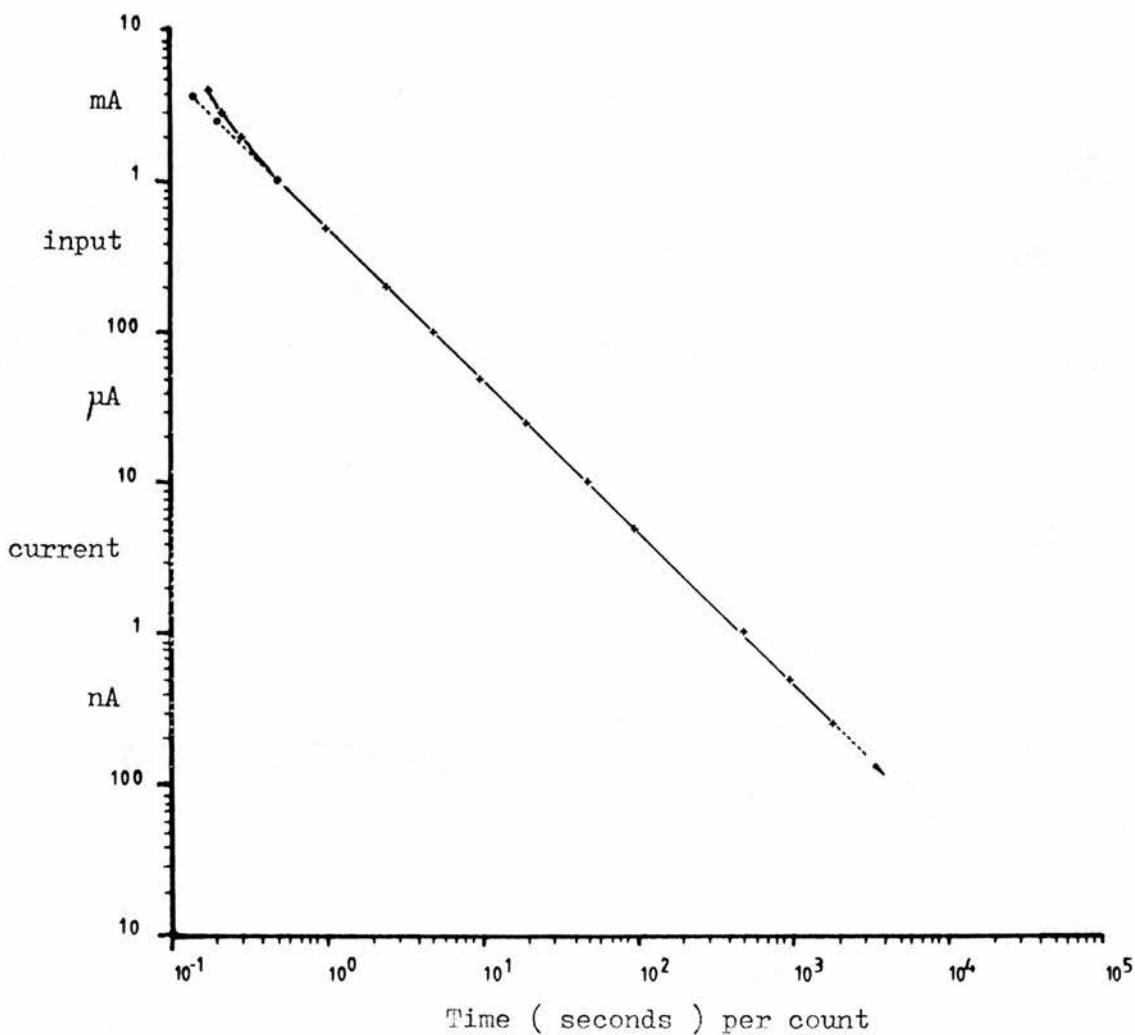


Fig. 65 Linearity of prototype integrator. Deviation from linearity at low currents (not here apparent) due to leakages in C6, C8, Q6 or D10 (Fig. 28); and at high currents due to mis-setting of R12 - here correctly set to 355 ohms. Graph shows effect of both presence and absence of linearity correction circuit.

also see Fig. 94

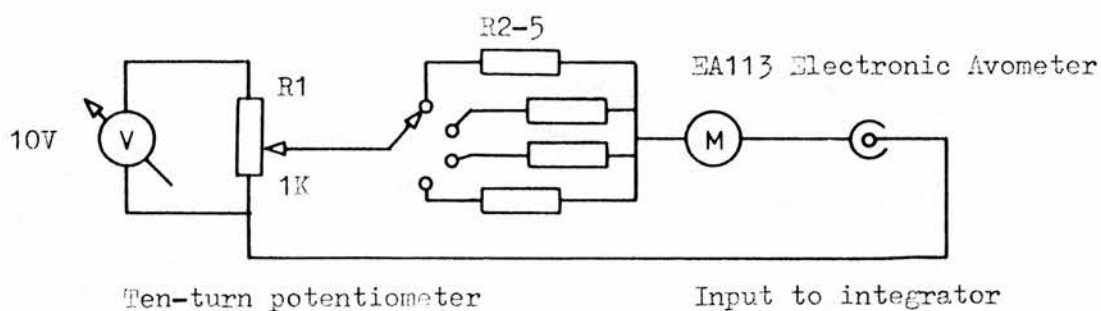


Fig. 64 Simple current source for integrator linearity tests

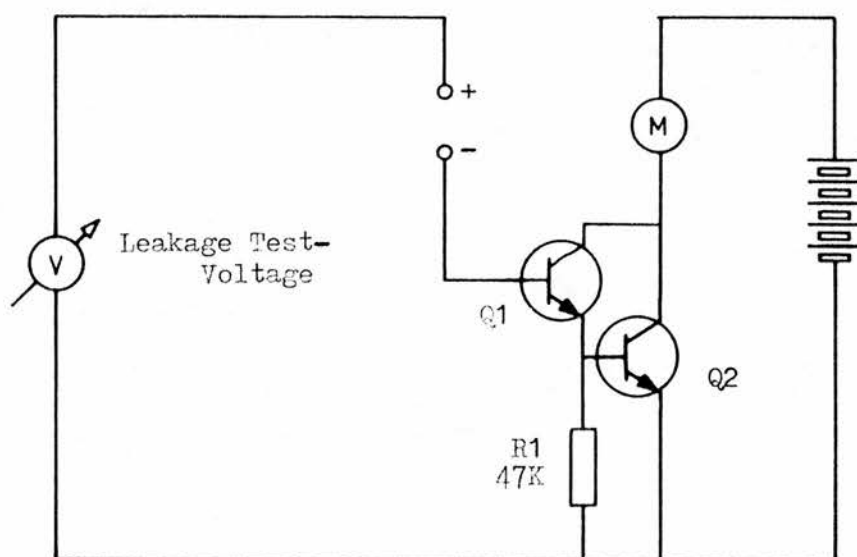


Fig. 66 Simple test circuit for evaluating semiconductor junction reverse leakage-current properties. Q1 and Q2 are almost any silicon planar transistors. Calibration is based on substituting known high value resistors for the test subject. M is an ordinary laboratory milliammeter.

5.H.3 Testing for thermal failure

As was mentioned in section 5.G.2, transistor gain falls considerably with decreasing temperature. On the other hand rising temperature increases semiconductor junction reverse leakage characteristics, this leakage current approximately doubling for each 10° Centigrade rise, see for example, Fig 57 . The most important of these leakage currents is that known as I_{ce0} , ie. the current flowing external to the transistor proper, but still through the material of the transistor, out of the collector region and back into the base. If there is no external resistance path between base and emitter, this current will flow into the base region, and be amplified to cause considerable static flow of collector current. Where there is such a path, as is provided, for example, by R3 in relation to Q1 (Fig. 28) it is found that the turn-on voltage of the b-e junction is rarely exceeded, and the leakage current flows safely out of the transistor to ground.

For these reasons, before time is spent on detailed evaluation of a circuit configuration, it is best tested with the extremes of temperature to be met with. For cold, an aerosol refrigerant is caused to evaporate on the surface of the semiconductors under test, a convenient product being RS Components 554-765. This is stated to reduce temperatures to -45°C , but that will depend on conditions of use, and for the present purposes a reduction of temperature to -25°C has been assumed. This refrigerant is an electrically insulating liquid which can readily be directed on to the components under examination by means of the narrow-bore tube attached to the can. For heating, a hair dryer is admirable.

In practise, a milliammeter is used to monitor circuit current flowing in the region under test, and this will give early warning of impending failure. In the case of the integrator, it is instructive to cool first Q4 and Q5 (Fig 28) then D6-8 and Q7, then all of these at once, and compare the effects on the static supply current to the circuit.

5.H.4 Testing the temperature co-efficients

The temperature co-efficient of the integrator was tested under six conditions - two temperature bands and three test currents (see page 106 for the measurements.)

The lower temperature was that of a deep-freeze. The integrator was enclosed in a polythene bag before being placed in the freezing compartment, to prevent problems of condensation in the circuit upon removal to the moist air of the room after the test. The power supply, input and output leads were lead out into the room, the soft gasket of the deep-freeze lid preserving the seal within, and the integrator was left for an hour to equilibrate.

The high temperature was obtained with a hair drier, the nozzle of which was inserted into a cardboard box containing the integrator. Since the flow of hot air through the box was high, it was assumed that the temperature inside was homogeneous, although the actual temperature was only measured in one spot. Since the air was moving, equilibrium was reached much more quickly than in the deep-freeze. In all cases, succeeding test periods were used until thermal equilibrium had been attained and no further change in the resulting co-efficient was apparent.

5.H.5 An abnormal state - the 'stalled' integrator

In early forms of the integrator, a worrying and faulty mode of operation would occasionally manifest itself. This may be designated 'stalling'. It is possible to envisage an electrically stable state in the integrator in which C6 (Fig 28) is totally discharged, there is no negative bias voltage on the gate of the Q8-Q9 combination (which therefore conducts); and C10 has charged so that R16 biasses Q7 on, as in the normal 'quiescent' state of the integrator. The only way to break this stalled state is to artificially switch Q7 off, using the press-switch SW1 to earth Q7 base momentarily.

The early versions of the integrator would occasionally pass into the stalled state when the current being integrated fell to nothing for long periods, as naturally would happen at night for a radiometric integrator. With no current being integrated, the dv/dt value on C6 falls to a very low level dictated by residual leakage currents in the circuit. When the lower threshold voltage on the capacitor C6 is passed very slowly, the corresponding change in voltage from high to low at points J-X (Fig 28a) will also be slow, especially if the gain of the Q8-Q9 pair is low. If this voltage change is exceedingly slow, C10 may not couple the change to Q7, which will therefore never initiate the recharge phase, and the integrator will pass into the stalled state just referred to.

One way of lessening the chances of stalling occurring is to increase the gain of the Q8-Q9 pair. Originally Q8 alone was present, but Q9 was added in a successful attempt to cure this problem. The

conditions of maximum likelihood for stalling to occur are those of lowest temperature, lowest battery voltage, and zero integrating current. Providing that the integrator remains functional under these conditions, there need be little fear of stalling occurring under normal operating conditions. When power is first applied to the integrator, it may start either by remaining in the stalled state until SW1 is momentarily pressed, or else the first operation will be a spontaneous recharge cycle. In all events, it is best to depress SW1 initially, to be sure that the integrator really is operational.

When testing the circuit for freedom from stalling tendencies, it is simplest to connect a voltmeter across the terminals of C6 (from E-H in Fig 28a) and observe the lower threshold voltage. The integrator will cycle fairly rapidly, owing to the current path provided by the internal resistance of the meter. With practice it is possible to shed most of the charge in C6 before removing the meter load and waiting to see if the spontaneous cycling of the circuit will occur. An oscilloscope with high-impedance probe, connected between points J-X (Fig 28) will show whether or not the circuit is 'alive', or has stalled.

As was revealed by Fig 38 , the circuit is very sensitive to extraneous electrical interference when the voltage on C6 approaches the lower threshold, and only great care and repeated testing will show that the circuit is genuinely stall-proof, and not merely responsive to noise voltages originating extraneously.

On occasion it has been found necessary to wait at least an hour for the expected recharge cycle to occur, and it is conceivable that the unhappy coincidence, within the one example of the

circuit, of almost perfect insulation in C6, and very low leakage in D10 and Q8 gate-source terminals, could result in the dv/dt value on C6 being so low that the circuit would inevitably stall. If this seems to be a possibility, the simplest answer is to 'slug' the circuit with a small false leak, to ensure a certain low background count, and sufficient dv/dt to be free of stalling. In practice, it has not so far been necessary to do this.

5.H.6 Testing D10, Q8 and C6 for low leakage

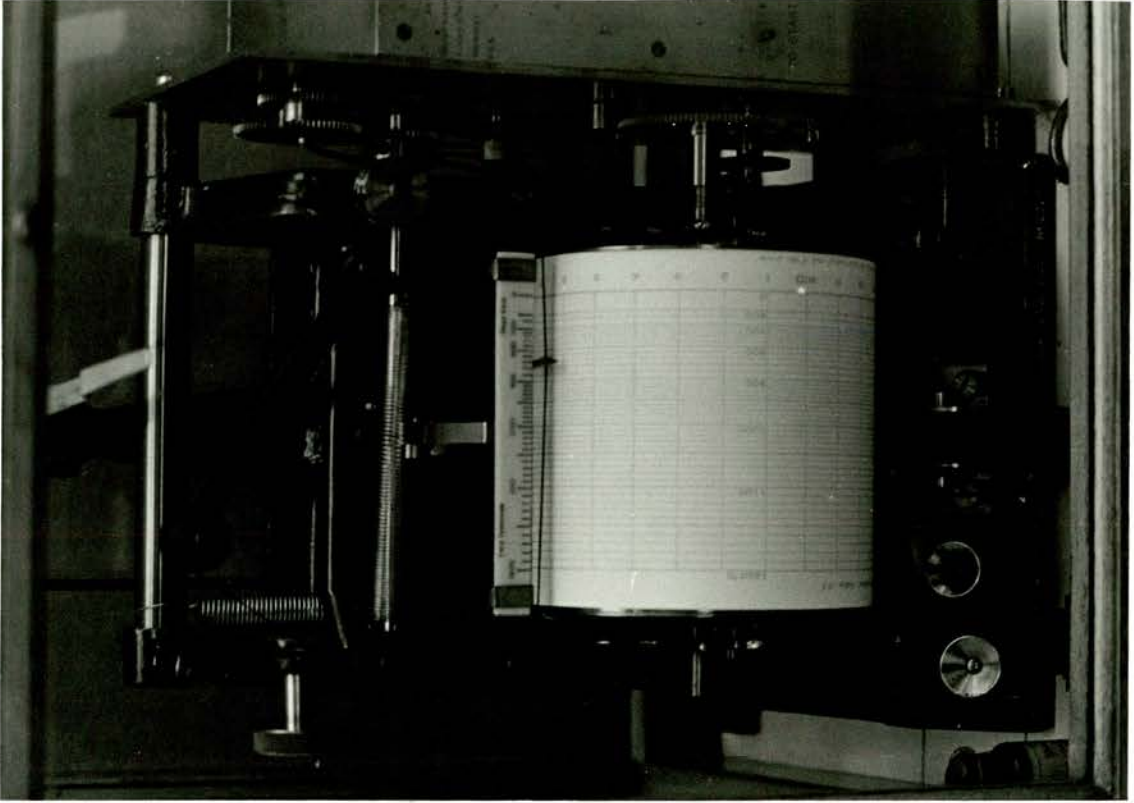
In view of what has been said in section 5.H.5., it might seem strange to wish to select samples of D10, Q8 and C6 for unusually low leakage. However, with C6 values reduced to nano- or picofarad values, the circuit can be used with extremely low integrating currents, as may be supplied by small-area radiometric sensors operating in environments of low irradiance, for example, moonlight.

In a procedure for selecting low leakage current, the simple circuit shown in Fig 66 is quite adequate for testing semiconductor junction leakage currents, on a 'best of the bunch' basis. M can be a simple laboratory multimeter, and almost any silicon planar NPN transistors will serve for Q1 and Q2. If the temperature of the room in which the circuit is used remains fairly constant, an approximate calibration in nanoamperes can be found using high-value resistances across the + and - terminals, (Fig 66), and varying the test voltage V.

Plate 1. An early production model of the Cambridge chopper bar recorder devised by Sir Horace Darwin (1905)

displayed in the Science Museum, London

Plate 2. Callendar's radiometer of 1898, consisting of blackened and bright platinum resistance thermometer elements connected in a bridge. Callendar used it in conjunction with his new recorder from 1897, more than one mile of cable separating the radiometer head from the recorder. The original instrument is now in the Science Museum, London. See Callendar (1898)



Plates 3 and 4

Two views, with cover and without, of the first chopper bar recording galvanometer, designed by August Raps (1897) and made by the firm Siemens and Halske. Taken from Elektrotechnische Zeitschrift.

see Raps (1897) and Heiden (1969)

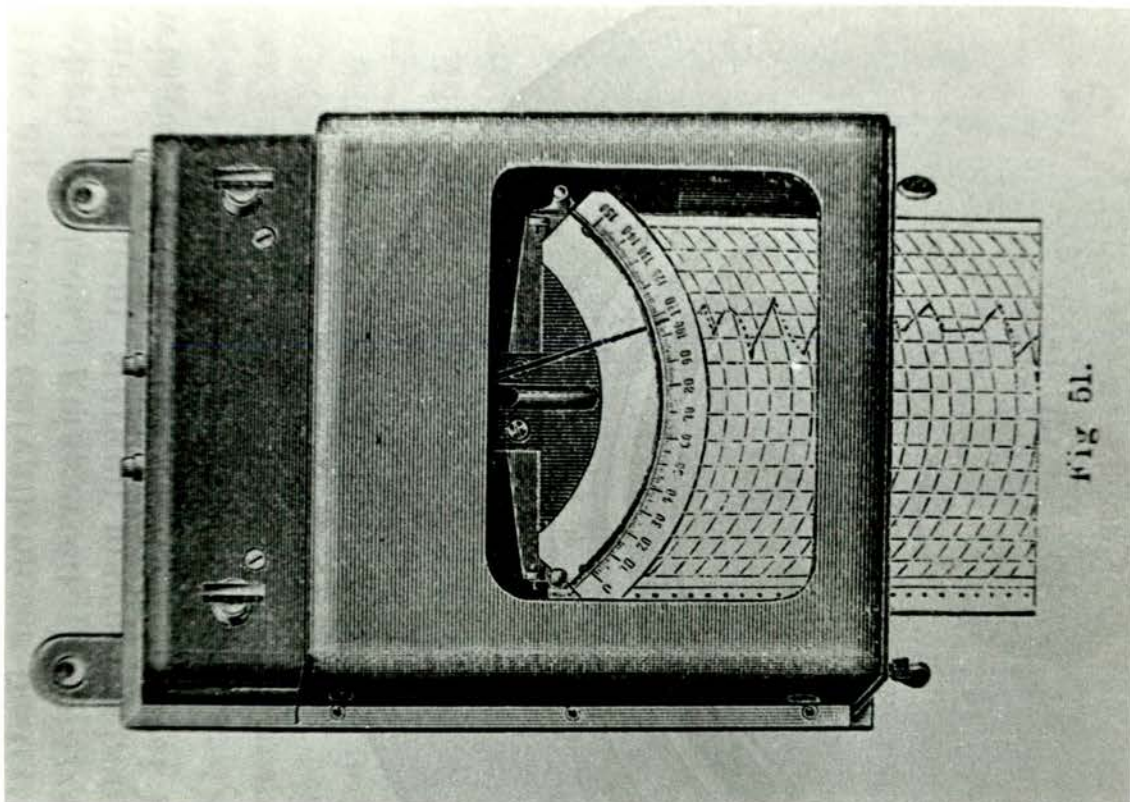


Fig 5L.

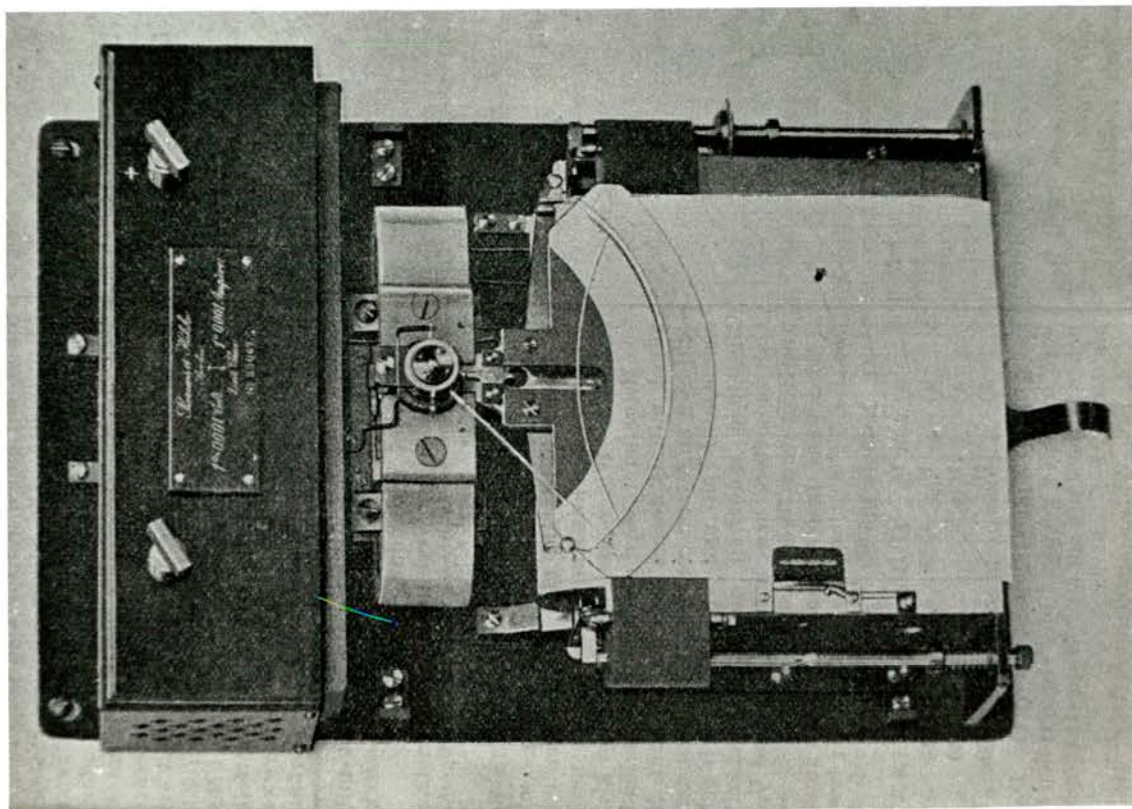


Plate 5. One of the first potentiometric chart recorders, of the design due to H.L. Callendar (1897), now on display in the Science Museum, London. For a description of the operation, see text, page 58.

Plate 6. Possibly the first chart recorder, this design of 1880, the 'Spannungsregistrier-apparat' of Siemens and Halske marked the paper with pin pricks at intervals. See text, page 58 for a description of operation, and also Heiden (1969)

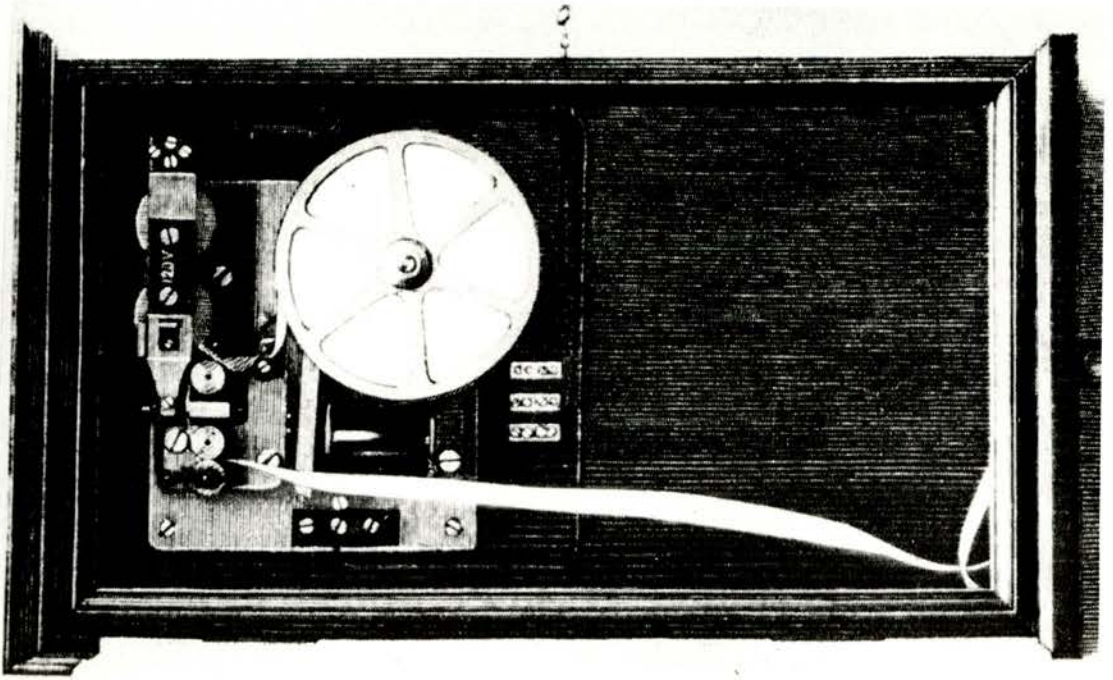
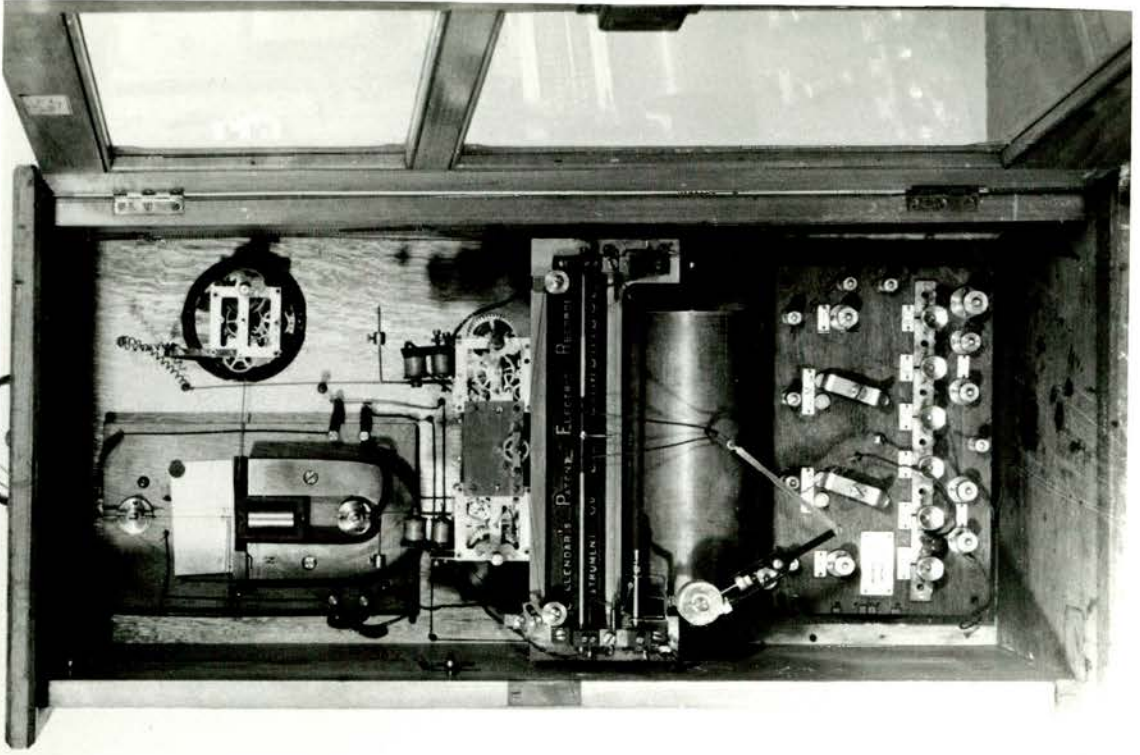


Plate 7. The new recorder, side view

Plate 8 The new recorder. Detail showing clearly the hot wire pen, path of paper tape, ratchet wheel and actuator.

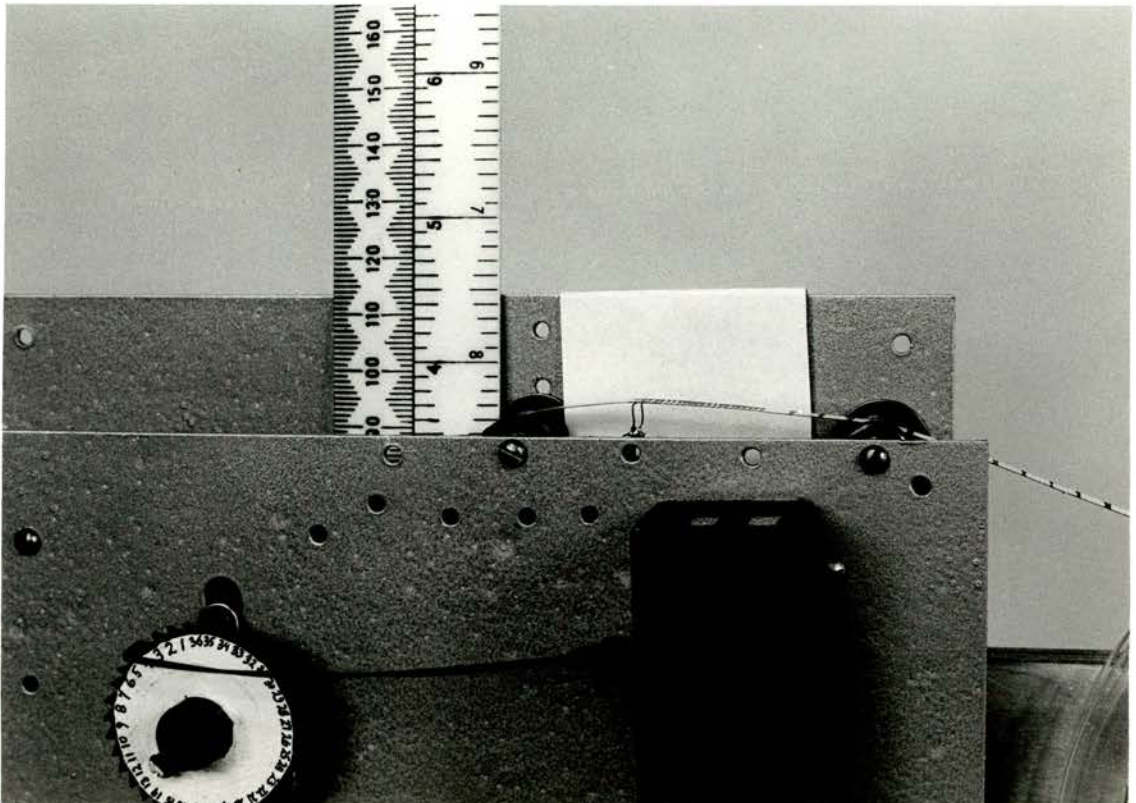
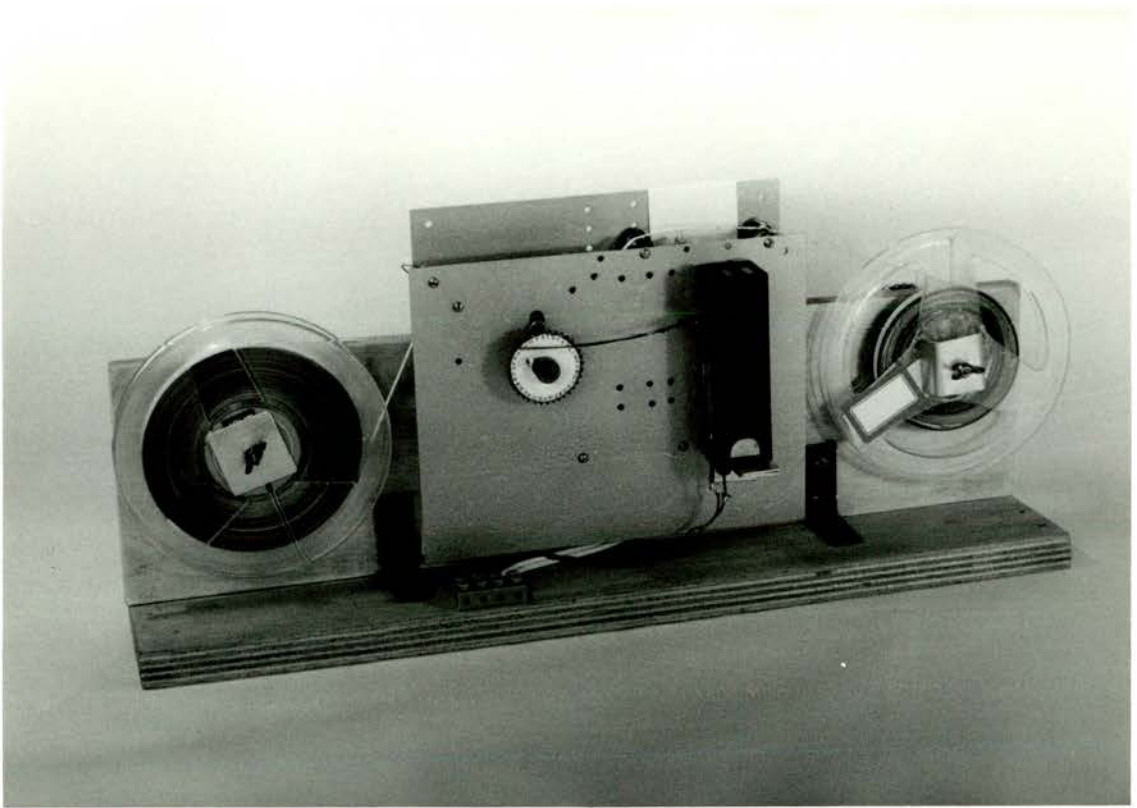
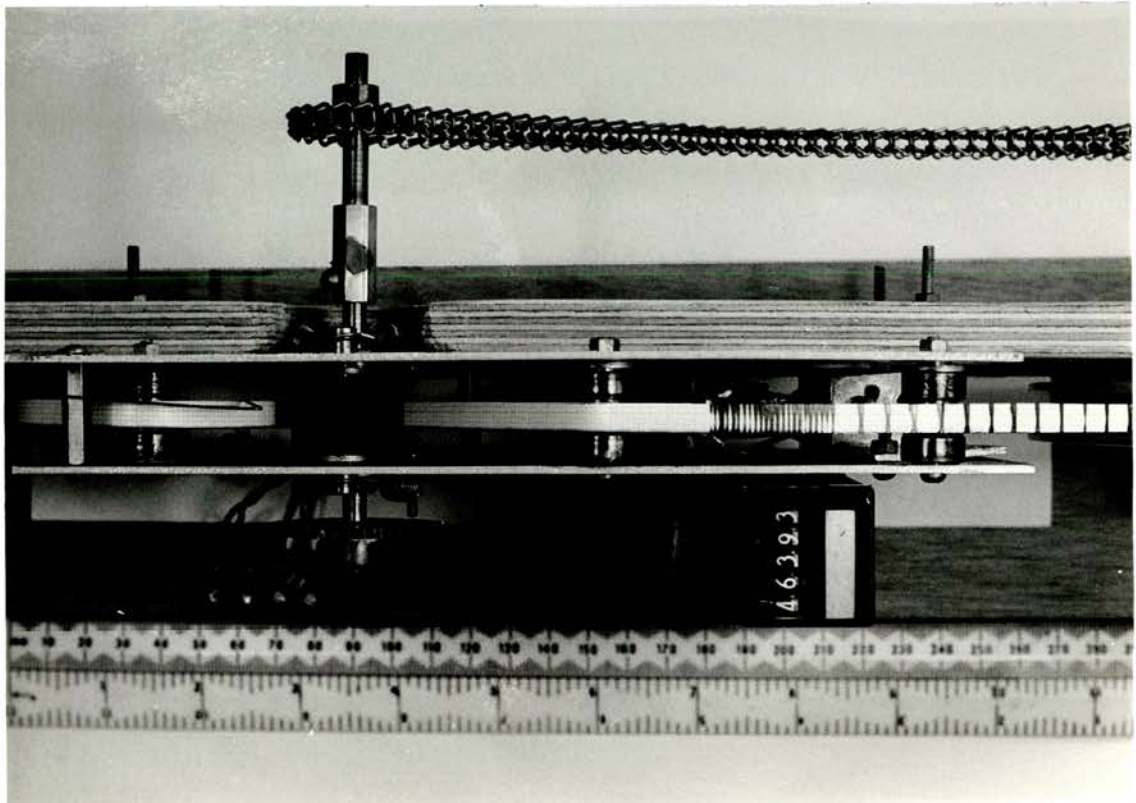
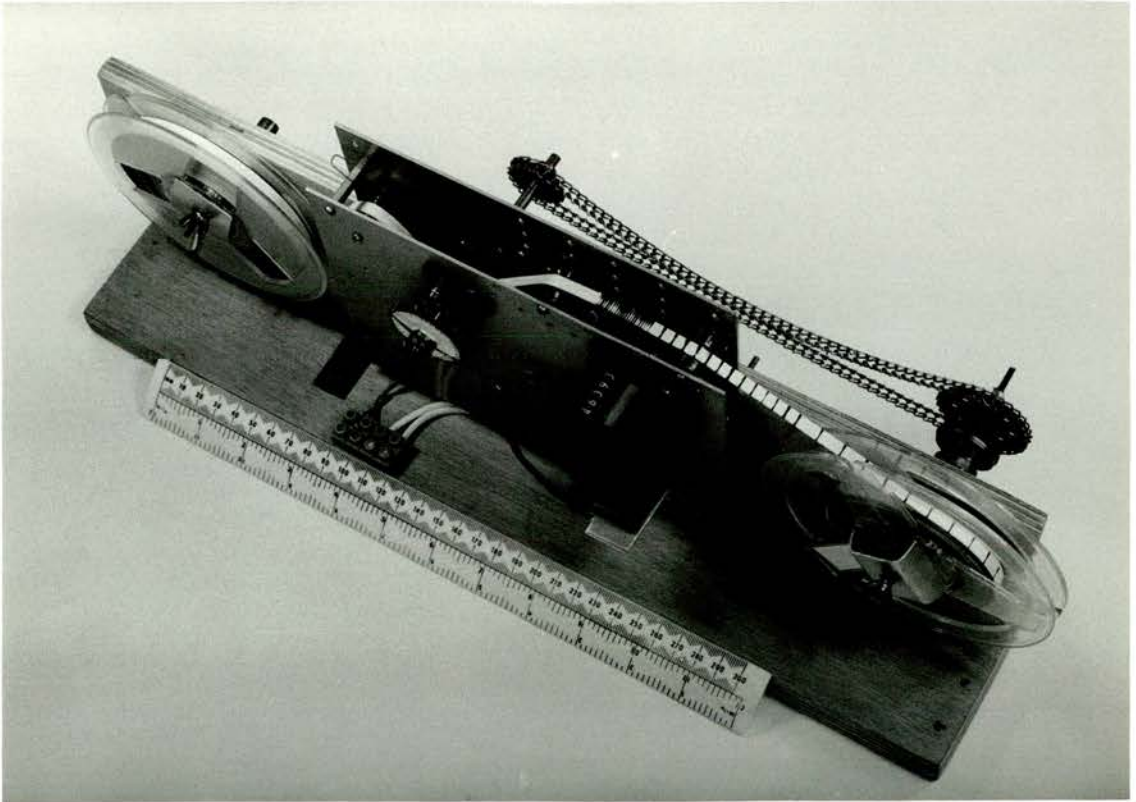


Plate 9. The new recorder. Oblique view. The diagram Fig. 24 identifies the parts visible in this photograph.

Plate 10. The new recorder. Vertical view, showing clearly the path of the tape, with time marks. Note the single tape supply-decoupling spring. See Fig. 25



For capacitors, the simplest test method, and the one applicable here, is to charge the capacitor under test to a suitable voltage, then disconnect all connections to the 'hot' end of the capacitor. The capacitor will then discharge only through its own leakage resistance, and its quality may be determined after a suitable time delay by momentarily measuring the residual voltage present across the terminals (with a voltmeter of suitable high impedance). MACHATTIE (1971) gives suitable circuits and discusses measurements further. FRANCE (1960) explains why more seemingly direct methods of measurement on capacitors are usually invalid. He states that even most manufacturers' data are erroneous because of their testing methods. However, it is also true that the self-time constants given for their products by manufacturers usually err greatly on the side of caution.

CHAPTER 6

THE DEVELOPMENT OF AN AUTO-RANGING CIRCUIT FOR USE WITH THE
INTEGRATOR-RECORDER COMBINATION

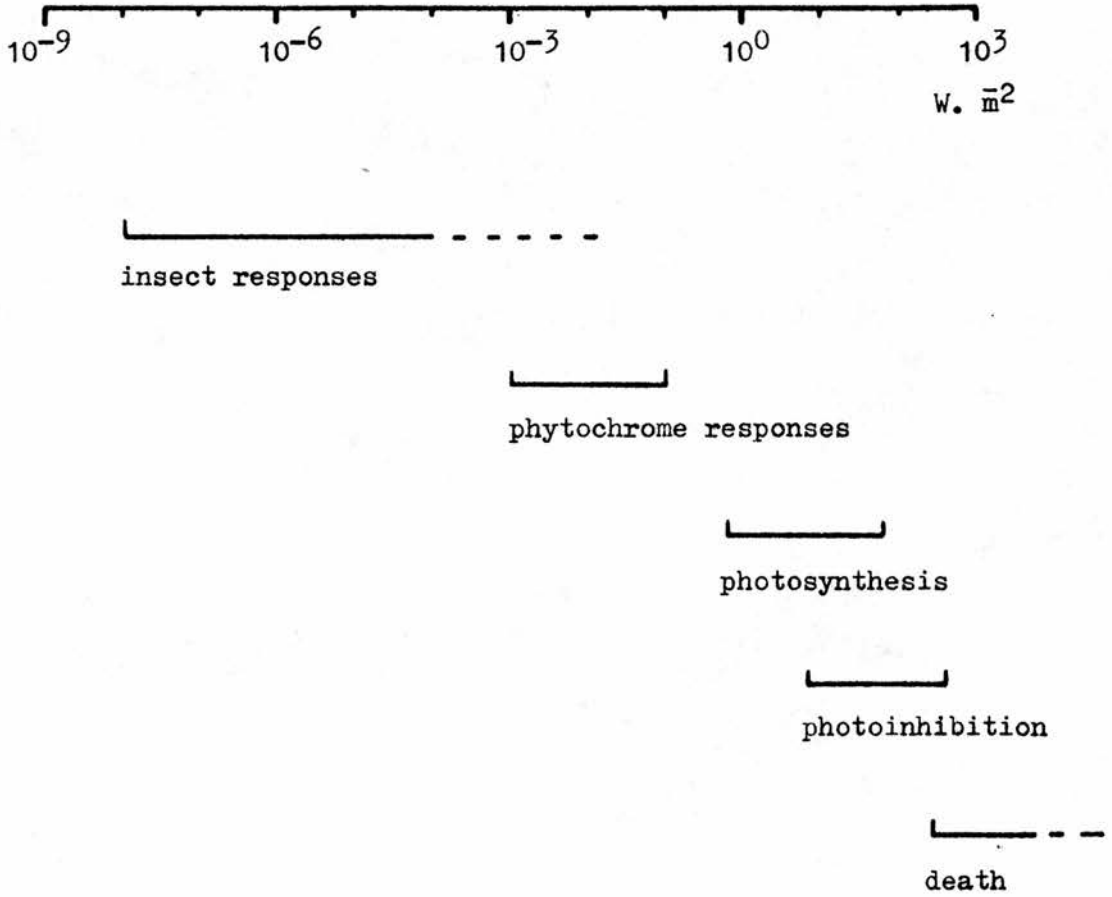


Fig. 67 Approximate natural irradiance levels and the operation of some natural responses, illustrating the extremely wide range of natural irradiance levels for which some kind of response occurs.

6 THE DEVELOPMENT OF AN AUTO-RANGING CIRCUIT FOR USE WITH THE INTEGRATOR-RECORDER COMBINATION

6.A.1 Background

The special problem inherent in radiometric measurement done in connection with ecological work is the enormous range of irradiances which evoke significant responses in the biosphere, as shown in Fig 67 , see opposite . A study of the irradiance graphs produced by the recorder and integrator in the single-sensitivity form (Figs 91 and 92) clearly shows that, for Fig 92 , much greater sensitivity in the integrator would have been an advantage. In chapter 5 , the basis for range-changing has already been laid down. In Fig 28 , in addition to C6 there is shown a smaller-value integrating capacitor, C7, either being selected by the relay contacts RL1. The means for monitoring the current being integrated is the resistance R13/1A, across which develops a voltage in proportion to the current being integrated. This voltage is used to control the operation of the automatic range-changer, and in Fig 28 is shown leading to a socket marked 'to level detector'.

6.A.2 The dynamics of radiometer auto-ranging

Before the voltage analogue of the irradiance signal passes from R13/1A (Fig 28) into the range changing unit proper, it passes to the damping network shown within the blue box in Fig 74 . This network, having two time-constants, modifies the rise and fall of the voltage passing through it, to give a fast rise and slow

decay. Additionally, the voltage sensor of the auto-range unit incorporates hysteresis, ie. if the sensor changes output from state A to state B when the input voltage rises above a certain value X, then when the voltage falls, it must pass considerably below value X before the sensor output will change from state B back to state A again.

The purpose of these complications in the response pattern of the auto-range unit is to prevent the integrator from responding to merely short-term fluctuations in irradiance values. In this way, change in sensitivity only occurs when general trends in irradiance levels make a change appropriate. The exception to this rule is that the unit has a rapid response to extreme changes from low irradiance to high irradiance, in order to prevent possible damage to the integrator through overloading.

The basic circuit for the damping network is shown in Fig 68 and Fig 69 shows the response time for the network when attached to the input of the range change switch. Resistor R13/1A (nomenclature as in Figs 28 and 73) is adjusted empirically to suit the prevailing field conditions. If, as is possible, the range changing is required to occur only at dawn and dusk, R13/1A will have a high value (100-200K) to produce the typical switching voltage of 1.0v from an input of only ca. $10\mu\text{A}$ photocurrent. Since the noon photocurrent on a Summer day can be about 100 times this value, an element of non-linearity is wired in parallel to R1A/13 (D1 and D2) ensuring that the maximum voltage drop of peak photocurrent does not much exceed 1.5V. In Fig 68 D1 and D2, two series connected silicon diodes are used, however this is an inflexible arrangement, and the variable 'pseudodiode' of Fig 70 and 71 is recommended instead.

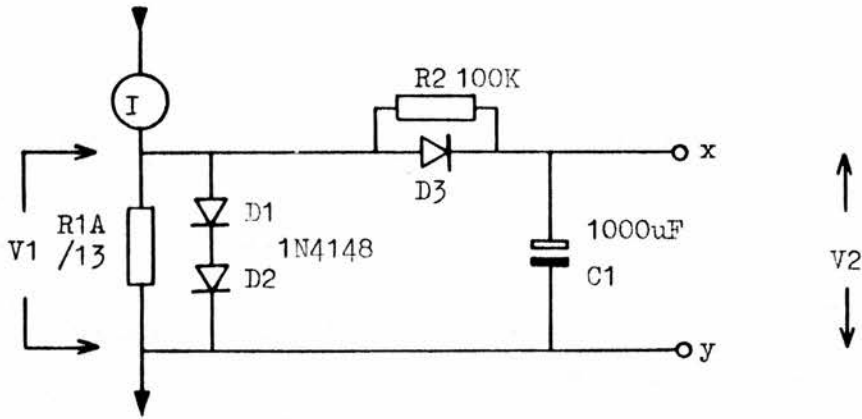


Fig. 68 Basic damping network employed at input to range-changing switch. The rise time is relatively fast and is set by extraneous impedance x $C1$, the slower fall time is set by $(R1 + R2)(C1)$

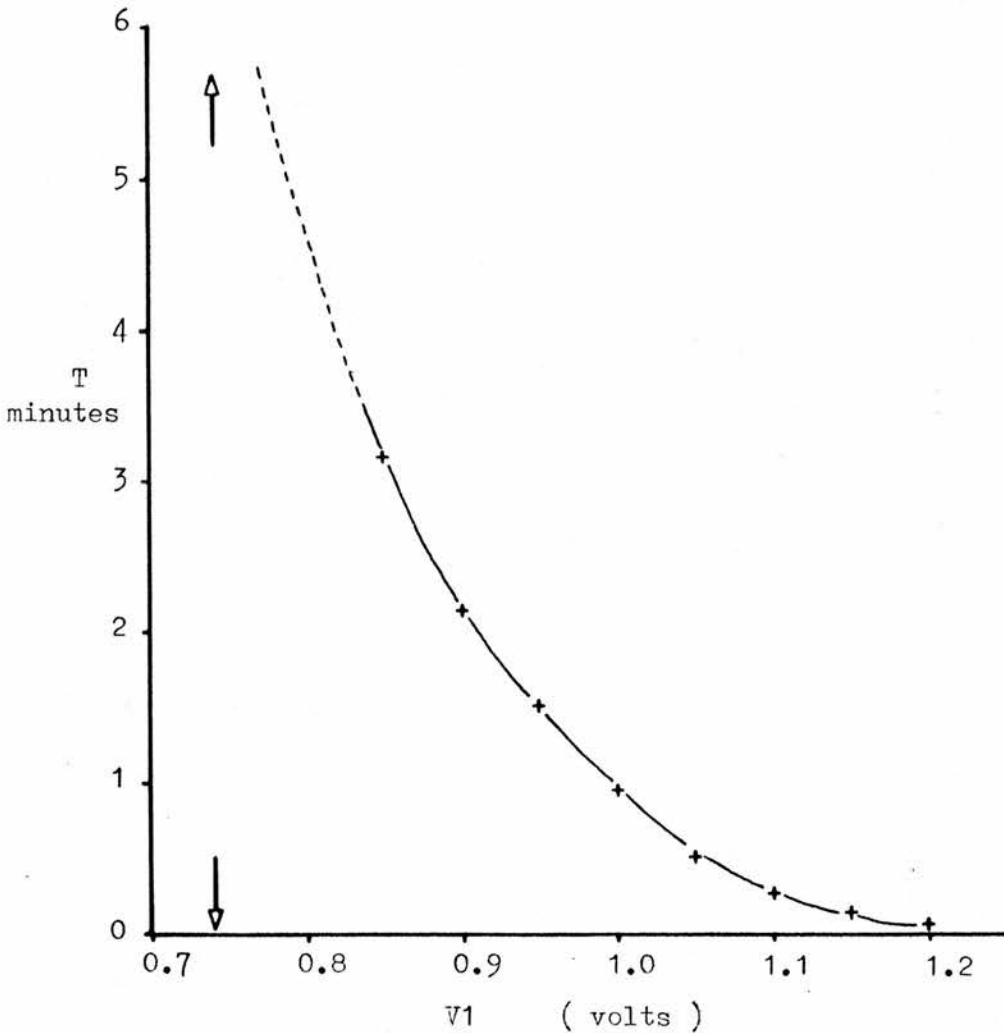


Fig. 69 Elapsed time before operation of range-change switch for basic circuit shown above. $R2$ effectively short-circuited by $D3$. Fall time much longer - not measured. Basic operating voltage of range change switch = 0.74 V. - depicted by arrow

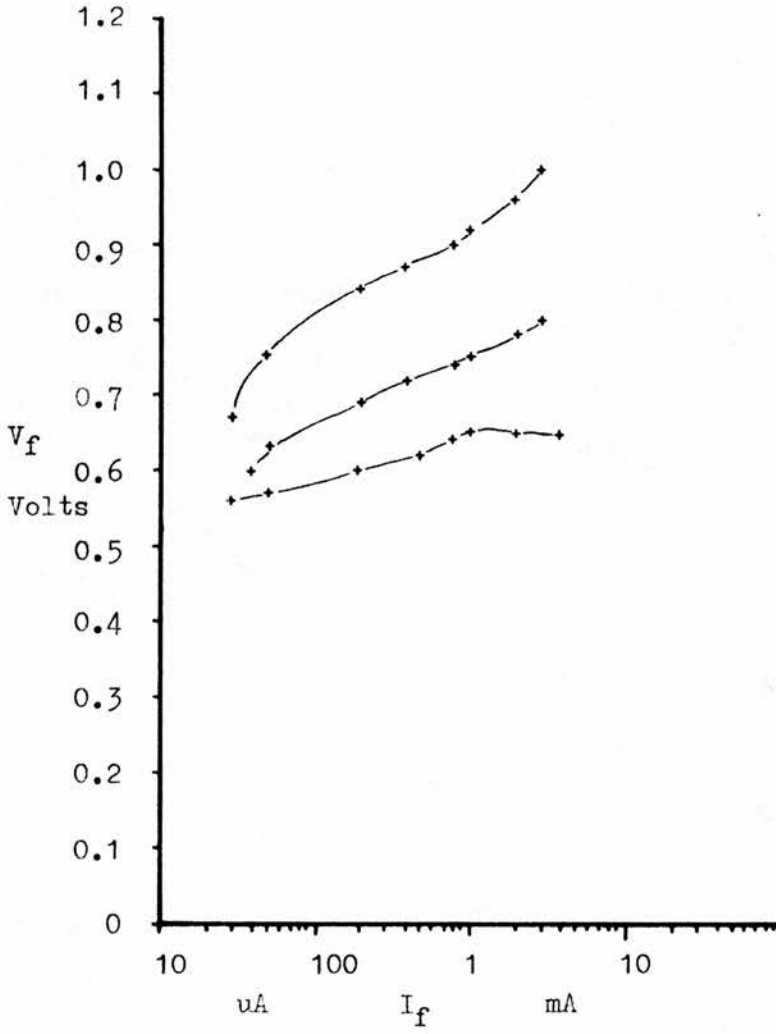


Fig. 70 V_f / I_f response for ' pseudo-diode ' for three arbitrary positions of the variable contact of R1 (see below, Fig 71)

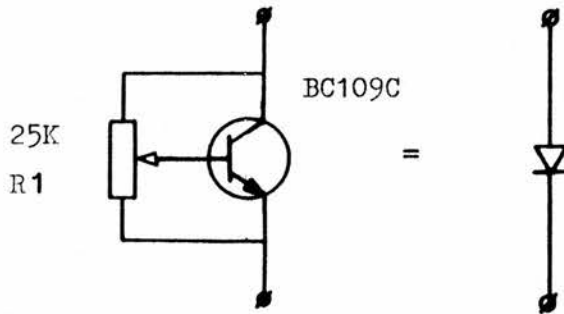


Fig. 71 Pseudo-diode

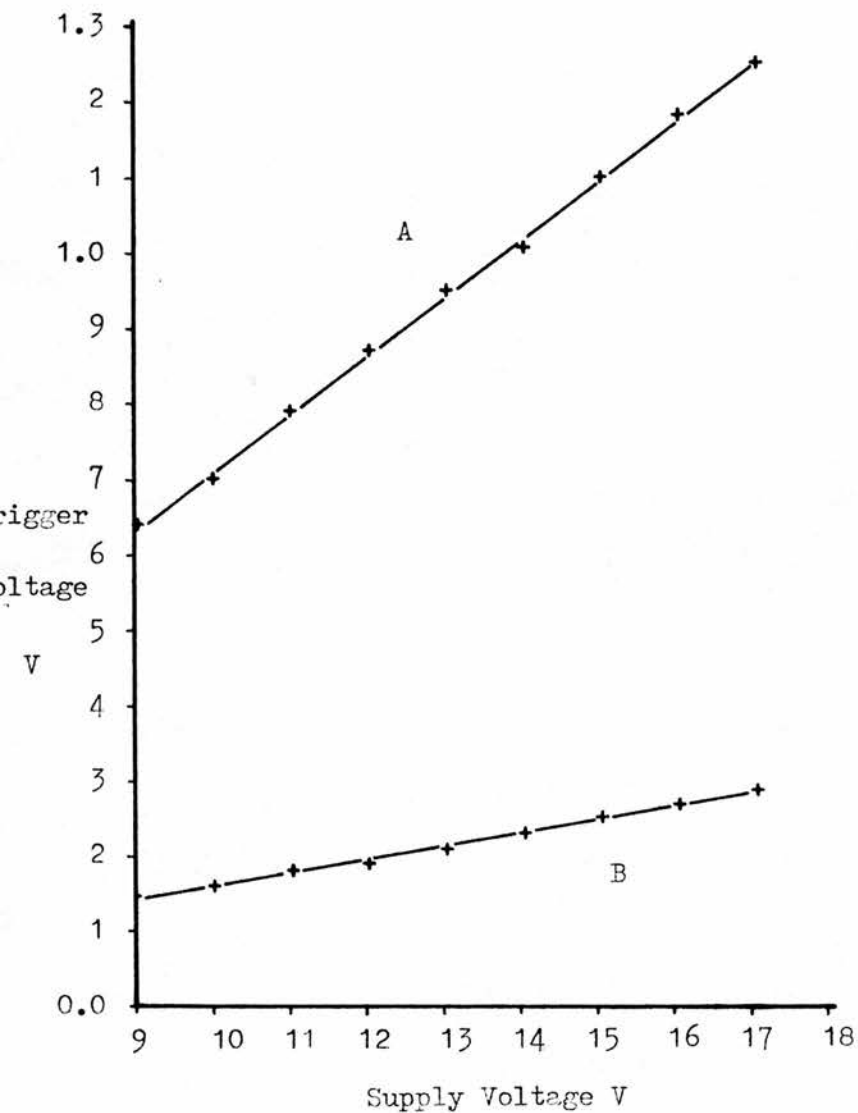


Fig. 72

Auto range change switch. Performance of voltage detector, with hysteresis. Curves A and B show the voltages at which output voltage of comparator (E-X in Fig. 73a) changes from A) low to high and B) high to low; in relation to battery supply voltage.

Damping unit disconnected, input voltage from Z-B (Fig 73). R6A, R7A set at arbitrary positions.

Table 7 Temperature Test

V_{supply}	$V_{Z-B \text{ A)}}$	$V_{Z-B \text{ B)}}$	T_{ambient}
12	0.85	0.19	+21°C
12	0.85	0.20	-25°C
8.5	0.60	0.16	-25°C

all readings in volts.

Environmental performance satisfactory.

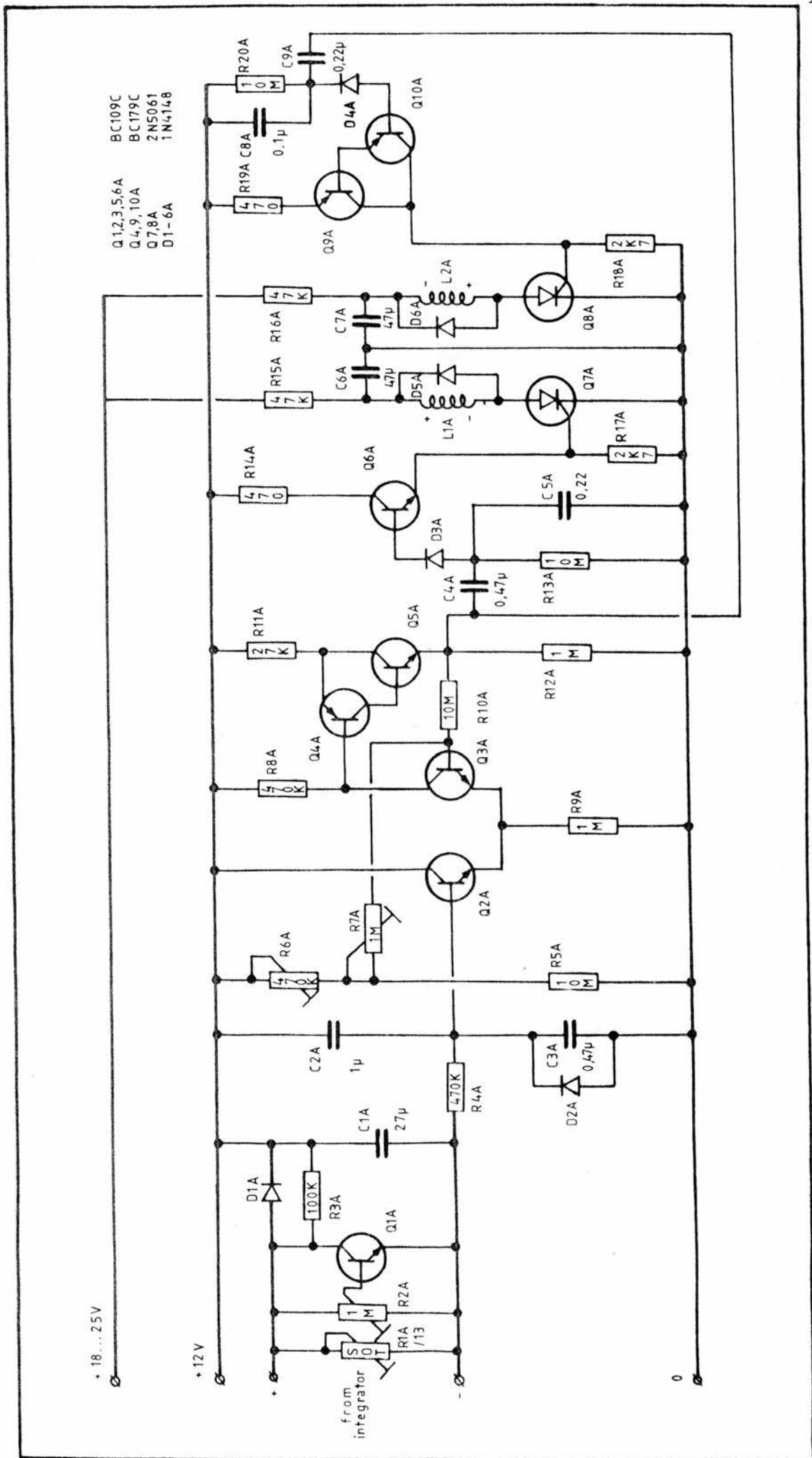


FIG 73 Circuit diagram of the auto range-change switch. See Chapter 6

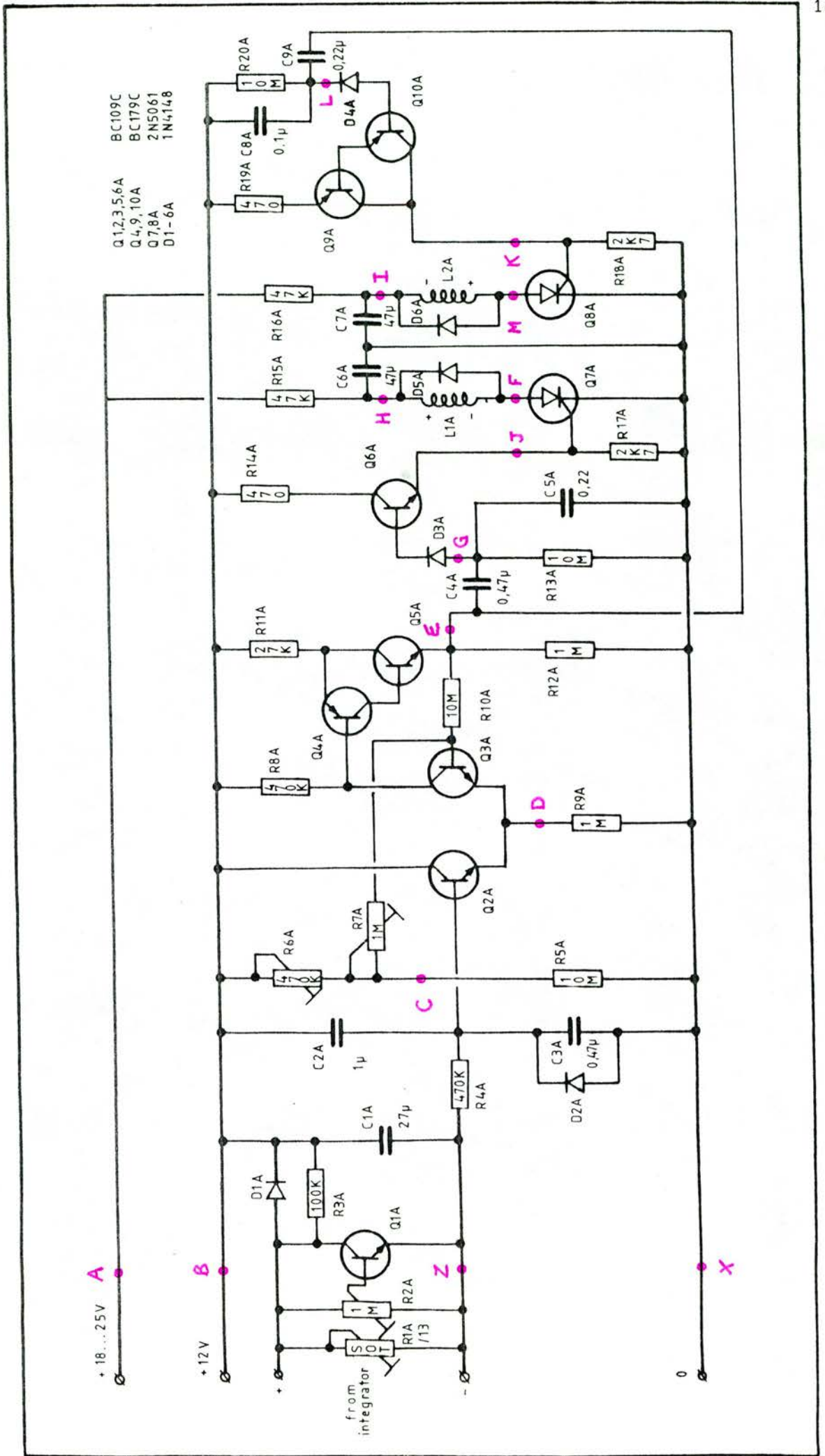
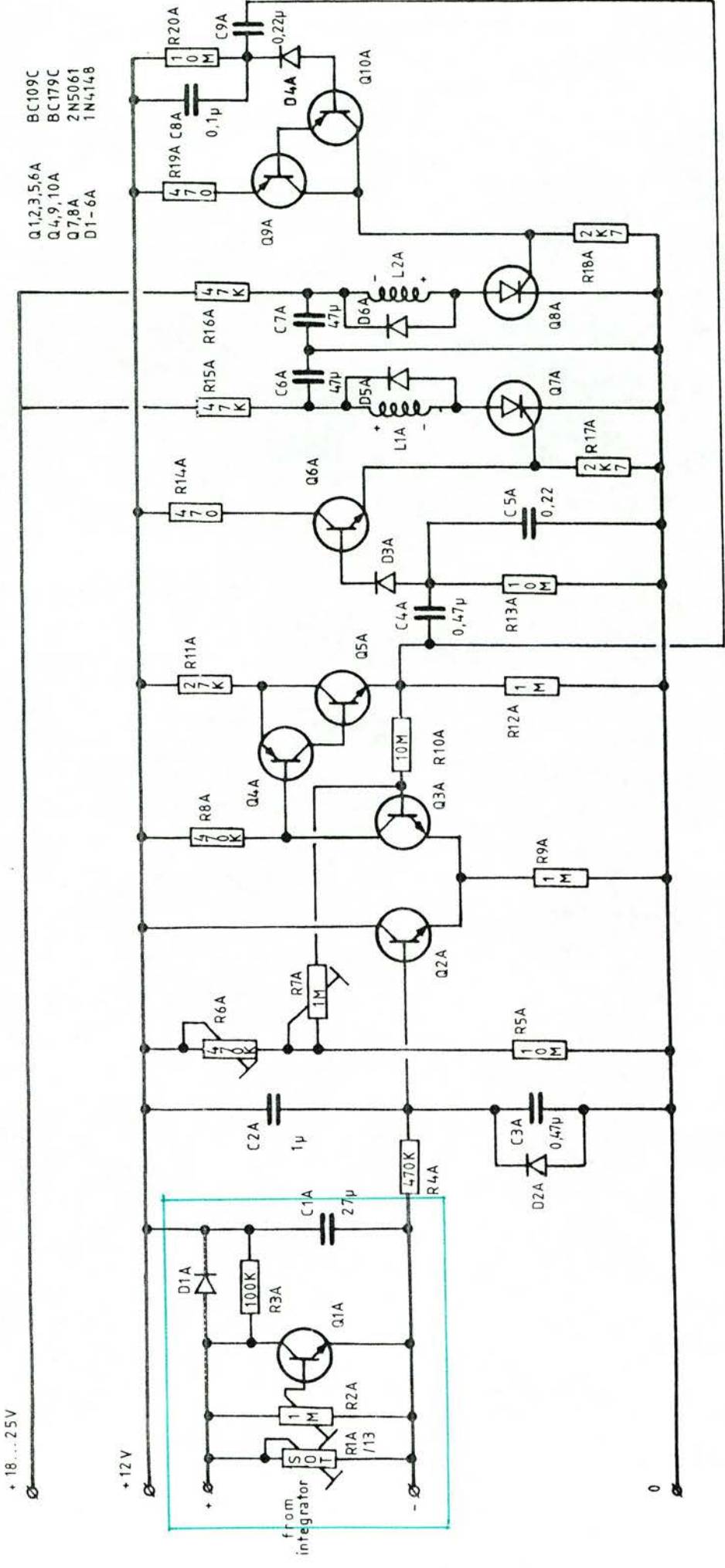


FIG 73a Measuring points for circuit tests shown in red. See text for explanation

+ 18... 25V

+ 12V



- Q1,2,3,5,6A BC109C
- Q4,9,10A BC179C
- Q7,8A 2N5061
- D1-6A 1N4148

FIG 74 Signal damping network for the auto range-change circuit shown within blue box. See section 6.A.2 for explanation, p. 136

6.A.3 Introduction to and characteristics of the most recent auto range-changing unit

The unit to be described below has been used to produce promising test-results, which are presented in section 7. However, in spite of this, the circuit is technically clumsy, and other means to the same end are available, and would repay investigation. For example, the ideal low-consumption monostable of FURUICHI and SASAKI (1968) has only recently come to hand, and, as tentatively incorporated in Fig 88 , should represent a much more elegant approach, dispensing with the need for thyristors of a specified high gate-sensitivity. However, if these are to be retained, Fig 87 shows a further tentative circuit which is more elegant. Part of the problem has been an extreme, and most unwelcome, sensitivity of the initial circuit to electrical impulsive interference, leading to random selection of the high-sensitivity mode of operation at times of high irradiance input. This in turn leads to damage to the integrator and the copious waste of scarce recorder tape. With the initial circuit, the only cure found was so to damp parts of the circuit, with C5a and C8A (Fig 73) that all responses, including those to desired inputs, have become very sluggish. More serious than this, in spite of full tests on the comparator section (round Q2A, 3A, 4A, 5A, Fig. 73) the auto ranger has failed to respond on occasion in the field tests, and for this there has been no explanation. In my view, where such materials are to hand, a more satisfactory circuit could be generated around the new CMOS operational amplifiers now on the market, using CMOS logic integrated circuits and bilateral switches to replace the latching relay. (See also section 1).

The tested performance of the unit is shown by Table 7 and Fig 72. The switching threshold voltages are closely bound to the battery supply voltages, since no stabilisation is incorporated. This was deliberate, to save power, and immaterial, since in practise the battery voltage will not range as widely as that shown, and the exact irradiance values (hence voltages on R13/1A (Figs 28 and 73) at which range-changing occurs will not usually be critical. Power consumption is less than $25\mu\text{A}$ at 12V.

6.B Analysis of Operation - 1

6.B.1 The comparator unit

The first half of the range change unit is a voltage comparator, in which the voltage developed across R13/1A (Fig 28 and 73) in proportion to the integrator photocurrent is compared with a pre-set reference voltage. Depending on whether or not the monitored voltage exceeds that of the reference, the output voltage of the comparator (measured from point E to point X in Fig 73) will be high or low. It is important to note that the +12V and 0V rails of the range change unit are separate and isolated from those feeding the integrator; if this were not so, the fact that R13/1A is shared by both circuits would cause neither circuit to work properly. This basic performance is complicated by hysteresis, producing the performance shown in Fig 72.

The comparator circuit originally investigated was a Schmitt trigger (see for example FERRANTI (1974), CRUMP (1967)), but this was abandoned since it did not prove possible to combine low switching voltage levels with enough hysteresis. Instead, the basic

circuit of WILLIAMS et al., (1976), and WILLIAMS (1968), shown in Fig 75 was used, after modification to resistor values to effect micropower operation. Q2A and Q3A (Fig 73) are a long-tailed pair differential amplifier. The base of Q3A is connected to a reference voltage with a value set by the variable resistance R6A, which acts as part of the voltage divider R6A-R5A, connected across the power supply rails. The base of Q2A samples the varying input voltage. The voltages at both bases are referred to the positive supply rail (+12V line). In operation, the voltage D-X (Fig 73 a) from the emitters of Q2A, Q3A always remains approximately constant or, more exactly, 'follows' the most positive base voltage present on the Q2A-Q3A pair. Imagine that R7A is short circuited. An increase in voltage across R13/1A will cause the voltage on Q2A base to become progressively more negative. Above a certain value, the b-e junction of Q2A will increasingly become cut off, but the voltage across R9A will be sustained through Q3A turning on as Q2A turns off. If Q3A turns on, however, its collector voltage (with respect to the positive supply rail) will fall, tending to cause Q4A and Q5A to turn on. The emitter of Q5A is coupled back to Q3A via R10A, and as a result of this positive feedback route Q3A, 4A and 5A, all turn on with a snap action. The reverse procedure holds true, and if once again Q2A is caused to conduct, Q3A begins to turn off, therefore so do Q4A and Q5A; the drive to Q3A via positive feed-back resistor R10A falls away, and by regeneration, the switching off of Q3A, 4A and 5A also proceeds with a snap action. The voltage across R6A corresponds to the threshold voltage 'B' shown in Fig 72 . As described so far, the circuit does not show much hysteresis; this was finally controlled by the preset variable resistance R7A placed in series with the reference voltage. This resistance has the

effect of modifying the apparent reference voltage, according to whether or not a load current is flowing through it at the moment when the circuit switches.

To express the performance of the comparator, the effects of varying R7A (the hysteresis control), R6A (the reference voltage control) and R4A (the input resistance) are shown in the graphs Figs 76 , 77 , and 78 . These make plainer the interactions of the components. For the first two graphs, R4A is eliminated (short-circuited) and the value of R6A is expressed directly as the reference voltage to which it corresponds, $V_{\text{input}} (V_{\text{B-Z}})$.

Fig 76 shows that the hysteresis is the difference between the two threshold voltages, A and B, at which the output voltage $V_{\text{E-X}}$ goes high or low, and not a percentage of either voltage. Fig 77 shows that adjusting R7A (the hysteresis control), produces the main change by affecting the turn-on voltage, A. The turn-off voltage threshold (B) is not much affected. In Fig 78 , the reference voltage (R6A) and hysteresis (R7A) remain fixed, but changing R4A alters the apparent reference voltage, though not the hysteresis.

In practice, it was decided to fix the value of R4A and use only variations in R6A and R7A to control the performance of the circuit. The output of the comparator is a rising or falling voltage, varying between just above the 0V rail and a voltage slightly below that of the positive battery rail.

6.B.2 The relay operating section

The heart of the range-change unit is an electromechanical bistable relay; this has two stable states, and momentary energising of the appropriate coil causes it to change state. Unlike the

conventional relay, no current flow is necessary to hold the relay in either of the two switched states.

When the comparator changes state, the capacitors C4A and C9A couple a current pulse to the two amplifiers Q6A and Q9A-Q10A, which handle respectively the positive and negative-going edges of the comparator output voltage waveform. In each case, the peak current output of the amplifying stage is limited to a safe value by a $470\ \Omega$ resistance, either R14A or R19A. The output pulses go to the thyristors Q7A and Q8A, and these turn on, discharging the capacitors C6A and C7A through the windings of the relay. In each case, the thyristor turns off when the capacitor has discharged, since even at the maximum operating temperature the residual current supplied by R15A and R16A remains below the holding current I_{HX} of the recommended thyristors.

In using this circuit arrangement, the penalty paid is that the time constants R15A-C6A and R16A-C7A are rather long. There is therefore a minimum recharging period during which the comparator must not change state, or else capacitors C6A and C7A will be unable to supply the necessary relay switching current pulses. For this reason, R4A and C2A are used to slug the response of the comparator, preventing rapidly alternating changes of state. In the prototype, the only available relay operated from 24 V (nominal); it is for this reason that the second battery supply marked +1825 V appears in Fig 73 . See Appendix 7 Electromechanical Relays.

6.C Analysis of Operation - II

As in the case of the integrator, the use of oscillographs

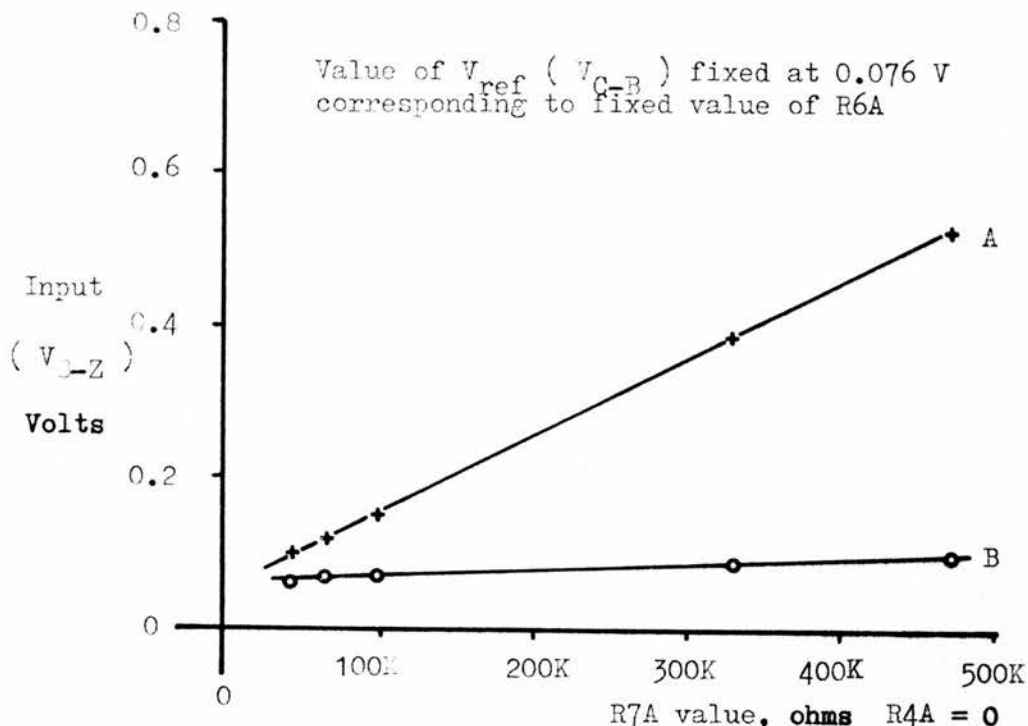


Fig. 77 Effect of varying $R7A$ value (Fig. 73) on hysteresis (turn-on - turn-off voltage). Note relative constancy of turn-off voltage, B.

Circuit values and component references relate to Fig. 73 . Circuits tested at room temperature ($+13^{\circ}C$) and the minimum battery voltage, 9V. Certain other component values used at this time differ from finally selected values, viz. $R8A = 47K$, $R9A = 470K$, $R12A = 470K$.

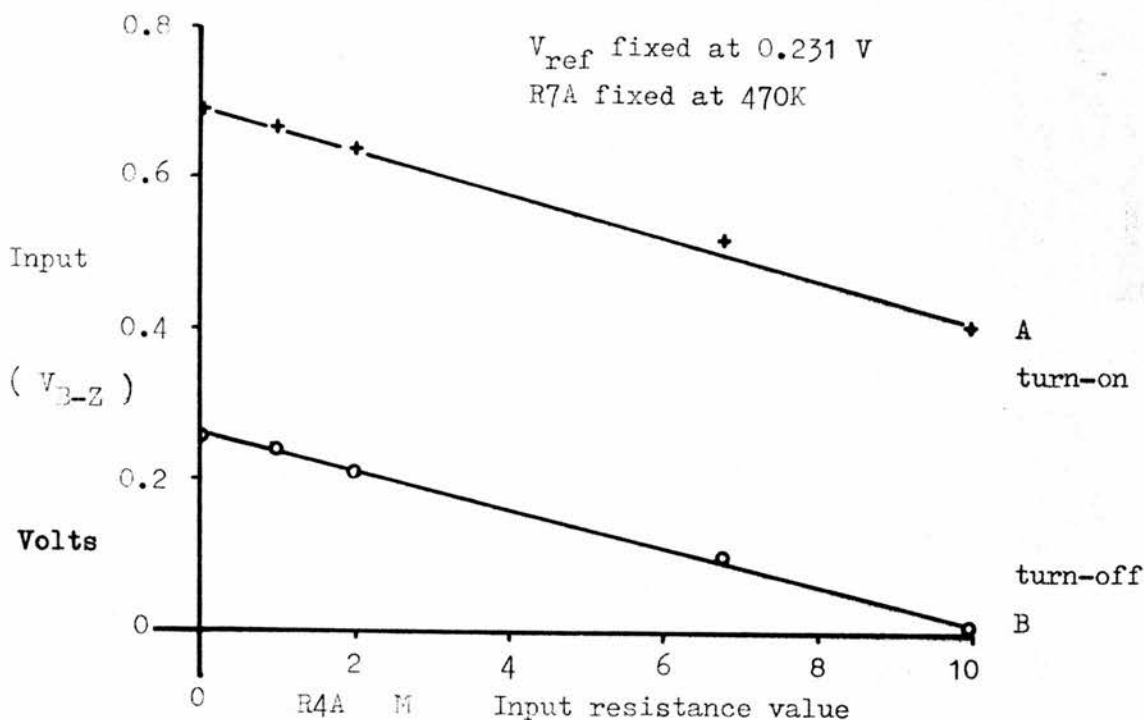


Fig. 78 If $R6A$ and $R7A$ (Fig. 73) remain fixed, variation of $R4A$ is expressed as a change in apparent reference voltage, but not in hysteresis. $R6A$ value here expressed as the V_{ref} value to which it corresponded during this test.

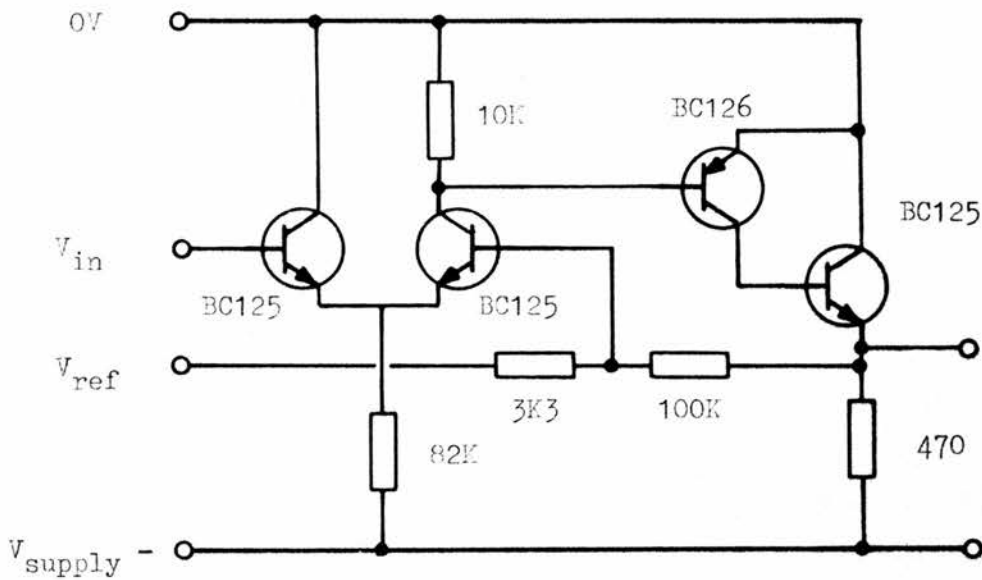


Fig. 75

Basic voltage comparator circuit, as given in WILLIAMS (1976) from which the circuit of Fig. 73 is derived.

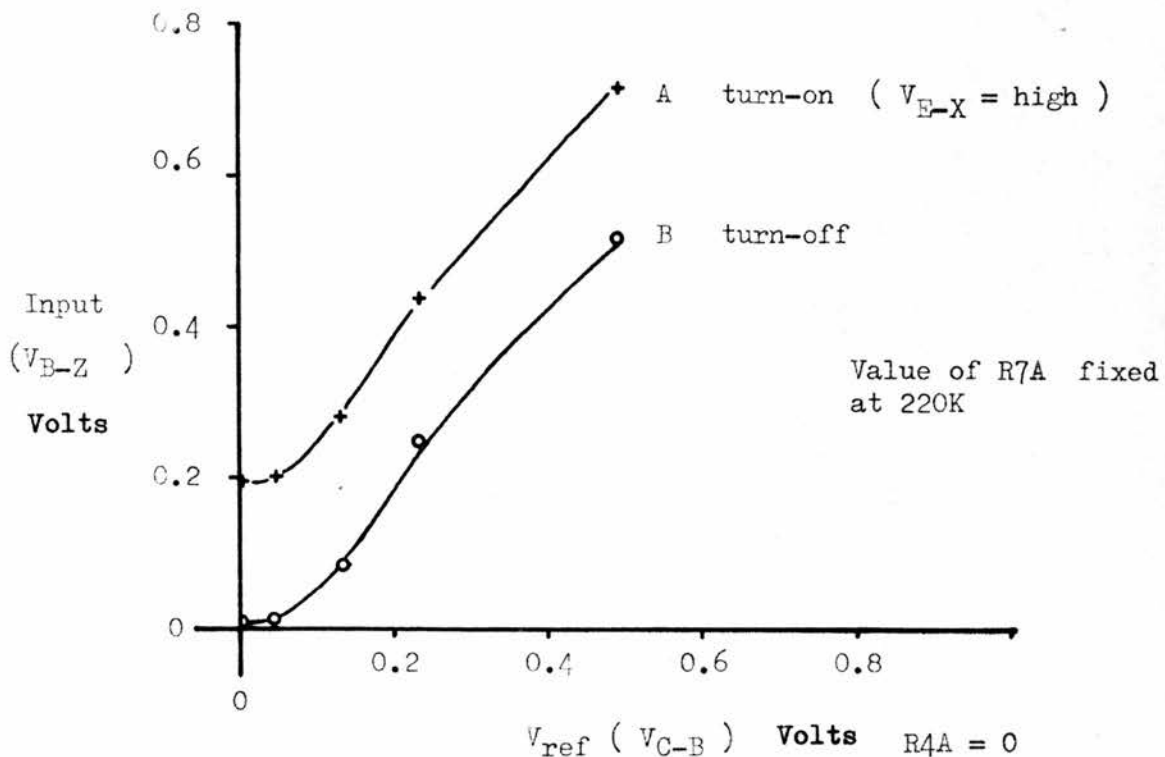


Fig. 76

Turn-on (A) and turn-off voltages of the comparator unit (Fig. 73) showing constant value of hysteresis voltage obtained with widely varying reference voltage.

to characterise the performance is invaluable. The method described in 5.D. was used, and the figures 79 to 86 are the result. All circuit references relate to Fig 73 , and the battery voltage was the minimum, 9.0 V, room temperature 13°C. These oscillographs should make clearer the information of 6.B.

6.C.1. Fig 79 Output waveform of comparator Probe position E-X

The output waveform shown approximates to a square wave, the voltage varying from 0.82 V above X to 7.9 V (ie. 1.1 V below the positive rail voltage). The rise and fall times of the waveform edges are slow, since the output impedance of the comparator is high, and both C4A and C9A are large. A worthwhile improvement would be to buffer the output of the comparator with a complementary emitter follower stage as shown in Fig 87 or 88.

6.C.2 Fig 80 Probe firstly positions B-L Live oscilloscope probe to L
Probe secondly positions G-X Live oscilloscope probe to G

The role of the capacitors C4A and C9A are clear from this pair of graphs. They serve to differentiate the output of the comparator (E-X) and to apply, for a short time, driving voltage to Q6A and Q9A-Q10A which are responsible for firing the thyristors.

6.C.3 Figs 81 and 82 Probe positions across 1.02 Ω resistance in series with gate of either Q7A or Q8A for the duration of the tests

Fig 81 displays an investigation of the time constant of C4A with

extraneous resistance, carried out to check that the current pulse supplied to the gate of Q7A is always sufficient to drive it, even if changes of state of the comparator were to follow rapidly. (The subsidiary limitation of the time-constant R15A-C6A has not, of course, been forgotten.) For this experiment, the comparator output E-X was sent 'high' for periods of ten seconds, separated by recovery periods of 5, 7, 10 and 15 seconds during which E-X was low. The effect of shortening recovery periods is to reduce the peak current (\hat{I}) available to the gate of the thyristor, and to shorten the time for which this drive current flows. At all times the gate drive current present exceeds the minimum requirement of the thyristor by a very large margin. ($I_{GT} \text{ max.} = 350 \mu\text{A}$).

Fig 82 shows the corresponding graph of drive current to Q8A from Q9A-Q10A. In this case, the comparator cycles were 20 seconds 'low' followed by 3, 5, 7, 10, 15 and 75 seconds 'high' prior to switching low again. In this case it is interesting to note that peak currents flowing to Q8A gate are marginally lower than analogous currents to Q7A, but they flow for a much longer time. The result of this is that each time Q8A fires it remains conducting for much longer than does Q7A in similar circumstances - as is shown by Figs 83 and 84. Note also the surprising fact that Q9A-Q10A, although a darlington pair, does not produce a peak output current as high as that which flows from Q6A. Currents were measured as voltage developed across test resistance of 1.02Ω , placed in series with each thyristor gate for the duration of the test.

Nevertheless, the circuits presented in Figs 87 and 88 are more elegant, and would repay investigation. Fig 87 interposes a buffer stage between the comparator and a simplified relay operating section, and Fig 88 substitutes relay operating circuitry according to the circuit of FURUICHI and SASAKI (1968) (see page 92). Both of these circuits have passed preliminary tests in 'breadboard' form.

If the mechanical relay could be replaced by a CMOS* analogue switch, an expensive and somewhat unreliable (see Appendix 7) component would be saved. Unlike a good relay, the CMOS analogue switch has a significant equivalent series resistance of about 100 ohms. This means that the switch could not be substituted for S1 (Fig 28) directly, but would have to be used as tentatively incorporated in Fig 89 . In selecting a value for R12, the switch resistance would need to be accounted for. The temperature coefficient of the switch resistance is not made very clear in most published data.

* Complementary Metal Oxide Semiconductor - Silicon Integrated circuits made using this technique are noted for their low power consumption, but also, under certain circumstances, for their fragility.

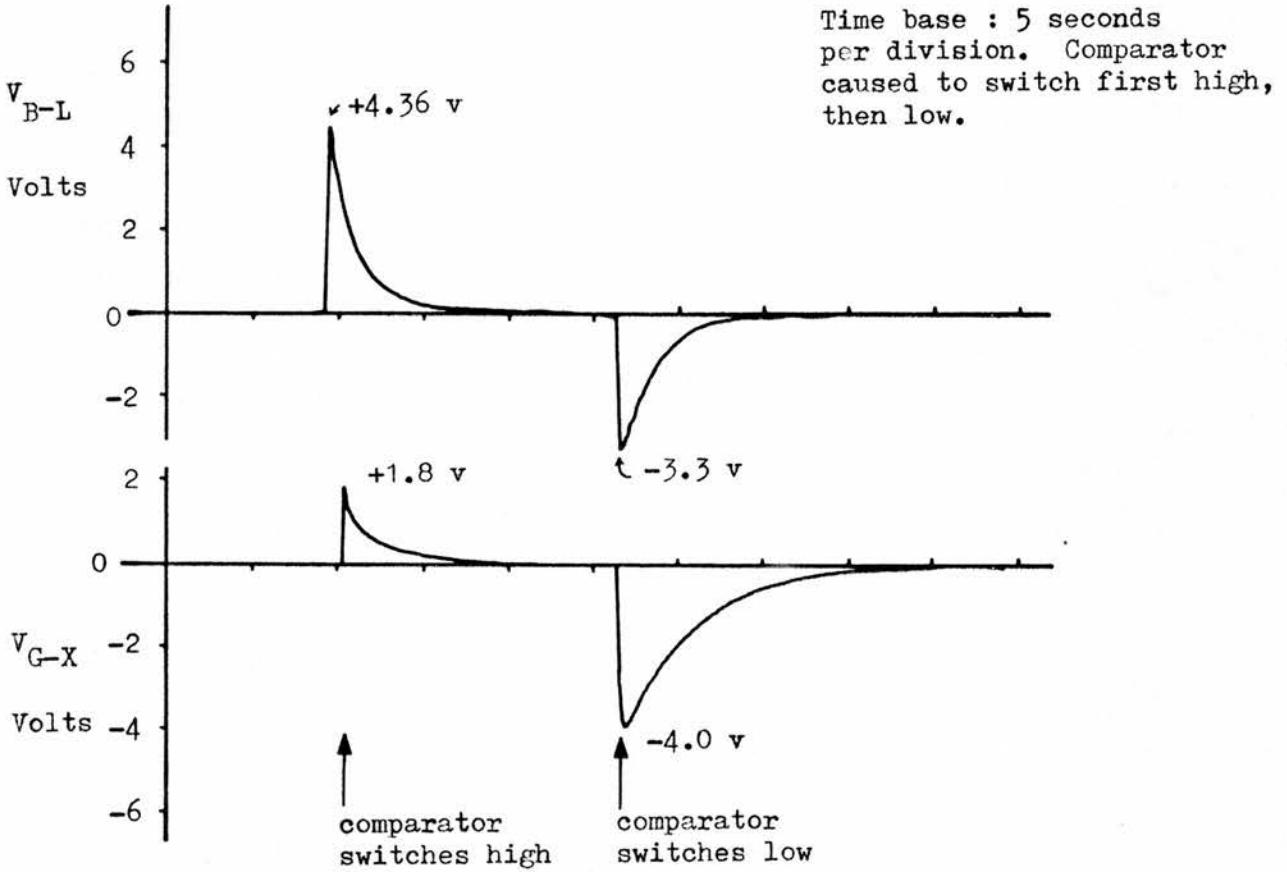


Fig. 80 Drive voltage present on thyristor-driving transistor bases, showing differentiating effect of C4A and C9A (Fig. 73) See text, page 150 .

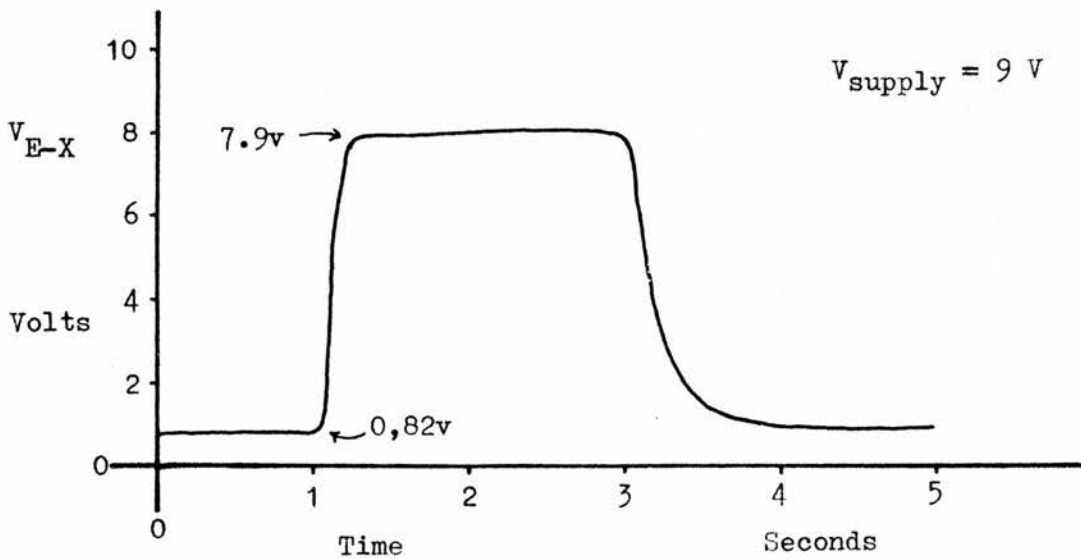


Fig. 79 Output voltage waveform of comparator, V_{E-X} of Fig. 73

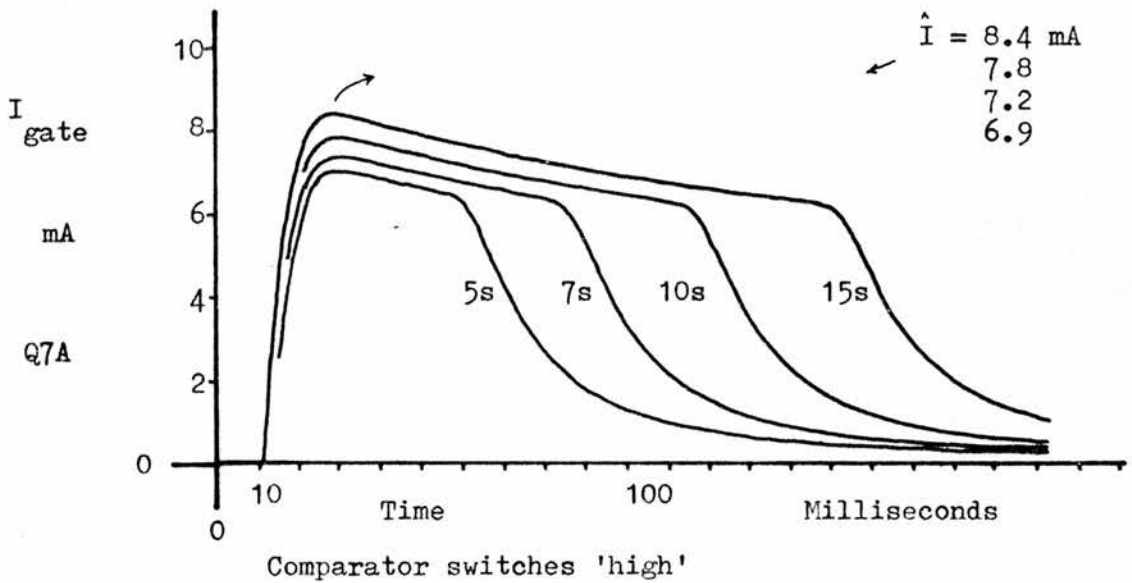


Fig. 81

Response of relay driving circuitry to V_{E-X} , comparator output, switching high for a 10-second period. Effect of four different recovery times (during which comparator output is low) on the coupling performance of C4A (Fig. 73), reflected in changing values of peak output current from Q6A.

N.B.

The differing time scales on these two graphs are correct.

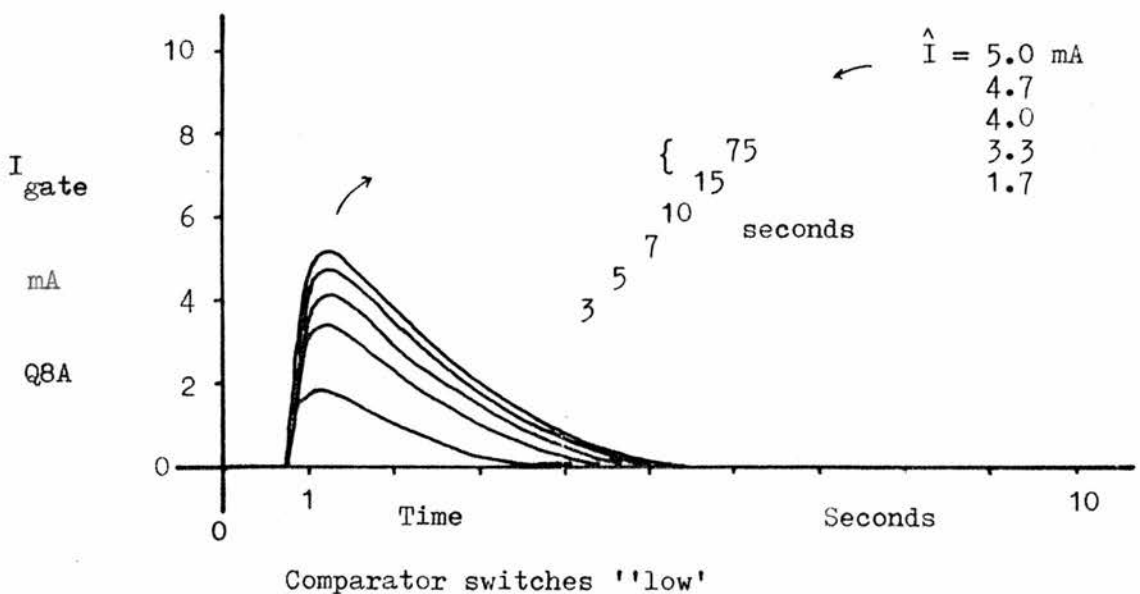


Fig. 82

The complement to Fig. 81 Comparator output switched low for 20-second periods, recovery times (during which comparator output is high) are indicated, for each graph, in the middle of the graph.

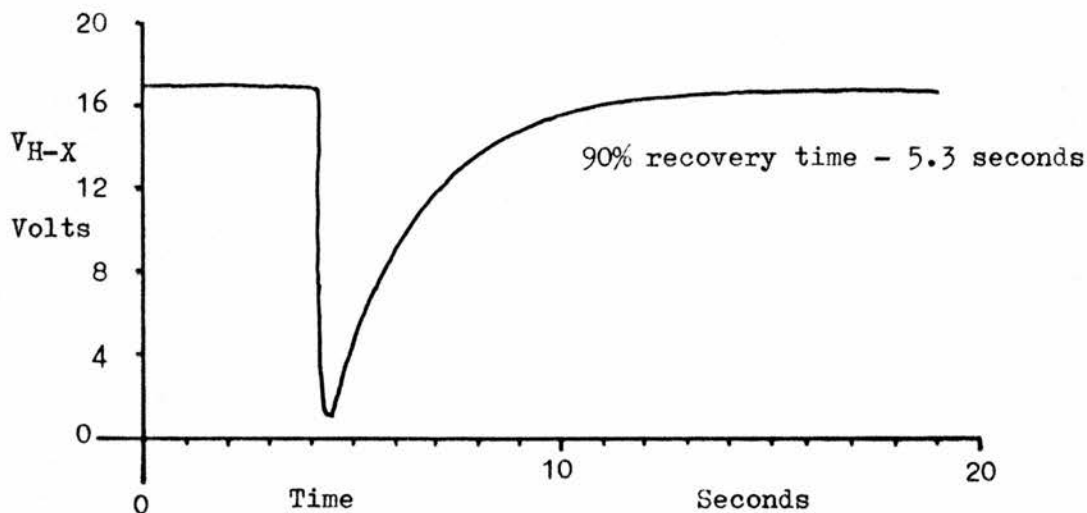


Fig. 83 Discharge and subsequent charging characteristic of the relay pulsing capacitor, C6A. The time-constant of R15A-C6A determines the recharge time. R15A has the lowest value consistent with never exceeding the minimum holding current, I_{hx} of the thyristor Q7A. Component references relate to Fig. 73

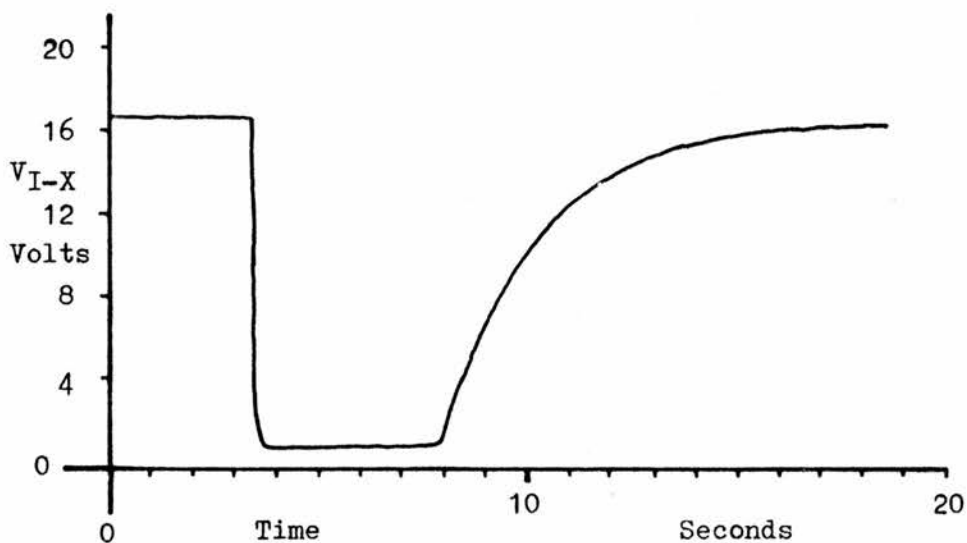


Fig. 84 The complement of Fig. 83, relating to R16A, C7A and Q8A. See page 152 for further comment on the difference between these graphs.

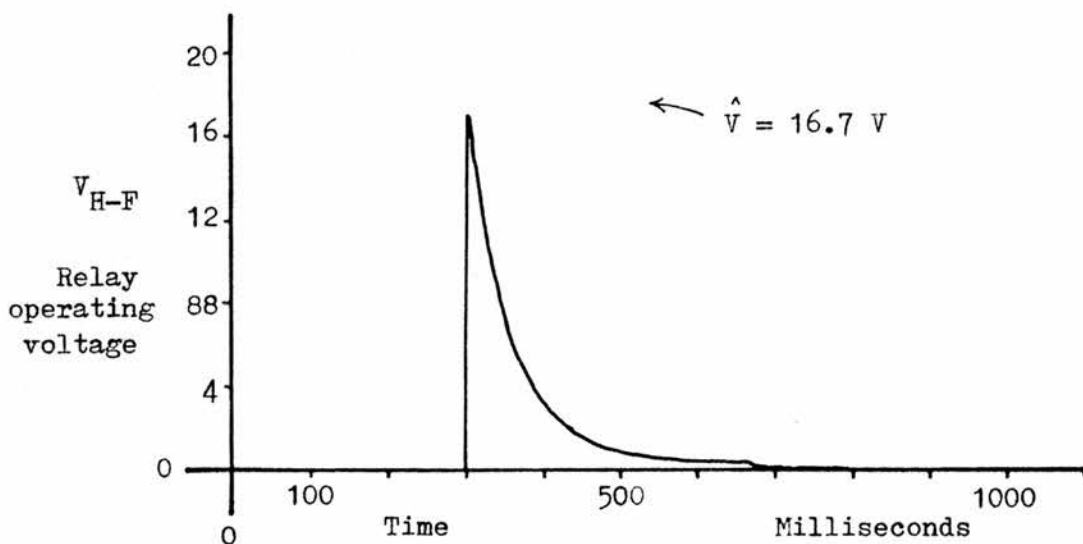


Fig. 85 Shape and size of voltage pulse causing relay coil to operate.

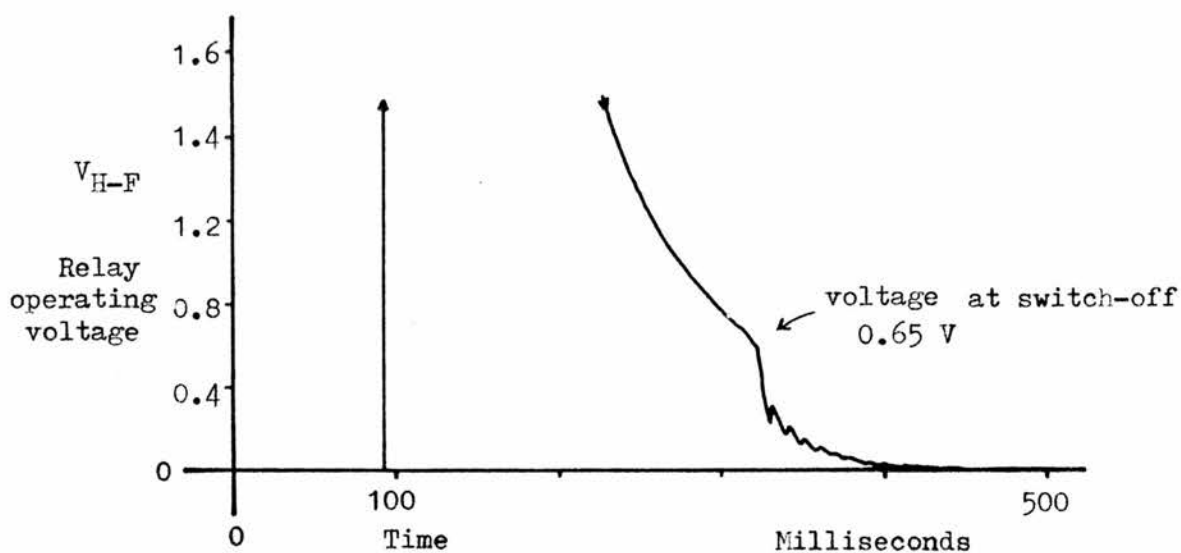


Fig. 86 Enlarged portion of 'tail' of the curve, above. The apparent discrepancy in the time-base values between Fig. 85 and Fig. 86 is due to differing length of thyristor driving pulse from Q6A, as demonstrated graphically in Fig. 81. Vertical scale 10X that in Fig. 85 above.

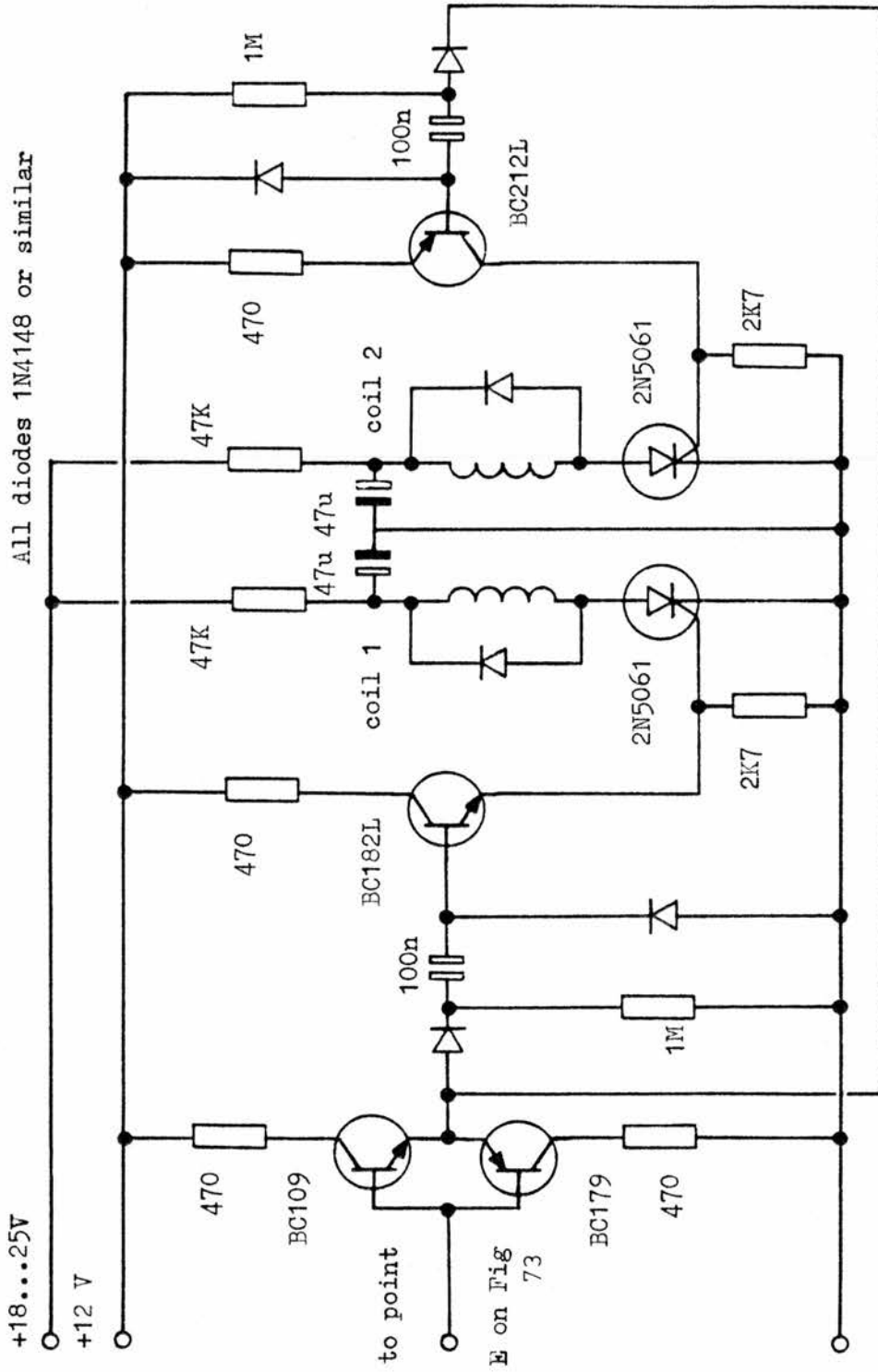


Fig. 87 Suggested improved version of relay-switching part of auto-range unit. This has not been fully tested. Note the inclusion of a buffer stage between point E (as in Fig. 73) and the relay-switching unit proper.

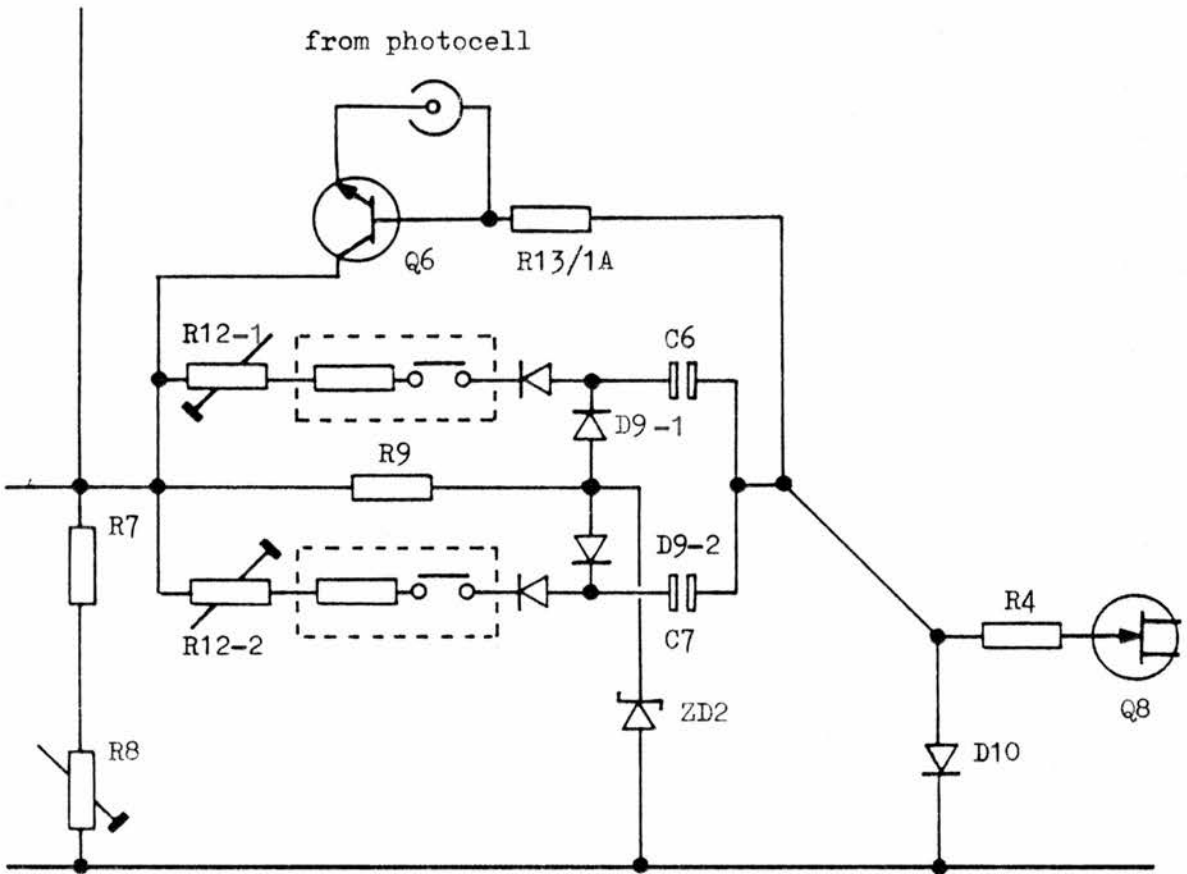


Fig. 89 Rearrangement of components (references as in Fig. 28) to accommodate the use of CMOS-analogue switches in place of the relay contacts, S1, (Fig. 28) for range changing. The circuit changes are necessary since unlike the relay, the solid-state state switches would be unable to pass the recharge currents for C6-C7. The inherent resistance of solid state switches is shown within the dashed boxes. See text, page 153 .

CHAPTER 7

FIELD TRIAL RESULTS

7 . EQUIPMENT TRIALS

A programme of laboratory and field trials was carried out to test the completed equipment. In the laboratory, the effects of ambient temperature on thermal time-marking efficiency were investigated, along with the effect of atmospheric humidity on dimensional stability of the recording paper. Statistical tests on recorder constancy were performed using full and empty supply and take-up spools, and the differences in the ability of 3 naive subjects to read irradiance records were investigated. The electronic parts (i.e. not the recorder mechanism or main battery) were given a 600 hour thermal stress test involving more than 30 sudden changes between two temperature extremes.

For the field trial the equipment was moved to Sutton Bonington * (53°N, 1°W). For this trial a radiometer head was constructed using one of the newly available HAMAMATSU gallium arseno-phosphide detectors, the theoretical spectral response curve being given in Fig 11 p. 253 . This head was designed according to the general precepts of Appendix 2, p.234, and is illustrated in plan and section in Fig. 121 . However, the goodness of the cosine correction and agreement of the spectral response with the theoretical are untested.

The reference solarimeter was the well-established KIPP & ZONEN pyranometer (Moll thermopile pattern) MOLL (1923), the output of which was divided between an electronic integrator (DELTA-T DEVICES; SAFFELL et al. (1979)) and a chart recorder (VITATRON). The equipment was operated at Sutton Bonington from June to September 1982, and was housed in a small hut near to an open instrument field. The radiometer head was set up as close as possible to the comparison Kipp Solarimeter and carefully levelled.

* University of Nottingham, Dept. of Physiology and Environmental Science

Effect of ambient temperature on thermal time-marks

See Fig. 90 . The recorder was operated in three different atmospheric temperatures; $+60^{\circ}\text{C}$, $+20^{\circ}\text{C}$, and -20°C . The current pulses for the time marks were supplied at the accelerated rate of 1 per 10 seconds; 36 times the normal operational rate. Even so, the hot-wire pen was off for the larger part of the time and excess heating appeared to be no problem.

Fig 90 shows in the photocopied form approximately 400 marks for each temperature regime, and in each case a small section of the original recorder tape has been pasted adjacent to the photocopied replica, enabling a clear idea of the temperature effect to be gained. It is apparent that usable marks are made over a wide range of temperatures. It might be worth introducing a temperature-dependent resistance or network in place of the simple timing resistance in the driving circuit for the hot-wire relay (Fig. 99, p.189) to prolong the heating current under cold ambient conditions.

It is also apparent from Fig. 90 how regular the movement of the tape is (supposedly 1.0 mm steps). There is some variation from step to step, but it is too small to be critical. However it is apparent that the recorder fails badly at -20°C , repeatedly sticking. The probable cause is increased viscosity of the lubrication, but this defect is not fundamental to the design of the recorder. See also the statistical test of recorder constancy, p. 172

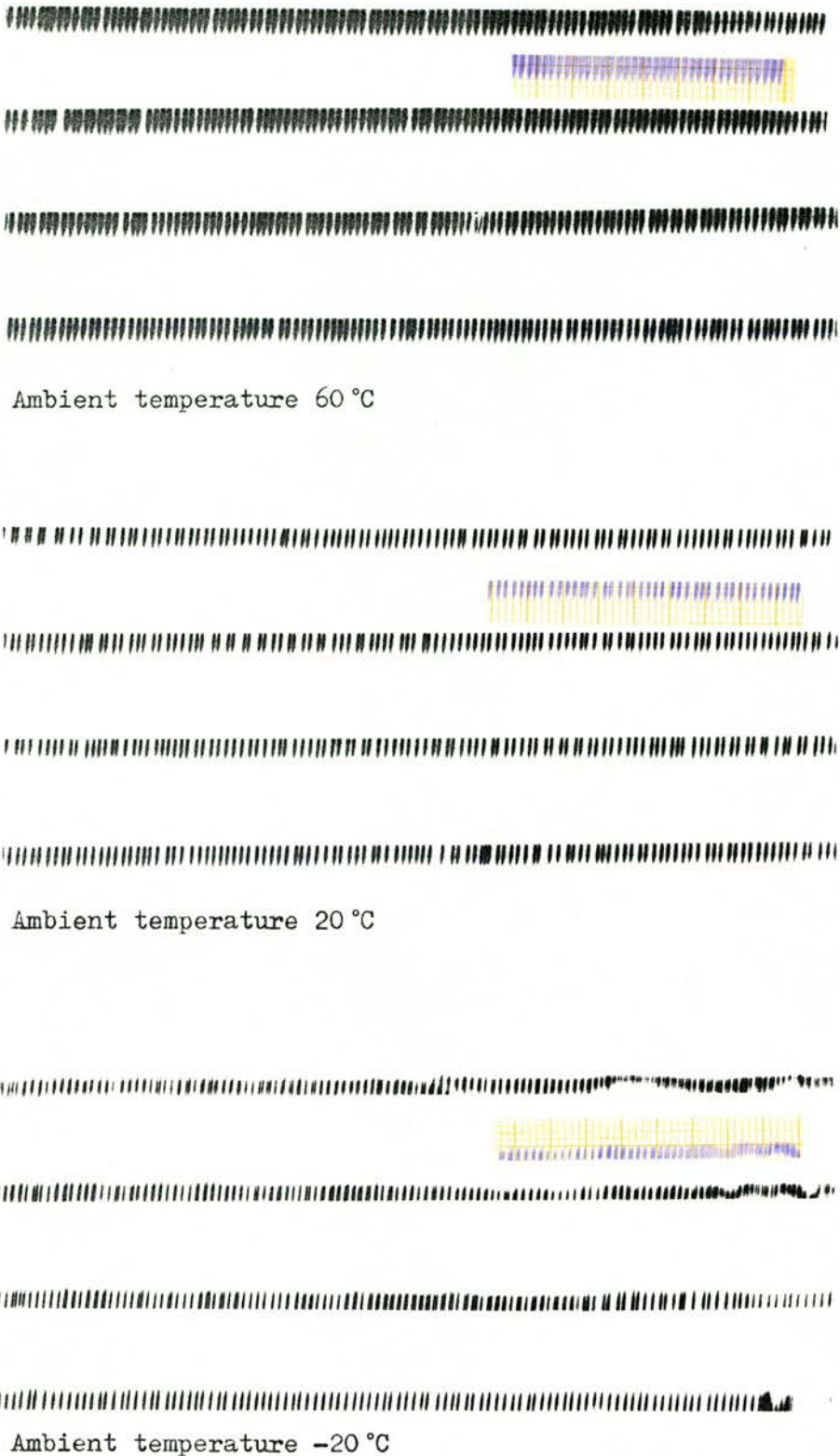


Fig. 90 Response of Heat Pen and Recorder Mechanism to Temperature Range

The hot-wire pen has a wide satisfactory operating temperature range, even without compensation to the heating time by electronic means. At low temperatures the viscosity of the lubricants causes erratic performance of the prototype recorder mechanism.

7.A.2 Dimensional stability of the recording paper

7.A.2a Introduction

Since the irradiance records from the new recorder are read against a separate scale of length, rather than with reference to a printed grid on the paper, a reasonable dimensional stability is necessary. The main cause of dimensional change in cellulose based papers is change in Relative Humidity (r.h.) of the ambient atmosphere. This acts by altering the hydration of the cellulose molecules, and forces generated can be very large - certainly sufficient to tear a clamped length of paper undergoing shrinkage.

British Standard 3880 Part 1 (1971) specifies acceptable limits for dimensional stability in papers for data processing and gives methods for testing them. It states:

" 1.5.3.1 The maximum variation of the dimension in the cross direction when the relative humidity is varied from 20% to 75% and also when it is varied from 75% to 20% shall not exceed 1% of the length measured at 50% r.h.

1.5.3.2 Under the same changes of relative humidity, the maximum variation in the machine direction shall not exceed 0.5% of the length measured at 50% r.h. "

Appendix D of BS3880 Part 1 specifies certain conditions for determining dimensional stability. These include:

D3	Upper relative humidity	75± 2% r.h.
	Lower relative humidity	20± 2% r.h.
	Temperature	23°C ± 2°C
	Speed of flow of conditioned air not less than	1.5 m. min ⁻¹

D4 (paraphrased)

Conditioning: The test sample must be conditioned for $\frac{1}{2}$ hour after the desired ambient conditions have been obtained.

Loading: Not greater than 0.2 N per 25.4 mm width of strip.

(\approx 8 g-wt per mm width of strip)

7.A.2b Test method

In the light of the foregoing a simple test was designed. No attempt was made to produce a statistical evaluation, because without special co-operation from the manufacturer only one ' sample ' of paper was available, i.e. the large mother roll from which all the stock paper had been cut.

A test chamber consisting of a glass tube sealed with rubber bungs, an air pump, and either a fine bubbler or a tube of ' drierite ' were the main components of the system. The system specifications were as follows:

Chamber	Material	glass
	Length	150 cm
	Diameter	5 cm
	Volume	ca. 3 l
Pump	Circulation	2.4 l.min ⁻¹
	Circulation time	\leq 1.5 min
Drying tube	Active material	Drierite - anhydrous calcium sulphate (self-indicating)
	Volume	30 cm ³
	Column length	10 cm

Hydration bottle - sintered bubbler under 5 cm of water

The tall glass tube making the test chamber was mounted with clips to a window frame, out of direct sunlight. The upper bung bore the outlet tube, a thermometer, and three hooks. Three lengths of paper tape were hung from the hooks, and at their lower ends they were tensioned with one of three masses of 3, 6 and 12 g, corresponding to 0.5, 1.0 and 2.0 g.mm⁻¹ width of tape. A short way above these

tensioning weights was a scale marked in mm attached to the chamber wall, and opposite the middle of the scale the test samples were marked with a datum line.

The test sample lengths were made as long as possible to maximise changes in length which occurred. The samples hung close to the scale, minimising parallax error, however they did show a slight tendency to twist in conditions of low humidity. Two conditions of relative humidity were used: as humid as possible, as obtained by fine bubbling of the air through water; and as dry as possible, by passing the air through anhydrous calcium sulphate. These conditions have been called ' $\leq 95\%$ r.h.' and ' $\geq 5\%$ r.h.' in the absence of more precise figures. The temperature of the air in the test chamber was about 25°C . The r.h. limits were as extreme as can be found in natural conditions, but the temperature was not taken to extremes because of the difficulties in doing so.

7.A.3 Results

Fig. 91 shows the results of changing the r.h. from the initial value to the lower, then upper, and then lower extremes. For this first test, the values were carefully observed to ascertain the rate-of-change which would be found, and to check reversibility. Clearly, the $\frac{1}{2}$ hour equilibration demanded by BS3880 is sufficient to elicit the maximum change; in this case equally clearly the atmosphere in the test chamber must have quite rapidly changed, as required, from one extreme to the other. In this context it is worth noting that the drierite tube becomes warm to the touch if fed with saturated air straight from the pump and bubbler, due to the rapidly proceeding exothermic hydration reaction.

From this first test, it is clear that the maximum change in length and therefore recording accuracy is less than 0.75% over the full humidity range; and also that for the range of loading employed little difference in change of length occurs. It is not easy to establish the loading tension which occurs in the actual operation of the new recorder, but it is very low.

Fig.92 shows the results of the second test, which was simply a prolongation of the first test through ten cycles of change over a period of seven days. The equilibrium time was always in excess of $\frac{1}{2}$ hour. As in the first test, the elongation continues to be reversible, and not apparently affected by the loading used in the three samples.

Worst-case elongation	+0.30 % r.h. ≥ 95 %
shrinkage	-0.84 % r.h. ≤ 5 %

This corresponds to a change of ± 0.6 % on the mean length.

The effect of humidity changes on the dimensional stability of the recording paper used (Sensitised Coatings Ltd. ' Heat Sensitive Thermal) have proved to be quite small, and in the context of normal operating values of relative humidity, unimportant.

The sole British manufacturer of the paper supplied by Sensitised Coatings Ltd. is JOINTINE PRODUCTS Ltd. (Wiggins Teape), and the particular paper used in the course of this work is now obsolete, and has been replaced by the very similar type T1101. The recommended storage conditions for this paper are r.h. 50 - 60% and temperature 20° - 22°C.

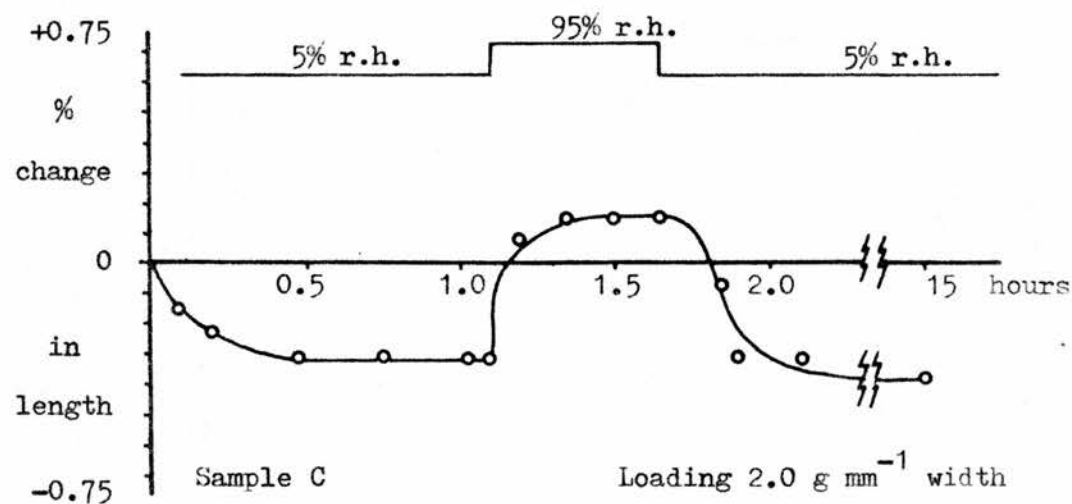
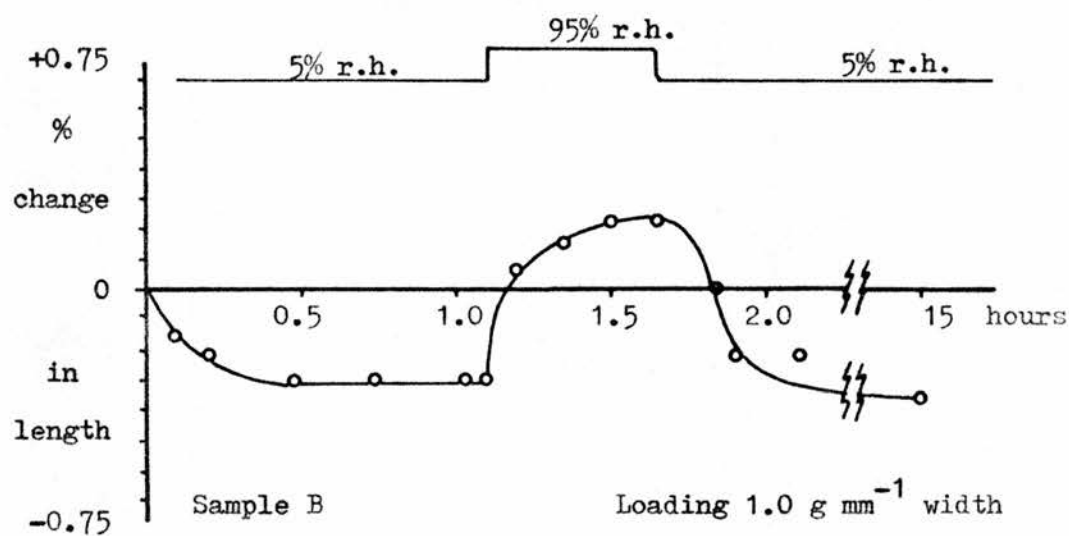
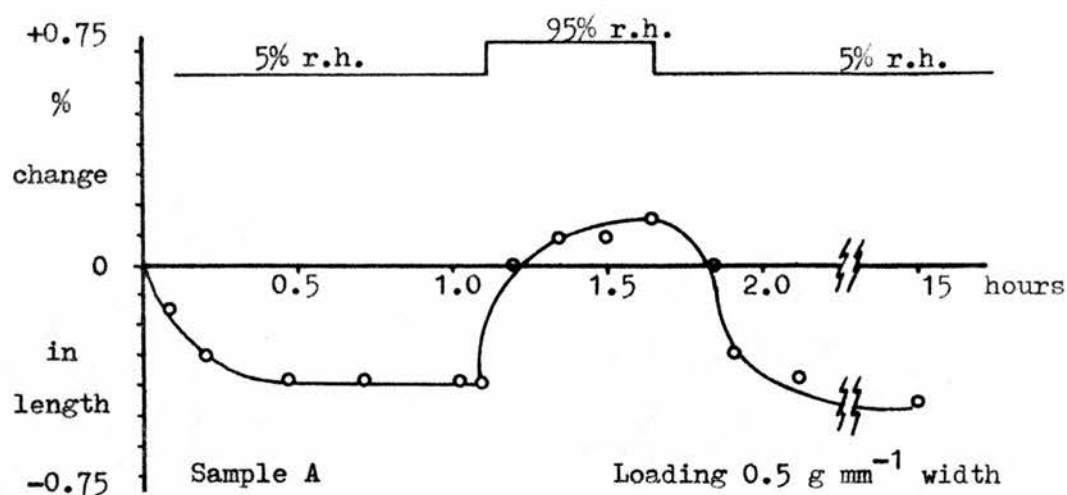


Fig. 91 Initial response of recording paper samples to extreme changes in relative humidity. r.h. at start... 54 % room temperature circa 20 °C

Date, Aug. 4 5 6 9 9 10 10 11 12
 Temp. °C 26 - - 23 23 24 26 25 25

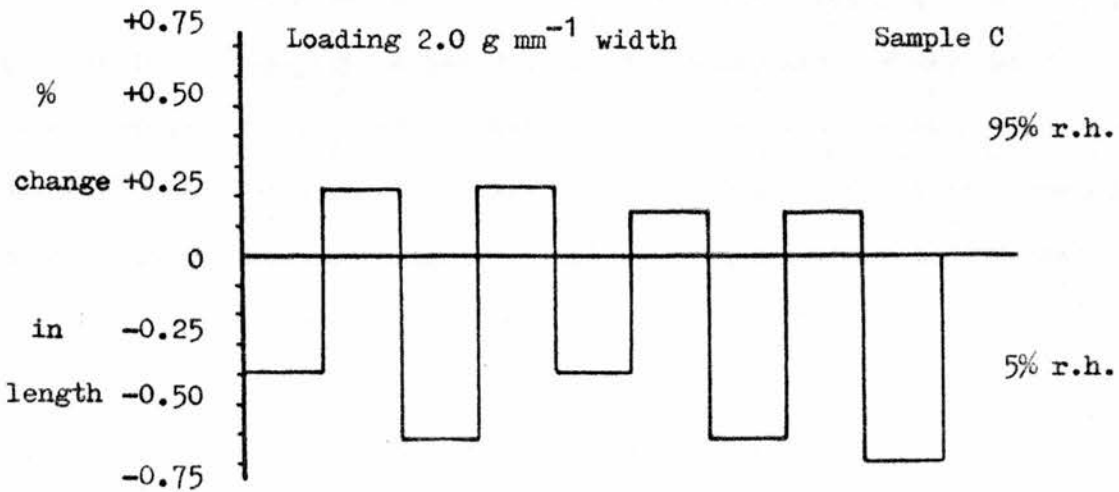
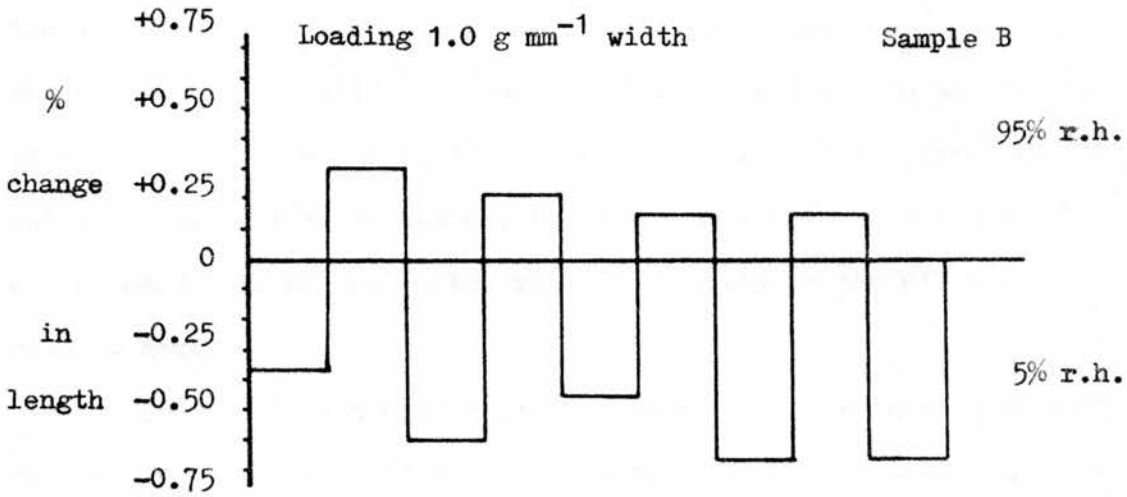
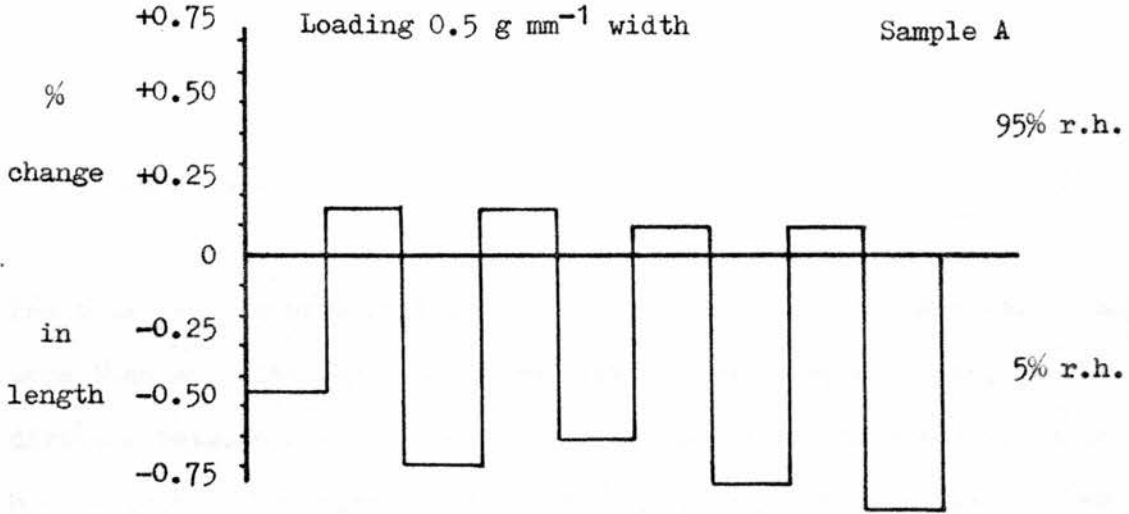


Fig. 92 Long-term response of recording paper samples to extreme changes in relative humidity. r.h. levels alternated between two extreme values over a period of 1 week.

7.B The interpretation of tape irradiance records

7.B.1 Introduction

The tape records were initially stored on their plastic spools. They were then annotated by hand in red ink, giving time and date, and the distance between each adjacent pair of time marks was transcribed into a note book. The irradiance value (E_e) is given by $k(l-1)$ where k is the calibration constant, and l tape length between time marks. At the outset k was not known, and it was simply the value of l in mm which was noted. To simplify the reading process, a template was set up in which the tape was passed under the scale of a transparent plastic rule. During this operation, the tape was stored in a loose pile in a cardboard box, and collected in a similar way on the other side of the reading desk.

Since it is intended that the tapes should be machine readable, red ink, which would not affect a red-light optical scanner, was used for annotations on the tapes.

For the purposes of presentation in this volume, the tapes for four individual days have been pasted to cards, and are presented as Figs. 104 to 107. One of these cards is original in each volume, the other three are photocopies. Each original is faced by its photocopy to facilitate comparison. The reading sense for the mounted tapes is from left to right, top to bottom.

7.B.2 Operator error and the reading of tape records

Clearly it is desirable that the tape records can be read by different people with the minimum of subjectivity. Therefore three

subjects were given photocopies of the records as in Figs. 104 to 107 , and lent the originals, and asked to measure the distances between time marks and write the results on the copies. They were asked to measure 'to the nearest millimetre' and to 'round up or down to the nearest millimetre'. Some subjects took this last instruction to mean 'round only up or down', the others 'round either up or down'. The results from three separate days were measured. In one case results from the same day were given to all three subjects - the second examples given to the subjects differed.

Table 8 gives the errors found and their distribution. In certain cases, where large errors occurred ($\geq \pm 5$ mm) the errors originated in the first measurements of the author. Such readings are ringed in the table. One of the subjects tended to mis-read a reading by ± 10 mm.

As is apparent from Table 8 , and as might have been anticipated, a misreading of ± 1 mm is the most common error found. About 25% of all readings differed by ± 1 mm from those of the author, except in one test where the rate was about 45%. Clearly, the longer the distance between time marks, the less the percentage error represented by ± 1 mm. There is therefore a conflict between good tape economy and the minimisation of operator error in reading tapes. See also Section 4D1 p. 69 .

7.C Recorder constancy

The test of goodness of the recorder and integrator system is to see the variability with which a nominally constant input signal can be recorded and decoded from the recordings.

The simplest way to check this is to replace the radiometer head with a current from a reference source (such as is described in Appendix 10 p. 226), and set the clock for a short timed period, e.g. 1 minute.

Table 8 Error scores for subjects reading irradiance records (Figs. 104 to 107)

Date	7 July 1982			26	2
	1	2	3	July	July
Subject	1	2	3	1	2
Error					
+28	0	0	0	①	0
+17	0	0	0	0	①
+10	0	3	2	0	0
+9	0	0	0	0	0
+8	0	0	0	1	0
+7	0	1	0	0	0
+6	0	0	0	0	0
+5	0	0	0	0	0
+4	0	0	0	1	0
+3	0	2	0	0	0
+2	0	18	1	0	6
+1	0	22	5	4	20
-1	102	20	54	46	20
-2	10	2	2	4	0
-3	0	0	0	2	0
-4	1	0	0	0	0
-5	0	0	2	①	0
-6	1	0	4	0	0
-7	0	0	0	①	0
-8	0	0	0	0	0
-9	0	0	0	0	0
-10	0	0	0	0	0
-19	0	0	0	①	0
-30	①	①	①	0	0
±1	102	42	59	50	40
(±1)%	43	18	25	21	17

N.B. Error figures given are length in millimetres, except where identified as percentages.

Ringed readings represent errors caused by wrong initial readings of the author

Subjects 1 and 3 usually rounded down, subject 2 rounded either up or down

In this way a suitable recording may be obtained quite rapidly. When natural irradiance is being recorded, the night-time periods, as recorded, present a good visual check in which unaccustomed variation can usually be discerned. The first and last few centimetres of the tapes presented in Figs. 104 to 107 give representative examples of this.

7.C.1 Statistical examination of recorder constancy

Using the methods outlined above, a new full tape was recorded, first with supply spool full and take-up spool empty, then with the conditions reversed. Two recordings each were made for both conditions, one at about five times the equivalent dummy irradiance value of the other. The results were:

Table 9 Statistical examination of recorder constancy

Supply reel : Take-up reel : Dummy irradiance level	Full		Empty	
	Empty A	B	Full A	B
Timed periods	50	53	58	44
Mean tape movement, mm	11.74	57.00	11.67 (-0.6%)	56.32 (-1.2%)
Standard deviation	0.66	1.22	0.75	0.79
Std. error of the Mean (S.E.)	0.09	0.17	0.10	0.12

Clearly, the dispersions of readings about their means is not great. The mean tape movement is slightly greater when the take-up spool is nearly empty than when it is nearly full. This may be because of a tendency of the higher torque to snatch tape through the capstan when the spool is empty; on the other hand the difficulty of setting the dummy irradiance level twice to exactly the same levels could give the same effect.

Further evidence of recorder constancy is given in Fig. 93 p. 176 . The abscissa shows mm of tape moved, the ordinate the number of motor pulses given to the recorder, as determined from readings of the solenoid counter (see Fig 24 p. 68). Each point represents results for one day, 39 days in all. From the raw data of Fig. 93 we find:

1. 1 solenoid counter movement corresponds to 1.024 mm tape moved.

Correlation tests of the values of abscissa and ordinate readings used for Fig. 93 give:

2. (all readings used)

Correlation coefficient	0.978
T value for $r = 0$	29.51
degrees of freedom	37

3. (four least correlated points excluded)

Correlation coefficient	0.995
T value for $r = 0$	61.87
degrees of freedom	33

These values, which incorporate human error in reading, as well as the true errors, are quite satisfactory.

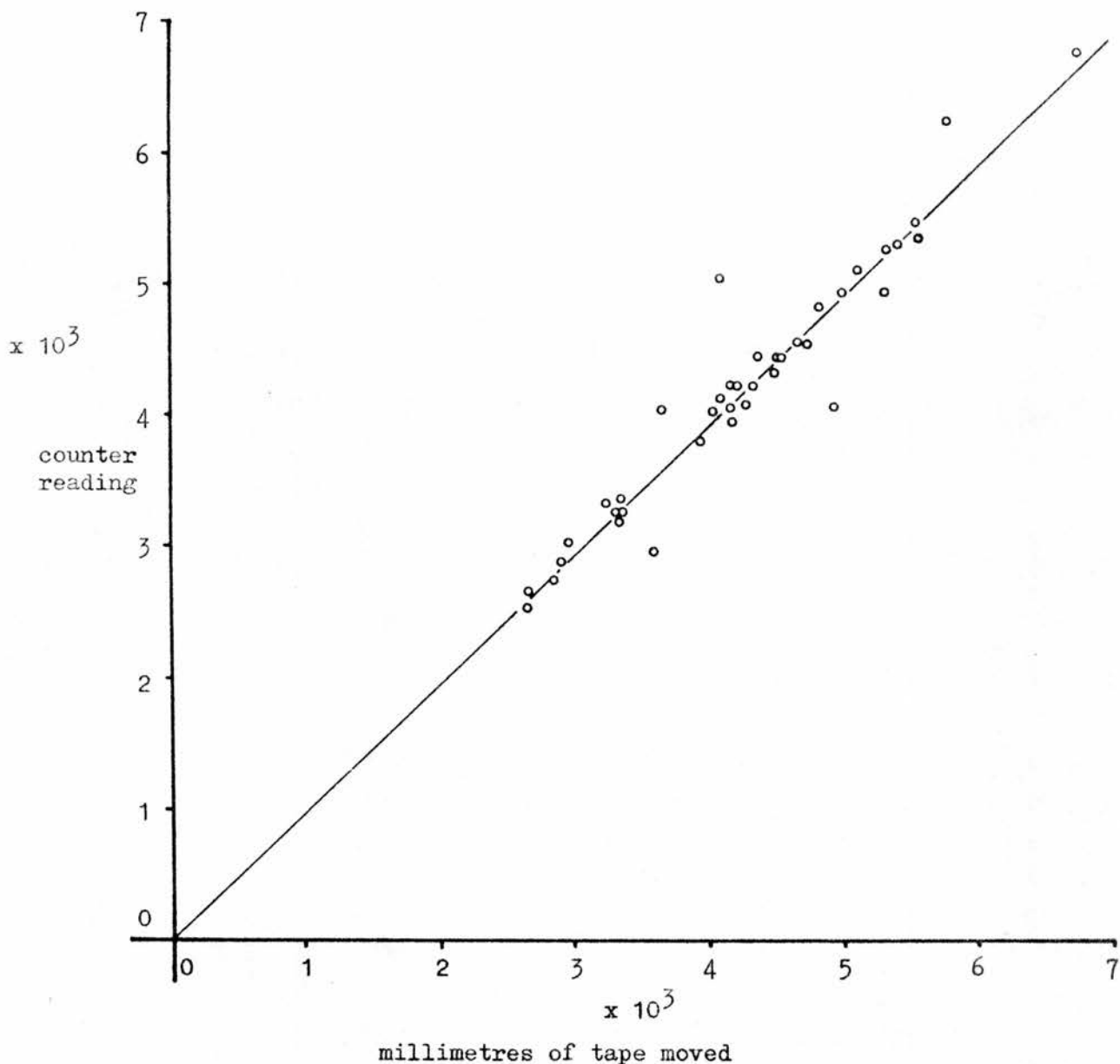


Fig. 93 A check on the relationship between actual paper movement and motor solenoid pulses registered on the recorder counter during field trials. The data points relate to daily totals for 39 days at Sutton Bonington, July - August 1982.

Correlation of the values of the x and y co-ordinates.

Correlation coefficient	0.978	0.995 *
T value for $r = 0$	29.51	61.87
Degrees of freedom	37	33

* These values apply when the four least correlated pairs of co-ordinates are excluded from consideration

7.D Integrator Calibration, drift of calibration, and temperature coefficient

7.D.1 Introduction

Before the field trials described in section 7E5 p.199 , the entire integrator, range change unit and a clock to the design of Appendix 11 p.280 were rebuilt into a die-cast box measuring 20 x 11 x 6 cm. To decrease the dependence of the range changer on battery voltage, resistors R5A, R9A and R12A (Fig. 73, p. 141) were all replaced by constant current sinks. In addition, whilst the performance of the integrator for the field trials was satisfactory, it was later found that the calibrations obtained immediately before and after the field trials were significantly different from earlier ones. This problem was traced to the inadvertent substitution of a different specimen of Q4 (p.113) into the stabiliser, which caused the output to fall below 7.5 volts. The indirect consequence of this was that the recharge voltage of the integrator capacitors C6 and C7 (p. 87) was too low to be clamped by ZD2 to 5.6 V, but was clamped via the effective emitter-follower of Q4 and Q5 to the stabiliser output. This provided reasonable stabilisation, but since it was not the intended operating rationale, the circuit was modified.

The change involved the removal of R10 and R11 (Fig. 28, p. 87) and the substitution of a $25\mu\text{A}$ constant current source between the un-stabilised battery supply (junction of D5 and C3) and the junction of Q5 base and D6 anode. The changes to integrator and range changer are made clear by Figs. 98 to 100 (p. 188) which show the final versions.

Because of these changes, a completely new series of tests was carried out. Since these do not invalidate the earlier calibration and temperature coefficient tests (section 5H, p. 119 ff.), these and

the relevant descriptions have been left in the text. The changes resulted in a decrease in sensitivity of less than 2.5% over the earlier ones.

7.D.2 Integrator calibration and drift

The simplest calibration factor for the integrator is the Time-Current Product, where time is measured between consecutive pulses. This should be a constant, dependent only on the integrating capacitor and the threshold voltages of the circuit. For the low-sensitivity range, C6, a 150 μ F tantalum wet electrolytic capacitor was used. To make the high-sensitivity range as nearly as possible 25 times more sensitive, capacitors were added in parallel on a breadboard until the correct ratio was obtained, to within $\pm 2\%$.

The calibrations were carried out with a supply voltage of 12.0 V, room temperature of 17° - 20°C and always the same current sources, AVO DA211 meter and stopwatch. They were carried out before and after a prolonged thermal stress test, described in the next section.

Fig. 94 , p.179 , gives the calibration graphs for figures obtained before the thermal stress test. (cf. Fig. 65, p. 126). The deviations of the sensitivity are given below the graph, and when combined give a range of integrated currents (and hence irradiance values) of 40,000:1 for $\pm 3\%$ error in integration (deviation in linearity). The corresponding figures obtained after the thermal stress test have not been graphed, since no difference would be apparent from the first graph. Fig. 95 p.180 does present both sets of information in such a way that the deviation from linear integration is apparent. In both cases, it is clear that the integrator was slightly more sensitive after the thermal stress test than before. The changes were $\leq +2\%$

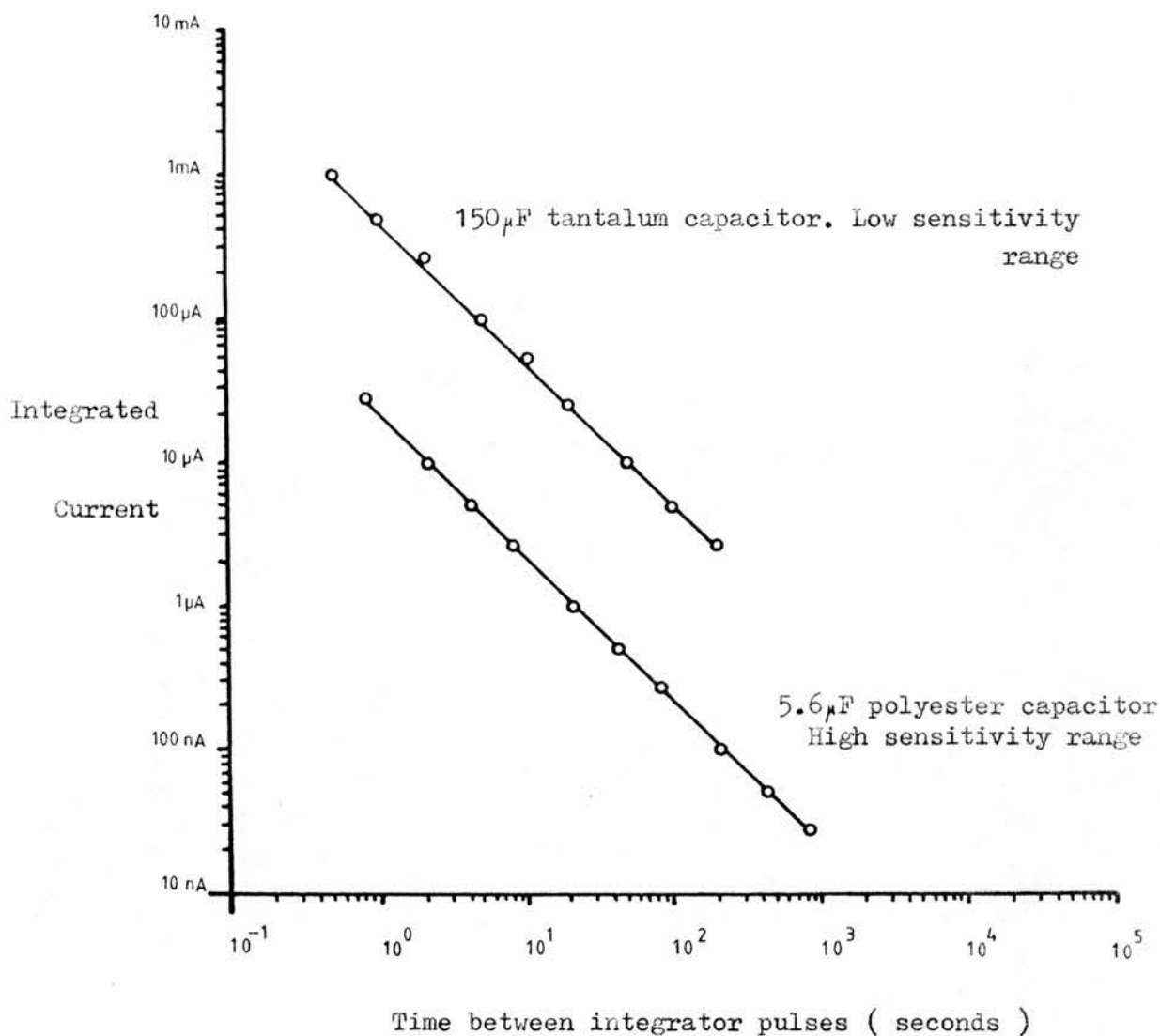
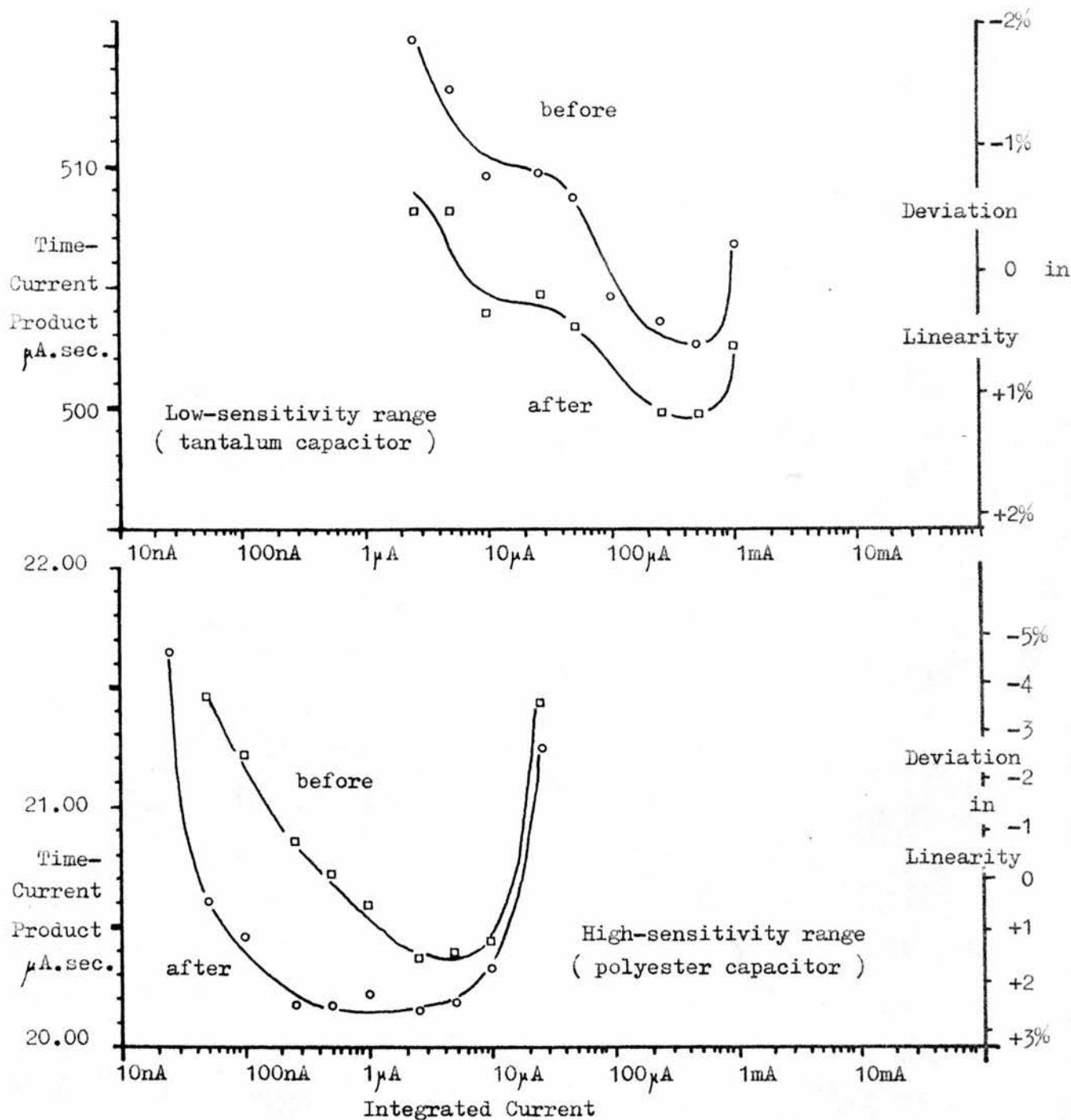


Fig. 94 Test calibration - before thermal stress tests

Integrating Capacitor C_{intg}	Dynamic Range	for	Deviation from perfect Linearity
150 μ F	400:1		$\leq \pm 1.5\%$
5.6 μ F	1000:1		$\leq \pm 3\%$

The combination of both ranges give a dynamic range of 40,000:1 for a deviation from perfect linearity of $\leq 3\%$

see also Fig. 95 p. 180



Ratio of sensitivities : before trial - 24.4:1
 after trial - 24.6:1 (25:1 nominal)

Fig. 95 Integrator non-linearity and drift in response to thermal stress

'Before' and 'After' relate to the thermal stress tests of Figs. 96 and 97 (see p. 182) The change in sensitivity as a result of these tests was $\leq +2\%$ for the high-sensitivity range (polyester capacitor) and $\leq +1\%$ for the low-sensitivity range (tantalum capacitor).

Also shown are percentage limits for deviation in the calibration about the mean values.

The Time-Current Product is derived from measurements in seconds and microamps, and is constant for a perfect integrator. The supply voltage to the integrator was carefully maintained at 12.0 V for these tests.

on the high sensitivity range and $\leq +1\%$ on the low sensitivity range (tantalum wet electrolytic capacitor). The values of actual deviation in linearity should be regarded with circumspection; non-linearity of the current meter used (AVO model DA 211) could very easily result in invalid readings. It is difficult to overcome this problem without recourse to expensive calibration against recognised standards. The measured ratio of sensitivities of the two ranges was 24.4:1 changing after the thermal stress test by $+0.8\%$ to 24.6 :1 (25:1 nominal).

Under more favourable temperature conditions, the drift in calibration can be very low. Just before the reconstruction of the integrator and change of circuit from that of Fig. 28, p. 32, the prototype integrator was given a second calibration check to see what change had occurred over the period of 5 years (± 1 month). The printed circuit board had been stored in a normal temperate room temperature and humidity, unprotected save for a coat of lacquer. The change in calibration was a mean decrease in sensitivity of $\leq 1\%$, checked over the current range of $1\mu\text{A}$ to $500\mu\text{A}$, and using the $150\mu\text{F}$ tantalum electrolytic capacitor.

7.D.3 Thermal stress test

To simulate the harshest conditions the integrator and electronics might be subjected to, the electronics, which were in the sealed metal box with some 'drierite' desiccant, were subjected to alternating temperatures of about $+55^\circ$ to 60°C and -20° to -30°C . These conditions were in a laboratory incubator and a communal deep-freeze. The recorder was replaced with a post-office pattern counter; and the counter, main battery (12 V) and connecting leads kept out of the hostile environment. The recorder prototype mechanism is not capable of withstanding

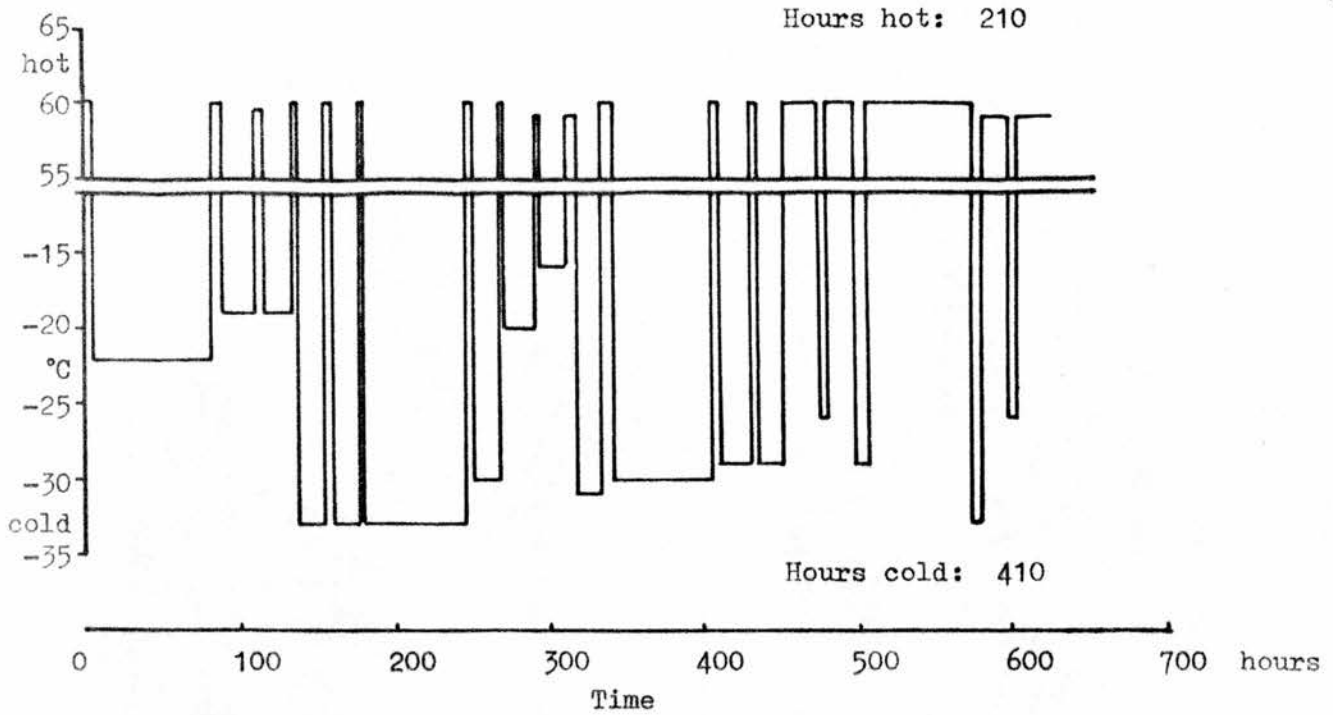


Fig. 96 Time and temperature record for the thermal stress test

Long spells of uniform temperature correspond to weekends. Temperature fluctuations had to be accepted, since the deep freeze used was communal. There were 34 changes from hot to cold, and vice versa.



Fig. 97 Effects of thermal stress on the Integrator/Range changer (N.B. The x axis is not linear in the diagram for the sake of clarity. See Fig. 96 above)

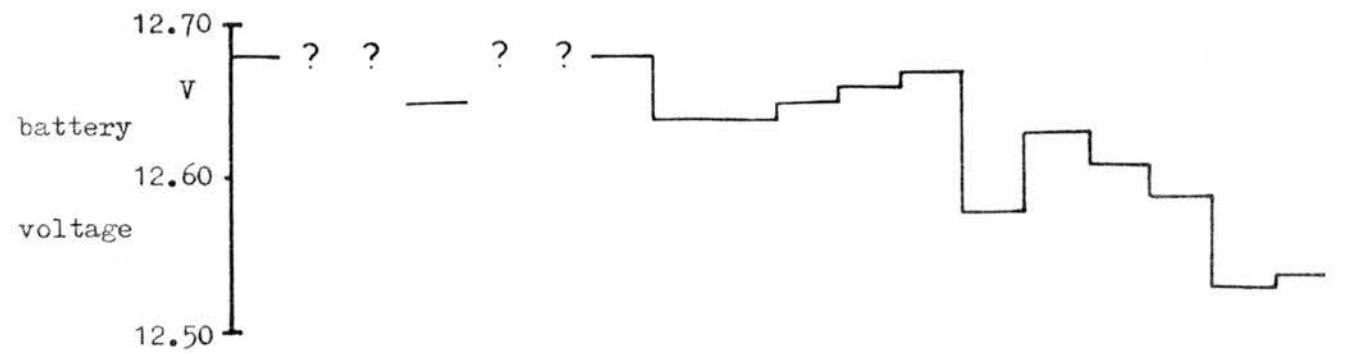
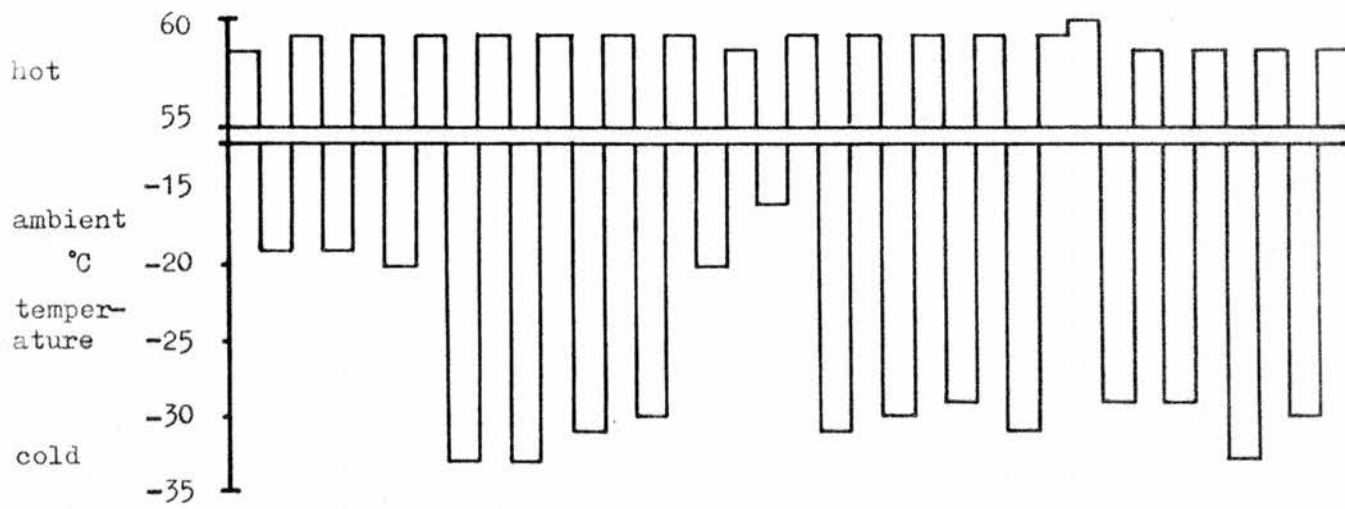
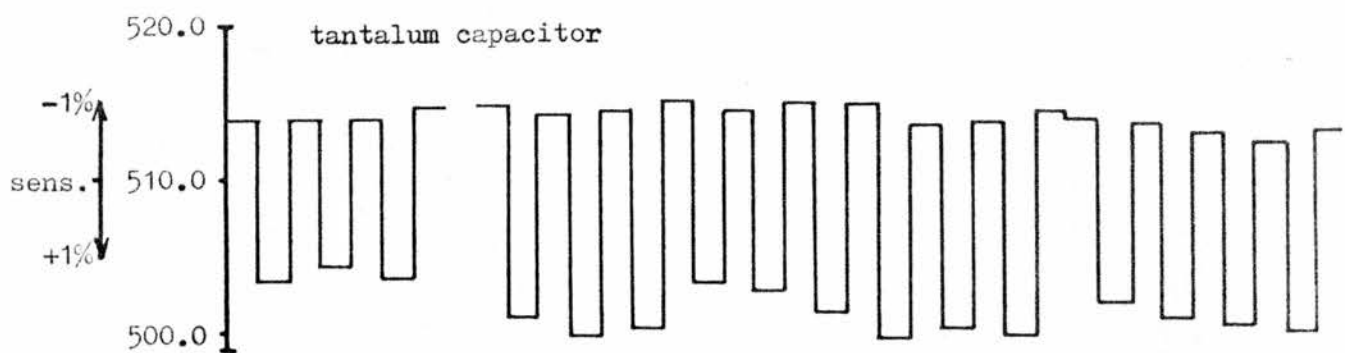
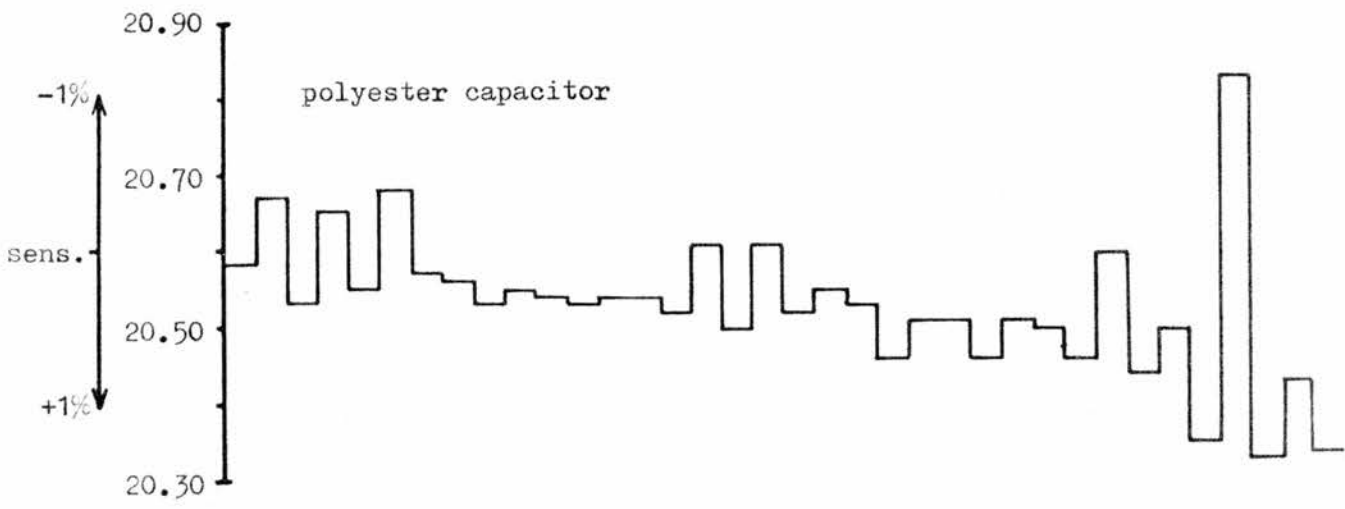
Note the difference in performance of the two ranges of the integrator, due largely to the characteristics of the integrating capacitor (C_{intg} Fig. 28). The polyester capacitor causes a lower temperature coefficient but gave a progressive change in sensitivity over the duration of the test. The tantalum capacitor gives a much greater, though still acceptable, temperature coefficient, but less drift. The gap in the record for the tantalum capacitor was caused by a problem with the range changer battery, unmasked by the continued temperature stress. (see p. 186 for further explanation)

The supply voltage was only recorded intermittently at first. The drift in sensitivity on the **high** sensitivity range may or may not be linked with the progressive fall in battery voltage - it is, however, unlikely and could be due to changes in hydration of the capacitor dielectric.

The sensitivity calibration is the Time-Current product, which is derived from measurements in seconds and microamps - it is constant in the 'ideal' integrator. (see also p.178)

START

FINISH



low temperatures in its present form; the question of batteries is dealt with in Appendix 4 p. 254 . However, the batteries for the range changer (2 x PP3 9 V leclanché pattern) are contained within the sealed box and so were subjected to the temperature extremes.

The effect of temperature on electronic parts is to modify resistance, transistor gain, semiconductor diode forward conduction voltages, leakage currents, insulation, ionic mobility (affecting electrolytic capacitors and batteries), the physical state of electrolytes, and (sometimes importantly) the flexibility and resistance to cracking of cables and insulation. Change in temperature, if too rapid, may through differential rates of heating and cooling, and hence expansion and contraction, cause broken seals, flaked insulation and resistive coatings, and semiconductors may suffer shearing of the encapsulation.

Where coefficients of expansion differ greatly, sustained temperature extremes will produce similar deleterious effects. Thus both extremes of temperature and rate of change of temperature may cause failure.

Changes between the high and low temperatures were made with the least possible delay; however the volume of the box and the static air within will have had a slowing effect on the rate of change of temperature of the electronic circuits. The times at which changes occurred were irregular, fitting in with other commitments. Fig. 97 , p. 183 shows a stylised representation of the temperatures encountered.

At least two hours were allowed for equilibration after each change of temperature, then the integrator and range changer were checked to see that they still worked, and the time between consecutive pulses and the current flowing were measured. Just one integrating current

was used on each range, $50\mu\text{A}$ on the low sensitivity range and $1.00\mu\text{A}$ on the high sensitivity range. The circuitry was electrically energised all the time, but the supply battery voltage was not stabilised; it fluctuated as shown in Fig. 97, probably following changes in ambient temperature.

The slow increase in sensitivity for the sensitive range (polyester capacitor) is quite clear, likewise the obvious temperature coefficient of the tantalum capacitor. Fig. 96 p. 182 shows the true time and temperature course during this test on a linear x - axis scale. The total hot time was 210 hours, the cold time 410 hours, with 34 reversals of temperature.

The drift in calibration resulting from this test, discussed in section 7D2 p. 178 was satisfactory. However, such a test does not guarantee the performance of duplicate equipments - a single component stressed beyond endurance will cause failure of the whole machine; inherently weak components cannot always be spotted, and a badly designed stress test carried out on all copies of an electronic instrument may produce a more unreliable product than if they all remained untested. This is because of damage caused by the tests.

7.D.4 Integrator temperature coefficient

At the close of the thermal stress tests, full calibration of the integrator was done at $+56^{\circ}\text{C}$ and -31°C , and then at 19°C . From these calibrations, the data given below was derived (Table 10 p. 186). From these data, it can be seen that for the worst case value, on the high sensitivity range, a seasonal temperature swing of 30° centigrade degrees will produce a swing in integrator sensitivity of 2.4%, or $\pm 1.2\%$ about the mean value.

Table 10 Integrator temperature coefficient

Integrator range	Low sensitivity		High sensitivity	
Capacitor	Tantalum, 150 μ F		Polyester, 5.6 μ F nom.	
Test Currents	1.0 μ A to 1.0mA		50nA to 1 μ A	
Temp. range, °C	-31° to +19°	+19° to +56°	-31° to + 19°	+19° to +56°
* Mean temp. coefficient	-0.02	-0.03	+0.05	+0.02
Highest recorded value	-0.03	-0.05	+0.08	+0.1
Lowest recorded value	-0.01	-0.02	+0.01	-0.01

* expressed as percentage change in sensitivity per centigrade degree rise in temperature.

7.D.5 Integrator response to fluctuating battery voltage

The integrator was designed to work properly from a 12 V (nominal) battery, with a supply range of 9 to 15 volts. As battery voltage is raised, the sensitivity of the integrator falls. This is probably due to the integrating capacitor (C6 or C7, Fig 28 p. 87) charging to a slightly higher voltage. It has been shown that the slightly fluctuating voltage on C9 is not the cause, by repeating the tests whilst varying the main supply voltage which feeds Q4 and Q5, but clamping steady the voltage on C9.

Table 11 gives the results. Effectively, the change is about $\pm 1\%$ over the course of a battery life passing from charged (13 V) to discharged (11 V)

7.D.6 Conclusions

Overall, the integrator test results have been very satisfactory. A current source such as that of Appendix 10 p. 278 is a worthwhile asset, and along with a stopwatch can be used rapidly to check the condition of the integrator. A minor problem occurred during the

thermal stress test, when the range changer failed to operate. The cause of this was found to be increasing internal resistance in the two small PP3 9V batteries, which together supply the 18 volts needed for the range changer. Increased decoupling, provided by those components asterisked in the amended circuit, Fig. 100 p.190 cured this problem.

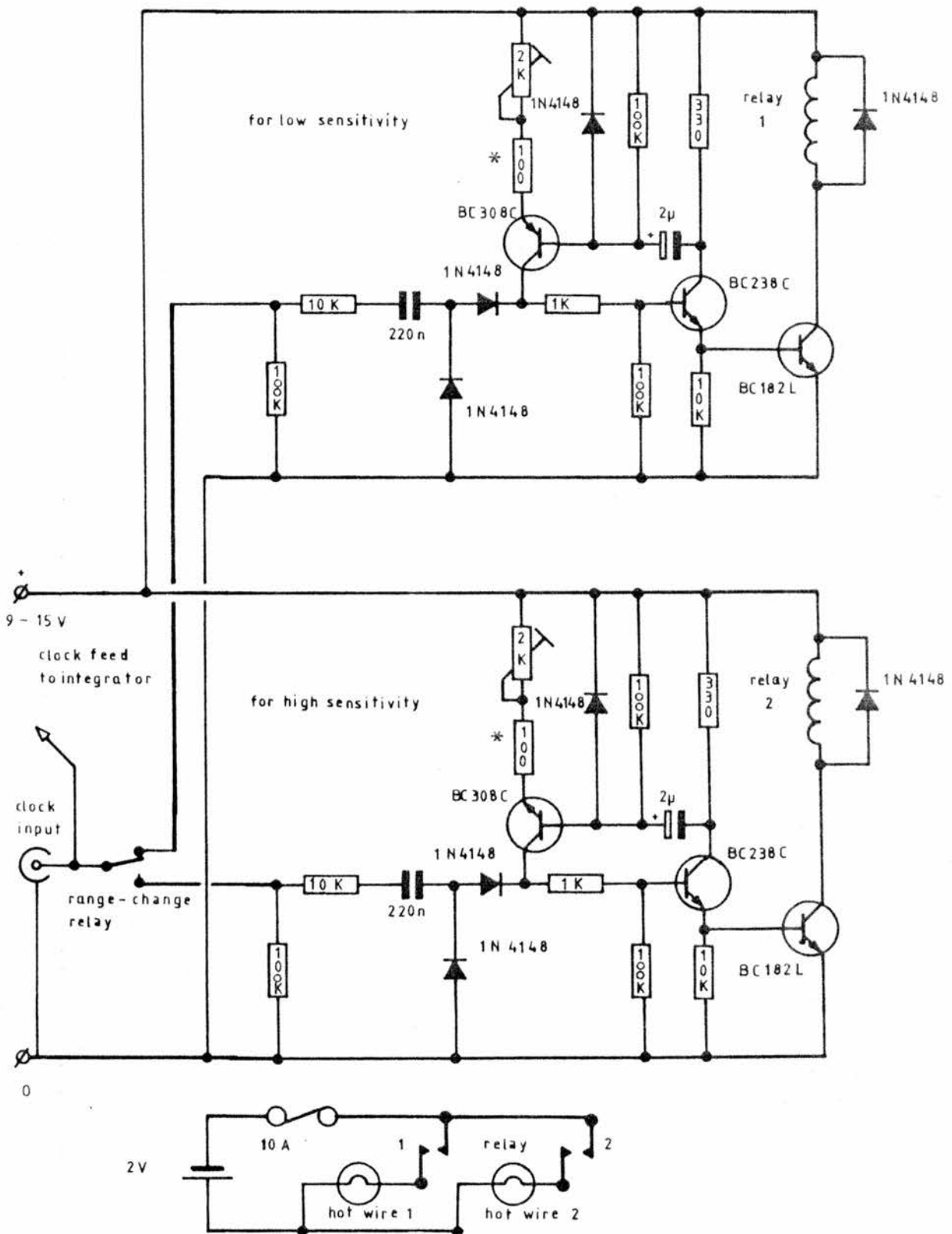
Table 10 Coefficient of battery voltage supply

for high sensitivity range, @ $1.0\mu\text{A}$ integrating current	V_{bat} 9.00 to 10.00	$-2.1\% \cdot \text{V}^{-1}$ *
	10.00 to 12.00	$-0.92\% \cdot \text{V}^{-1}$
	12.00 to 15.00	$-0.91\% \cdot \text{V}^{-1}$
for low sensitivity range, @ $25\mu\text{A}$ integrating current	V_{bat} 9.00 to 10.00	$-2.5\% \cdot \text{V}^{-1}$
	10.00 to 12.00	$-1.06\% \cdot \text{V}^{-1}$
	12.00 to 15.00	$-0.90\% \cdot \text{V}^{-1}$

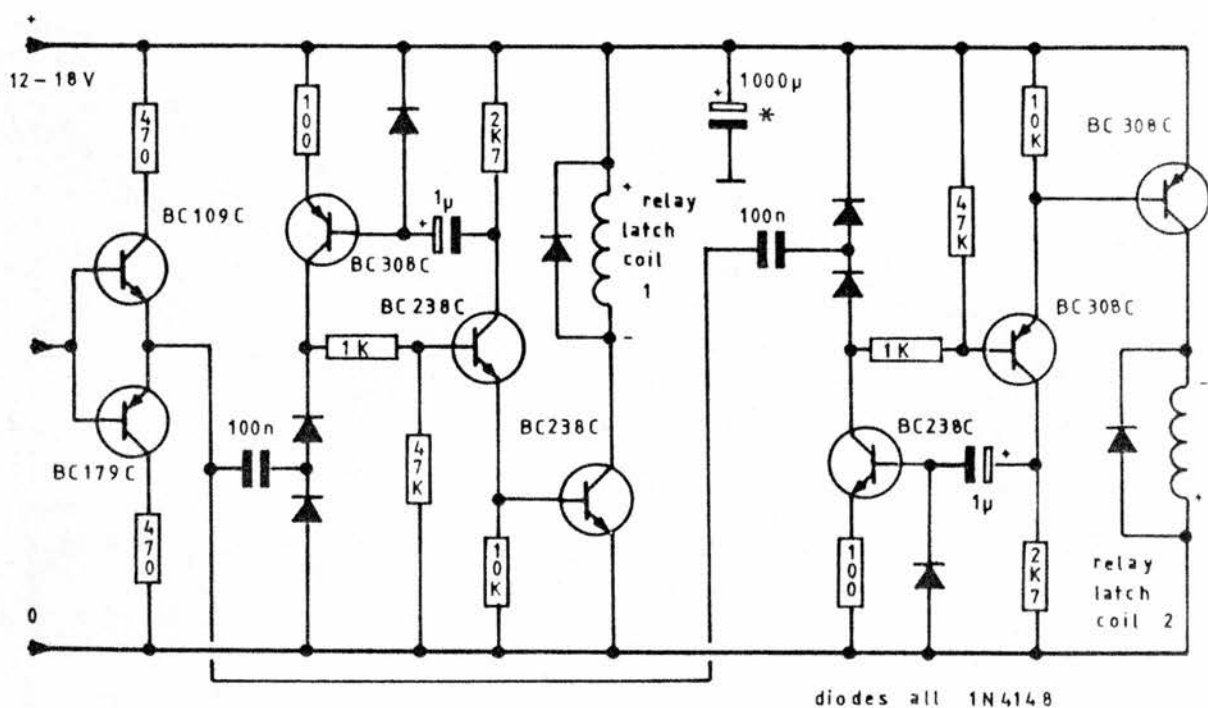
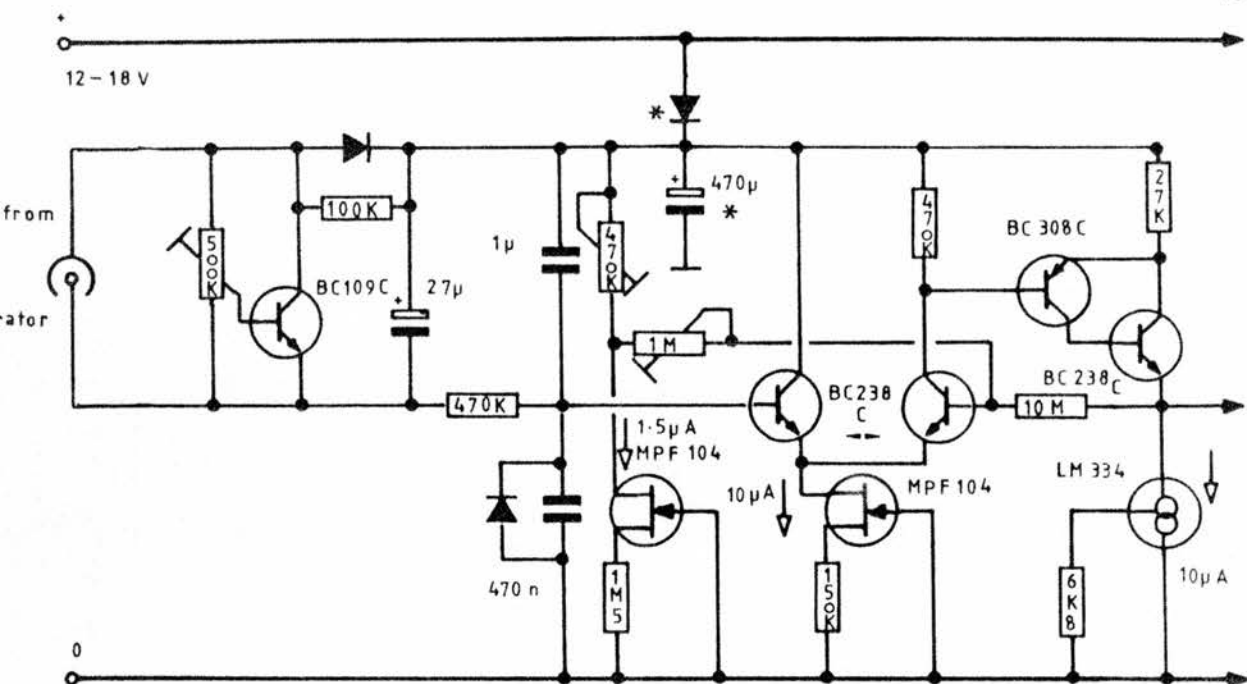
at room temperature 20°C .

* expressed as a change in the sensitivity of the integrator for an increase in battery supply voltage.

Fig. 99 Recorder Hot-wire pen operating circuitry



According to which integrator range is in operation, the second contact set on the range-change relay routes the clock signal to the appropriate pen drive circuitry. Two independently adjustable monostables are used to compensate for differences in sensitivity in the two parts of the hot-wire pen. Where needed, temperature compensation could be provided by using thermistors in the asterisked positions on the circuit diagram.



diodes all 1N4148

Fig. 100 Final circuit of range changer for subjection to thermal stress test.

The asterisked components were installed after the early failure of the circuit in the thermal stress trial. They decouple the relay drive from the threshold detecting circuit and eliminate the effect of high battery resistance. In the range-changer, the constant current 'tails' provide complete proofing against changes in threshold voltages resulting from changes in battery voltage. At a drain of $25\mu\text{A}$, as here, 2 x PP3 batteries will power the unit for many months.

7.E FIELD TRIAL RESULTS

7.E.1 Introduction

On p. 162(equipment trials) the basic information on the trial is given, and as noted in section 7D1 p.177 different calibration factors pertained to the integrator during this field trial from those established, after modifications were made, before the thermal stress test.

The original intention was to measure the incoming photosynthetically active radiation (PhAR) directly, in the manner of SZEICZ (1966,1974). Two Kipp solarimeters (pyranometers) were set up, one with a standard all-wavelength passing glass dome, the other with a SCHOTT RG695 (formerly known as RG8) glass dome. The RG695 is an infra-red passing glass with 10% and 90% transmittances (τ) of 690 nm and 710 nm respectively. The 50 % τ is at 700 nm wavelength. By subtraction of readings from the i.r. sensing radiometer from those of the all-sensing radiometer, the PhAR values may be found (also see Appendix 1, p. 227). The outputs from the two radiometers were split between electronic integrators and the two channels of the twin chart-recorder. The integrators were to be switched over to duplicate channels at 00.00 hours GMT, using an automatic switch, allowing the previous days' totals to be noted during laboratory working hours. The chart records were to be available for comparison with graphs constructed from the data coming from the new recorder under test.

Unhappily, only the total irradiance integrals could be recorded electronically from 00.00 to 24.00 hours, because no spare switch channel was available for the second (i.r.) integrator. Had the chart recorder worked well, this would merely have been an inconvenience, and

both the integrals could have been obtained from the chart records by planimetry (and the total irradiance values from chart and electronic integrator compared, to provide additional corroboration). However, the chart recorder showed a tendency to drifting of the baseline in both channels, and to prolonged sticking of the pen in the total irradiance channel.

Fortunately, it is generally held (SZEICZ, (1974); McCREE (1981) and STANHILL & FUCHS (1977) that the PhAR can be taken to be 50 % of the total irradiance (global) measured with a thermopile pyranometer, and this figure was applied to produce an estimate of PhAR from the total-irradiance Kipp figures.

7.E.2 Results - I Long term: Performance of the radiometer head, and calibrations.

Good data for comparison was obtained for 36 days. The calibrations for the new recorder, integrator and radiometer head were all derived from the mean performances of the equipment over these thirty six days, which covered a wide range of weather conditions. The raw Kipp pyranometer integrated total was multiplied by 0.50 to convert this total to a PhAR measure, and divided by the raw reading from the new recorder tapes. (This raw reading was at this stage expressed as millimetres of tape: for this purpose, the tape lengths recorded at high sensitivity were divided by 25 and summed with the low sensitivity counterpart to make a days' total). This ratio of integrated Kipp total to millimetres-of-tape total was used as a calibration factor, as explained in the next paragraphs. In fact, the 36 days results produced 36 different calibration factors. The four worst of these were eliminated, and the mean of the remaining 32 values ($\bar{x} = 2.81, \sigma_n = 0.11$)

was used as the overall calibration factor.

At the time of the trials, the calibration factor given for the combined integrator and total irradiance Kipp pyranometer then in use was

$$\begin{array}{l} \left(\frac{\text{raw figure}}{1.27} \right) \quad \text{gives} \quad \text{kJ. m}^{-2} \quad \left(\text{radiant} \right. \\ \text{or raw figure} \times 7.874 \times 10^{-4} \quad \text{gives} \quad \text{MJ. m}^{-2} \quad \left. \text{energy} \right) \end{array}$$

The basic Kipp pyranometer output was given as:

$$12.75 \text{ mV. kW}^{-1} \cdot \text{m}^{-2}$$

The electronically integrated totals were expressed as a five-digit number. The conversion factor for lengths of tape is thus:

$$\text{length (mm)} \times 2.81 \times 7.874 \times 10^{-4} \quad \text{gives} \quad \text{MJ. m}^{-2} \\ \left(\text{radiant} \right. \\ \left. \text{energy} \right)$$

where the factor ' 2.81 ' is the calibration mentioned at the bottom of the previous page.

The correlation coefficient for the thirty six Kipp-obtained PhAR estimates and the new recorder counterparts was found to be 0.982, and the T - value for coefficient = 0 was 31.0 with 34 degrees of freedom. These results are presented in Fig. 101p.197 as a scatter graph, along with boundaries for $\pm 10\%$ deviation of the new recorder results from those of the Kipp pyranometer. The prevalent weather during each recording is also shown.

Clearly, the daily totals of PhAR estimated with the new recorder mostly fall within 10% of the values found using the reference Kipp and Zonen pyranometer, and since these errors include the deviation of the actual PhAR from the assumed 50% of the total irradiance, as well as the errors of reading and analysing much tape, this is encouraging.

It would also seem worthwhile to test the radiometer head more thoroughly, to see if it could be worthy of more widespread use, with or without the new recorder and integrator.

7.E.3 Calibration of integrator with radiometer head, and radiometer head alone.

The calibration factor for the conversion of mm of tape to MJ. m⁻² for the new recorder system was found to be (section 7E2 above) x (2.81 x 7.874 x 10⁻⁴) or x 2.213 x 10⁻³. Since the quantity of tape moved per recorder count is not exactly 1.000 but 1.024 mm, (see p. 175) the conversion factor for integrator counts will be:

$$\begin{aligned} 1 \text{ count} &= 2.213 \times 10^{-3} \times \frac{1}{1.024} \\ &= 2.161 \times 10^{-3} \quad \text{MJ. m}^{-2} \text{ (radiant energy)} \end{aligned}$$

Or, expressing these figures in terms of power:

$$\begin{aligned} 1 \text{ count per hour} &= \frac{2.161 \times 10^{-3} \times 10^6}{60 \times 60} \\ &= 0.6003 \quad \text{W. m}^{-2} \text{ (irradiance)} \end{aligned}$$

and

$$\begin{aligned} 1 \text{ count per timed period of 0.1 hour} &= 6.003 \text{ W. m}^{-2} \\ \text{(as employed throughout these recordings)} &\quad \text{(irradiance)} \end{aligned}$$

The mean calibration factor ($\mu\text{A Seconds}$) for the low sensitivity range of the integrator during these trials was 314.2 (see section 7E4 below, p. 196). Therefore the integration current corresponding to a known count rate will be, for 1 count per timed period of 0.1 hours:

$$\frac{it}{t}$$

$$= \frac{314.2}{360}$$

$$= 0.873 \mu\text{A} \quad (\text{ @ } 6.003 \text{ W. m}^{-2} \text{ irradiance })$$

and it follows from this that:

1.00 μA of radiometer head current (from photodiode)
corresponds to:

$$\frac{1.00}{0.873} \times 6.003$$

$$= 6.878 \text{ W. m}^{-2} \quad (\text{ irradiance })$$

and:

A PhAR irradiance of 1.00 W. m^{-2} incident on the radiometer head
will produce an output current of:

$$\frac{0.873}{6.003}$$

$$= 0.145 \mu\text{A}$$

7.E.4 Drift in the integrator calibration during the field trial

Before and after the use of the new equipment at Sutton Bonington,
in June and November 1982, it was calibrated. This was a simplified

procedure to check the integrator for drift over the course of the trials. Therefore the range of currents corresponding to the radio-meter head output was limited to 10 : 1 for each sensitivity range.

Table 12 Integrator calibration factors

Capacitor	Current range	June i.t (μ A.Sec)	November i.t	Mean	Sensi- tivity change
polyester	250nA to 2 μ A	12.47	13.10	12.79	-5.1 %
tantalum	5.0 μ A to 50 μ A	314.4	314.0	314.2	+0.13 %

polyester = 5.6 μ F for high sensitivity range; tantalum = 150 μ F for low i.t = current-time product. see p.178 s. 7D2 (sensitivity range.

Possibly unwisely, the polyester capacitors used at this time were of the 'stacked foil' construction (SIEMENS MKH B32560/1 series). These are not hermetically sealed, and the absorption of moisture causes an increase in capacitance. Conversely, the five month period in the artificially dry atmosphere of the sealed integrator box should have resulted in drying out, a decrease in capacitance and an increase in sensitivity. There is no very obvious explanation for the decrease in sensitivity. For the thermal stress test, these capacitors were replaced by sealed types from the SIEMENS MKH 32234 range (see p. 178.) The low sensitivity range capacitor was a hermetically sealed tantalum wet electrolytic type.

Since the radiant energy integrated on the high-sensitivity range was very small, the -5.1 % change in sensitivity can be ignored; the +0.13 % change in sensitivity of the low-sensitivity range is satisfactory.

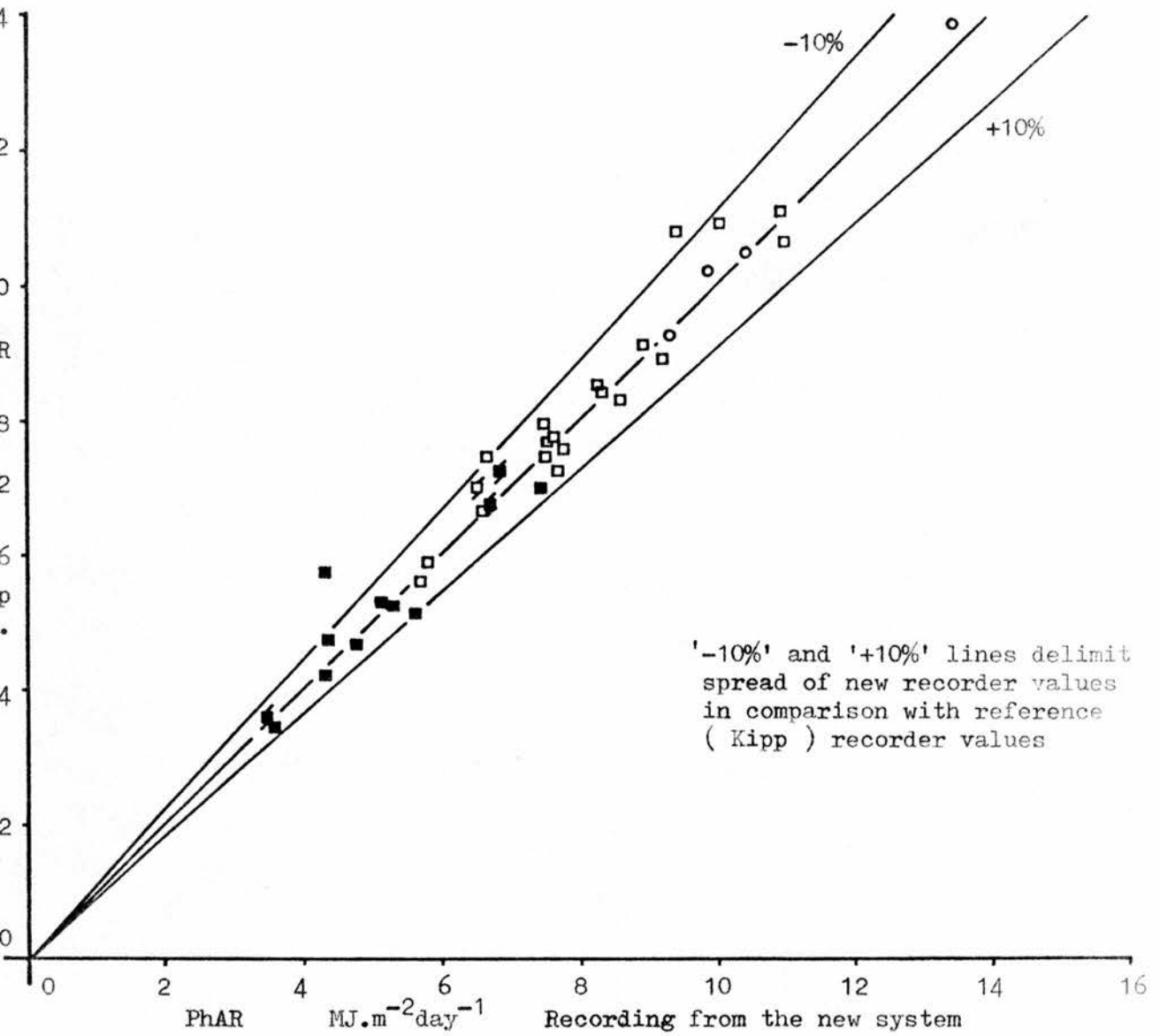


Fig.101 PhAR values: Comparison of New and Reference system recorded values

- bright sun
- alternating sun and cloud (broken cloud)
- overcast
- ◐ ◑ overcast, or broken cloud with thunderstorm

For the PhAR estimation (y-axis) PhAR was assumed to be 50% of the total irradiance as recorded from a thermopile (Kipp and Zonen) pyranometer.

36 pairs of co-ordinates	
Correlation coefficient	0.982
T value for coefficient = 0	31.0
Degrees of freedom	34

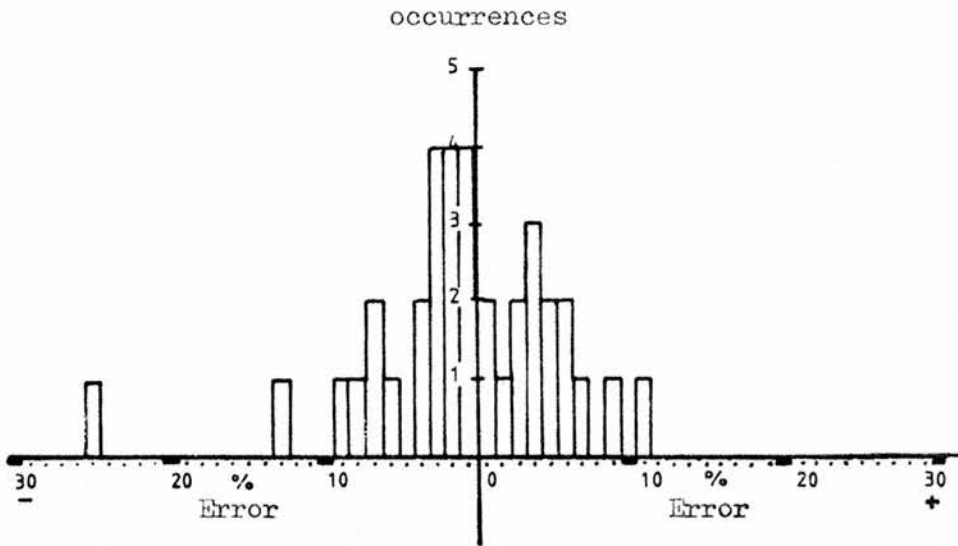
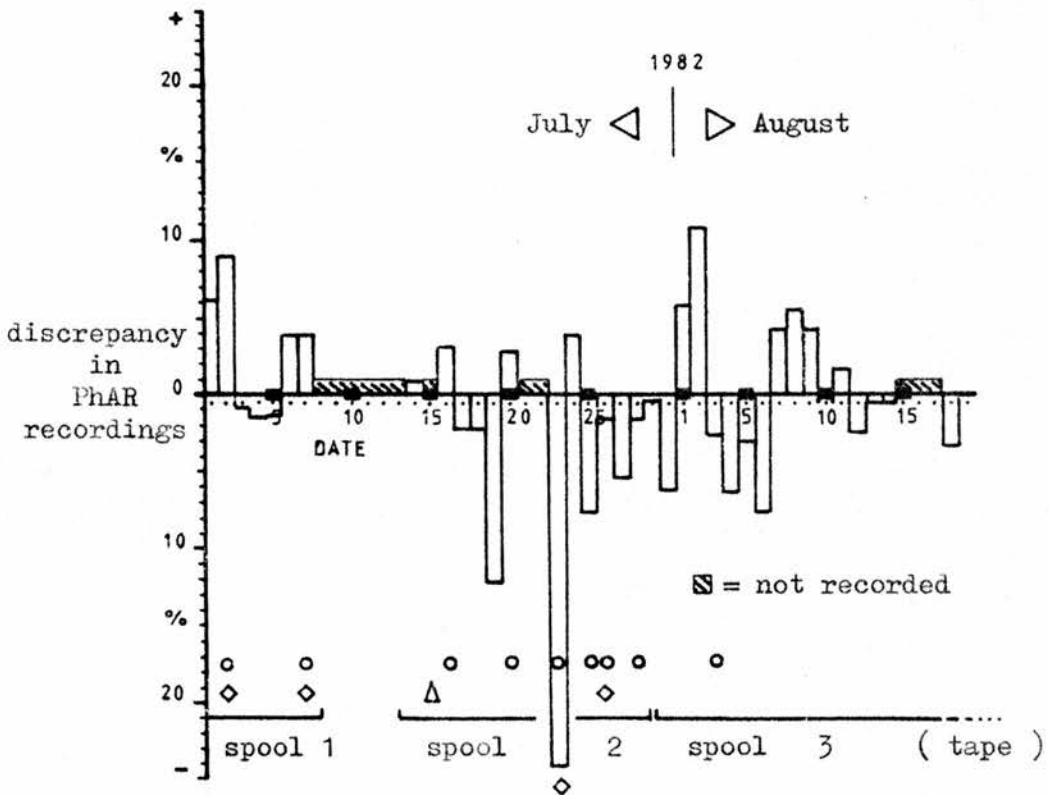


Fig. 102 Histogram showing distribution and size of errors for the 36 days' PhAR totals obtained independently from the New Recorder System and the reference Kipp pyranometer. Note the roughly gaussian shape of the curve. S.D. = $\pm 6\%$



- Δ = day lost because of defect in Kipp irradiance (recording)
- \diamond = recorded tapes presented as Figs 104 to 107 .
- \circ = short-term irradiance records given as Figs. 108 to 116 .

Fig. 103 Error in recordings from the New Recorder System, given as deviation in % from values derived from Kipp and Zonen pyranometer concurrently.

7.E.5 Results - 2 Short Term: Comparison of irradiance records (short term) from chart recorder and new recorder systems.

Fig.103 p198 shows in a day by day record the difference between radiant energy totals from the new recorder system compared with those from the reference Kipp pyranometer. The hatched sections indicate days in which the new recorder was not operating. The first break, July 8th to July 13th. was due to shortage of recording paper, the break from July 21st to 22nd caused by sticking of the new recorder, and that from Aug. 16th. to 18th. caused by a discharged marker-pen battery. As shown in Fig.103, selected days (diamonds and circles indicate which) are presented as tape records, Figs.104 to 107 , or else transcribed as histograms for comparison with chart-recorder graphs from the Kipp and Zonen pyranometer, Figs. 108 to 116 , respectively.

The tape records were pasted on to cards with a polyvinyl acetate wood glue, suitably thinned with water. The annotations in red emerge as being upside down, but the reading sense of the tapes is left to right, top to bottom, and putting the annotations the correct way up would reverse this. The tape of July 23rd gives no clue why the discrepancy between the PhAR-Kipp radiant energy total and the new system total should be so large.

7.E.6 Presentation of the irradiance graphs

These were recorded on standard 9" recorder paper, and the reading sense (i.e. time on the x-axes) ran from right to left, the reverse of normal. Straightforward reduction produced a very obtrusive graticule pattern, so the records selected for presentation here were traced and inverted before being photoreduced. The transcribed readings from the

the new recorder shows evidence of slippage in the relationship of time, due to missed time marks over the course of the day. For example, the first obvious trough in the Kipp chart record, at 08.40 hours is matched by one at '08.10' on the lower graph, but towards the end of the day's records, the trough at 17.30 hours (upper graph) is matched by one at '16.50' hours (lower graph). There are two obviously high readings on the lower graph, marked by question marks, which if split into two would have been more plausible and would have kept the time record correct by restoring the two lost 0.1 hour timed periods. The first one, at about 11.15 hours GMT (lower graph) occurred just after a splice in the tape, which would very likely have disrupted the contact between tape and time marker hot wire. No clue is apparent in the tape record to explain the second one at ca. 15.00 hours GMT .

Date: 17th. July 1982 Radiant energy measurement error: - 2.5 %

Again the Kipp pyranometer record on the chart recorder was partially lost, and the recorder had to be activated at 09.00 hours GMT. The dip in irradiance on the lower graph (new system) at 11.00 hours GMT was not matched on the upper graph. The two brief fourfold falls in irradiance, shown in the upper instantaneous record just after noon are naturally shown differently in the lower graph, where they show up as a small difference to the short term radiant energy totals.

Date: 20th. July 1982 Radiant energy measurement error: +2.7 %

In this case, both the reference Kipp pyranometer and the new system were apparently working to their optimum capabilities.

Date: 23rd. July 1982 Radiant energy measurement error: -24.2 %

The Kipp recorder was stuck at dawn and dusk, but freed itself. The cause of discrepancy (new recorder reading nearly 25 % low) is not known. It could have been, for example, bird droppings on the radiometric receiver head. It does not appear, from the graphs, to be connected with complete failure of the new recording system at any one time, and the cause is likely to remain a mystery.

Date: 25th. July 1982 Radiant energy measurement error: - 7.8 %

The Kipp chart recorder was again unstuck at 09.00 hours GMT. Planimetry of the upper trace would be quite difficult. It is the frequent alternation of sunshine and cloud in a day such as this which is not revealed by the new recording system, but in most cases the short term integrals which are here recorded are more useful.

Date: 26th. July 1982 Radiant energy measurement error: - 1.8 %

The Kipp chart recorder again became stuck during the previous night, being freed at 07.50 hours GMT, and was again stuck during the day from 10.40 to 11.30 hours GMT. Where the records are complete, they compare favourably.

Date: 28th July 1982 Radiant energy measurement error: - 1.9 %

The chart recorder was again unstuck at 07.50 hours GMT. The time on the lower (new recording system) graph is clearly slightly slow compared with the Kipp pyranometer record.

Date: 3rd. August 1962 Radiant energy measurement error : -2.9 %

Chart recorder unstuck at 08.20 hours GMT. Brief clouding at about noon makes it clear that the new recording system is running slow by about 15 minutes. Bright though the sun was on this day (total radiant energy PhAR 10.2 MJ. m^{-2}) it was exceeded on July 17th, which gave a total radiant energy PhAR value of 13.9 MJ. m^{-2} .

7.E.8 Discussion of the irradiance graphs

Overall these graphs seem quite promising. The system is vulnerable to the loss of the absolute time-keeping properties, because of the risk of the time-marks failing to occur. If this is happening, it should be clear that the 'midnight' time established by following the sequence of time marks will begin on consecutive days not to fall exactly half way between dawn and dusk. Obviously, cloud conditions will make dawn and dusk occur earlier or later than they would occur under cloudless circumstances, but a regularly worsening lop-sidedness should make the observer question the time accuracy. As mentioned on p. 60, SUMNER (1959) used a lens and slit so that the sun's image could be used to burn a mark in the chart record for corroboration. Other aspects of the recorded graphs have been considered in Section 4D1 p.69. A second electromagnetic counter in parallel with the solenoid counter would show if this last was losing integrator counts, through sticking.

Figs. 104 - 107

These four figures give photocopied and pasted out recording tapes for selected days from Figs. 108 - 116. In each case, the 'reading sense' of the tape is from left to right and top to bottom. One only of these four is faced by the original tape to which it corresponds; however this only applies to the first four copies of the thesis.

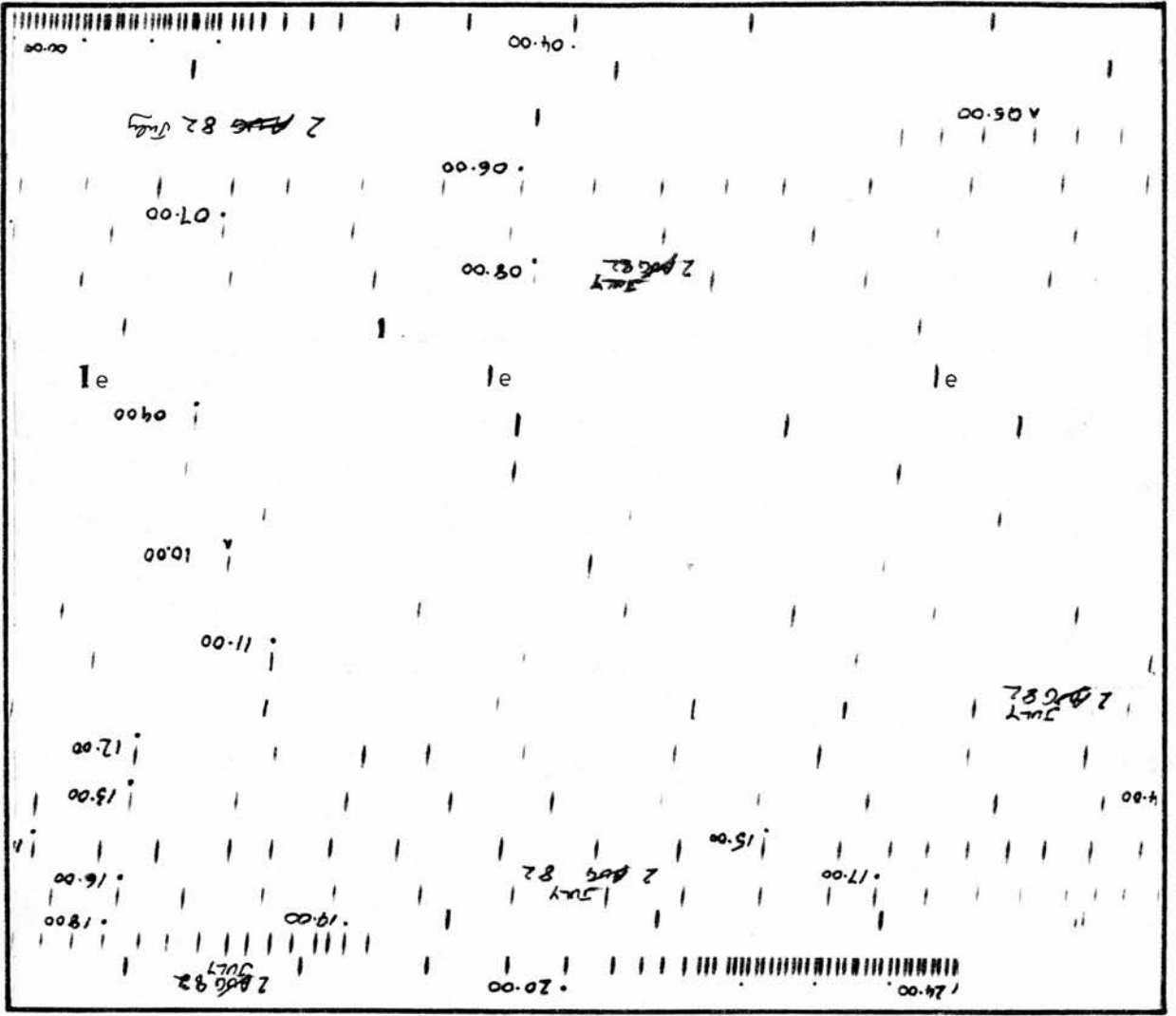


Fig. 104 2nd. July 1982 see p. 171 and 204

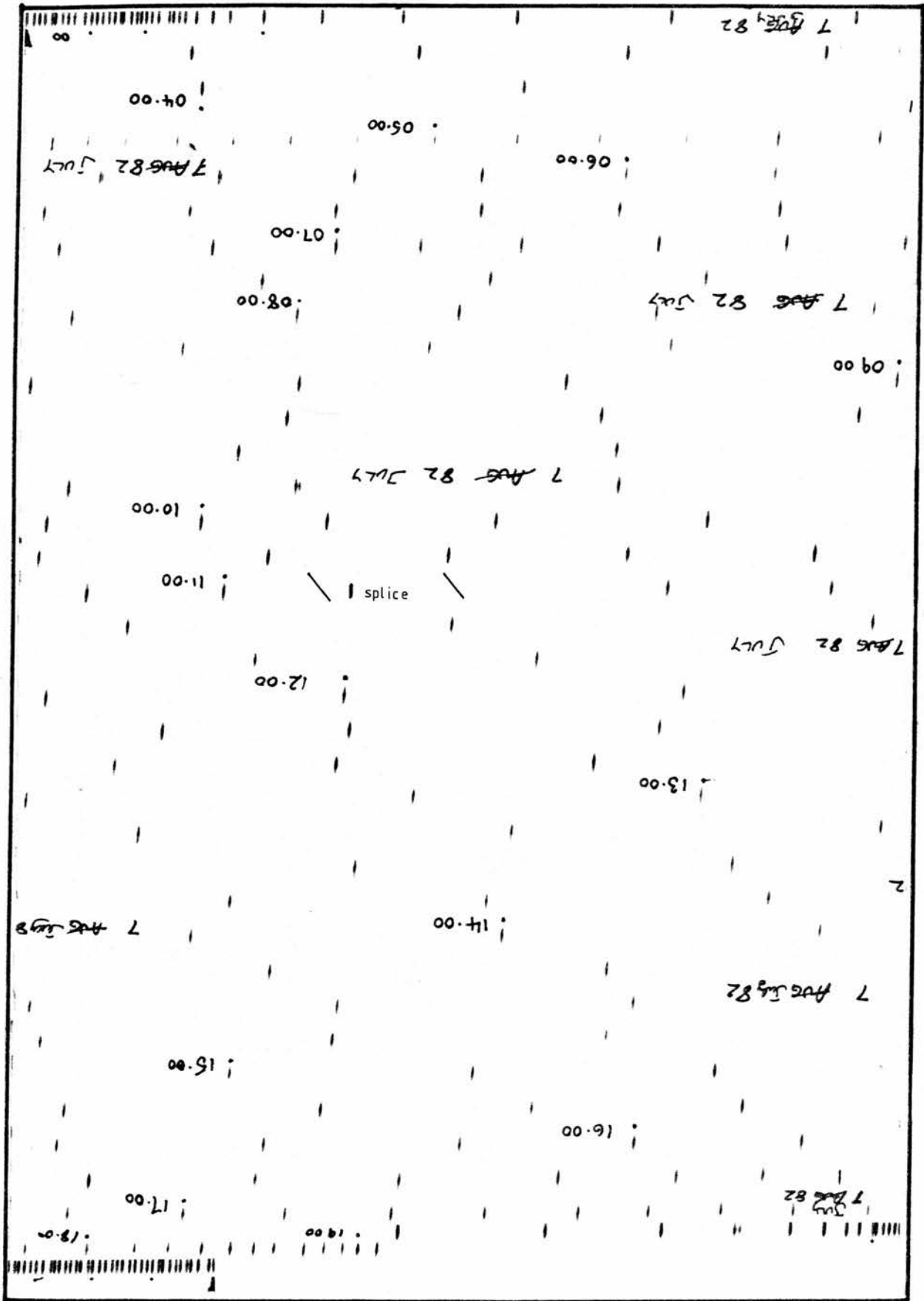


Fig. 105 7th. June 1982 see p. 171 and 204

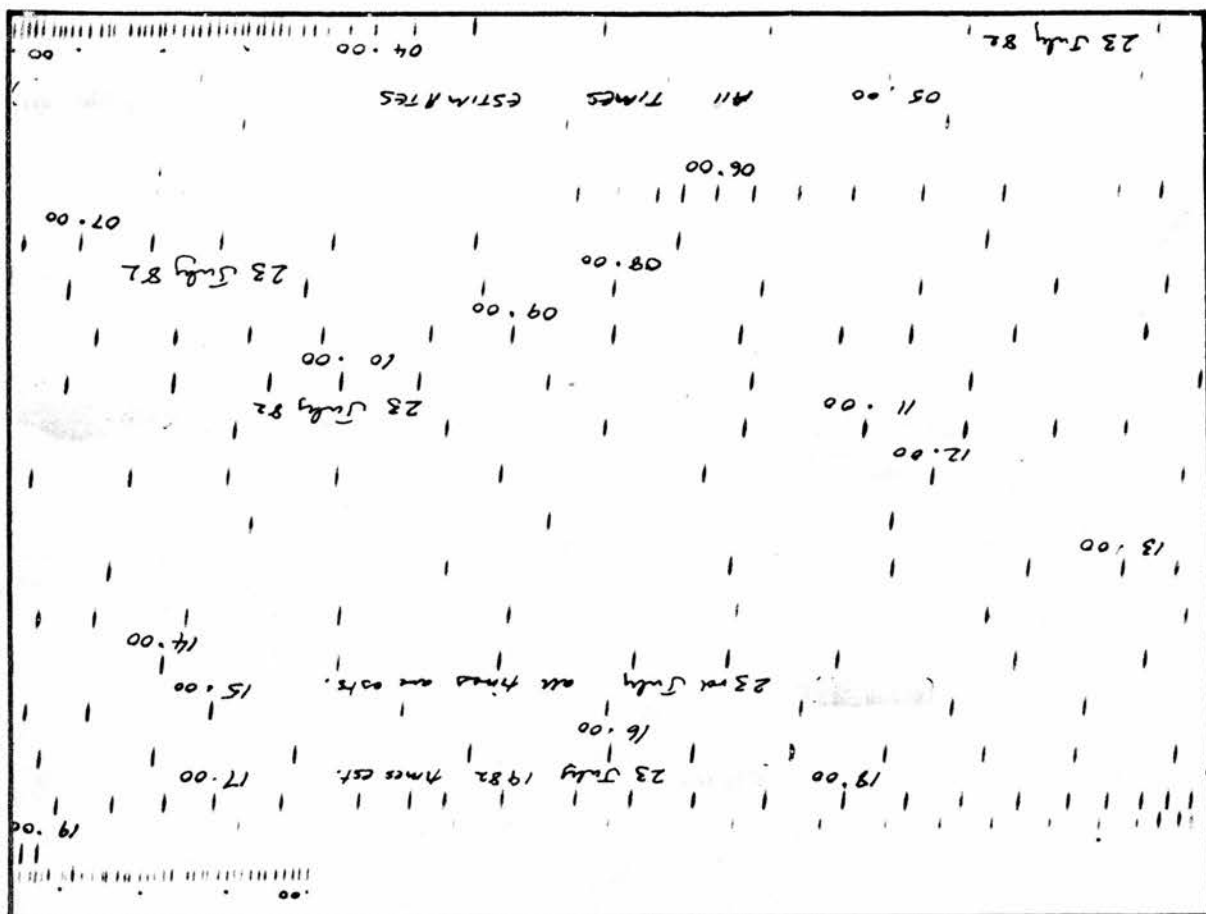
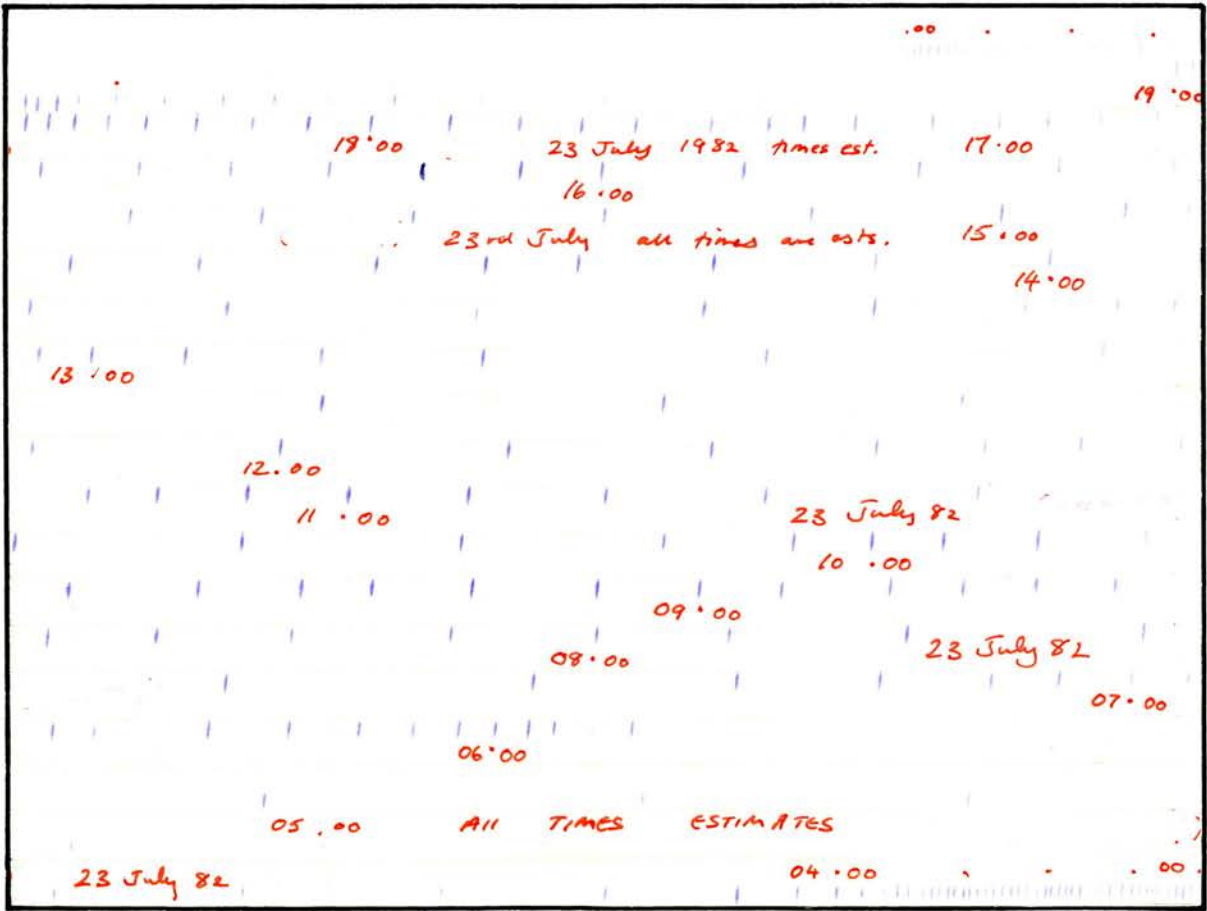


Fig. 106 23rd. July 1982 see p. 171 and 204



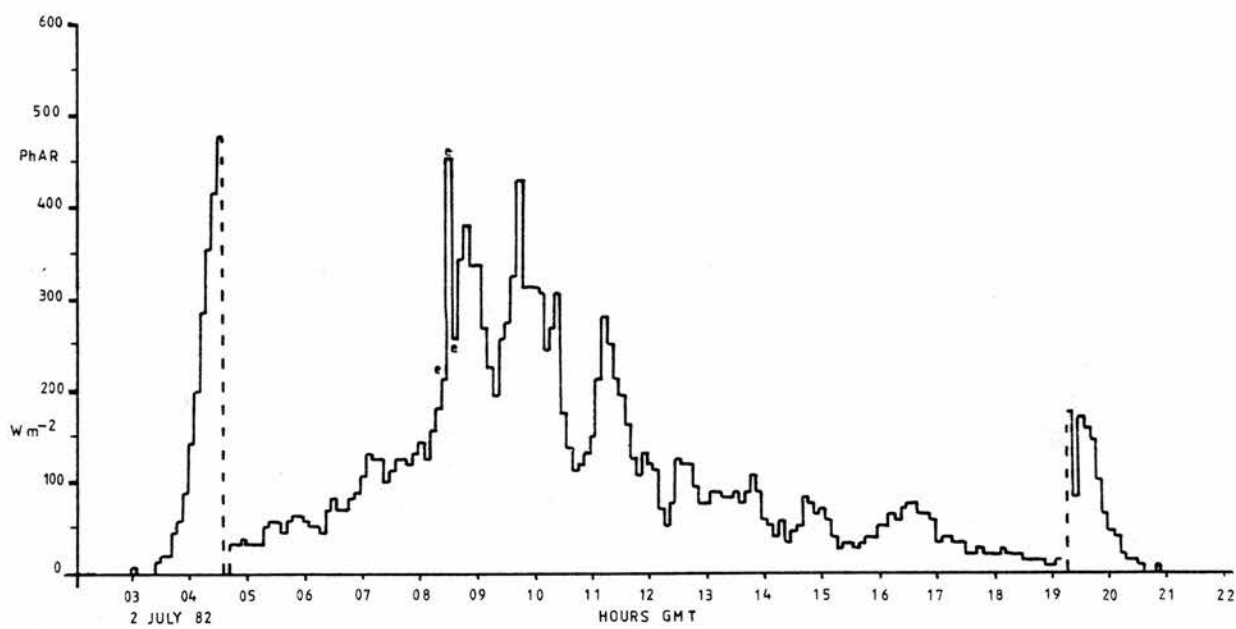
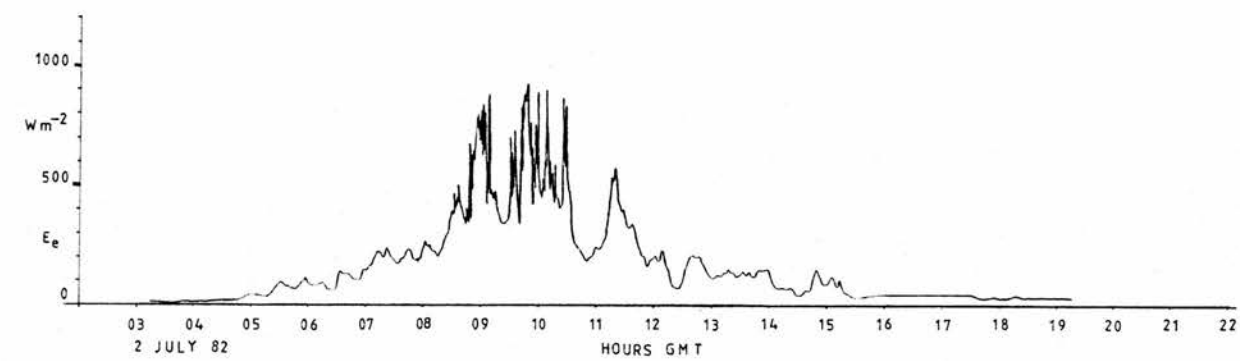


Fig. 108 see p. 199 for discussion

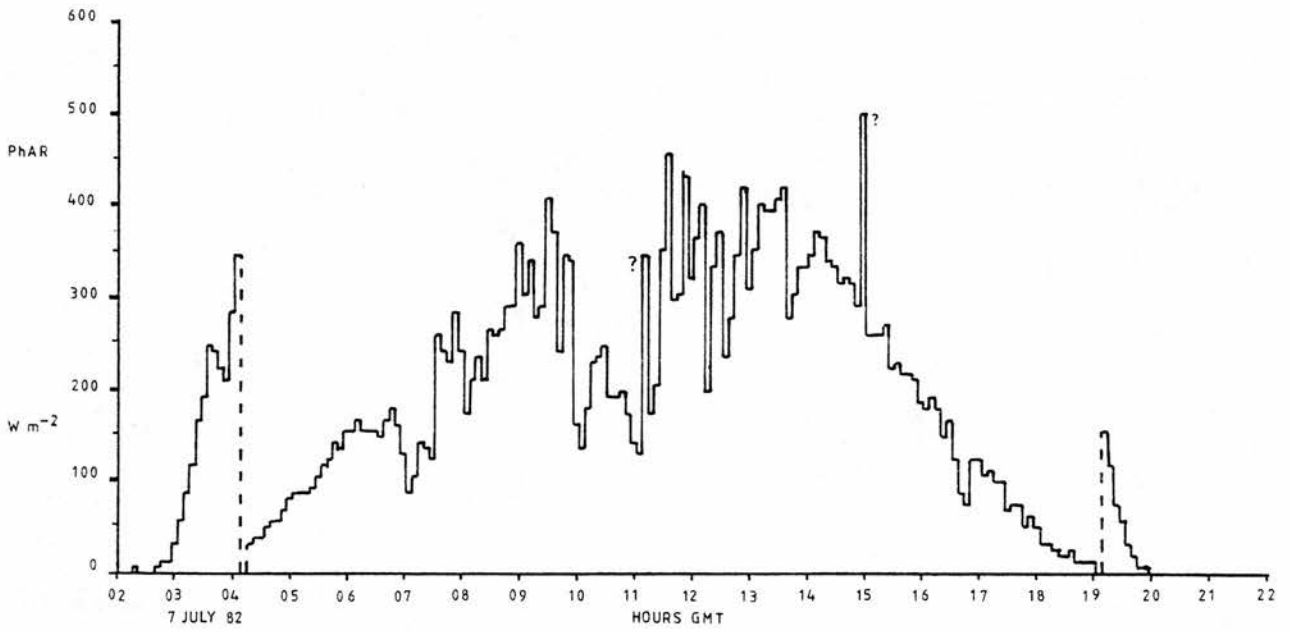
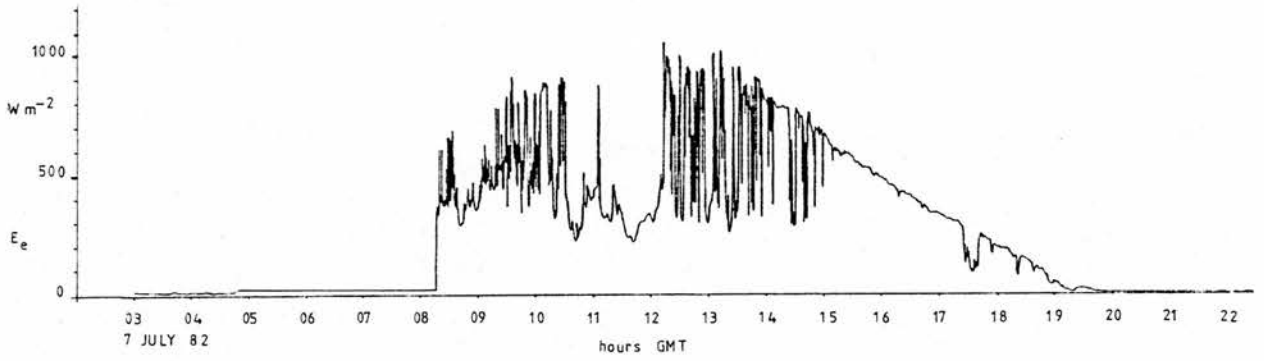


Fig. 109 see p. 199 for discussion

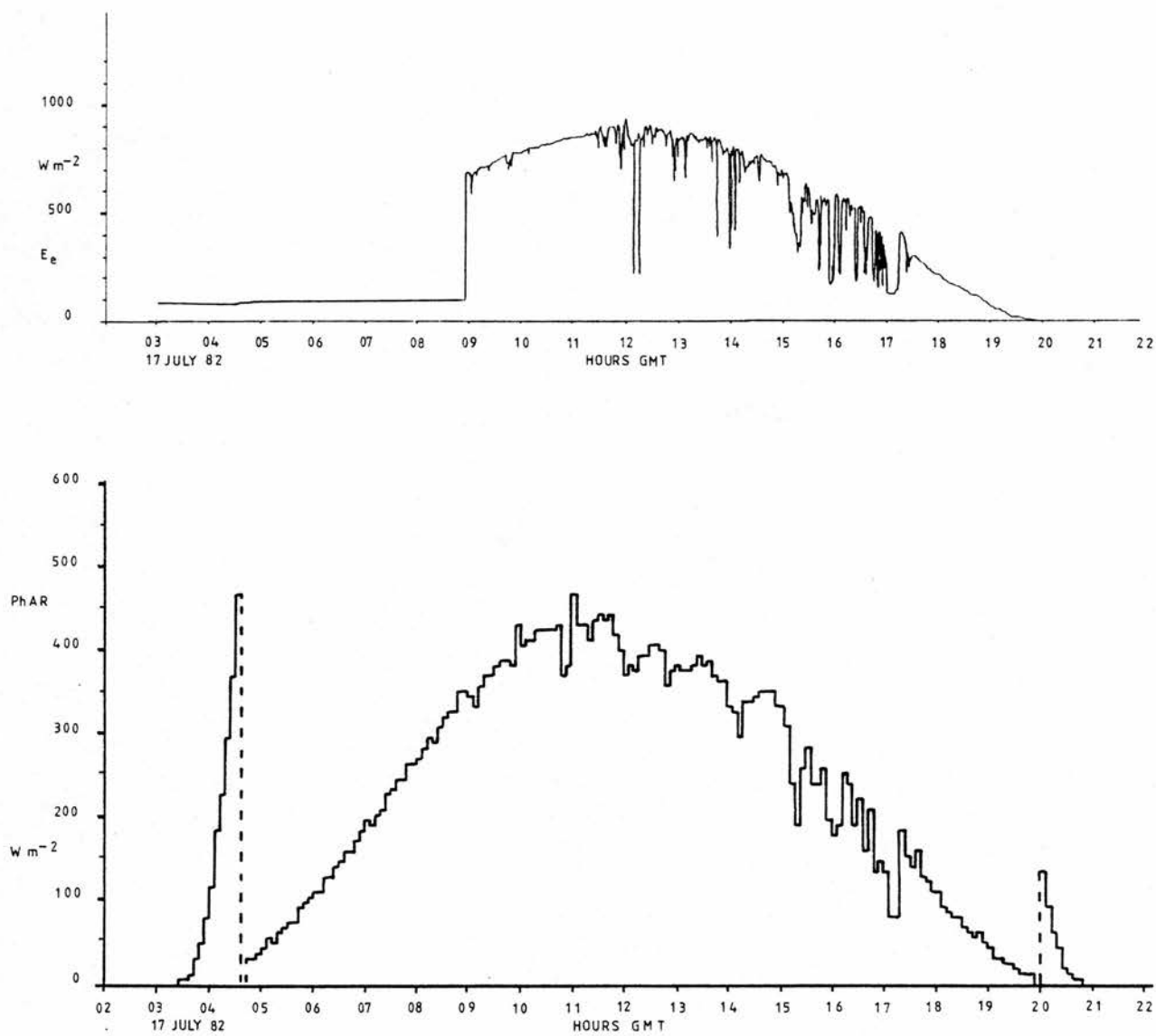


Fig. 110 see p.200 for discussion

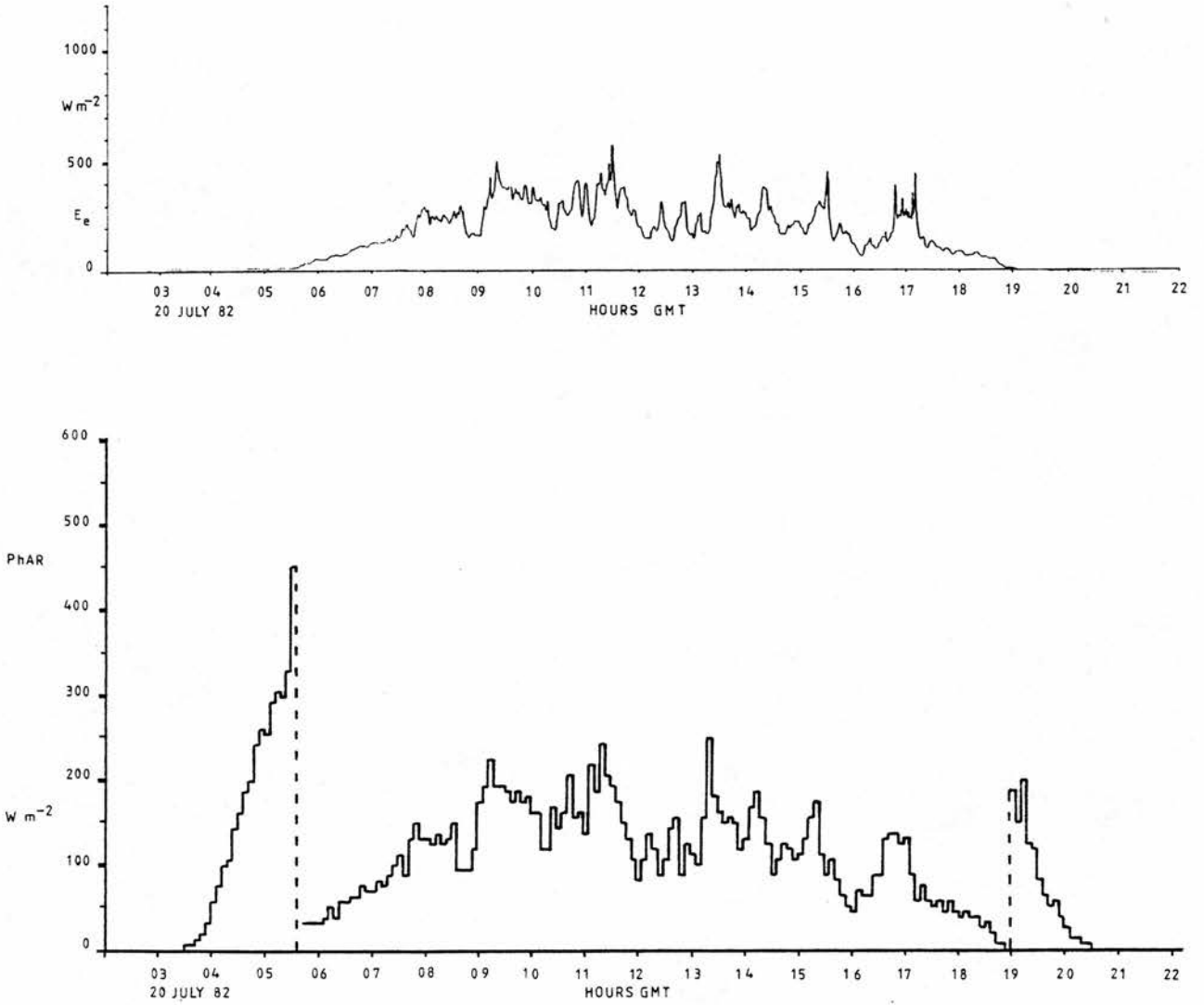


Fig. 111 see p. 200 for discussion

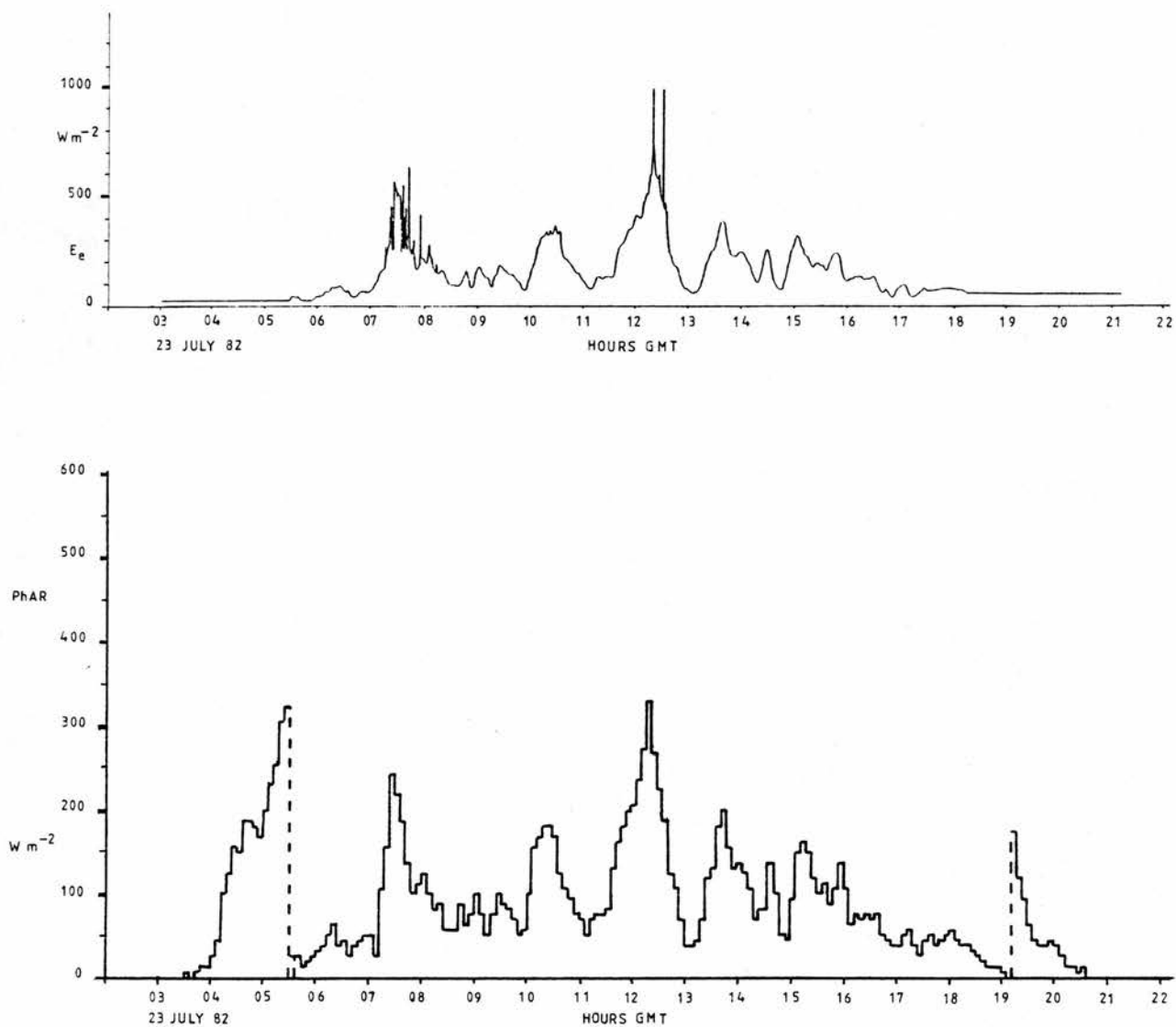


Fig. 112 see p. 201 for discussion

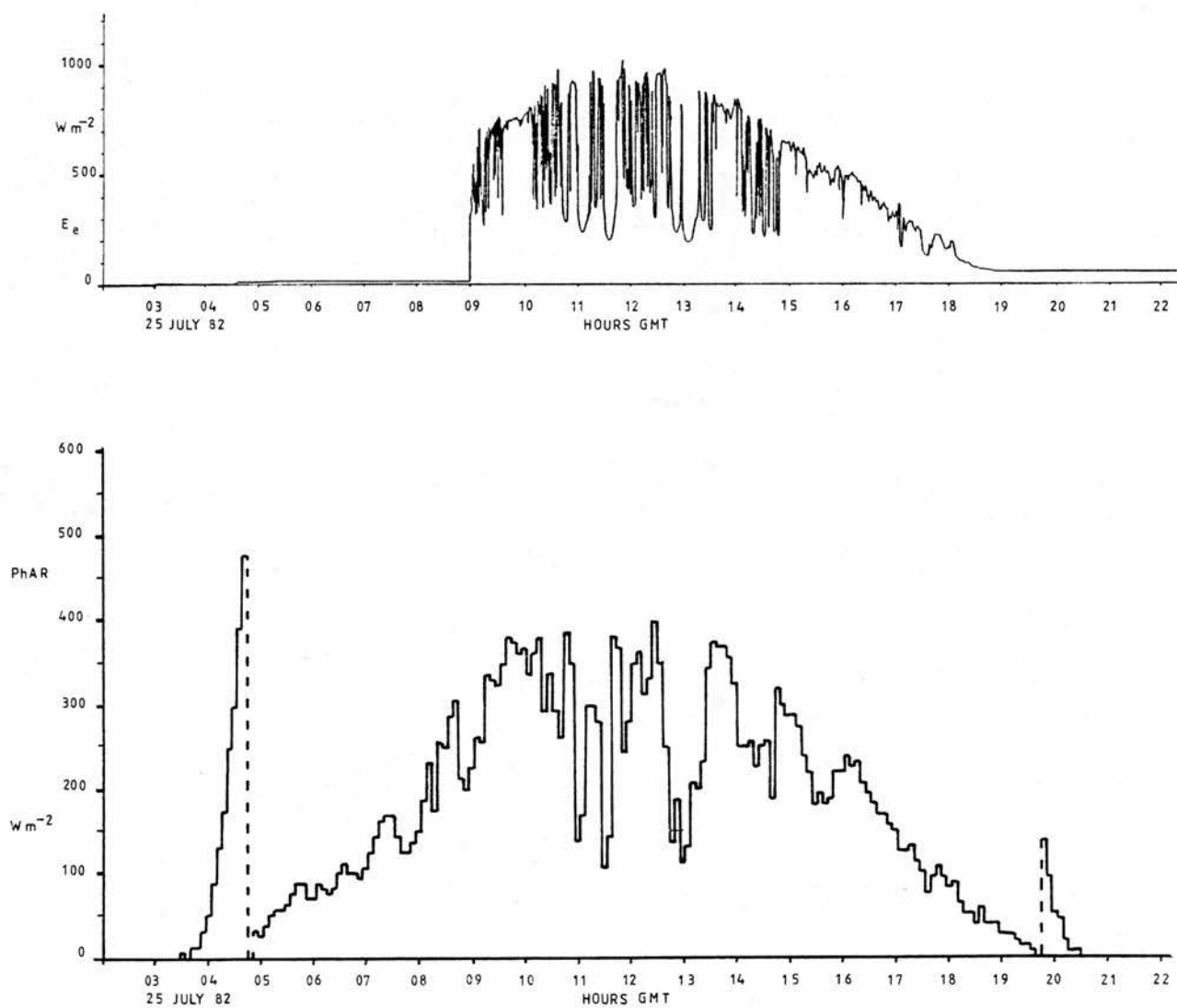


Fig. 113 see p. 201 for discussion

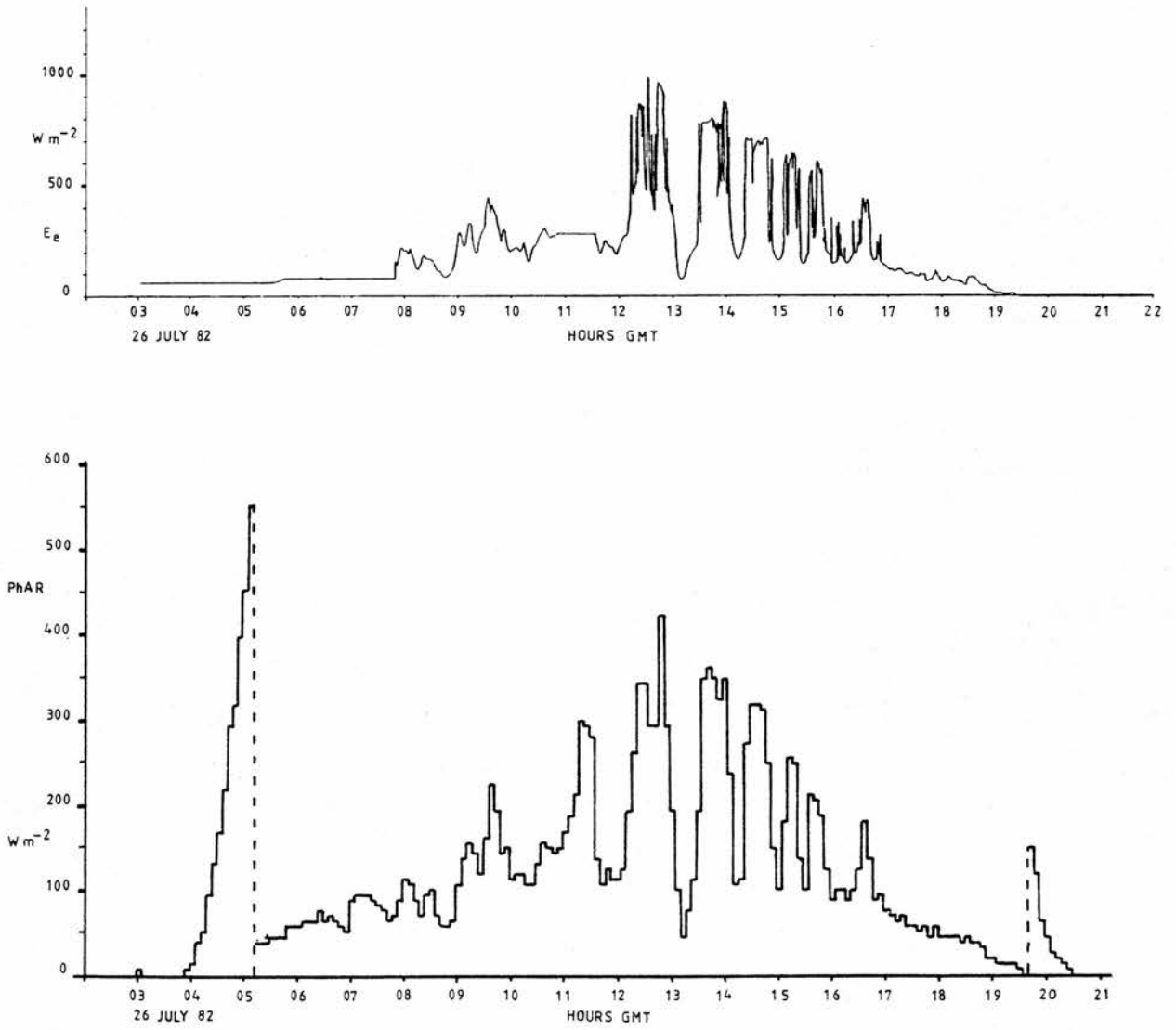


Fig. 114 see p. 201 for discussion

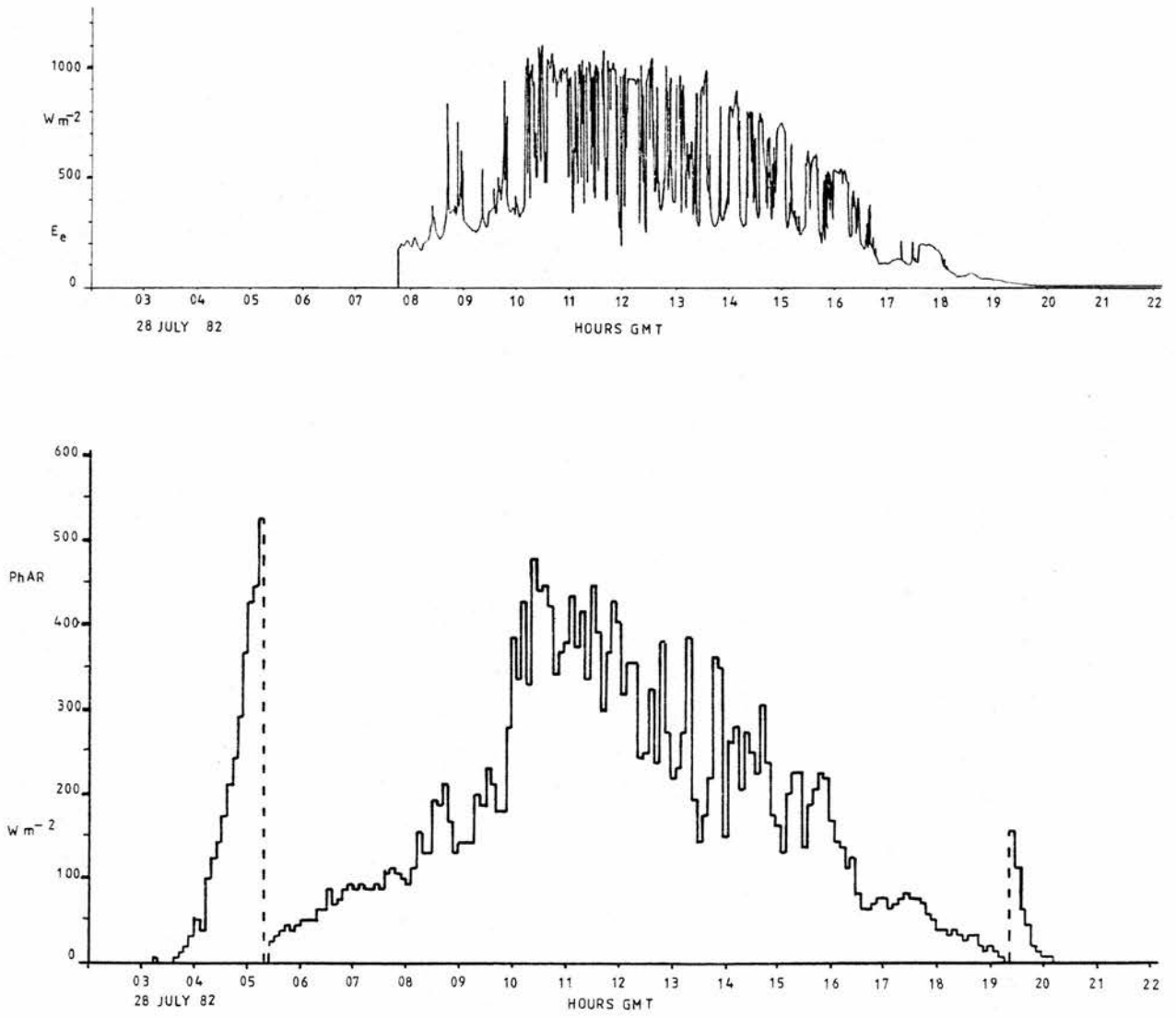


Fig. 115 see p. 201 for discussion

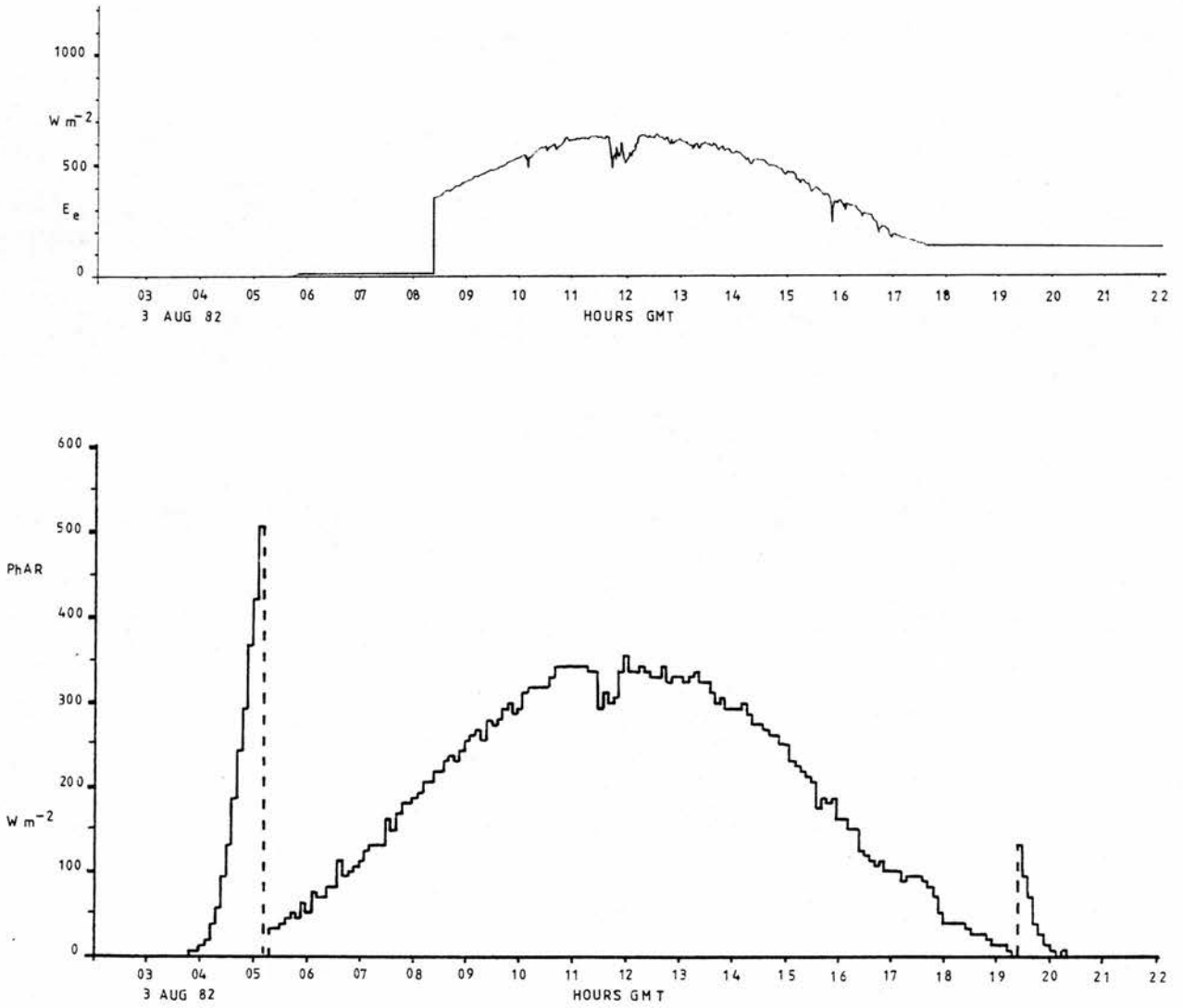


Fig. 116 see p. 202 for discussion

- 7.E.9 Results - 3 : Additional ways of using the new recorder system
- 7.E.10 Twilight levels of irradiance

If the range change unit is available, the apparatus becomes much more versatile. To the entomologist, low irradiance levels associated with moonlight and the rapidly changing irradiance levels at morning and evening twilight are of great interest. (also see p. 4) The phenomenon of diapause - a resting state which may affect insects at any stage in the life cycle - may be controlled by day length, or by rate-of-change of day length (as, e.g. for *Anthrenus* larvae in autumn (WIGGLESWORTH (1964). Referring to the mechanism controlling diapause, BRADSHAW and PHILLIPS (1980) say, " there is a basic conflict in the selective forces determining the sensitivity of the photoperiodic clock to light. On the one hand, the clock would be least affected by varying weather conditions if the underlying chromophore was stimulated during late civil twilight, when light intensity is changing at its maximum rate. On the other hand, too great a sensitivity to light would subject the clock to perturbation by the light of the full moon. The sensitivity of the *Wyeomyia* photoperiodic clock may thus represent an adaptive compromise to these conflicting forces of selection. "

Figs. 117 and 118 show recordings of the twilight period of two May nights in St. Andrews (56°15' N). Note the logarithmic irradiance scale. The minimum irradiance levels which apparently occur in Fig. are several times greater than for the previous night, and this is probably due to the light from the city of Dundee being reflected and scattered back to earth by cloud. The lopsidedness of these curves is possibly due to a genuine cause, or an inaccurate alignment of the radiometer

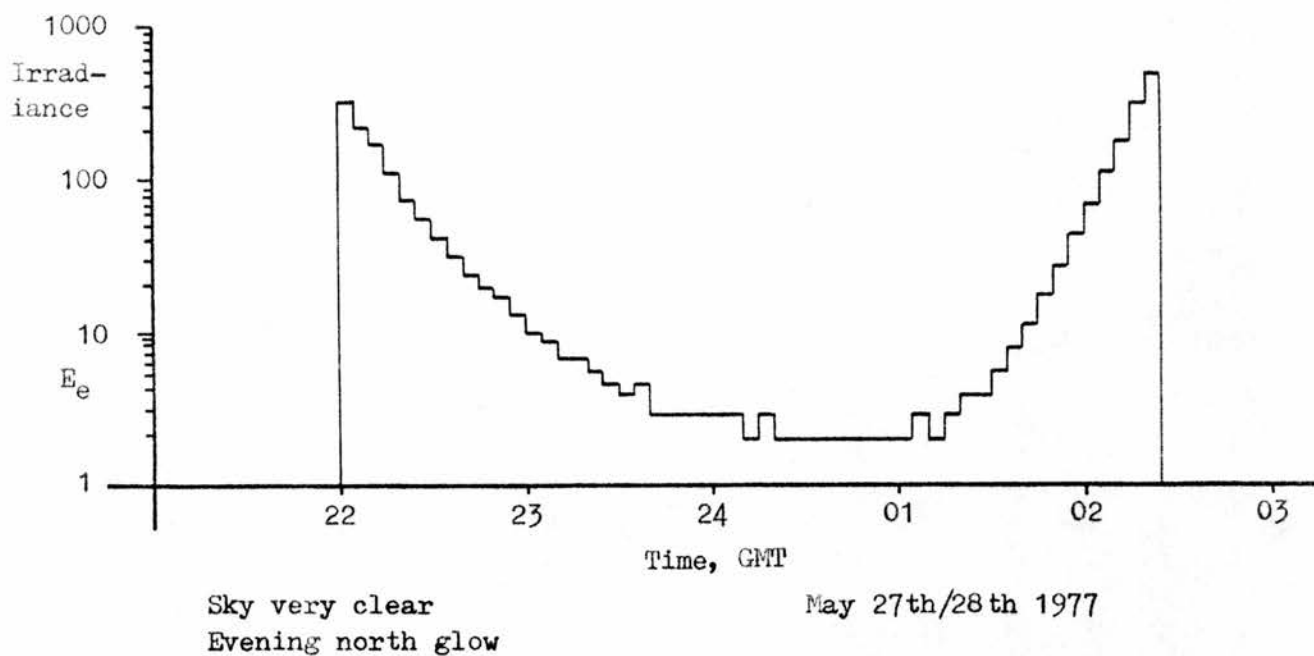


Fig. 117

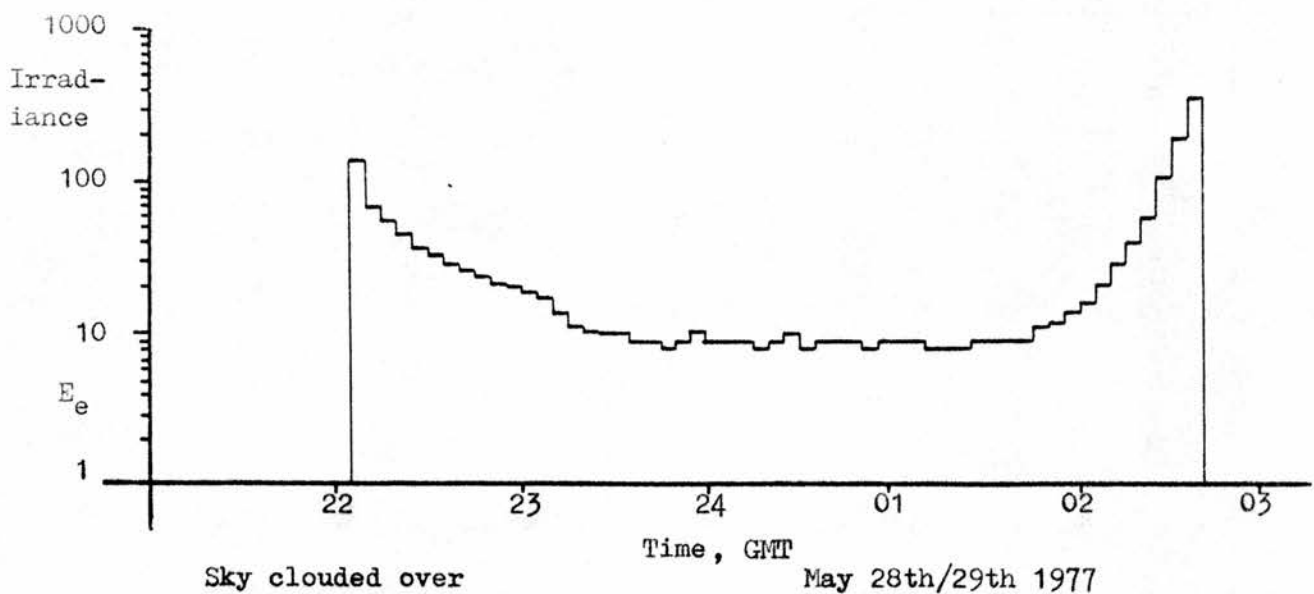


Fig. 118

See section 7.E.10 Twilight records obtained for two May nights in St. Andrews (56 15' N). Note the lower minimum irradiance levels occurring during the cloudless night.

head with the zenith, or to slight shading effects from part of a roof, which could not be avoided, or to the lag in responsiveness of the cadmium sulphide photocells; (see Appendix 3). These responses were obtained from a simple radiometer head containing three ORP12 (BULLARD/PHILIPS) photoresistive detectors wired in parallel. Partial cosine correction was attempted using a front opal disc collector, but this design aspect was not tested. To secure adequate photo-current in these low-irradiance conditions, the photocell driving voltage was set at the high value of 36 V, with a current limit (see Fig 61, p. 123) preventing damage to the photocells under higher irradiance conditions. The range changer disconnected the integrator during the daytime, but the clock and recorder continued to preserve the time record.

7.E.11、 The recording of temperature

Recording temperature proved to be simple, and either the thermistor (negative temperature co-efficient resistor) or one of the newer temperature-sensitive semiconductors, e.g. the ANALOG DEVICES AD590 temperature-dependant current source may be used. See TIMKO (1976).

In this instance, two ordinary disk thermistors (SIEMENS K164 100K) were connected in series directly across the capacitor C6 (Fig. 28 p.87). For resistive sensors, the constant current circuitry need not be used. The thermistors were sealed in a polythene bag and calibrated against a mercury thermometer in a water bath. Thermistor resistance is not linearly related to temperature, and the calibration obtained in this case is shown in Fig.120. Here, the temperature is directly expressed as the length of paper recording tape moved between time marks, over a range of naturally occurring temperatures. The upper trace is for two thermistors, series connected, the lower for just one thermistor, which allows better

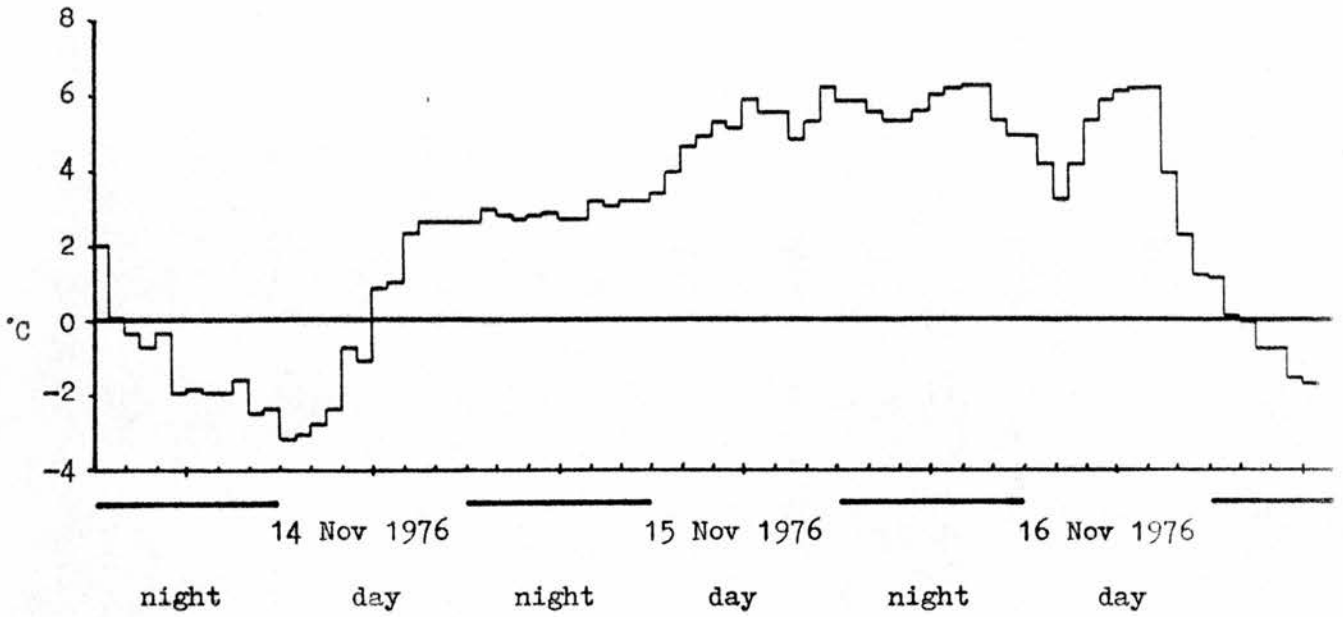


Fig. 119

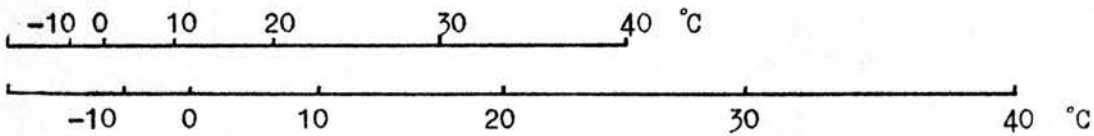


Fig. 120

The new recorder may be used to record temperature, as shown here. In this example, Siemens K164 100K thermistors (negative temperature coefficient resistors were used, as described in section 7.E.11 For interpretation of the recorded tape, a template, directly calibrated in °C, may be constructed. Fig.120 shows the scale for two such templates, the upper one for 2 x series-connected thermistors (for good resolution at higher temperatures), the lower one (one thermistor) giving better resolution at lower temperatures .

resolution at low temperatures. Balance has to be struck between poor resolution at low temperatures, and waste of paper at higher temperatures.

7.F Power and paper consumption in the recorder and integrator

Table 13 shows a breakdown of the consumptions of paper and electricity which contribute to the mean consumption overall. The values are given in relation to the example recordings of Figs.110 and 112 .

The unit consumptions are expressed as watt-seconds or joules, and on the basis of 240 units per day (10 per hour) are then expressed as a power consumption in watts, averaged over the entire day. The current flowing through the hot-wire time marker was originally measured using an oscilloscope to judge the voltage drop across a very small resistance (1 milliohm) placed in series with the pen. This resistance was made from 3 x 36.75 cm pieces of 16 SWG copper wire, in parallel, on the basis of the resistance value given by SCROGGIE (1971) as $0.008162 \Omega \cdot m^{-1}$ (temperature not specified).

As is apparent from this data, the power consumption is extremely low, raising the possibility of powering the whole system with a small bank of solar cells. The question of battery choice is dealt with in Appendix 4.

Table 13

Analysis of power and paper consumption in integrator and recorder for conditions occurring in Figs. 110 and 112.

1. Unit consumption

One paper movement:	12 V 1 A for 60 mS	0.72 J
One time mark:	1.5 V 4 A for 100 mS	0.60 J
Time marks, 1 day, at 10 per hour		240 marks

2. Standby Consumptions

Integrator:	12 V 50 μ A	6 x 10 ⁻⁴ W
Clock:	4 V 35 μ A	1.4 x 10 ⁻⁴ W
240 x paper movements (240 mm paper)		20.0 x 10 ⁻⁴ W
240 x time marks		16.6 x 10 ⁻⁴ W
	sub-total (A)	38.0 x 10 ⁻⁴ W

3. Specific consumptions

17th. July 1982 (Fig. 110)		
6462 tape movements (B)	54	x 10 ⁻³ W
23rd. July 1982 (Fig. 112)		
2503 tape movements (C)	21	x 10 ⁻³ W

4. Total consumptions

17th. July 1982	- electricity	58	x 10 ⁻³ W
	(sub-totals (A) + (B))		
	- paper (6462+240 mm)	6.7	m
23rd. July 1982	- electricity	25	x 10 ⁻³ W
	(sub-totals (A) + (C))		
	- paper (2503+240 mm)	2.7	m

ooo0ooo

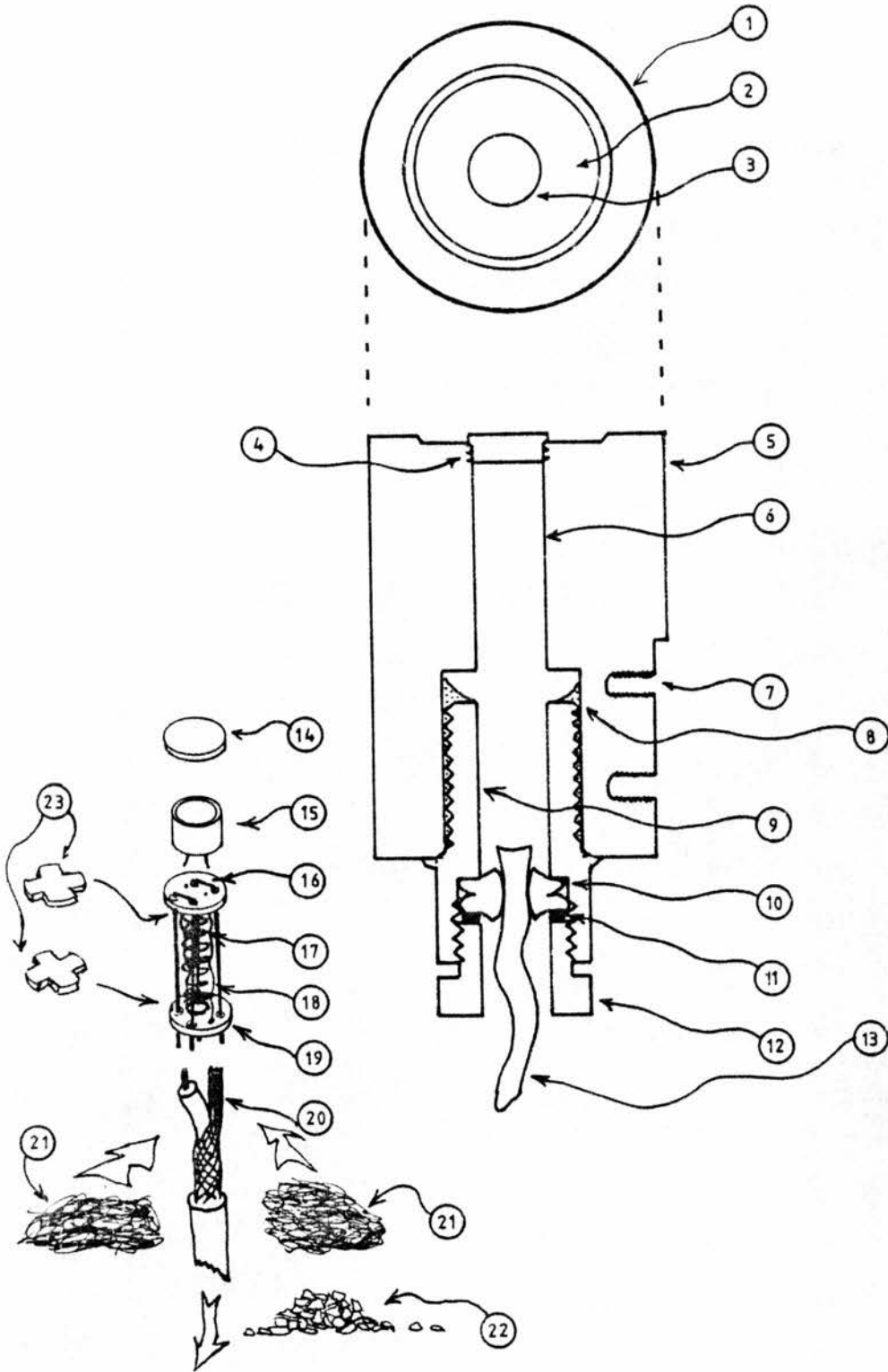
To place these power consumptions in context: 250 ml of water, enough for a mug of tea, raised in temperature from 10°C to 100°C, would consume 94,000 J in the process. This would take 43 days to supply at the rate of consumption on 23rd, July 1982. Rather more than 2 kg of manganese alkaline batteries would run the whole system for one year.

Fig.121 Radiometer Receiver designed for use during Recorder Trials
at Sutton Bonington

This design follows from the considerations discussed in Appendices 2 and 3. The theoretical radiometric response curve is given by Fig.11 , p. 253 .

Legends.

- 1 Outer edge of cylindrical body
- 2 Recessed part of the top surface
- 3 Opal perspex receiving surface, proud of the top surface of recess, level with outer edge
- 4 Ridged surfaces of opal disk and tube wall. Opal disk glued in with araldite
- 5 Solid dural bar, recessed at the top. Recess etched with sodium hydroxide solution and painted with matt black paint. Outer wall painted with aluminium paint to keep down solar heating.
- 6 Cylindrical space in which the photodetector and ancillaries are housed
- 7 Tapped hole (2 BA) into 3 cm x 1 cm milled flat in outer wall of cylinder, for fixing outdoors.
- 8 Araldite glueing in plastic cable gland (WEST HYDE DEVELOPMENTS)
- 9 Inner wall of cable gland (type CAGP M16 thread)
- 10 Compression bush (nitrile rubber)
- 11 washer
- 12 Clamping bush (nylon)
- 13 Cable, co-axial, 50 ohms, 4.95 mm O.D. Type CRG58CV from FARNELL ELECTRIC COMPONENTS
- 14 SCHOTT FG3 glass, 1 mm x 10 mm dia. (prepared by PRECISION OPTICAL INSTRUMENTS)
- 15 Gallium arseno-phosphide photodiode, active area 25 mm² . Type HAMAMATSU G1126
- 16 U - folded piano wire runners
- 17 Compression spring to enforce good contact between 3 , 14 and 15
- 18 Insulated lead wire from photodiode
- 19 One of two small printed circuit boards which carry the connections for the photodetector . The upper one also has the piano wires soldered into pads on the undersurface
- 20 Connections to the cable
- 21 Cotton wool to keep dust from 22 excluded
- 22 Drierite (no. 8 mesh preferred) self-indicating calcium sulphate desiccant (BDH Ltd.)
- 23 PTFE insulators to prevent spring 17 from interfering with electrical connections on the printed circuit boards



8. CONCLUSION

This thesis presents the history of development and *raison d'etre* of a complete field recording instrument, optimised for the measurement of biologically active, especially photosynthetically active radiation. The electronics sections, which may be used in a variety of simplifications and combinations, are mostly fully developed, and may be used with confidence.

The new recorder section, whilst fulfilling all the demands made of it, would benefit from a reworking by a competent mechanical engineer. In spite of that, most of the elements necessary for optimum operation have been incorporated in the original design.

The recorder may be used in isolation from the integrator, and can be used with any simple contact-closure device as an event recorder. Future work might include (a) development and full assessment of a computer link, and it is to be hoped, (b) first field trials in which the data recorded will be put to a significant use.

APPENDIX 1

THE CHOICE OF SPECTRAL RESPONSE PROPERTIES FOR SENSORS OF
PHOTOSYNTHETICALLY ACTIVE RADIATION (PhAR)

* "The varied pigment contents and chromatic adaptability of a mixed marine phytoplankton population is such that, for all practical purposes, the only parameter that needs to be measured in photosynthetic studies is the total radiant energy between 380nm and 720nm" STRICKLAND STRICKLAND (1958)

* "Most farm crops reach light saturation at visible intensities as small as $0.3 - 0.4 \text{ cal cm}^{-2} \text{ min}^{-1}$ ($12.5 \text{ kJ.m}^{-2} \text{ min}^{-1} - 17 \text{ kJm}^{-2} \text{ min}^{-1}$) - with important exceptions including maize and sugar cane - hence they will respond equally to different wavelengths." SZEICZ (1966)

* "The new unit "(for the measurement of photosynthetically active radiation)" should be an energy (radiant power) unit with boundaries either at 400nm and 700nm or 380nm and 710nm. It should be an MKS unit, and a suitable name might be 'plantwatt m^{-2} ' " McCREE (1966)

* "In photobiology, the incident energy flux (irradiance) is a prime example of an irrelevant physical parameter." McCREE (1973)

* "Thus, despite the fact that photosynthesis is a quantum process, the relations of photosynthesis to irradiance, in natural waters, can be studied on the basis of energetic values (watts, joules) as well as of quanta values without significant error." MOREL and SMITH (1974)

- * NORMAN, THURTELL and TANNER (1969) designed their PhAR sensor for flat quantum response.
- * GEORGIEV (1974) designed a PhAR sensor to have an energy response matching the action spectrum of certain green plants in certain (unspecified) conditions.
- * FITTER, KNAPP and WARREN WILSON (1980) designed their PhAr sensor for flat energy response.

A.1.1. Flat quantum - or flat energy response?

The quotations and statements gathered above give a certain idea of the confusion of strongly held views which have held sway in the field of the measurement of photosynthetically active radiation (PhAR). It is currently fashionable to make measurements in terms of a sensor spectral bandwidth with a flat quantum response, on the assumption that since photosynthesis is a photon operated process, this is more appropriate than using a flat energy response. On the other hand, the action spectrum for photosynthesis of an "average field crop leaf" (McCREE 1971) redrawn as Fig 1 does not present an ideal "flat-topped" response curve either for photons or energy. Add to this the effects of saturation (SZEICZ, 1966 above), temperature, chromatic and intensity adaptations, and there would seem to be little reason to prefer a flat quantum response sensor to a flat power response sensor except for highly specific uses where it would be appropriate.

However, an interesting (and comforting) piece of research by MOREL and SMITH (1974) has shown that in air and under most types of natural waters, irradiance measurements made in quantum and energy terms are usually interconvertible. Their conversion factors are given here, and are given as being irrespective of weather conditions and for solar elevations exceeding 22° .

Above Water (400 - 700nm)
 $2.77 \pm 0.16 \times 10^{18}$ quanta sec^{-1} = 1 watt ($\pm 0.6\%$)

Below Water (400 - 700nm)

For all waters:
 $2.5 \pm 0.25 \times 10^{18}$ quanta sec^{-1} 1 watt ($\pm 10\%$)

For blue water:
 $2.35 \pm 0.13 \times 10^{18}$ quanta sec^{-1} 1 watt ($\pm 5\%$)

For blue-green water
 $2.50 \pm 0.13 \times 10^{18}$ quanta sec^{-1} 1 watt ($\pm 5\%$)

For green water
 $2.65 \pm 0.13 \times 10^{18}$ quanta sec^{-1} 1 watt ($\pm 5\%$)

It should not need restressing here that lux and other photometric units are wholly inappropriate for other than vision studies. TYLER (1973) has shown that the ratio of quanta to lux measured at different depths in oceanic waters can vary by a factor of more than 6:1.

A.1.2 The response bandwidth of sensors

For PhAR studies the recommended short and long wavelengths bounding the passband is usually specified as being about 400 - 700nm. A list of some authors and their recommendations is given overleaf.

The choice of short-wavelength cut-off should receive attention particularly if the irradiance sensor is for use under water.

MOREL and SMITH (1974) note that "in blue waters the wavelength range from 350 - 400nm may contain as much as 10% of the total quanta in the range from 350 - 700nm." Similar care should be given to the placement and sharpness of cut-off at long wavelengths, especially if the sensor is to be used below plant canopies. This is because green plant leaves have a transmission co-efficient which increases very sharply just beyond 700nm (see Fig 3), which can lead to considerable over estimation of PhAR in, for example, woodlands, GAASTRA (1968). The problem is made worse when the otherwise attractive silicon photodiode is used as the radiometric sensor, since this type of device has its peak sensitivity in the 700 - 900nm range. See Appendix 3.

If PhAR is to be related to other than terrestrial green plants, for example marine algae, special sensor response curves may become appropriate to deal with the unique action spectra of many of these, and the fact that saturation effects, with their flattening effect on response curves will be less common in the deeper aquatic environments. See, for example, HAXO and BLINKS (1950), HALLDAL (1974) and PRIEUR (1970).

HALLDAL (1967) deals with the somewhat less well explored field of the ultraviolet action spectrum.

Author	Pass-band cut-off wavelengths	
	Short Wavelength	Long Wavelength
NICHIPOROVICH (1960) PhAR	380 nm	710 nm
Energy Balance	380	3000
SCOR working party (1965) PhAR	350	700
WESTLAKE (1965)	390 ± 10	710 ± 10
McCREE (1965)	380 - 400	700 - 710
GEORGIEV (1974)	380	720
BEINHAUER (1977)	400	700

See also:

BLINKS (1964)
BROOKS (1964)
CHAPMAN and CAMPBELL (1975)
DODILLET (1961)
GABRIELSEN et al., (1961)
EVANS (1969)
GULYAEV (1964)
McCREE (1973b)
McPHERSON (1969)
RVACHEV (1963)
SAUBERER (1962)
SHROPSHIRE (1971)
STEEMANN NIELSEN and HANSEN (1961)
SZEICZ (1974)
UCHIJIMA (1968)
VOLLENWEIDER (1969)

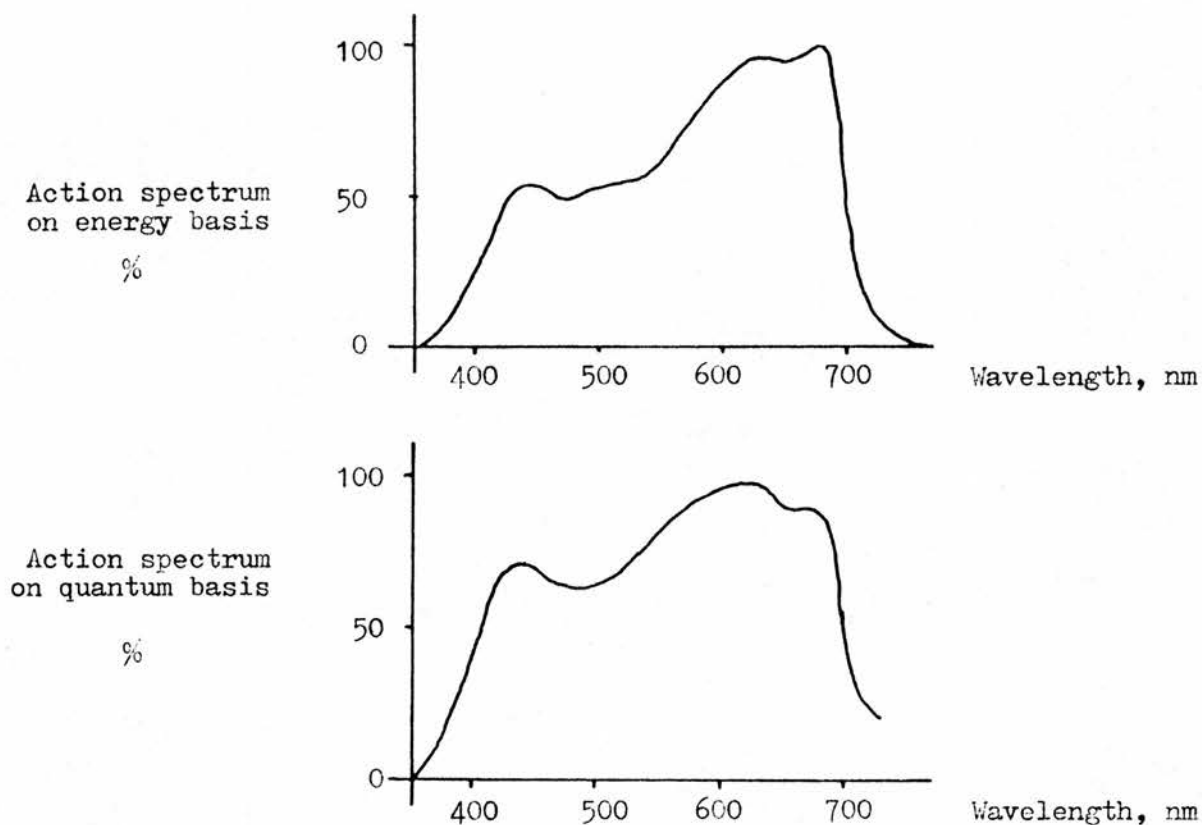


Fig. 1 Energy and quantum action spectra for an " average field crop leaf "
(redrawn from McCREE (1973)

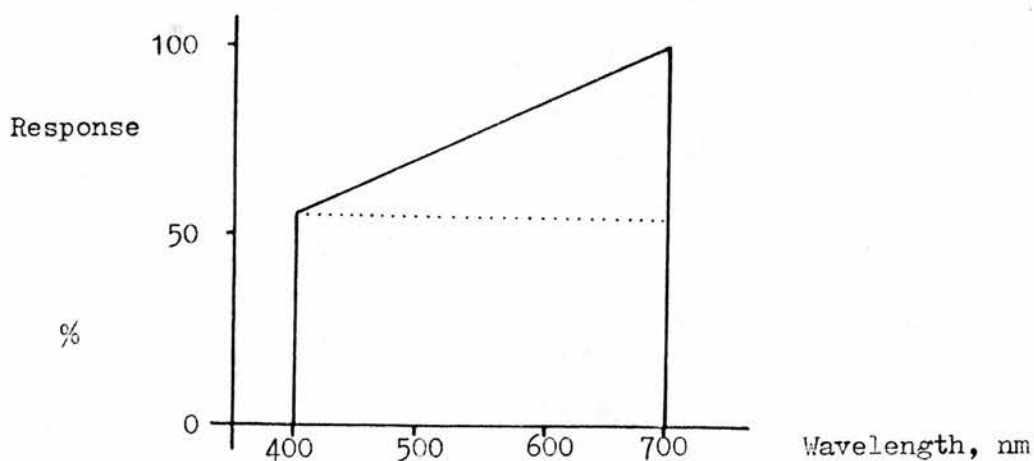


Fig. 2 Energy response of radiometric sensor with flat energy response
(dotted line) and flat quantum response (continuous line)
for input of equal power per unit area per unit bandwidth.

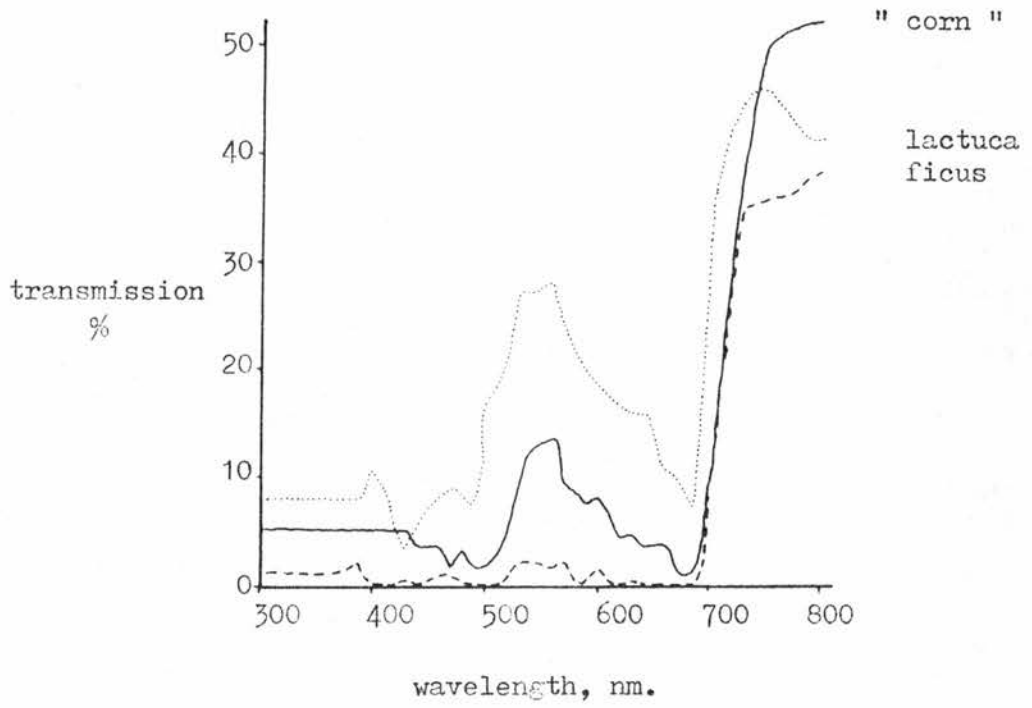


Fig 3.

Spectral transmission coefficients of three leaf types in the region 300 - 800 nm.

(Redrawn from GAASTRA (1968))

APPENDIX 2

RADIOMETRIC SENSOR DESIGN

A.2.1. Introduction

There is a considerable body of literature on the subject of the design of the radiometric sensors, and the aim of this appendix is to introduce some of the factors involved.

A.2.2. Receiver directional response

Three basic response patterns for radiometric receivers are recognised; spherical, hemispherical and cosine, of which the cosine response is most commonly used. The spherical response receiver (or sensor) is totally unresponsive to the direction of supply of the irradiance being registered, giving the same quantitative response in all cases. Typical receivers of this type use a globe of opal diffusing material, which in turn irradiates the flat surface of a radiometric detector, which is typically located unobtrusively at the end of a tube which points at an opal disk built into the base of the globe. MIDDLETON (1953), KROCHMANN (1964) and KUBIN (1971) consider such designs. Hemispherical receivers are similar, but use a hemisphere of diffusive material above the radiometric detector surface. The cosine response receiver in which the detector output is proportional to $\text{Cos } \theta^*$, the angle of incidence* of the incoming irradiance, is the most commonly used response pattern. In theory a disk of perfectly absorbing (matt black) material has this response, but since few radiometric detectors are like this, the response has

*the angle of declination from the normal to the plane of the sensor face

to be generated by artifice. In practise a disk or shaped dome of opal diffusing material is used as a secondary source, scattering and absorbing most of the incident radiant flux. Reflection losses, due to small angles of incidence, are corrected by a slight doming of the surface of the diffuser, or more often, by raising the edge of the diffuser slightly proud of the casing of the sensor. Whilst this technique successfully compensates for the loss due to reflection, it results in a response from the sensor when the angle of incidence θ is 90° . This response is usually suppressed by a shielding ring encircling the opal disk, and extending proud to such an extent that the anomalous response is corrected. BOYD (1951) cited in SMITH (1969) is credited with originating this design. With minor modifications, it has been used by KERR et al., (1967), BIGGS et al., (1971), KUBIN (1974) and FITTER et al., (1980). The LAMBDA INSTRUMENTS sensor is derived from that of BIGGS et al., (1971). SMITH (1969) emphasises that in the construction of "cosine corrected" heads dimensions do not scale up or down linearly; therefore testing and adjusting are most important. The size of sensors constructed to this pattern varies greatly; that of SMITH (1969) is more than 16 cm. in diameter; those of BIGGS et al., (1971), NORMAN et al., (1969) and FITTER et al., (1980) being smaller at 6 cm., 2 cm. and 2 cm. diameter, respectively.

Another pattern of cosine-corrected detector, not very popular for field studies on account of its size, is the integrating Larché or Ulbricht sphere, which has a perfectly reflecting inner surface, with a hole at the upper pole, covered with a transparent dome. The inside is coated with optical white paint and there is a

baffle which prevents directly incident irradiance from striking the photocell, which is sited down a tube attached to the lower pole of the sphere. See EVANS (1969) and KUBIN (1974).

A.2.3. Problems relating to radiometric sensor design

Some authorities (KUBIN 1971) contend that opal diffusers should be roughened, which gives a better cosine response if the sensor is to be used dry; on the other hand, if the sensor is to remain underwater or out of doors, a polished surface gives less of a "key" for the adherence of dirt or living organisms. See also WESTLAKE (1965). Cleaning can be quite a problem in the field; KAIN (1971) records that in her survey the radiometric sensors needed cleaning by divers every week if possible. On calm days in silt-laden waters it is possible for the sensor to be totally obscured by a layer of silt. A possible feature which might be worth building into radiometric sensors intended to operate in such conditions would be a ring of tuyeres through which compressed air could be passed at intervals, the turbulence produced serving to clean the opal.

Other problems relate to filters; FITTER et al., (1980) records that certain gelatin filters (WRATTEN type) fade with continued exposure to daylight. Where such filters must be used, it might be possible to alleviate the effect by ensuring that they are positioned on the photocell side of any neutral-density or glass-based filters which together make up the filter pack. WRATTEN type neutral-density filters have a rather uneven spectral response; that is because they are designed for good image passing quality for photography rather than for radiometric accuracy.

Ordinary opal perspex does not pass radiation of shorter wave-

length than 400nm. For this reason SMITH (1969) used ROHM and HAAS Plexiglass II- UVT. Filters are available from BARR and STROUD, CHANCE-PILKINGTON, SCHOTT, CORNING, BALZERS and KODAK (WRATTEN type). If interference filters are to be used, it is necessary to use a collimating structure, since the wavelength of peak transmission shifts according the angle of incidence of the irradiance. For filter calculations, see DAVIES and WYSZECKI (1962).

A.2.4. Unusual techniques: Photomultipliers, quantum counters and spectroradiometry

Most of the simpler field radiometric sensors use silicon or selenium photodetectors, but some, for example ACKEFORS et al., (1969) PRIEUR (1970), CRAIG and LAWRIE (1962) have used photomultipliers. These pose problems of bulk, high electrical voltage and insulation requirements, and fragility. They also need a very constant voltage supply unless they are operated with a constant anode current. This is possibly a better mode of operation, and there is also little likelihood of damage occurring to the photomultiplier tube in the event of exposure to high irradiance levels. However, as silicon photodetectors improve, the need for the use of photomultipliers lessens, except in conditions of extremely low irradiance levels. See CUNNINGHAM (1974).

Certain sensors have been designed using fluorescence techniques to convert irradiance of short wavelength to another of more readily detectable nature. SPITZER and WERNAND (1978) have used Rhodamine-B to produce a sensor with a flat quantum response. Phosphor plates of magnesium tungstate (RUFF 1970) and silver activated zinc/cadmium sulphide have been used (HARRIS 1968) for ultra violet radiometry to convert the uv into wavelengths in the middle of the response band of the selenium cell used.

Underwater spectroradiometers have been built by, amongst others, SAUBERER (1962) and TYLER and SMITH (1966). These usually use graded spectrum filters and mechanical systems to scan the waveband, but recently, photodiode self-scanning matrices have appeared on the market (INTEGRATED PHOTOMATRIX Ltd) which offer the prospect of miniaturised spectroradiometers with no moving parts. HAMAMATSU make slit photodiodes suitable for use with graded spectrum filters, which may be obtained from BARR and STROUD and SCHOTT.

See also:

ARNOLD (1975)
GORCZYNSKI (1936)
KAHN et al., (1975)
MONTEITH (1959)
PREVOST et al., (1971)
TYLER (1973)
WESTON and PAIX (1960)
WOODWARD and YAQUB (1979)

APPENDIX 3

RADIOMETRIC DETECTORS

A.3.1. Introduction

The aim of this appendix is briefly to survey the field of radiometric detectors; to present response-curves for some devices which represent the best now available, and to draw attention to the more important references. KUBIN (1971) and CLARKE (1964) present impartial surveys; with the semi-technical press and with scientific contributions which originate in commercial laboratories, it is harder to be so sure. Manufacturers seem to be extremely loth to provide information on the tolerances to which their sensors are made, particularly in regard to deviations from the published spectral response.

Most recently, the gallium arseno-phosphide (GaAsP) photodiode has come into commercial production (HAMAMATSU TELEVISION CO. and NIPPON ELECTRIC COMPANY) and this device, which is insensitive to infra-red and which has dark currents in the picoampere range, would seem to offer promise as a detector of PhAR, to replace the selenium cell. For reference to thermoelectric, thermomechanical, pneumatic, photoemissive and photomultiplier detectors, see KUBIN (1971).

A.3.2. Selenium photocells

Selenium photocells, or more correctly barrier-layer photovoltaic generators are one of the older types of radiometric detector. They have the same equivalent circuit as that for the

silicon photodetector shown in Fig 1 , consisting essentially of a constant current source of output proportional to incoming irradiance, in parallel with a shunting diode. Traditionally the output of the cell is passed to a low-resistance milliammeter, and providing the voltage generated across this load does not exceed a few tenths of a volt, the milliammeter reading will be linearly related to irradiance. Higher voltages cause the diode which inherently shunts the current source to turn on, shunting the milliammeter and causing non-linearity. There are certain advantages which have caused these cells to be widely used. They are cheap and readily fabricated in any shape and in areas of up to several square centimetres. Their wavelength response curve naturally covers the 400 - 700 nm band, and is fairly easy to correct, and importantly for certain types of work, they are naturally insensitive to the near infra-red. (cf. silicon cells). Against this, and unlike silicon and GaAsP cells (see below) they may suffer from instability, fatigue effects (from irradiance from over intense sources, eg. direct sunlight) hysteresis (ie. where a subsequent response is dependent on the irradiance prevailing for the previous one) and slow drift in characteristics and calibration. Fig 5 shows a family of curves for four varieties of selenium cell from MEGATRON Ltd.

See also

SAUBERER (1962)

WORNER (1955)

KUBIN (1971)

GULYAEV (1964)

for full discussions.

A.3.3. Photoresistive cells

In photoresistive cells the conductance of the cell is more or less linearly proportional to the irradiance falling on it. Their main advantage is that since they can withstand high applied voltages their sensitivities are second only to photomultipliers and can be amazingly high. The usual construction takes the form of a ceramic element coated on the surface with a layer of cadmium sulphide or selenide (or a mixture) with interdigitating contact electrodes deposited on the surface. They are available in very small sizes, circa 0.5 cm up to 3 cm diameter. Fig 7 shows curves of typical wavelength response patterns for three varieties of cell (CLAIREX). Unfortunately, photoresistive cells are even worse than selenium cells in respect of hysteresis, non-linearity and fatigue. Furthermore, at low levels of irradiance, the temperature coefficient can be extremely bad. FORSTNER and RUTZLER (1970) claim that the stability of some of these can be improved by boiling them in water for some hours before use, but this seems unlikely, in view of the fact that the photoresistive element is already prepared by sintering at a high temperature, and this advice cannot be recommended.

The wavelength response curves vary greatly according to the condition of manufacture, and some firms claim better degrees of linearity for their cells than do others.

See also

de GIER et al., (1959)
GUHA (1972).

Manufacturers include CLAIREX, HAMMAMATSU, MULLARD, PHILIPS and RCA.

A.3.4. Silicon and gallium arseno-phosphide cells

This category of radiometric detectors is today the most important for use in field instruments. Similar in many ways to selenium cells, they are unlike in exhibiting good stability, no hysteresis or fatigue effects and excellent linearity (over 6 decades of irradiance levels for silicon and 10 for gallium arseno-phosphide detectors). The equivalent electrical circuit of these devices is shown in Fig 1 and consists of a perfect irradiance-controlled constant current source, in parallel with a diode, a capacitance and a resistance. There is also a series resistance, largely made up of the distributed resistance of the thin front layer of the cell which serves to gather the electrons liberated in the junction by photon action. The so-called "solar cell" and "photodiode" are the same device, but the first is optimised for the generation of solar power, the second for photoconduction in the reverse-biased mode: Fig 2 makes this clearer. The detector is a large-area semiconductor diode, and like any other diode has a forward conduction characteristic and a reverse current blocking characteristic, up to the point where avalanche breakdown begins to occur. In Fig 2 there is a family of five curves. The upper one is for a detector in total darkness, and is identical to that of an ordinary diode. Almost no current flows in the forward direction until the ordinary forward voltage drop of perhaps 0.6 volts has been exceeded, after which the current increases rapidly and non-linearly. In the reverse direction, no current flows until breakdown occurs. The remaining four curves in Fig 2 are for four different levels of irradiance, of one to four times the basic level. The effect on the diode curve is to lower it bodily down the current axis (y-axis) in proportion to the irradiance level.

The fourth quadrant of the graph gives the photovoltaic (photogenerative) mode of operation - and current can be drawn from the detector and measured. Provided that the diode does not reach its minimum conduction voltage, that current will be proportional to the level of irradiance. This means that only a low-resistance current meter may be used, or ideally (in case the diode is leaky) a measuring circuit of zero effective impedance - easily arranged with an operational amplifier. See WITHERELL and FAULHABER (1970) and EPPELDAUER (1973). If the irradiance is very large, and with it the photocurrent, the voltage drop across R_s , the internal series resistance, may be sufficient to cause the diode to conduct, shunting the photocurrent. This is a fundamental cause of non-linearity at the highest irradiance levels.

Quadrant three displays the reverse-bias characteristic. The same photocurrent will flow at constant irradiance, provided that the bias voltage does not exceed the point where avalanche breakdown begins to occur. The flatness of this characteristic is one measure of the quality of the detector; unfortunately, R_{sh} (the shunt resistance) is another inherent feature, giving increased "dark current" with increasing reverse bias. If it is important to measure low irradiance levels, the bias voltage must be kept low, ideally 0 V, so that the dark current will be at the minimum.

In practice, the design of these photodetectors is a matter of compromise; photoconductive photodiodes have the characteristics displayed in Fig 3 and display poor Quadrant IV characteristics, whilst for photovoltaic detectors Quadrant III performance (reverse leakage) is bad, and the characteristic in Fig 4 pertains.

"Solar cells" operating in the Quadrant IV photovoltaic mode need to have a low value of R_s (series resistance, Fig 1) for good power conversion efficiency. Unfortunately, this usually comes from having a relatively thick front "window" to the cell with a low sheet

resistance; good short wavelength performance and a thick front window are incompatible. For this reason, the better quality radiometric silicon diodes are used in the photoconductive or reverse-biassed mode. See PRINCE and WOLF (1958) and WILLIAMS (1962) for good general accounts.

See also

DANAHY (1970)
CUNNINGHAM (1974)
DAVIS (1973)

Figs 8 , 9 , and 10 show some of the best currently available photoconductive cell responses. The y - axes give Responsivity in Amps. Watt⁻¹ (amps of photocurrent per watt of irradiance incident on the face of the detector: since the detector response is linear over a wide range of irradiances, the cell area and irradiance distribution pattern does not need to be specified). Fig 8 line 1 is for a FERRANTI visible radiation optimised cell and exhibits a relatively poor blue response. Lines 2 and 3 are for two so-called uv-enhanced photoconductive diodes from UDT and EG and G respectively. 2 is a Schottky-barrier type detector (see DAVIS, 1973). Fig 9 shows the responses of four cells from the Hamamatsu company. 3 and 4 are silicon photoconductive diodes; good blue and uv responsivity comes from the adoption of the SiO₂ inversion layer type of cell window (see HANSEN, (1978) and SUZUKI and YAMAMOTO (1976). 2 and 1 are ordinary and Schottky-barrier type gallium arsenophosphide detectors, notable for the absence of response in the near infra red, and also for having a dark current two orders of magnitude smaller than that for the typical silicon photodiode.

See also

SUZUKI et al., (1977)
BERKELIEV et al., (1976)
STIRN and YEH (1977)

If a good uv performance is required, simple removal of the

glass cell window (WHITING 1968) is unsatisfactory, even if doing so causes increased ultra violet responsivity. DANAHY and KAISER (1976) note that an unprotected silicon photoconductive diode may, under the influence of strong 254nm (mercury line) irradiance increase its response by several hundred percent, reversibly, possibly due to the formation of an unstable anti-reflective oxide layer on the surface of the silicon. Photodiodes for this spectral region have to be designed and tested for this use.

Suppression of the infra red response of a silicon photodiode is difficult to arrange without filters, but if the total junction region is made very thin, photons of infra red wavelengths may pass right through the cell without creating hole-electron pairs. This is the basis of the cell, the response of which is shown in Fig 10 ,2 . It is also probably the method by which the SHARP SBC - silicon blue cell obtains its response. These cells have been used by BIGGS et al., (1971), McLAUGHLIN and ALLAN (1976) and FITTER et al., (1980). The SHARP - SBC cell response is shown in Fig 6 , along with the responses of the Schottky-barrier and ordinary GaAsP photodiodes (redrawn from Fig 9), and that of one further SHARP cell, the BS100C which has a built-in filter. These responses may be compared with those of the selenium cells (MEGATRON) in Fig 5 above. Response 1 in Fig 10 relates to a HAMAMATSU filtered cell, the S1087.

Fig 11 shows a suggested PhAR sensor response produced by the combination of 1mm of SCHOTT FG3 filter glass and a HAMAMATSU schottky-barrier gallium arsenophosphide photodiode. The lack of response in the near infra red fits it for woodland studies.

For any photodetector, the formula for finding the quantum efficiency at any wavelength from the responsivity is as follows:

Where R = Responsivity, A.Watt⁻¹

λ = Wavelength, nm

$$\text{Q.E.} = R \left(\frac{1239.5}{\lambda} \right) \times 100\%$$

See also:

JONES (1959)
SELCUK and YELLOTT (1962)
WOLF and RAUSCHENBACH (1963)
RAUSCHENBACH and MAIDEN (1972)
LINDMAYER and ALLISON (1973)
BOGUS (1974)
TSUJI (1976)
AHRENKIEL et al., (1977)
FRANZ et al., (1977)
KIMURA (1978)
SCHRODER (1978)
GEHRING and LACHMANN (1979)

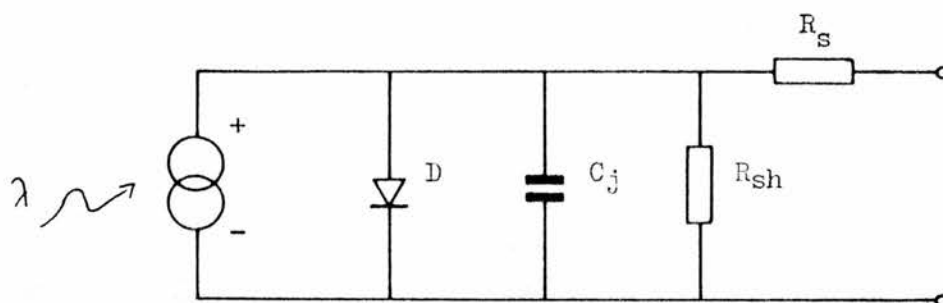


Fig. 1 Equivalent circuit of the silicon photodetector

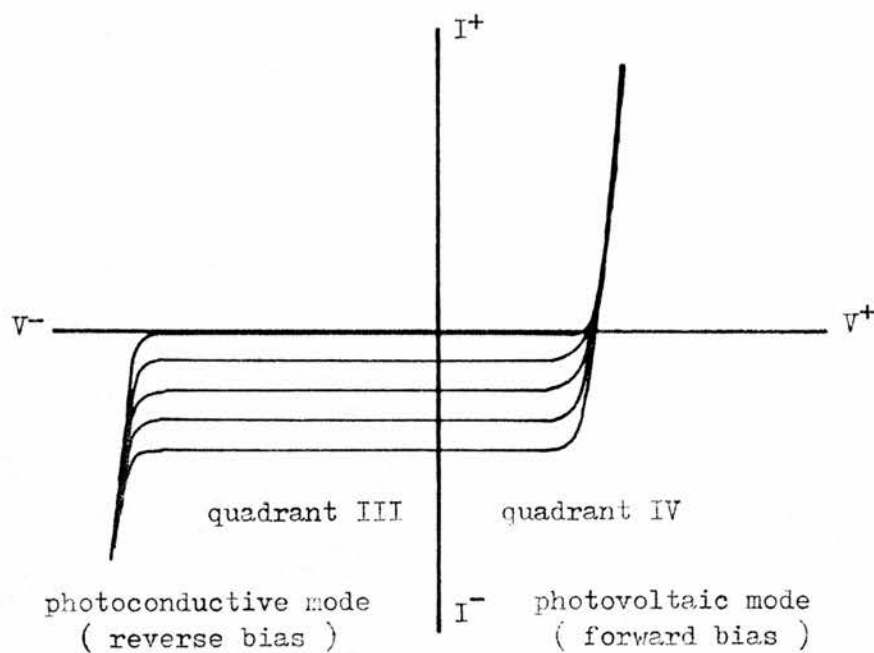


Fig. 2 Curves for darkness (uppermost) and four levels of irradiance incident on face of photodetector

Idealised response curve of silicon and GaAsP photodetector

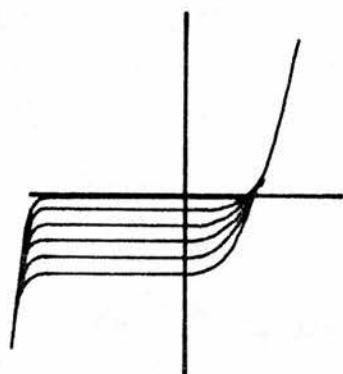


Fig. 3

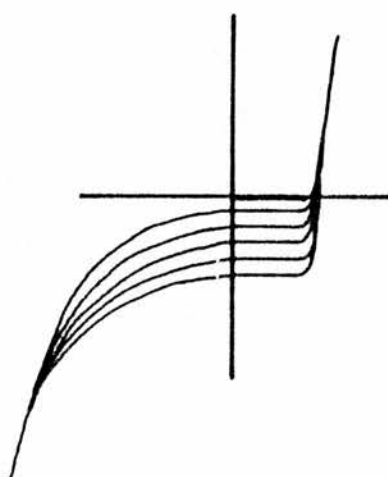


Fig. 4

Typical device response curves : left hand device optimised for photoconductive use, right hand for photovoltaic (photogenerative) operation

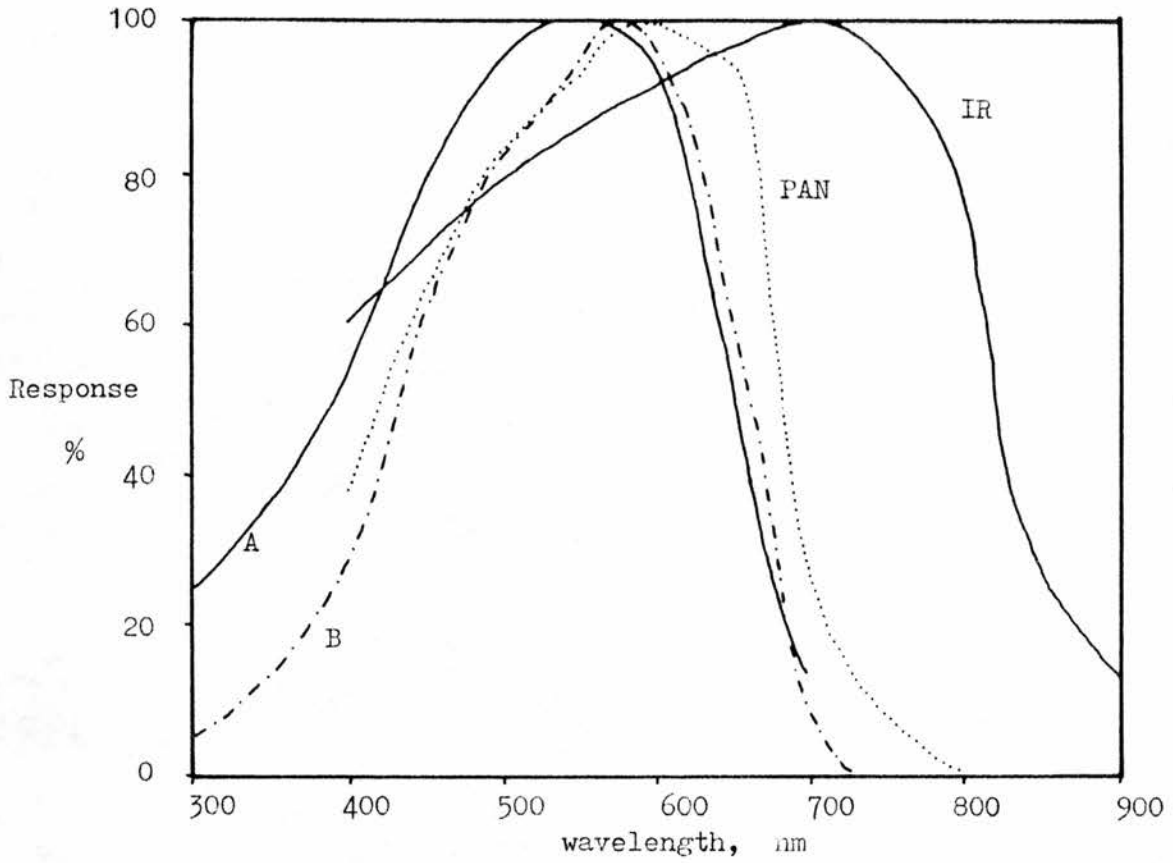


Fig. 5 Typical response curves for four types of selenium cell

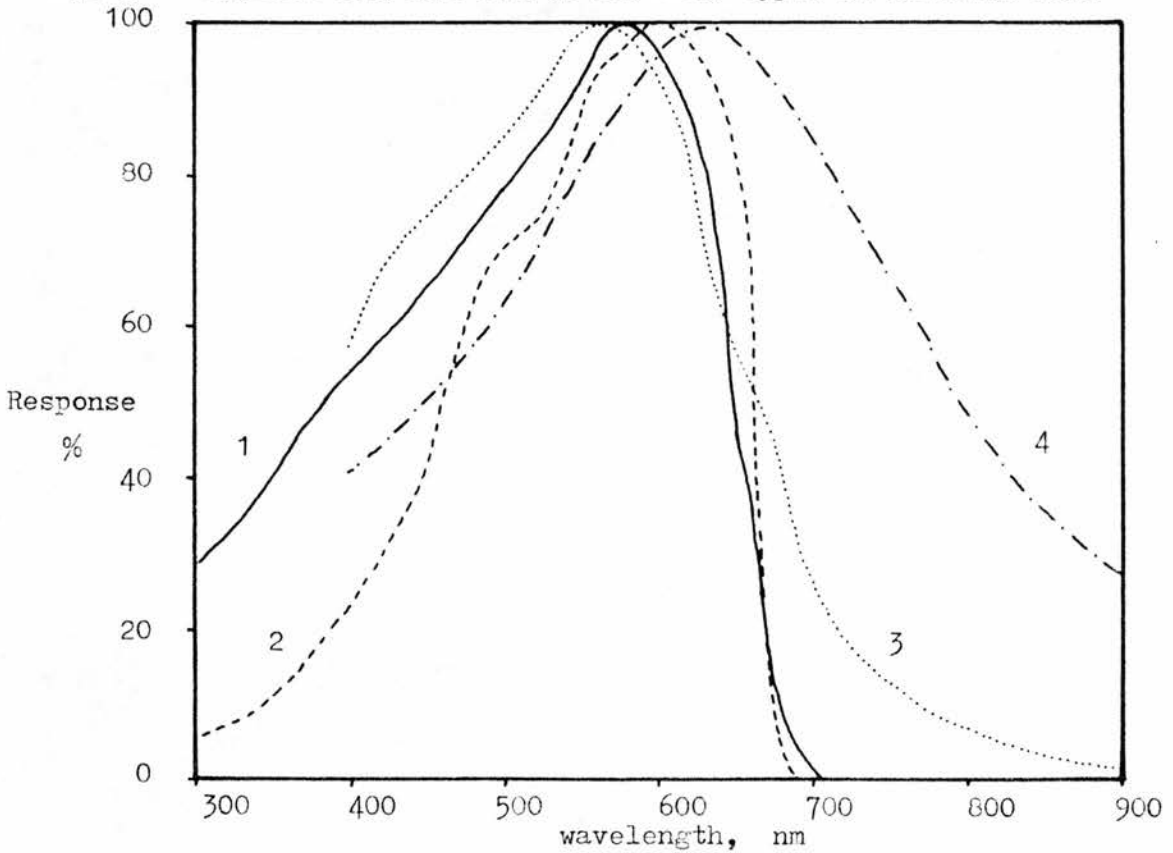


Fig. 6 Typical response curves for: 1 Schottky-barrier GaAsP photodiode
2 Ordinary GaAsP photodiode
3 SHARP BS100C filtered silicon photodiode
4 SHARP SRC series silicon blue cell
(1 and 2 from HANAFATSU data)

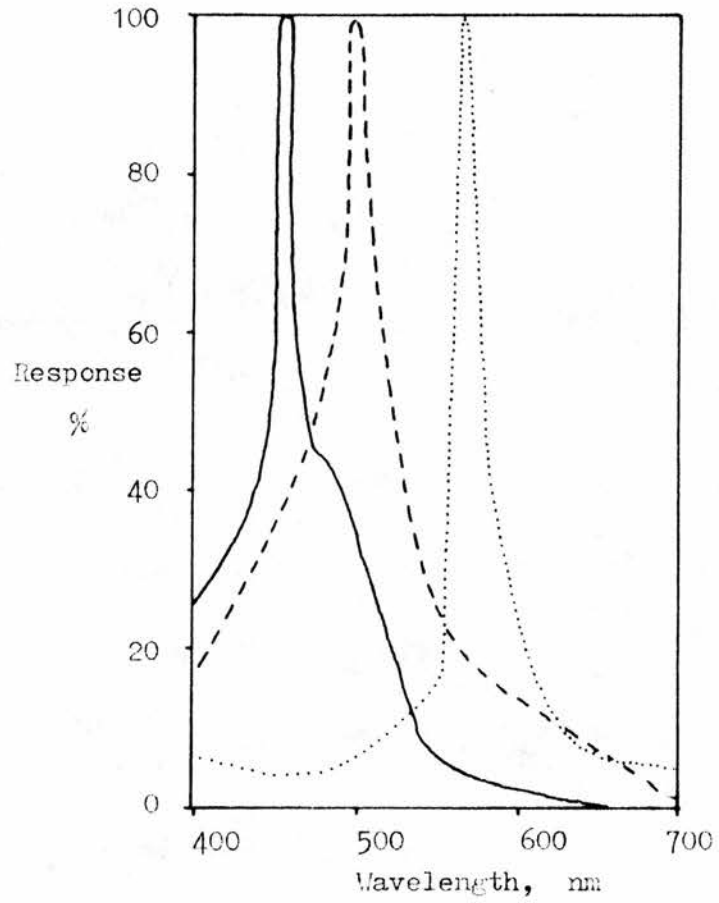


Fig 7

Response curves for three examples of photoresistive detector of the cadmium sulphide or selenide type.

(Redrawn from CLAIREX data)

Some varieties of these cells exhibit a broader response curve, e.g. those of NULLARD

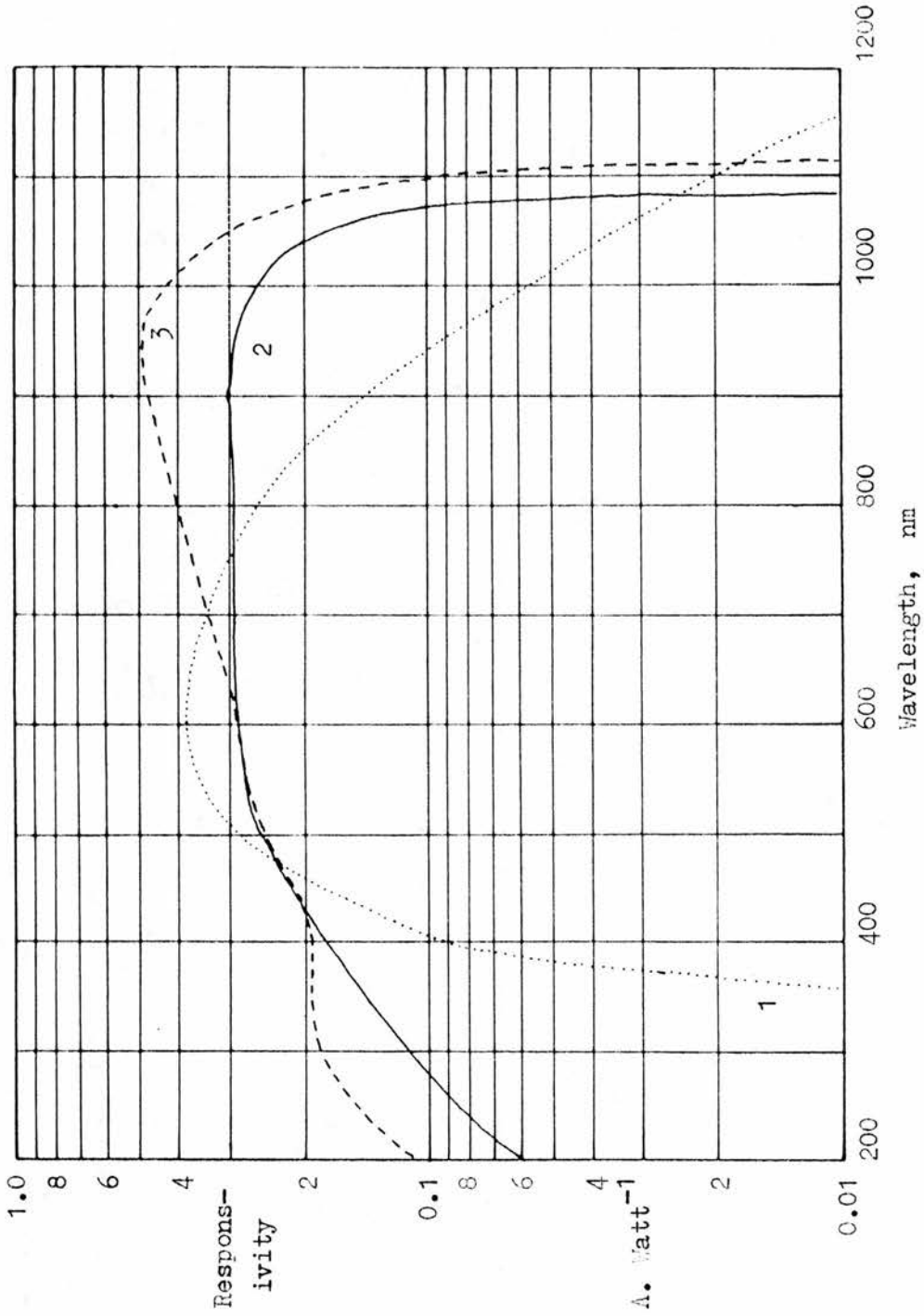


Fig. 8 Sensitivity of three silicon photodetectors:
 1. FERRANTI PS600 series visible spectrum detector
 2. UDT schottky-barrier uv enhanced detector
 3. EG & G Ltd. uv enhanced detector

(redrawn from manufacturers information)

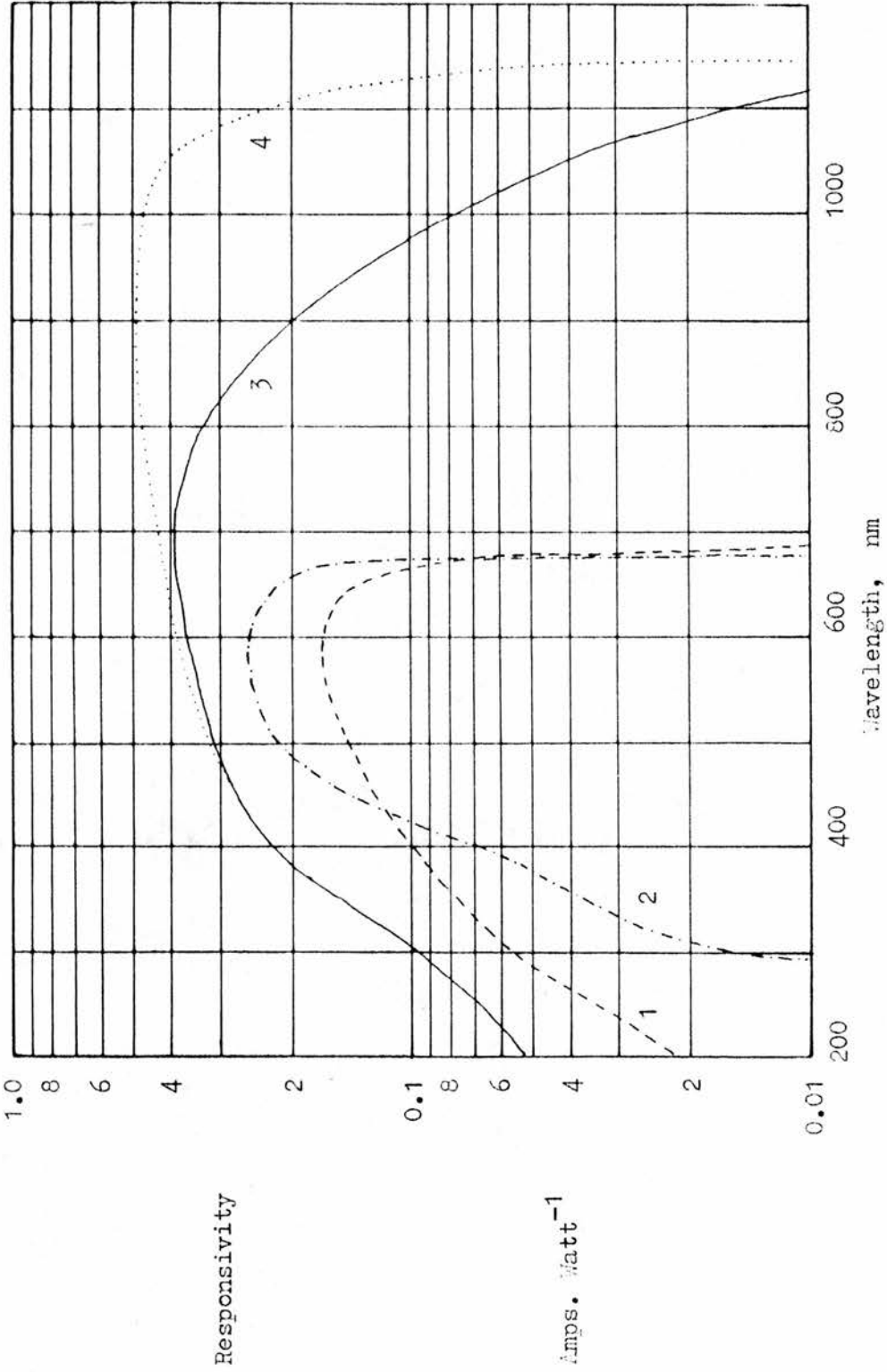


Fig. 9 Sensitivity of four photodetectors from the HAMAMATSU range

- 1. Schottky-barrier gallium arseno-phosphide detector
- 2. Ordinary gallium arseno-phosphide detector
- 3. uv-enhanced SiO₂ inversion layer silicon detector type S1226
- 4. " " " " " " type S1336

(redrawn from manufacturers information)

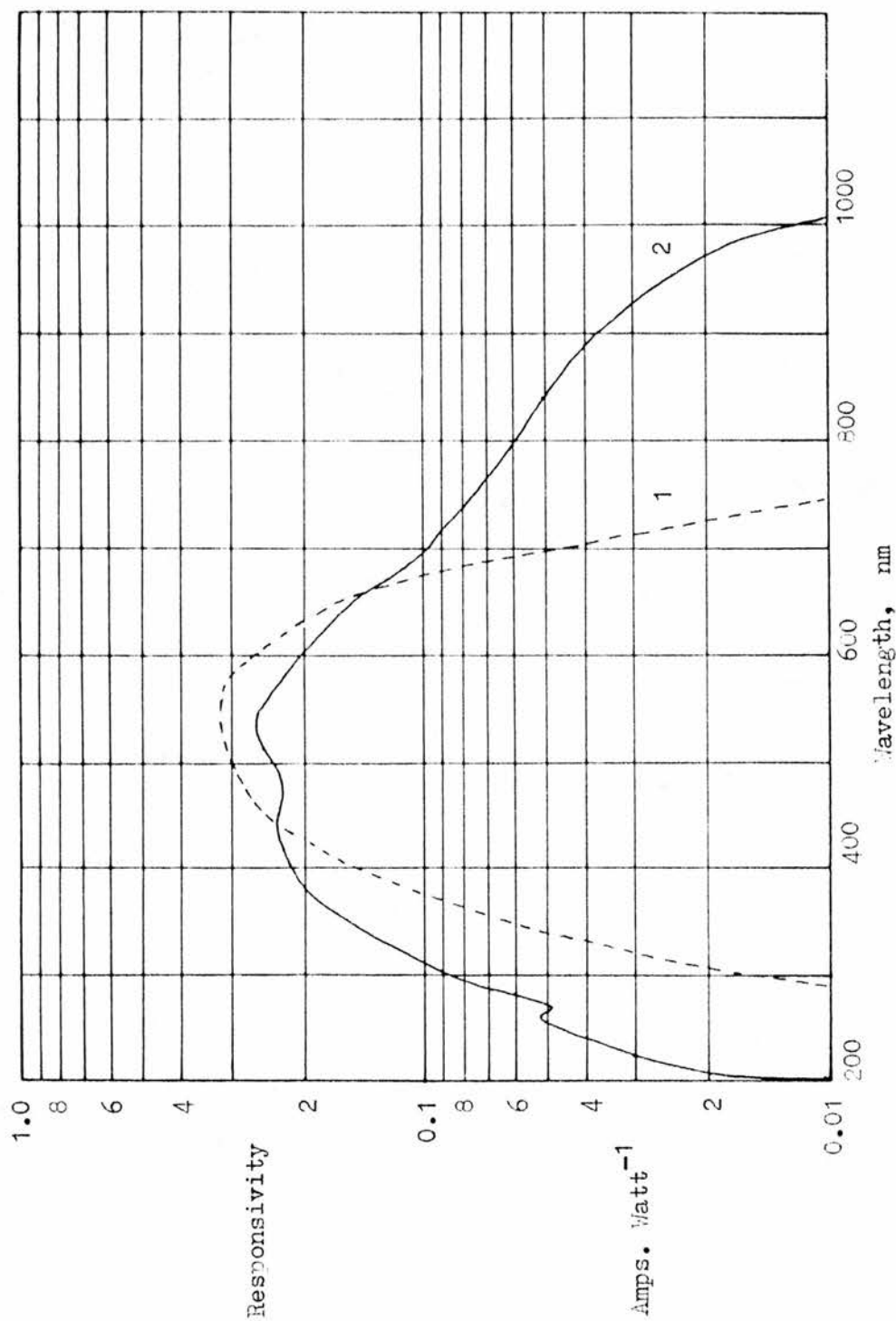


Fig. 10

Sensitivity of two HAMAMATSU silicon photodetectors

1. Silicon detector with built-in filter (type S1087)
2. Experimental HAMAMATSU inversion-layer type photodiode using an epitaxial p on n substrate instead of a plain p one.

(redrawn from HAMAMATSU data and from SUZUKI and YAMAMOTO (1976))

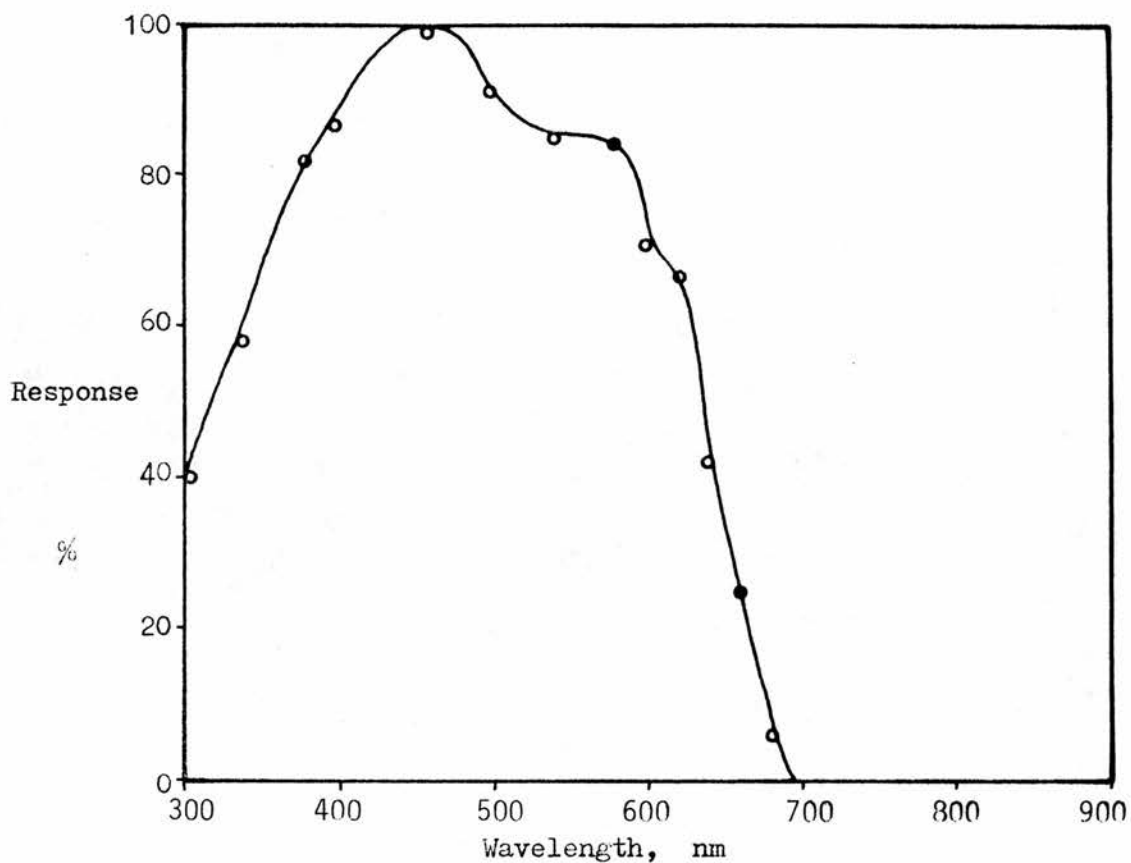


Fig. 11 Calculated response curve for suggested PhAR sensor using a schottky-barrier gallium arseno-phosphide diode filtered with 1 mm of SCHOTT FG3 coloured glass. Note the lack of sensitivity to the near infra-red and good response preserved into the blue. (photodetector from the HAMAMATSU range, e.g. G1125, G1126, or G1127)

(prepared using manufacturers data)

APPENDIX 4 .

A.4.1. BATTERIES

"An army" runs the saying, "marches on its belly", and by the same token, the choice of batteries powering a field instrument is quite important. Being electrochemical rather than electronic components, batteries are the most unreliable component used in electronic equipment. They decompose in storage, it is often not possible to determine their state of charge, and in most cases (with the exception of the new lithium cells) their available capacity decreases badly at low temperatures, because of the lowered ionic mobility of the constituents.

However, certain types, the manganese-alkaline cells and the sealed nickel-cadmium and lead-acid types of battery (DRYFIT-PC and CYCLON, NOT the ordinary motor car starter battery) have quite a good performance. In practise, it is sensible to allow 100% spare capacity in estimating battery life, replacing the cells after they have been half spent and using the old ones for less important purposes. For rechargeable nickel-cadmium cells, the same applies, the used battery being completely discharged with a fairly high load (C/2 rate: ie. the load which would flatten a fully charged battery in two hours) and then recharged. Lead acid batteries must never be left discharged for more than a couple of days.

Table 1 gives the salient properties of the more usual types of cell. The manufacturers data should be consulted since there is a wide variation in many of the properties, depending on the manufacturer.

A.4.2. Leclanché cells (primary)

This type of cell is one of the oldest, the most widely available and the cheapest. It is fairly satisfactory for very light current drains, and where the loading is intermittent, giving the battery time to recover in between demands. If the loading is continuous, the battery will have a very short service life, and the cell will supply only a fraction of the number of watt-hours of which it is capable. When used on low loads, the so-called "high power" types do not show much advantage over the standard cells. See TYE (1980).

A.4.3. Manganese-alkaline cells (primary)

This type of cell is much better than the ordinary leclanché in many ways; loss of capacity in storage is very low, the energy density is at least twice that of the leclanché cell, and the low temperature performance superior. The construction has a double-walled steel shell and is virtually leakproof. They are widely available, fairly inexpensive and are made by several manufacturers, like the leclanché cell. See DANIEL et al., (1963).

A.4.4. Mercury (mercuric oxide-zinc) cells (primary)

Mercury cells have the benefit of being one of the most compact primary electrical energy sources, exceeded only by lithium, and the voltage remains very constant at 1.35 V (1.4 for some varieties) over a wide range of loads. This type of cell does not perform well at low

temperatures, and is very expensive - about five times the price of manganese-alkaline cells on an equal energy basis. Because of the rarity and toxicity of the mercury, these cells should be returned to the makers for salvage when exhausted.

A.4.5. Lithium cells (primary)

Lithium cells are the newest type to reach commercial production, and are significantly better than most other primary systems. It is to be expected that they will become more readily available, and at the time of writing (1981) they are about the same price as mercury cells. There are a number of systems in use, giving different cell voltages, eg. Lithium-polycarbonmonofluoride Matsushita (See FUKUDA and IIJIMA (1975) and OGAWA and OKAZAKI (1978)); Lithium-sulphur dioxide (DURACELL-MALLORY) (See BRO et al., (1975) and LINDEN and McDONALD (1980)); Lithium-manganese dioxide (SANYO and BEREC) (See IKEDA et al., 1980). All have voltages of 3 volts. Lithium ferric sulphide cells (BEREC) have a working voltage of 1.45 V, but they have an open circuit voltage of up to 3 volts.

The lithium-sulphur dioxide battery can exist because of a thin film of lithium dithionite which forms on the lithium cathode, rendering it passive. As a result of this layer, the shelf life is outstanding. According to LINDEN and McDONALD (1980), this type of cell is ideally suited to discharge through a very small load. At 21°C, over ninety per cent of the available energy can be extracted over a four year long discharge period. The electrolytes for these cells are, of course, organic. That for the lithium-sulphur dioxide system is 1.8 M lithium bromide dissolved in a mixture of acetonitrile, propylene carbonate and liquid sulphur

dioxide. Internal pressure is 3 - 4 atmospheres at 21°C (LINDEN and McDONALD, 1980) for an undischarged cell. For low loads at low temperatures, the performance of the lithium-sulphur dioxide battery is excellent. If the discharge rate is lower than the 500 hour rate, over 80% of the rated capacity for discharge at 21°C can still be obtained at -40°C. It is possible that for certain conditions these batteries would be ideal for running the integrator-recorder combination. Like mercury batteries, these should be returned to the makers for salvage.

A.4.6. Nickel-cadmium cells (secondary)

This type of secondary cell is now well-known in its sealed form. Unfortunately, they have a tendency not to store charge well, and worse, to become short circuited on standing. They do not respond well to the type of regime which the integrator recorder imposes - that is, continuous discharge into a very small load. Unfortunately, manufacturers are content to keep silent about these problems, which are probably due to recrystallisation of the cadmium resulting in the formation of thin prismatic crystals which pierce the separators, JOHNSON (1977). The internally short-circuited cell can sometimes be brought back into service by subjecting it to the passage of a pulsed current sufficient to fuse the short-circuiting elements.

The correct way to use these batteries with loads such as the integrator is to alternate two sets of batteries, exchanging them at service visits. The exchanged set should be subjected to one or two full discharge-charge cycles at the 1-hour rate before finally being recharged for service. It is not difficult to design a charger which will perform this function automatically.

Providing that the charging and cycling requirements are met, these cells can give reliable service, and at low temperatures. It is important that batteries are charged near the time of use, because of the poor charge-retention properties.

See manufacturers data from

VARTA, BEREC and SAFT; and DANIEL (1963)
 THOMAS (1963)
 DEAC (1967)
 SIEMENS (1968)
 ATKIN et al., (1975)
 HODGE et al., (1975)
 HODGEMAN (1976)
 BENJAMIN (1977)
 FEICHTINGER (1977)
 SCHNEGG (1977)

A.4.7. Sealed lead-acid cells (secondary)

Another type of sealed battery with a reputation for uncertain performance and short life is the DRYFIT battery (ACCUMULATORENFABRIK SONNENSCHNEIN). This reputation is no longer well deserved, provided that such a battery is always recharged promptly when it has undergone a complete discharge. Failure to do so results in rapid "sulphation" of the plates, increase in internal resistance and loss of capacity. They should always be stored fully charged, and given a charge every 16 months when kept in store.

Versions of DRYFIT batteries made in the last ten years, the DRYFIT - PC series (EBERTS 1970), are distinguished from the older type of DRYFIT by the alloying of the lead in the plates with calcium, and the inclusion of phosphoric acid in the electrolyte. Standard motor vehicle type open accumulators discharge themselves to 50% capacity in about three months at 20°C: the corresponding figure for the DRYFIT battery is 16 months at 20°C and 25 months at 8°C. The poor performance in conventional batteries is due to the antimony

alloyed with the lead to harden the plates. The inclusion of phosphoric acid in the DRYFIT - PC series batteries has increased the cycle life by a factor of four over the older DRYFIT type, and the claimed cycle life for the A200 series is at least 200 full cycles. For methods of charging, see EBERTS (1970) or the manufacturers information. It is essential that the charging voltage used with these batteries does not exceed 2.3 volts per cell at any time (at 20°C).

A different approach to the sealed lead-acid cell is exemplified by the CHLORIDE - GATES "CYCLON" range of batteries, in which an oxygen recombination cycle similar to that used in the nickel-cadmium cell is employed. These have pure lead grids which give low corrosion. The cycle life depends on the depth of discharge, ranging from 250 cycles for 100% discharge to 600 cycles for 60% discharge. Hence these cells, unlike nickel-cadmium types, should not be cycled before charging. The self-discharge time is about 8 months to 50% capacity, and they should be recharged after about 18 months standing idle.

A.4.8. Silver-zinc cells (secondary)

Sealed silver-zinc cells are also available in button format like some of their nickel-cadmium counterparts. They have a higher operating voltage (1.5 volts) and a very flat discharge curve like that of the mercury cell, and a substantially greater energy per unit volume ratio than do nickel-cadmium cells. In the mid - 1970's,

they were similar in cost to nickel-cadmium cells, but the recent increases in the world silver prices means that that is no longer so. Their charge retention is very good compared with nickel-cadmium cells, but it is not clear from the manufacturers normal data what the cycle lifetime of these cells might be. See HAJDU and ZAHORAN (1972) and (1974). The manufacturers are MEDICHARGE Ltd.

CHARACTERISTICS OF ELECTROCHEMICAL CELL TYPES DISCUSSED IN TEXT

Column	A	B	C	D	E	F	
Cell type							
PRIMARY							
Leclanché	180	102	0		24	1.6	
Manganese-alk.	100	260	-20		35 to 90%	2.7	G
Mercury	120	440	0	50%	24	3.8	H
Lithium	350	560	-54	50	60 to 90%	1.6	I
SECONDARY							
Pb - acid DRYFIT	31	74	-25	50	17	2.3	J
Pb - acid CYCLON	25	60	-40	50	8	2.4	K
Nickel - cadmium	38	110	-35	50	3	2.8	L
Silver - zinc	36	160	-10	50	12	4.4	M

Columns

A	Milliwatt hours per gram
B	Milliwatt hours per millilitre
C	Minimum recommended discharge temperature; °C
D	Effective capacity at (C) compared with capacity at 20°C
E	Storage life, at 20°C, to 50% capacity except where stated (in months)
F	Density, grams per millilitre

Remarks

G	Based on Mn-1300 cell, R20 (U2) size, 10 Ah, 1.5 V
H	" RM 42 cell, " , 14 Ah, 1.4 V
I	" LO26S cell, (DURACELL LTD) 10 Ah, 3.0 V
J	" SONNENSCHHEIN DRYFIT type A312 5.7 Ah, 12 V
K	" CHLORIDE - CYCLON cell pack 5.0 Ah, 12 V
L	" SAFT VR4 cell, R20 (U2) size, 4 Ah, 1.2 V
M	" MEDICHARGE B450 button cell 0.45 Ah, 1.5 V

NB. Minimum discharge temperatures and effective capacities at those temperatures are highly dependant on rates of discharge. Storage properties improve at low temperatures, but the electrolyte must usually not be allowed to freeze. The lithium battery has the best properties of the primary types, and the cost, in 1981, is similar to that of the mercury cell. Mercury cells and lithium types should be returned to the makers for safe disposal.

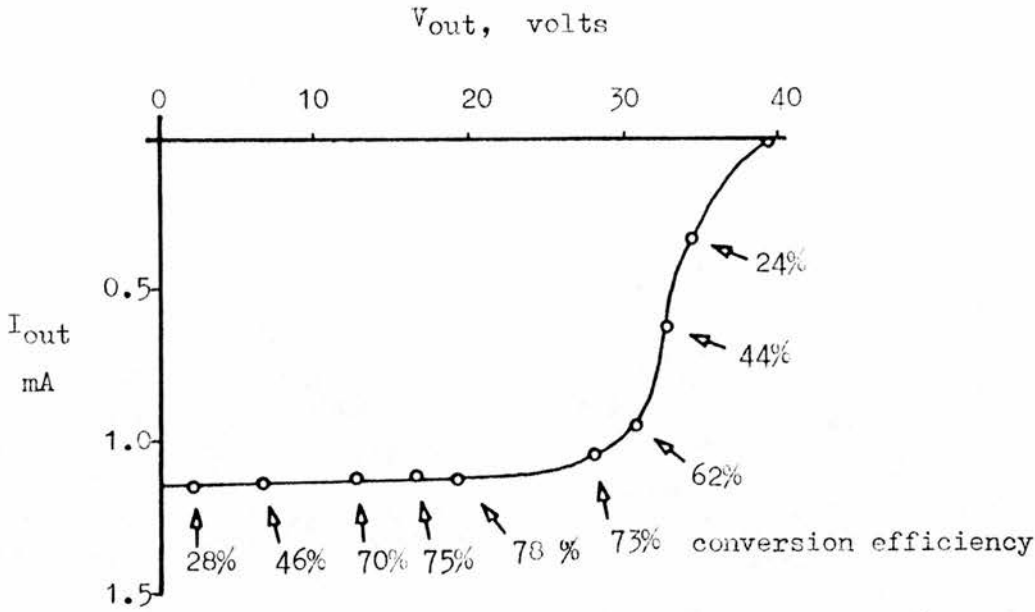


Fig. 1 Performance of inverter in circuit of Fig. 2 - input constant current 30 mA across two silicon diodes; simulated battery load (zener diode, 14 V) replaced by variable load resistance. Note optimum conversion efficiency obtained at 19 volts output.

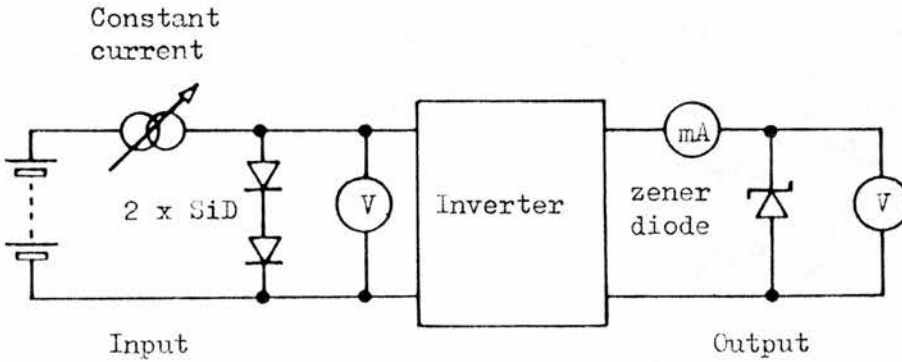


Fig. 2 14 V zener diode = 12 V battery

	Input Current mA	Voltage developed V	Inverter	Voltage developed V	Output current	% Conversion
min	0.4	0.88	→	14.2	15 μ A	60
max	200	1.10		15.6	3.4mA	60
	30	0.89		15.6	1.24mA	72 peak eff.

Inverter designed for conversion of 6.0 to 150 volts - for details see GOING (1981). Conversion efficiency exceeded 60% between the range of input currents tested, above.

Performance of solar cell battery charger using transistor oscillator - transformer conversion instead of a large number of photovoltaic cells.

APPENDIX 5

SOLAR ENERGY FOR THE INTEGRATOR AND RECORDER

The notion of powering a solar irradiance recorder entirely from the sun is aesthetically attractive, but since service visits to check the apparatus and replace the reels of recording tape are already necessary, the cost of arranging solar powered charging of the batteries would seem unwarranted.

From 31 to 36 silicon photo-voltaic cells are needed to produce adequate voltage to charge a 12 volt battery. Where a low current only is needed, it may be cheaper to use two cells feeding a DC to DC inverter rather than using an array of 32 small photo-voltaic cells, which at present (1981) are still very expensive. GOING (1981) has described a small transistorised inverter which, whilst not designed for the purpose, gives a conversion efficiency of over 60% for a wide range of input currents from just two series-connected silicon photo-voltaic diodes. The optimum load for this combination is the secondary storage battery, which was simulated in this test using a 14 volt zener diode as a load. The solar cells were simulated using a constant current source feeding two series connected silicon diodes. See information on the opposite page.

See also

SPENCER (1961)
SPENCER (1963)
BOLLEN (1966)
RICHARDS (1975)
COURTNEY (1976)
TSUJI (1976)
DIJKSTRA and FRANX (1978)
KIMURA (1978)
KUWANO (1980)
JOHNSTON (1980)
TREBBLE (1980)

APPENDIX 6

ELECTROLYTIC CAPACITORS

The leakage properties of electrolytic capacitors are non-linearly related to temperature and working voltage. For tantalum capacitors, the use of high working voltage types at low working voltages results in much improved leakage properties, and the sintered pellet wet electrolyte version has the best leakage performance. The measurement of leakage current in capacitors is difficult, made worse by such factors as dielectric absorption, and FRANCE (1980) states that many of the commercially quoted insulation resistance values are invalid. For application to the integrator, it is probably better to select and reject particular capacitor types on the basis of actual linearity tests on the integrator. See ALLISON et al., (1960), FRANKLIN (1962), CAMPBELL (1971) and company literature from, for example, SIEMENS and PLESSEY.

The capacitors used in the integrator, Fig 28 C6 and C7 were:

150 μ F 30 Volts Working Plessey type 'R' sintered tantalum
wet electrolytic

and

2.2 μ F 250 Volts Working MULLARD metallised polyester type C280 AE

APPENDIX 7

ELECTROMAGNETIC RELAYS

The relay used in the auto-range changing unit was a Clare-Elliott magnetic latching relay, type LF 2301 K00 (Associated Automation). This unit is a high-quality hermetically sealed nitrogen filled type, with gold-plated contacts. A quantity of these were obtained, unused, on the surplus market; they are very costly when new. Since it is anticipated that electronic circuitry containing the relays would normally be housed in a protective case, it is probably not necessary to use hermetically sealed ones.

It is, however, essential to use gold-plated contacts, designed for so-called 'dry circuit switching' when dealing with low-voltage signal loads. Such relays must never be used for switching high current loads unless it is intended that they will never be called upon to handle small signal loads again. This is because the gold plating is destroyed by the arcing which occurs when higher current loads are broken, leaving the basic silver contacts unharmed for use with power loads. There is a wide range of suitable relays, some manufacturers of which are listed below.

For more information on relays, see

GAYFORD (1969)
ASSOCIATED AUTOMATION LTD
B & R RELAYS LTD
OLIVER PELL CONTROLS LTD
THORN ELECTRICAL COMPONENTS LTD
ZETTLER (UK) LTD

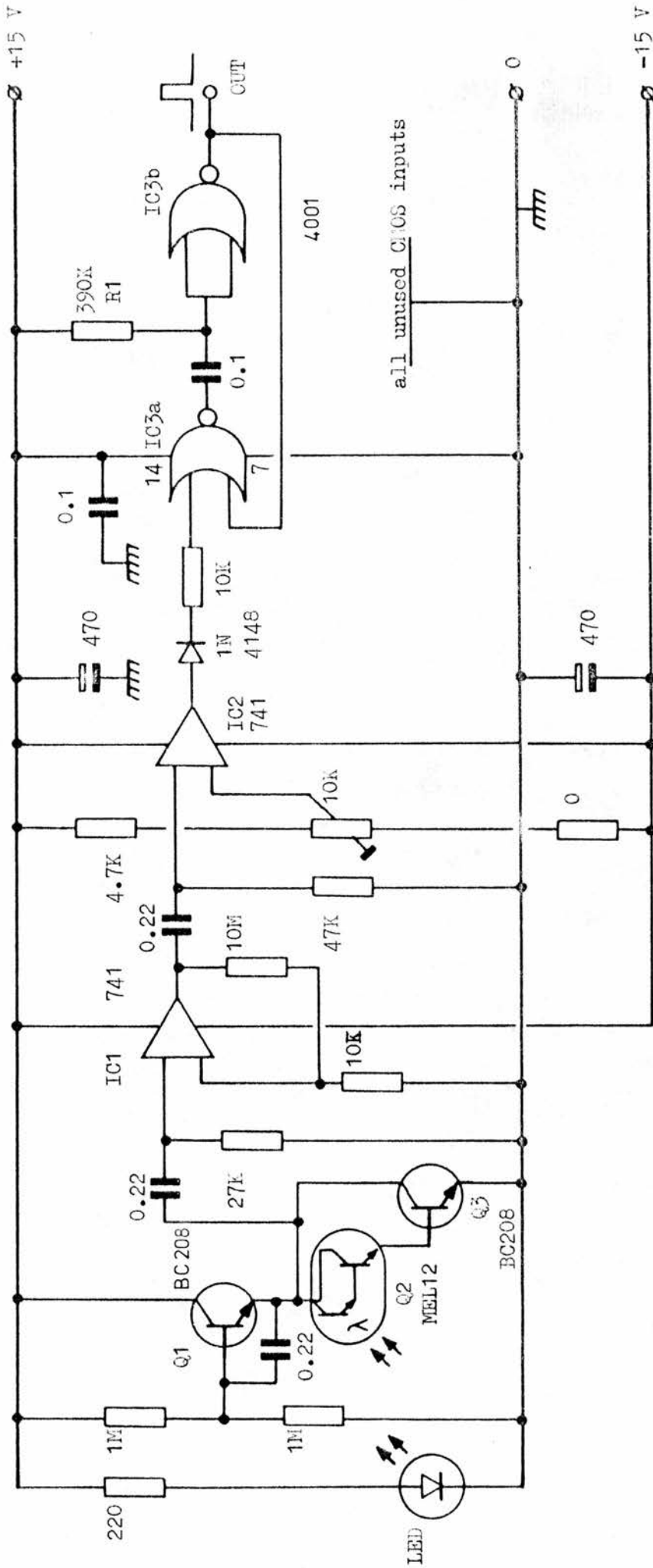


Fig 1. Circuit for optical scanner and 'front end' for reading paper tapes. see text

APPENDIX 8

AN AUTOMATED READER FOR TAPE RECORDS

Presented here are the first stages in making a computer link for the machine processing of recorded tapes. The tape is moved at constant speed past a reflective optical scanner, and the pulse train which results has intervals between pulses proportional to the signal level recorded. Each pulse can signal the start of the subsequent recording period. It would not be difficult to convert this information into stored data values on a magnetic disk, ready for re-plotting as histograms, or for mathematical operations.

An old magnetic tape recorder, speed of tape transport 95mm. per second, was stripped of electronics and an optical slit scanner was installed. This was made of black-painted perspex and contains a high power (50 mA) red light emitting diode, which irradiates the passing paper tape through a narrow slit (0.2 mm. wide). The light reflected from this is detected by Q2, a photodarlington transistor. The electrical output from Q2 is extremely small, and the network around and including Q1, derived from KRAUSE and KEINER (1974) is designed to eliminate interfering offset currents resulting from changed reflectivity in different batches of recording paper, stray light, and the temperature dependance of leakage current in Q2. The output pulses then pass through IC 1, a X 1000 amplifier; IC 2, a pulse squarer; and finally IC 3a and b which give each pulse a constant width of 10 milliseconds. At the tape speed used, 95 mm. per second, there can be 48 pulses per second maximum, and therefore about 20

milliseconds between the rising edges of adjacent pulses. For this reason, the time-constant of RC_1 is adjusted to give output pulse lengths of about 10 milliseconds. Further work remains to be done on this circuit.

Appendix 9 Parts list and assembly drawings of the new recorder

Reference

- Fig 1 A Top view of tape channel
- a ' meccano ' chain drive to clutch
 - b position of action of heat pen (not shown)
 - c duralumin side plate 1/16 "
 - d Post office pattern counter
 - e piano wire actuator
 - f plane through which Fig 2 B passes
- Fig 1 B Heat pen - detail
- a strips of clock spring, 1/16 "
 - b linking loop of copper wire
 - c overall coating of araldite as electrical insulator
 - d eureka hot-wire element in place for glueing
 - e end of hot-wire looped into tag form
 - f second coat of araldite embedding hot-wire
 - F' pre-formed hot-wire element from front
 - S " " " " side
 - T " " " " top
- Fig 1 C Heat pen
- a glued hot-wire assembly
 - b connecting tag
 - c aluminium bracket
 - d paxolin insulating plate
 - e bolt, 6 BA
 - f clock spring strip

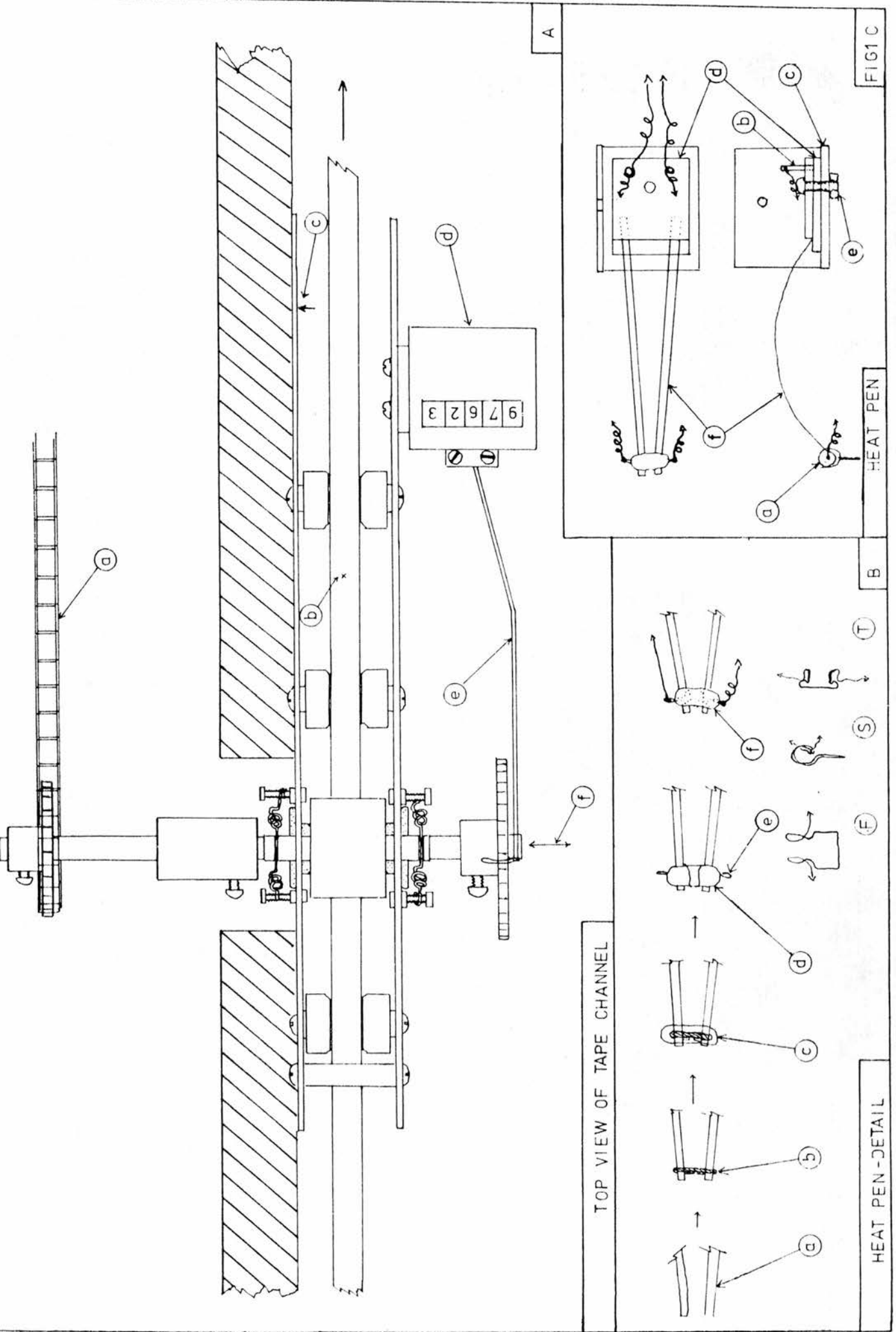


FIG 1 C

HEAT PEN

B

TOP VIEW OF TAPE CHANNEL

HEAT PEN - DETAIL

A

Reference Fig 2 Section of capstan and pinch wheel assembly

Fig 2 B

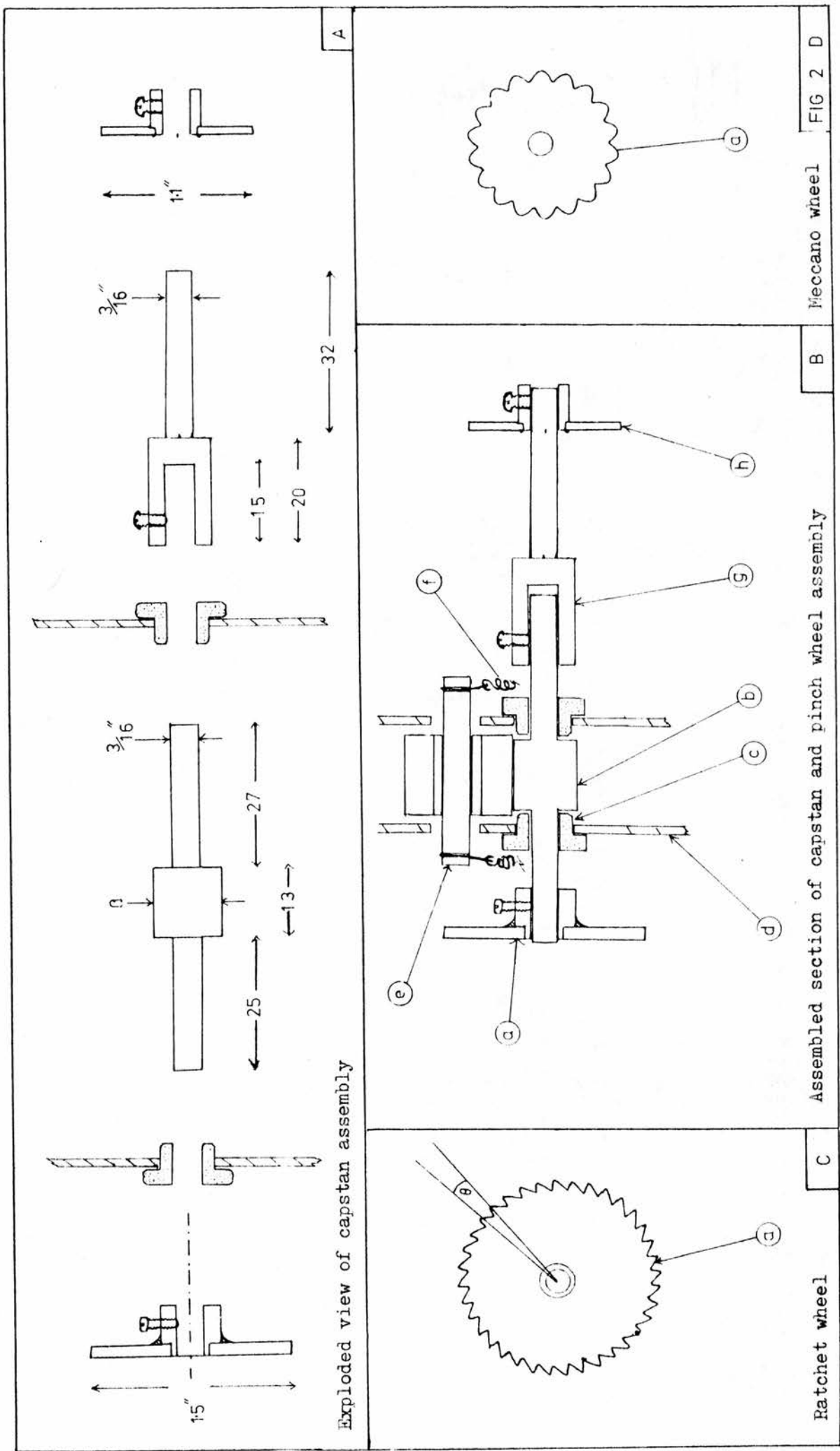
- a ratchet wheel
- b capstan
- c sintered bronze bush
- d duralumin side plate
- e roller bearing for pinch wheel
- f tension spring for pinch wheel
- g brass extension
- h 'meccano' wheel

Fig 2 C

- a one of 36 filed teeth
- θ 10°

Fig 2 D

- a one of 18 teeth



Exploded view of capstan assembly

Assembled section of capstan and pinch wheel assembly

Ratchet wheel

Meccano wheel

FIG 2 D

Reference Fig 3 Section of spool carrier assembly

Fig 3 B

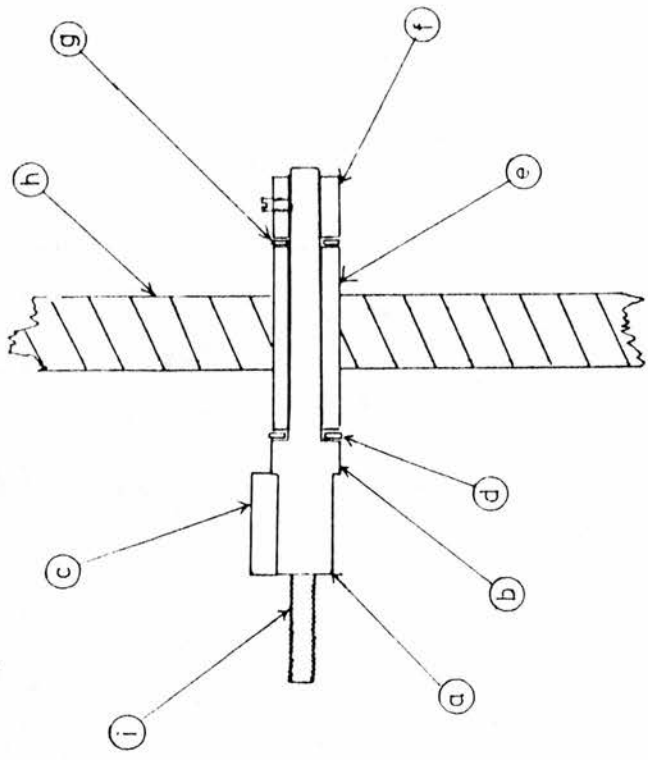
- a brass spool carrier
- b locating boss
- c spool locating fin
- d felt oil washer
- e mild steel sleeve bearing
- f spindle fixing
- g felt oil washer

Fig 3 C

- a mild steel tape roller
- b tape locating groove
- c mild steel spindle
- d end view of roller

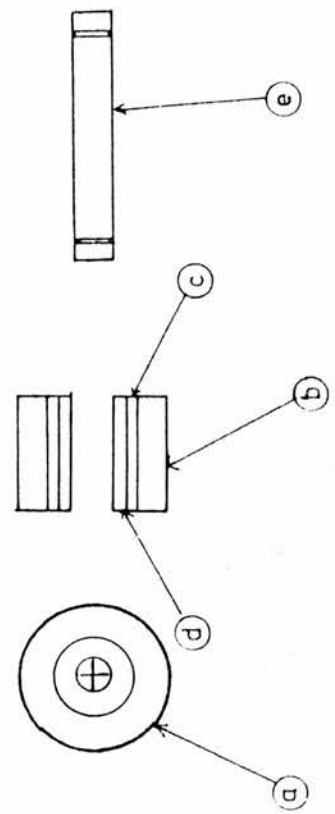
Fig 3 D

- a end view of pinch wheel
- b rubber outer layer of wheel
- c inner steel sleeve
- d sintered bronze bearing
- e spindle

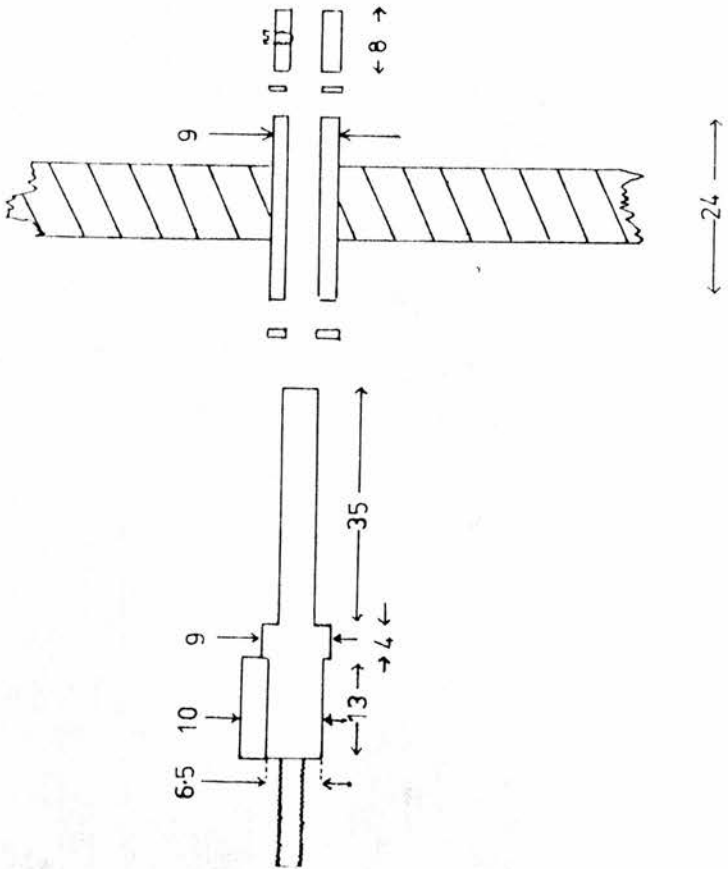


Assembled section of spool carrier

FIG 3D

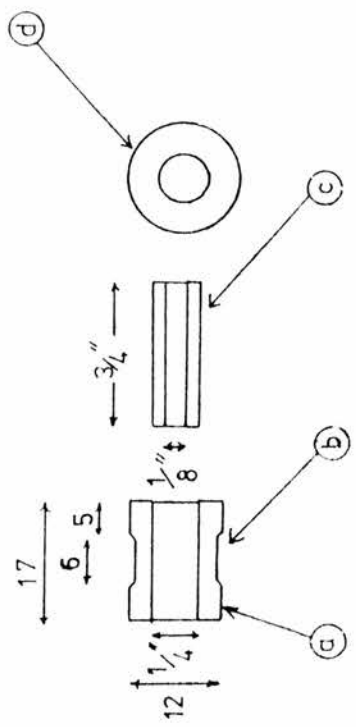


Rubber pinch wheel and spindle



Exploded section of spool carrier

A



Roller and spindle

C

Reference Fig 4 Section of clutch assembly

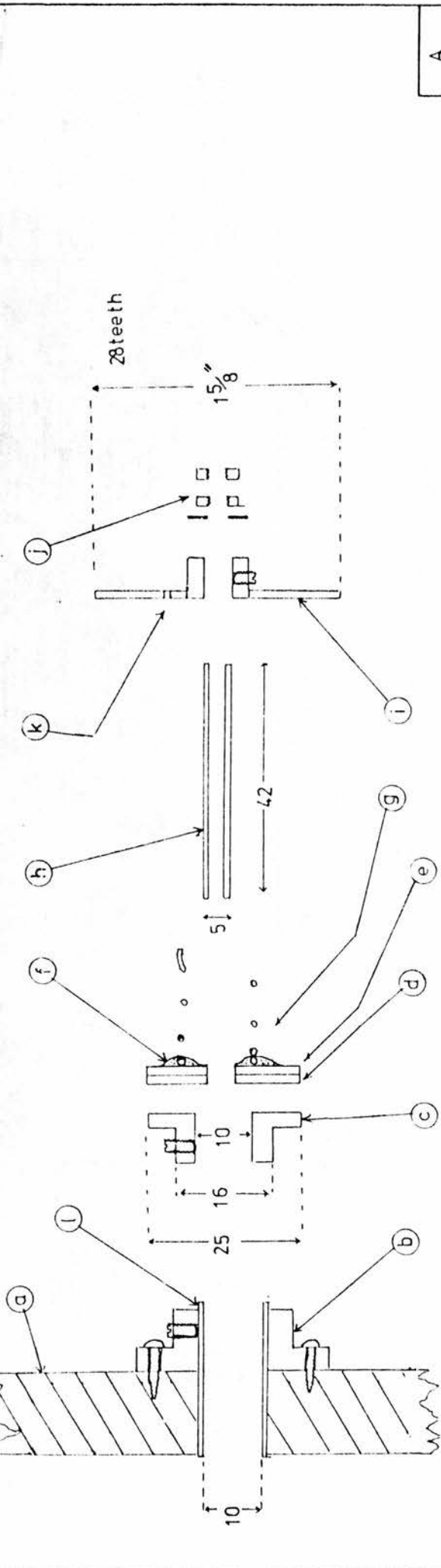
Fig 4 A

- a wooden panel, 8 ply
- b brass bush
- c steel clutch plate
- d cardboard clutch plate
- e paxolin supporting plate
- f glued end of spring
- g spring
- h inner spindle
- i meccano wheel
- j assembly locking nuts
- k hole for locating spring end
- l sleeve bearing, mild steel

Fig 4 C

- a spool locating fin
- b outer spindle
- c hole for inner spindle
- d assembly locking nuts
- e spool clamping plate
- f tension rod (6 BA brass studding)

All dimensions in millimetres unless shown as inches



A

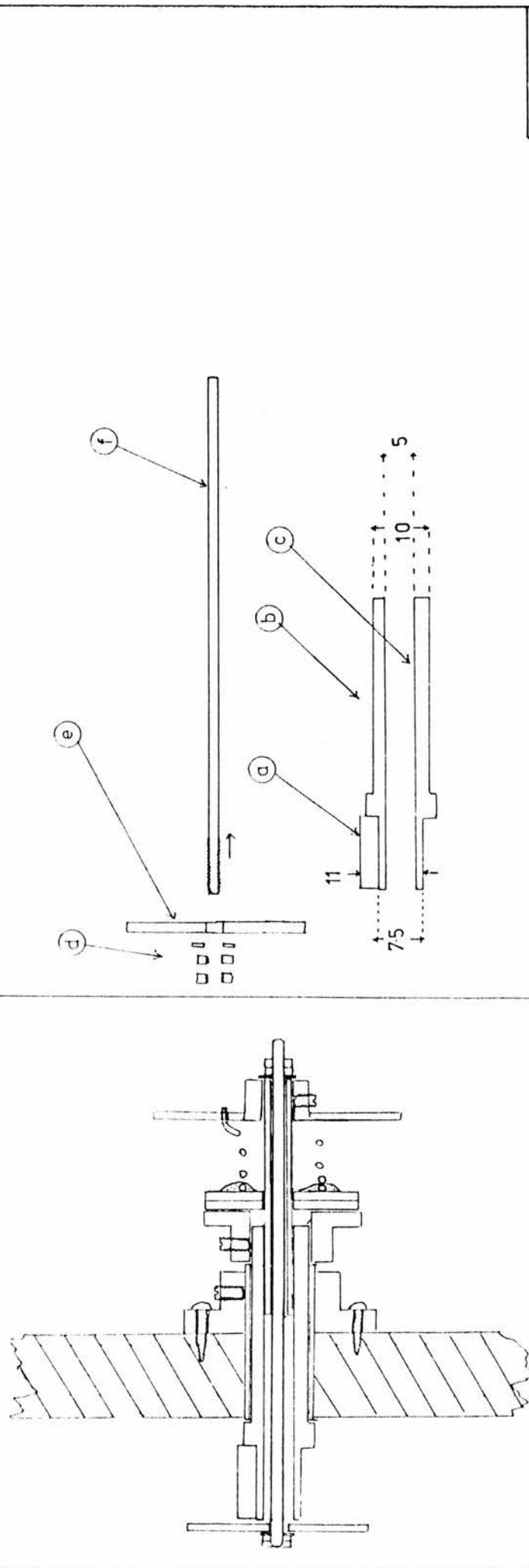


FIG 4 C

Exploded and assembled views of clutch

B

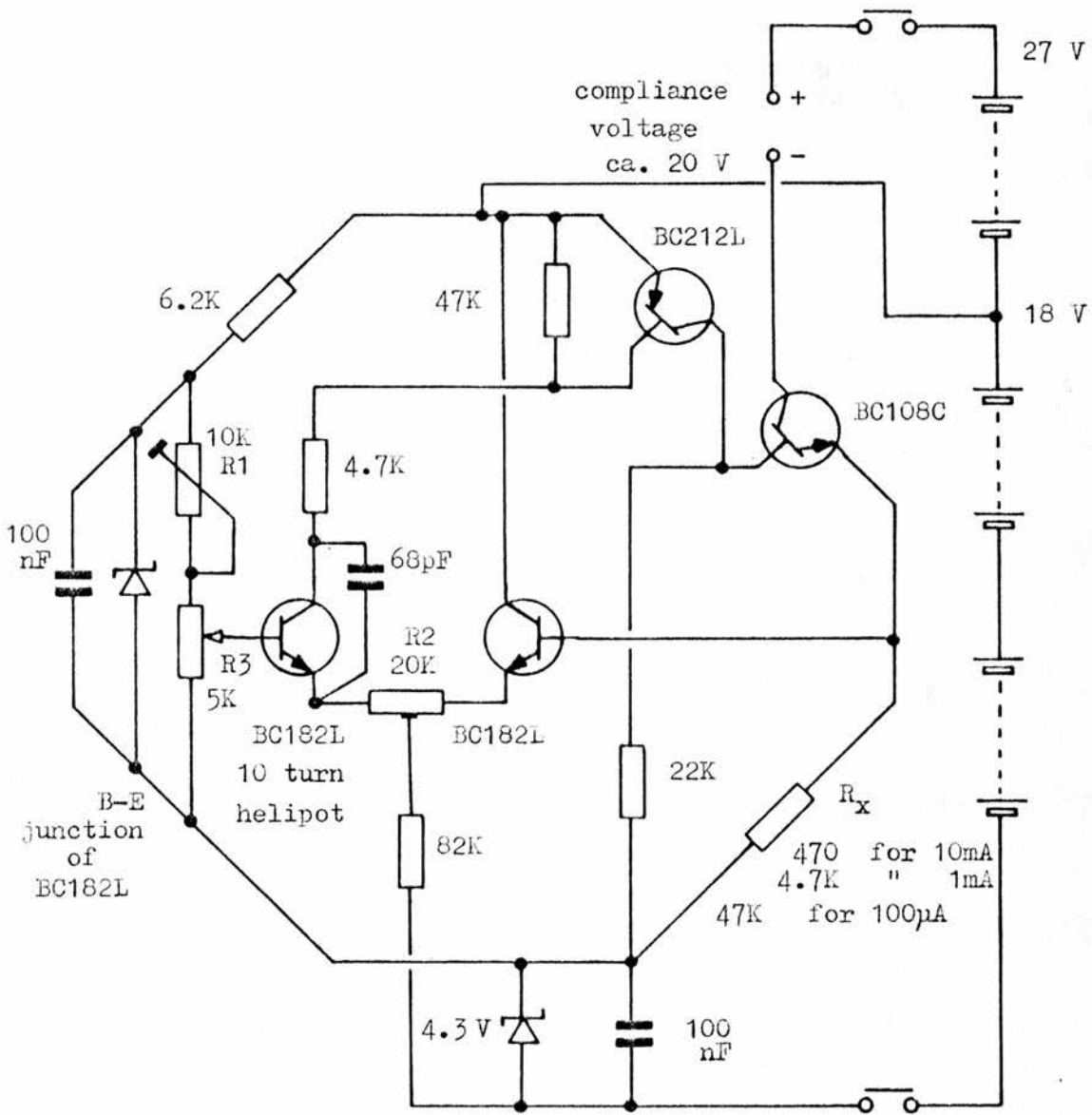


Fig. 1 Circuit for integrator calibration aid: a constant current generator. R_x value (switchable) depends on range of maximum output current. Current selected on 10-turn Beckman-pattern helipot with high resolution calibrated dial, R_3 . Setting-up procedure: R_3 set to 00µA on 100µA range, R_2 adjusted for zero output. R_3 then set to 100 on dial, and R_1 adjusted for 100µA output. For maximum accuracy on all ranges, R_x values must be selected so that one setting of R_1 is correct for all ranges. This circuit has not been tested in this form, being an adaptation of a high voltage current source (Going, unpublished)

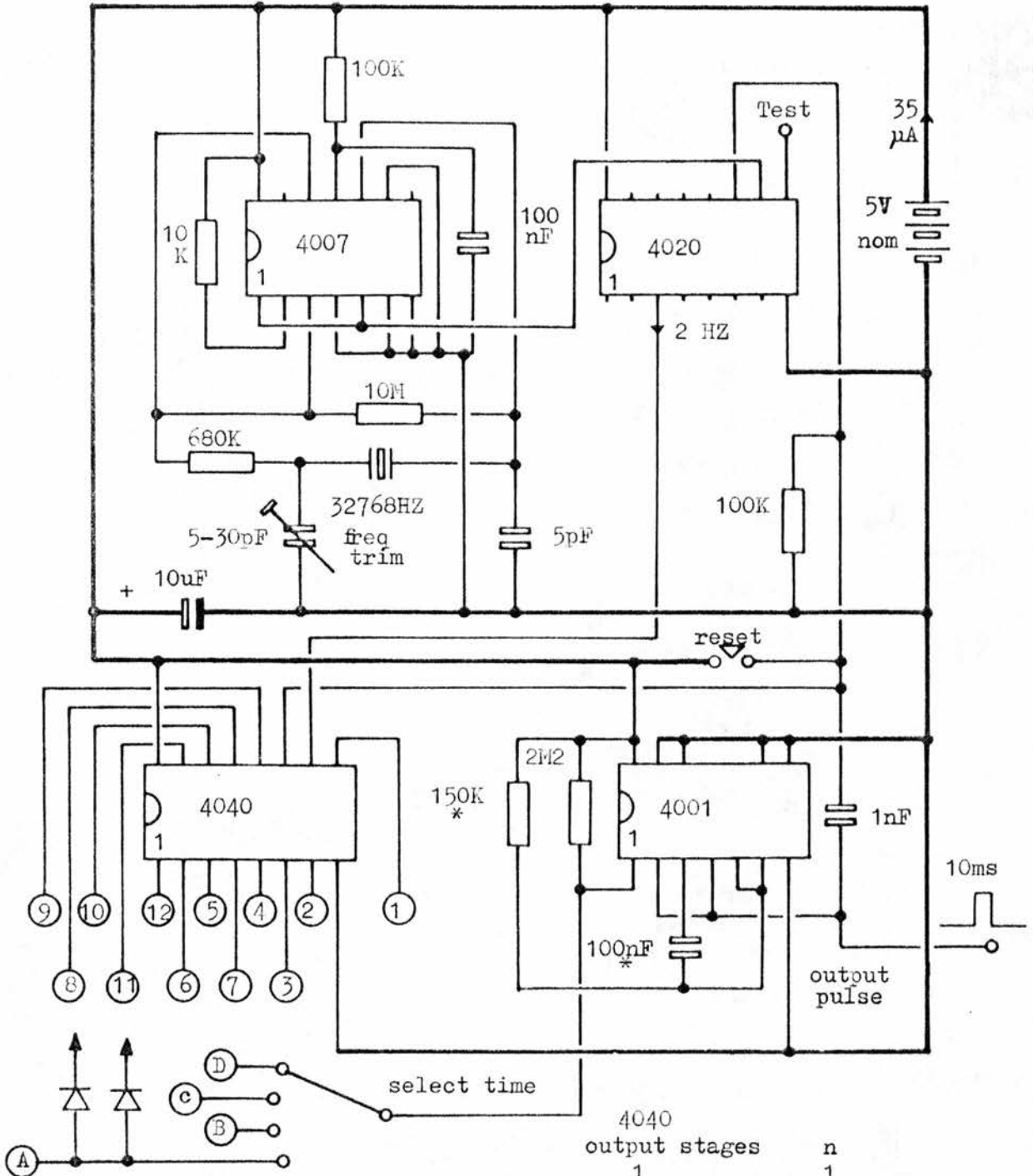
APPENDIX 10

A CALIBRATION AID: A CONSTANT CURRENT SOURCE

The circuit on the page opposite is for a simple current source based on a design (GOING) which has given satisfactory laboratory performance for the past two years. The current is selected on the calibrated dial of a ten-turn potentiometer; no meter is used, dispensing with a vulnerable component not well suited to field use. The circuit, slightly modified in comparison with the original form, has not been tested in this version.

See also

LEACH (1977)



Units of $n = \frac{1}{2}$ sec. (for 2 HZ clock)
 For a given time t sec, multiply t
 by 2; determine those 4040 output
 stages for which the sum of n values
 equals $t \times 2$. Connect chosen line
 A, B, C, or D to those 4040 outputs
 via 1N4148 diodes (cathodes to
 4040 outputs)

4040 output stages	n
1	1
2	2
3	4
4	8
5	16
6	32
7	64
8	128
9	256
10	512
11	1024
12	2048

For accurate timing monitor frequency at 'test' point and adjust
 trimmer capacitor to give a value of 16384 HZ. Minimum battery
 voltage is 3.6 V

This circuit was designed by Mr.C. Eley

APPENDIX 11

A CRYSTAL CONTROLLED CLOCK FOR THE RECORDER

The clock circuit presented in Fig, 1, facing, was kindly designed for me by my erstwhile colleague, Mr. Christopher Eley. It was used during the field trials of the recorder, when it performed in a satisfactory fashion. The circuit uses CMOS logic integrated circuits, which should be of ceramic encapsulation ' military ' grade if the circuit is to be used at low temperatures. The crystal, of frequency 32,768 Hz, is a miniature electronic watch component, or, better, a tuning-fork pattern crystal, e.g. type STATEK CX1V.

Appendix 12 - Selected Manufacturers' names and addresses

A.P.R. - A.P.E.M. (France)

U.K. Agents: P. Caro and Associates Ltd.
(miniature waterproof panel switches)

Accumulatorenfabrik Sonnenschein GmbH

U.K. agents : F.W.O. Bauch Ltd (lead-acid batteries)

Ambulatory Monitoring, Inc.

731, Saw Mill River Road, Ardsley, NY 10502 USA
(solid state heart-rate recorder)

Analog Devices Ltd.

Central Avenue, East Molesey, Surrey, KT8 0SN
(AD590 temperature measuring device)

Associated Automation Ltd.

70, Ludden Hill Lane, Neasden, London, NW10
(sealed relays)

B & R Relays Ltd.

Temple Fields, Harlow, Essex, CM20 2BG.
(Siemens relays)

Balzers High Vacuum Ltd.

Northbridge Road, Berkhamsted, Hertfordshire
(optical interference filters)

Barr & Stroud Ltd.

Caxton Street, Anniesland, Glasgow, W3
(Optical colour glass and interference filters)

Bauch, F.W.O. Ltd.

49, Theobald Street,
Boreham Wood, Hertfordshire, WD6 4RZ.
(agents for Sonnenschein batteries)

Berec Ltd

1255, High Road, Whetstone, London, N20 0EF
(Ever Ready batteries)

Bisset - Berman Inc.

division of Plessey Inc. Electrochemical Division ,
3860 Centinela Avenue, Los Angeles, California 90066
(Electrolytic integrating cells)

P. Caro & Associates Ltd.,

2457, Coventry Road, Birmingham, B26 3LS
(agents for A.P.R. - A.P.E.M. switches)

C.F. Cassella & Co. Ltd.,

Regent House, Britannia Walk, London, N.1
(meteorological Instruments)

Centronic Ltd.

Centronic House, King Henry's Drive, New Addington,
Croydon, CR9 0BC.
(silicon photodetectors)

Chance - Pilkington Ltd.

Glascoed Road, St. Asaph, Flintshire, Wales
(colour filter glasses Agents: Precision Optical Instruments Ltd.)

Chloride - Gates Energy Ltd.,

15, Elizabeth Street, London, SW1W 9RH
(sealed lead - acid accumulators)

Clairex Inc.

U.K. Agents : Hird - Brown Electronics Ltd. Lever Street,
Bolton, Lancashire, BL3 6BJ
(Cadmium sulphide photodetectors)

Corning Inc.

U.K. Agents : Precision Optical Instruments (Fulham) Ltd.
(coloured filter glass)

Cristie Electronics Ltd.

Rodney House, Church Street, Stroud, Gloucestershire, GL15 1JL
(data loggers)

Curtis Instruments Inc.

351, Lexington Avenue, Mount Kisco, New York, N.Y. U.S.A.
(mercury coulometers)

Duracell UK Ltd.

Duracell House, Gatwick Road, Crawley, West Sussex, RH10 2UQ
(batteries (primary))

E.G. & G Ltd

Electro - optics Division, 35, Congress Street, Salem,
Massachusetts, 01970 U.S.A.
(silicon photodetectors)

Electromethods Ltd

Stevenage, Hertfordshire.
(integrating motors)

Ferranti Electronics Ltd.

Fields New Road, Chadderton, Oldham, Lancashire, OL9 8NP
(silicon photodetectors and photovoltaic cells)

Hakuto International

159, Chase Side, Enfield, Middlesex, EN2 0PW
(U.K. Agent for Hamamatsu T.V. Co.)

Hamamatsu T.V. Co. (Japan)

U.K. Agents : Hakuto International
(silicon and gallium arsenophosphide photodetectors)

I.C.I. Ltd, Plastics Division

P.O.Box 6, Bessemer Road, Welwyn Garden City, Hertfordshire
AL7 1HD.
(perspex brand of polymethyl methacrylate)

Integrated Photomatrix Ltd.

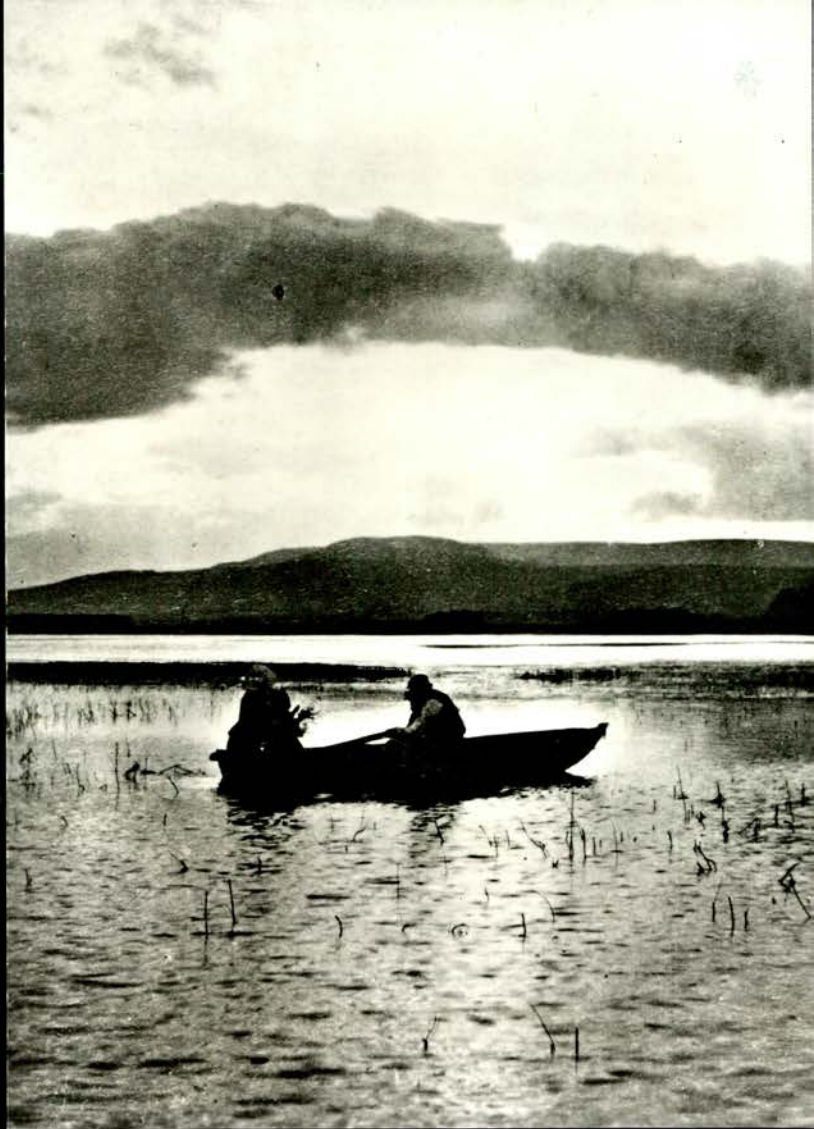
The Grove Trading Estate, Dorchester, Dorset, DT 1 1SY
(self - scanning photodiode arrays)

Interface Quartz Devices Ltd.,

27, Market Street, Crewkerne, Somerset, TA18 7JU
(Statek quartz crystals)

- Kodak Ltd.,
Victoria Road, Ruislip, Middlesex, HA4 0QJ
(gelatin Wratten filters)
- H. Kuhnke Ltd.,
St. John's Road, Penn, Nr. High Wycombe, Buckinghamshire
(solenoid operated valves)
- Lambda Instruments Inc.
2933, North 36th., Lincoln, Nebraska 68504, UBA
(underwater radiometric receiver and radiometer)
- Lintronic Ltd.
54-58, Bartholomew Close, London, EC1
(meteorological instruments)
- Lucas Ltd.,
parts and service division, Crat Hampton Street, Birmingham,
B18 6AV
(solar photovoltaic cells)
- Medicharge Ltd
Tolpits Industrial Estate, Tolpits Lane, Watford, Hertfordshire
WS1 8QY
(silver - zinc rechargeable batteries)
- Megatron Ltd.
165, Marlborough Road, Hornsey, London N19 4NE
(selenium photodetectors)
- Nippon Electric Company
43, Civic Square, Motherwell, Lanarkshire, ML1 1TH
(gallium arsenophosphide photodetectors)
- Oliver Pell Controls Ltd.
Cambridge Row, Burrage Street, Woolwich, London, SE18
(relays)
- Plessey Components Ltd.
Wood Burcote Way, Towcester, Northamptonshire, NN12 7JN
(tantalum capacitors)
- Precision Optical Instruments (Fulham) Ltd.
158, Fulham Palace Road, London, W6
U.K Agents for, and fabricators using, Corning, Schott and
Chance - Pilkington glass filters.
- Pye Electrodevices Ltd.
Controls Division, Exning Road, Newmarket, Suffolk, CB8 0AX
(solenoid operated valves)
- R.S. Components Ltd.
P.O. Box 427, Epworth Street, London, EC2P 2HA
(general suppliers of electronic components)
- Rapco Electronics Ltd.
Joule Road, Houndmills Industrial Estate, Basingstoke, Hampshire
RG21 2XF
(data logging equipment)

- Rauchfuss Instruments and Staff Pty.
11, Florence Street, Burwood, Victoria, Australia, 3125
(recorders and meteorological instruments)
- Rohm and Haas (U.K.) Ltd.
Lennig House, Masons Avenue, Croydon, Surrey.
(plexiglass brand of polymethyl methacrylate)
- Rustrak Instruments Division,
Manchester, N.H. 03103, U.S.A.
(portable chart recorders)
- Saft (U.K.) Ltd.
Station Road, Hampton, Middlesex, TW12 2BY
(nickel-cadmium batteries)
- Sensitised Coatings, Ltd.
Bergen Way, North Lynn Industrial Estate, Kings Lynn,
Norfolk, PE30 2JL
(heat sensitive thermal recording paper)
- Sharp Corporation
Semiconductor division, 2613-1, Ichinomoto, Tenri - City,
Nara 632, Japan.
(silicon blue photodetectors)
- Siemens (U.K.) Ltd.
Sunbury on Thames, Middlesex, TW16 7HS
(semiconductors, thermistors and general electronics)
- H.V. Skan Ltd.
425 - 433 Stratford Road, Shirley, Solihull, Warwickshire,
B90 4AE
(agents for Schott (Mainz))
- Statek Inc.
U.K. Agents: Interface Quartz Devices Ltd.
(quartz crystals)
- Thorn Electrical Components Ltd.
Great Cambridge Road, Enfield, Middlesex, EN1 1UL
(relays)
- United Detector Technology Inc. (U.S.A.)
15, South Street, Farnham, Surrey, GU9 7QU
(silicon photodetectors)
- Varta Ltd.
Hermitage Street, Crewkerne, Somerset, TA18 8EY
(nickel - cadmium batteries)
- West Hyde Developments Ltd.
Unit 9, Park Street Industrial Estate, Aylesbury,
Buckinghamshire, HP20 1ET
(cable glands, instrument housings)
- Zettler (U.K. Division)
Brember Road, Harrow, Middlesex, HA2 8AS
(relays)



two ecologists, believed to be
making irradiance measurements

REFERENCES

- Ackefors, H., Ahnstrom, G., Rosen, C., (1969) *Limnol. Oceanogr.* 14, 613-617, Construction and performance of a sensitive light meter for underwater use.
- Ahrenkiel, R.K. et al., (1977) *J. appl. Phys.* 48, 267-269, Low dark-current photodiodes using GaAs O.6 P O.4.
- Allan, A.H., McKree, K.J. (1955) *J. scient. Instrum.* 32, 422-424, Integrating meters for comparing light intensities in plant growth studies.
- Allison, W.M., Bubriski, S.W., Hazzard, H.O., Millard, R.J. (1960) *I.R.E. Trans. compon. Parts CP(7)*, pp. 88-105. Symposium on Tantalum capacitors.
- Anderson, M.C. (1971) *Radiation and Crop Structure in Plant Photosynthetic Production - Manual of Methods.* ed. Šestak, Z, Čatský, J., Jarvis, P.G. Den Haag: Dr. W. Junk N.V.
- Anderson, W.T., Robinson, F.W. (1925) *J. Am. chem. Soc.* 47, 718-725, Oxalic acid-Uranyl sulfate ultraviolet radiometer.
- Arnold, G.P. (1975) in *Light as an Ecological Factor II*, ed. Evans, G.C., Bainbridge, R, Rackham, O. Oxford: Blackwell. The Measurement of irradiance with particular reference to marine biology.
- Atkin, J. Bonnatere, R. Laurent, J.P. (1974), *Power Sources (5)* Collins, D.H. ed. pp. 91-101, paper 8, Sealed nickel cadmium and lead acid batteries: comparison of functioning mechanisms (proc. 9th. int. symp. Brighton on research and dev. of non-mech electrical power sources), London: Academic Press.
- Austin, R.W. (1964), *Appl. Opt.* 3, 5, pp. 584-587, Visibility VIII Techniques of measurement.
- Baharestani, H. Tompkins, W.J., Webster, J.G. (1979) *Med. and Biol. Eng.* 17, pp 719-723, Heart rate recorder.
- Barry, R.G., Chorley, R.J. (1968) *Atmosphere, weather and climate*, pp. 319, London: Methuen
- Beinhauer, R. (1977) *Gartenbauwissenschaft*, 42, 3, pp. 109-113 Photosynthetisch aktive strahlung in Gewachshaus.
- Bell, L.N., Chmora, W.N., Kornilev, V.P. (1959) *Fiziologiya. Rast.* 6, 504-507, Pribor dlya opredeleniya kolichestva oblucheniya (fotointegrator).
- Berkeliev, A., Gol'dberg, Yu. et al., (1976), *Sov. Phys. Semicond.* 10, 8, pp. 908-911, Photodetectors of visible and ultra violet radiation based on GaAs_{1-x}P_x surface barrier structures.
- Berry, R.E., Raney, L.W. (1968) *Ecology*, 49, 1, 161-162, A recording photometer for biological studies.

- Berthet, P. (1960) *Vegetatio* 9, 197-207, La Mésure écologique de la température par détermination de la vitesse d'inversion du saccharose.
- Biggs, W.W., Edison, A.R., Eastin, J.D., Brown, K.W., Maranville, J.W., Clegg, M.D. (1971) *Ecology*, 52, 1, pp. 125-131, Photosynthesis light meter and sensor.
- Bindloss, M.G. (1976) *Freshwater Biol.* 6, 501-508, The light climate of Loch Leven, a shallow Scottish loch, in relation to primary production by phytoplankton.
- Björkman, O. (1981) Responses to different quantum flux densities pp. 57-108 in Lange, O.L. et al., q.v.
- Blackman, G.E., Black, J.N., Martin, R.P. (1953) *Ann. Bot. (N.S.)* 17, 529-537, Physiological and ecological studies in the analysis of plant environment. VIII An inexpensive integrating recorder for the measurement of daylight.
- Blinks, L.R. (1964) *Accessory Pigments and photosynthesis* Ch. 7, pp. 199-221, *Photophysiology*, ed. Giese, A.C., London and New York: Academic Press.
- Bogenschutz, A.F. (1974) tr. Silman, H. Surface treatment and electroplating in the electronics industry. London: Portcullis Press.
- Bogus, K. (1974) *Elektron Int. (Austria)* No. 23-24, pp. 418-421, Photoelectric properties of silicon photodetectors for light and radiation measurements. (in German).
- Bollen, D. (1965) *Wireless Wld.* 71, pp. 381-383, Miniature DC converters.
- Bowen, E.J. (1936) *Proc. R. Soc. ser. A.* 134, pp. 349-353, Heterochromatic photometry of the ultraviolet region.
- Boyd, R.A. (1951) The development of prismatic glass block and the daylighting laboratory. *Research Bull, Engng. Res. Inst. Univ. of Michigan*, No. 32, App C, 64-68.
- Brach, E.J., Mack, A.R., St. Amour, G. (1969) *Electron. Engng.* 94-97, Integrator resetting switch using a combination of unijunction and thyristor.
- Bradshaw, W.E., Phillips, D.L. (1980) *Oecologia (Berl.)* 44, 311-316, Photoperiodism and the photic environment of the pitcher plant mosquito *Wyeomyia smithii*.
- Breimesser, F., Poppinger, M., Schwaier, A. (1981) *Siemens Forsch. u-Entwickl. Ber.* 10, 2, pp. 72-77, Piezoresistive pressure sensor with silicon diaphragm.
- Bro, P., Holmes, R., Marincic, N., Taylor, H. (1975) in *Power Sources 5* ed. Collins, D.H. London: Academic Press pp. 703-712, The discharge characteristics of the Li-SO₂ battery system.
- Brooks, F.A. (1964) *Bot. Rev.* 30, pp. 263-291, Agricultural needs for special and extensive observations of solar radiation.

- Buckley, D.J. (1976) *Agric. Meteorol.* 16, 353-358, A micropower digital temperature integrator
- Byrne, G.F. (1970) *Agric. Meteorol.* 7, pp. 415-418, Data logging and scanning rate considerations in micro-meteorological experiments.
- Cain, J.C. (1969) *Hortscience* 4, 2, pp. 123-125, A portable economical instrument for measuring light and temperature intensity-time integrals.
- Caldwell, M.M. (1981) Plant response to solar ultra violet radiation pp. 161-198 in Lange, O.L. et al., q.v.
- Callahan, P.S. (1964) *J. Econ. Ent.* 57, 5, 758-760, An inexpensive actinometer for continuous recording of moonlight, daylight, and low intensity evening light.
- Callendar, H.L. (1897) *British Patent* 16, 718.
- Callendar, H.L. (1898) Report of the British Association pp. 796-797 A quantitative bolometric sunshine recorder.
- Campbell, D.S. (1971) *The radio and Electronic Engineer* 41, 1, pp. 5-16, Electrolytic Capacitors.
- Campbell, G.S. (1974) *Agric. Meteorol.* 13, 399-404, A micropower electronic integrator for meteorological applications.
- Campbell, G.S. (1981) Fundamentals of radiation and temperature temperature relations. pp 11-40, in Lange, O.L. et al, q.v.
- Cernusca A. (1968) *Photosynthetica* 2, (4) pp. 238-244, The use of automatic data recording systems for climate- ecological studies within productivity research. (Ger).
- Chapman, A.R.O., Campbell, C.C.M. (1975) *Limnol. Oceanogr.* 20, 3, p. 496 only, Quanta vs. Watts.
- Chapman, A.R.O., Hoyt, B., Paton, B.E., (1976) *Mar. Biol.* 38, pp. 91-94, A self-contained instrument for logarithmic recording of submarine quantum irradiance.
- Clarke, F.J.J. (1964) *Photochem. and Photobiol.* 3, pp. 91-96, Comparison table of the performance of twenty-five types of radiation detector.
- Clegg, M.D., Biggs, W.M., Eastin, J.D., Maranville, J.W., Sullivan, C.Y. (1974) *Agron. J.* 66, pp. 471-476, Light transmission in field communities of sorghum.
- Coker, P.D., Coker, A.M. (1972) *J. Appl. Ecol.* 9, 767-770, Multipleday digital event recorder: some possible applications.
- Collins, B.G. (1973) *Austral. Meteorol. Mag.* 21, 113-117, Ultraviolet radiation as Aspendale, Victoria.
- Cooper, G.R., Hilborn, M.T., Hepler, P.R. (1958) *Maine Farm Res.* 5, 7-9 (January), A totalising light-meter for biological research.
- Courtney, R.G. (1976) *Archit. Sci. Rev.* 19, 2, pp.44-49, or Solar energy utilisation in the UK. Current Research and future prospects.

- Courvoisier, P., Wierzejewski, H. (1954), Arch. Met. Geophys. Bioklim. (Ser. B) 5, 413-446, Das Kugelpyranometer Bellani. Beiträge zur strahlungsmessmethodik V.
- Craig, R.E., Lawrie, R.G. (1962) Limnol. Oceanogr. 7, 2, 259-261, An underwater light intensity meter.
- Crump, A.E. (1967) Wireless Wld. 73, pp. 122-127 (March) pp. 175-177 (April), Design of Schmitt-trigger circuits.
- Cunningham, R.C. (1974) Electro-opt. Syst. Des. 6, 8, 21-26, Silicon photodiode or photomultiplier tube?
- Czopek, M., Starzecki, W., Lagisz, J., Motyka, B. (1965) Photosynthetica 1, 1-2, pp. 65-68, An automatic registrator as a supplement of an electronic integrator of PhAR and their adaptation to ecophysiological studies.
- Danahy, E.L. (1970) Electro-opt. Syst. Des. 2, 5, 36-43, The real world of silicon photodiodes.
- Danahy, E.L., Kaiser, K. (1976) 27th Ann. Conf. Analy. Chem. and Appl. Spectros. Cleveland Ohio USA March 1-5, Ultra stable silicon photodiode for low-level light detection in the V.U.V., UV, and visible spectrum-abstract only.
- Daniel, A.F. (1963) in Batteries: Proc. 3rd., Int. Symp. Zinc-Alkaline MnO_2 dry cells. Collins, D.H. Ed. Oxford: Pergamon.
- Darwin, H. (1905) British Patent 10844.
- Davies, W.E.R., Wyszecski, G. (1962) J. opt. Soc. Am. 52, 6, 679-685, Physical approximation of colour mixture functions.
- Davis, P.H., () United Detector Technology, The Schottky barrier silicon photodetector in perspective with other devices in the 200nm-1100nm range, 1st European electro-optics markets and technology conference, Geneva, Switzerland, 13-15 Sept. 1972 (Guildford, England: IPC Sci. Technol. Press (1973) pp. 393-399).
- Deac, G.B. (1967) Des. Electron. April, pp , Use and abuse of hermetically sealed rechargeable accumulators.
- De Wilde, J. (1962) A. Rev. Ent. 7, pp. 1-26, Photoperiodism in insects and mites.
- Dijkstra, H.R., Franx, C. (1978) Mullard Technical Publication TP1700 United Kingdom: Mitcham 16pp, Solar panels for terrestrial applications.
- Dobson, G.M.B. (1963) Exploring the atmosphere, Oxford: Oxford University Press.
- Dodillet, H.J., (1961) Lichttechnik, Berl. 13, 11, pp. 556-558, Der maximalwert des phyto-photometrischen strahlungsäquivalentes.
- Dore, W.G. (1958) Ecology, 39, 151-152, A simple chemical light meter.

- Drew, E.A. (1972) *New Phytol.* 71, 407-413, A simple integrating photometer
- Dunsheath, P. (1962), *A history of electrical engineering*, London: Faber and Faber.
- Eberts, K. (1970) in: *Power Sources 2*, ed. Collins, D.H. Oxford: Pergamon Press, pp. 69-92, Specific properties of small closed lead accumulators using an immobilised electrolyte.
- Engelsma, G. (1978/9) *Philips tech. Rev.* 38, 3, pp. 89-100, Phenol synthesis and photomorphogenesis.
- Engineering Equipment Users Association (1968) *Specification and selection of data-logging equipment*, EEUA Handbook 28, London: Constable and Company.
- Eppeldauer, G. (1973) *App. Opt.* 12, pp. 408-409, Some problems of photocurrent measurement of photo-voltaic cells.
- Evans, G.C., (1969) *J. Ecol.* 57, pp. 109-125, The spectral composition of light in the field I. Its measurement and ecological importance
- Feichtinger, H. (1977) *Funkschau*, 12, 555-557, Gasdicht NiCd Akkumulatoren - Tips für Anwender.
- Ferranti Ltd (1974) *Applications of the E-line plastic encapsulated transistor* 7th edition, March, Oldham: Ferranti Ltd.
- Fitter, D.J., Knapp, P.H., Warren-Wilson, J. (1980) *J. appl. Ecol.* 17, 183-193, Stand Structure and light penetration, IV A sensor for measuring photosynthetically active radiation.
- Forstner, H., Rutzler, K. (1970) *Oceanogr. and Mar. Biol. Ann. Rev.* 8, 225-249, Measurements of the microclimate in littoral marine habitats
- Foss, N.A. (1971) *IEEE J. Quantum Electron.* QE7, 6, p.285 para.5.5 (June), Metal-oxide semiconductor photodiode for ultraviolet laser detection (Abstract only).
- France, R.W. (1960) *I.R.E. Trans. compon. Parts* CP7, pp.106-112, (Sept), The transient effect in capacitor leakage resistance measurement.
- Franklin, R.W., (1962) *Proc. Instn. elect. Engrs. Part B. Sup.* 22 109, 525-536, Electrolytic Capacitors.
- Franz, S., Kent, G., Anderson, R.L. (1977) *J. Electron. Mater.* 6, 2, pp. 107-123, Heterojunction Solar cells of SnO_2/Si .
- Fritschen, L.J. (1977) *Agric. Meteorol.* 18, 321-325, A millivolt to volt and pulse to volt integrator for meteorological purposes.
- Fukuda, M., Iijima, T., (1975) in *Power Sources 5*, ed. Collins, D.H. London: Academic Press pp. 713-728, Lithium polycarbonmono-fluoride cylindrical type batteries.

- Furuichi, K., Sasaki, A. (1968) *Electronic Engineering* Dec. __, __, pp. 678-679, Monostable multivibrator with zero stand-by power consumption.
- Gayford, M.L., (1969) *Modern Relay Techniques*, London: Butterworth.
- Gehring, G., Lachmann, U. (1979) *Siemens Forschung u. Entwickl. Ber.* 8, 264-267, Integrated light sensor device with broad operating range and enhanced blue spectral response.
- Georgiev, G.D. (1974) *Imeko proceedings, Budapest, Hungary*, A new photoreceiver for quantitative valuation of photosynthetic efficiency of optical radiation. 6th. Internat. Symp. of the Tech. Committee on photodetectors, Siofok, Hungary, Sept. 16-19.
- de Gier, N.A., van Gool, W., van Santen, J.G. (1958/9) *Philips tech. Rev.* 20, 10, 277-308, Photoresistors made of compressed and sintered cadmium sulphide.
- Going, T.C.H. (1981) *J. Phys. E.:Sci. Instrum.* 14, 1128-30 A very high efficiency DC to DC inverter, optimised for supplying high voltages in battery operated equipment.
- Gorczyński, L. (1936) *Met. Mag., Lond.* 71, 1-5, Measurements of solar radiation instruments, and some results.
- Guha, S.K. (1972) *Light. Res. and Technol.* 4, 3, pp. 166-170, Application of photoconductive cells in portable photometers.
- Gulyaev, B.I., (1964) *Soviet Plant Physiology or Plant Physiology (USSR)* 10, pp. 433-441, *Fiziologiya Rastanii (Pl. Physiol., Wash.)* 10, 5, (Sept/Oct 1963) pp.513-524, Measurement of Photosynthetically Active Radiation.
- Hajdu, L., Zahoran, J. (1974) *Acta tech. Hung.* 76, 1-2, 153-175, Hermetically-sealed silver-zinc batteries operating in the Silver I oxide (Ag_2O) phase.
- Hajdu, L., Zahoran, J. (1972) *Acta tech. Hung.* 73, 1-2, 117-141, Recent research results in the field of hermetically sealed miniature silver-zinc storage batteries.
- Halldal, P. (1967) *Photochem. and Photobiol.* 6, pp. 445-460, Ultraviolet action spectra in Algae.
- Halldal, P., (1974) Chapter 15 of Steeman Nielsen, E., Jerlov, H.G. eds. *Optical Aspects of Oceanography*, London and New York: Academic Press, Light and photosynthesis of different algal groups.
- Hanks, R.J., Gardner, H.R. (1964) *Proc. Soil Sci. Soc. Am.* 28, 449-450, Portable integrator for net radiation, total radiation and soil heat flux.
- Hansen, K., Hagemann, K. (1967) *Oikos*, 18, 14-24, Micro-thermic measurements in arctic vegetation with a transistor-probe and integrating Cu-voltmeter.
- Hansen, T.E., (1978) *Phys. Scr.* 18, pp. 471-475, Silicon UV-photodiodes using natural inversion layers.

- Harris, P.B., (1968) J. Phys. E: Sci. Instrum. Ser. 2, 1, 1007-1010, A simple ultra-violet sensor and integrating recorder for long-term field operation.
- Hart, B.L., Barker, R.W.J. (1974) J. Phys. E: Sci. Instrum. 7, pp. 921-123, A low-level current source for extended duration time-base sweeps.
- Haxo and Blinks, (1950) J. gen. Physiol. 33, 389-422, Photosynthetic action spectra of marine algae.
- Heiden, R.H. (1969) Technica No. 17, pp. 1579-1586, Geschichte der elektrischen Messtechnik: Messwert-schreiber.
- Heinicke, (1963) Can. J. Plant Sci. 43, 561-568, Light measurement with the uranyl oxalate actinometer.
- Hill, R.H. (1966) J. scient. Instrum. 43, 829-890, An attachment for the Sumner long-term recorder that integrates a radiometer output.
- Hillman, G.R. (1976) Med and Biol. Eng. Sept. , 589-590, Automatic over-range device for strip-chart recorders.
- Hodge, B.J.R., Bonnaterre, R., Putois, F., (1974) Power sources - 5 paper 14, pp. 211-231, Collins D.H. ed., Fast charging of sealed nickel-cadmium batteries, theory and practice. (Proc. 9th Int. Symp. Brighton 1974 on Res. and Dev. in non-mech. electr. power sources) London: Academic Press
- Hodgmann, J.S. (1976) Elektrotechnik, Berl. 58, Heft 19, 'Merkt' sich die Behandlung: Der Gedachtniseffekt bei Nickel Kadmium Batterien.
- Holden, S.H. (1905) J. Instn. elect. Engrs. 36, 393-405, Two new electrolytic meters.
- Holmes, M.G., Smith, H. (I, II and IV) (1977) Photochem. and Photobiol. 25, pp. 533-538, 539-545, 551-557, the function of phytochrome in the natural environment.
 I-Characterisation of daylight for studies in photomorphogenesis and photoperiodism
 II-The influence of vegetation canopies on the spectral energy distribution of natural daylight.
 IV-Light quality and plant development
 for III, see Smith, H., and Holmes, M.G.
- Holmes M.G., McCartney, H.A. (1976) Spectral energy distribution in the natural environment and its implications for phytochrome function. pp 467-476 in Smith H. (ed) q.v.
- Horiguchi, I. (1976) J. agric. Met., Tokyo 31, 4, pp. 171-176, Some characteristics of radiation instruments for measurement of very low intensity under artificial light sources.
- Hughes, A.P. (1965) New Phytol. 64, 55-64, Plant growth and the aerial environment VII. The growth of *Impatiens parviflora* in very low light intensities.

- Hughes, M.K., Lincoln, E. (1969) *Oikos*, 20, 161-165, A simple integrator for use with solarimeters
- Huntington, K.A., Johnstone, D.R. (1973) London: Centre for Overseas Pest Research, A remote-recording field installation for monitoring micrometeorological variables during spray trials.
- Hurd, R.M., Jordan, W.H. (1960) *Platin. Metals. Rev.* 4, 42-47, The principles of the solion - a new range of electrochemical control devices.
- Ikeda, H. (1975-8) Sanyo House Symposium, Osaka University, Chapter 18, Watford: Sanyo (UK) Ltd, Solid state electrochemical cell (memoriode).
- Ikeda, H., Hara, M., Narukawa, S. (1980) *Jap. Electron. Eng.* 17, 157, pp.79-81, Sanyo Lithium batteries feature enhanced energy densities.
- Ikeda, H., Tada, K. (1976) *Jap. electron.Eng. Dec.* pp. 59-62, Memoriode: An ionic superman breaks through.
- Institute of Terrestrial Ecology (1972/3) *Proc. R. Soc. Edinb. B.* 74, IBP programme Loch Leven study.
- Iwaszkiewicz, T., Mazurek, S., et al., (1977) *Pomiar Autom. Kontrola* 5, pp. 186-187, Integrator hybridowy o długim czasie całkowania.
- Jackson, J.E., Slater, C.H.W. (1967), *J. appl. Ecology* 4, 421-424, An integrating photometer for outdoor use particularly in trees.
- Jackson, J.E. (1970) *J. appl. Ecology* 7, 2, 207 - 216
Aspects of light climate within apple orchards
- Jeffrey, S.W. (1981) Responses to light in aquatic plants pp. 249-276 in Lange, O.L. et al. q.v.
- Johnson, K.C. (1977) *Wireless Wld.* 83, 47-48, Nickel Cadmium Cells - experiments in reviving cells you would otherwise discard.
- Jones, J.I.P. (1965) *J. scient. Instrum.* 42, pp. 414-417, A portable sensitive anemometer with proportional DC output and a matching wind-velocity component resolver.
- Jones, J.I.P., (1970) *J. Phys. E: Sci. Instrum.* 3, pp. 9-14, A new recording wind vane.
- Jones, R.C. (1959) *Proc. Inst. Radio Engrs.* 47, No. 9, pp. 1495-1502, Phenomenological description of the response and detecting ability of radiation detectors.
- Jung, W. (1980), *IC Op-Amp Cookbook*, Indianapolis: Howard Sams.

- Kain, J.M. (1971) European Marine Biology Symposium 4th, Bangor 1969, ed. Crisp, D.J., Continuous recording of underwater light in relation to Laminaria distribution Cambridge: C.U.P.
- Kerr, J.P., Thurtell, G.W., Tanner, C.B., (1967) J. appl. Meteorol. 6, pp. 788-794, An integrating pyranometer for climatological observer stations and mesoscale networks (sic).
- King, A.B.S. (1974) J. appl. Ecol. 11, 127-131, An integrating photometer for measuring light penetration through cocoa canopies.
- Kimura, K. (1978) Jap. electron. Eng. pp. 42-45 (April), Silicon ribbon cells increase efficiency and reduce costs.
- Kirby, R.P., (1972/3) Proc. R. Soc. Edinb. (B), 74, 4, pp. 57-67, The morphological history of Loch Leven, Kinross.
- Klein, W.H., Goldberg, B., Shropshire, W. (1977) Sol. Energy, 19, pp. 115-122, Instrumentation for the measurement of the variation, quantity, and quality of sun and sky radiation.
- Kóie, M. (1952/3) Oikos 4, 2, 180-186, A self-recording light integrator and a portable integrator for light-percentage measurements.
- Kahn, D.A. et al., (1975) IERE Conference Proceedings 32, pp.81-90, Underwater logarithmic irradiance meter for primary production and associated studies. (Instrumentation in Oceanography Conference, Bangor Wales, 23-25 Sept).
- Krause, G., Keiner, F. (1974) Components Report 9, 4, pp. 110-111, Suppression of DC component in photocurrent of transistors.
- Krochmann, J. (1964) Lichttechnik, Berl. 16, 180-181, Über ein neues Raumbelichtungs-Messgerät.
- Kubín, Š. (1971) Measurement of radiant energy in: Plant photosynthetic production - manual of methods, Šesták, Z., Čatský, J., Jarvis, P.G. eds. The Hague: Dr. W. Junk N.V.
- Kubín, Š., Hladek, L. (1963) Pl. Cell Physiol., Tokyo, 4, 153-168, An integrating recorder for photosynthetically active radiant energy with improved resolution.
- Kuhn, L., Podogrocki, J. (1969) Gazeta Obs. pánst. Inst. hydrol.-met. 22, 10, pp. 14-16, New Integrators in Actinometry (in Polish).
- Kuwano, Y. (1980) Jap. electron. Eng. 17, 167, pp. 72-78, Amorphous silicon solar cell and integrated cell module.
- Lange, O.L., Nobel, P.S., Osmond, C.B., Ziegler, H., (1981)
Encyclopedia of Plant Physiology, New Series, 12a:
Physiological Plant Ecology - I
Berlin: Springer Verlag
- Leach, M.F. (1977) J. Phys. E: Sci. Instrum. 10, pp. 879-880, A wide-range, constant-current generator for use with Hall measurements.
- Lehfeldt, R.A. (1902) Lond. Edinb. Dubl. Phil. Mag. 6th series, 3, pp. 158-159, A voltameter for small currents.

- Leighton, W.G., Forbes, G.S. (1930), J. Am. chem. Soc. 52, 3139-3152, Precision actinometry with uranyl oxalate.
- Levring, T. (1947) Göteborgsk. Vetensk.-o. Vitterh-samm. Handl. Series B, 5, 6, 5-36, Submarine daylight and the photosynthesis of marine algae.
- Liberman, A.M. (1970) Lightning Empiricist (Teledyne Philbrick Nexus) 18, pp. 6-7, The current reflector as a circuit element.
- Linden, D., McDonald, B. (1980) J. Power Sources 5, pp. 35-55, The Lithium-Sulphur Dioxide primary battery - its characteristics, performance and applications.
- Lindmayer, J., Allison, J.F., (1973) Comsat Tech. Rev. 3, 1-22, The violet cell: an improved silicon solar cell.
- Luckow, C. (1865), Dinglers Polytechn. 177, 231.
- McComb, A.L., Iyambo, D.E., (1968) Federal Dept. of Research, Samaru, Nigeria, Research Leaflet 1, (July), Some solar radiation measurements at Samaru, Nigeria with an actinograph and radiation integrators.
- McCartney, H.A., Unsworth, M.H., (1978) Q. J. Roy. Met. Soc. 104, pp. 699-718 Spectral distribution of Solar Radiation
I - Direct radiation
pp. 911-926 Spectral distribution of Solar Radiation
II - Global and diffuse
- Macfadyan, A., Webb, N.R.C. (1968) Oikos 19, 1, 19-27, An improved temperature integrator for use in Ecology.
- MacHattie, L. (1971) Wireless Wld. 77, pp. 13-15, Voltmeter uses FETs measures capacitor Insulation resistance.
- McKee, G.B., (1963) Agron. J. 55, 6, pp. 580-583, A self-powered integrator for ecological research.
- McCree, K.J. (1973) Sol Energy 15, pp. 83-87, The measurement of photosynthetically active radiation.
- McCree, K.J. (1966) Agric. Meteorol. 3, 353-366, A solarimeter for measuring photosynthetically active radiation.
- McCree, K.J. (1973) Curr. Adv. Plant-Sci. No. 5 (Oct), PP.39-43, A rational approach to light measurement in plant ecology.
- McCree, K.J. (1981) Photosynthetically active radiation pp. 41-56 in Lange, O.L. et al, q.v.
- McKnight, J.G. (1964) J. Audio Engng. Soc. 12, 2, pp. 140-146, Mechanical damping in tape transports.
- McLaughlin, N.B., Allan, J.R. (1976) J. Phys. E: Sci. Instrum. 9, pp. 651-653, An inexpensive radiant energy integrator.
- McPherson, H.G. (1969) Agric. Meteorol. 6, pp. 347-356, Photocell-filter combinations for measuring photosynthetically active radiation.

- Maggs, D.H., Alexander, D.McE. (1970) *J. appl. Ecol.* 7, (5) 639-646, Tests of a uranyl oxalate light integrator for use in fruit tree canopies.
- Manley, W. (1969) *Qd. J. agric. Sci.* 26, pp. 625-628, A minimal intensity photometer.
- Martin, J.W., Cox, J.R. (1962) *Electronics (America)* 35, March 23rd issue, pp. 46-47, Solion tetrode integrates chromatograph signals.
- Maxwell, J. (1977) National Semiconductors applications note. A novel FET micropower voltage regulator.
- Melhuish, W.H. (1962) *J. opt. Soc. Am.* 52, 11, pp. 1256-1258, Calibration of spectrofluorimeters for measuring corrected emission spectra.
- Middleton, W.E.K. (1953) *Ecology*, 34, 2, pp. 416-421, Spherical illumination as an ecological parameter.
- Mobley, R.C. (1962) *Rev. Sci. Instrum.* 33, 177-180, Precision continuous current integrators.
- Moir, J. (1961) *High Quality Sound Reproduction*, London: Chapman and Hall Ltd.
- Moll, W.J.H. (1923) *Proc. phys. Soc. London*, 35, 257-260, A thermopile for measuring radiation.
- Monteith, J.L. (1959) *J. scient. Instrum.* 36, pp. 341-346, Solarimeter for field use.
- Monteith, J.L. (1972) *Survey of Instruments for Micrometeorology (International Biological Programme Handbook No. 22)* Oxford: Blackwell Scientific Publications.
- Monteith, J.L. (1973) *Principles of Environmental Physics (Contemporary Biology Series)* pp.241, London: Edward Arnold.
- Monteith, J.L. (1976) *Spectral distribution of light in leaves and foliage.* pp 447-460 in Smith H. (ed.) *q.v.*
- Monteith, J.L., Szeicz, G. (1960), *Q. Jl. R. met. Soc.* 86, 91-94, The performance of a Gunn-Bellani radiation integrator.
- Monteith, J.L., Szeicz, G. (1962) *Arch. Met. Geophys. Bioklim. (Wien)* B-11, pp. 491-500, Simple devices for radiation measurement.
- Morel, A., Smith, R.C. (1974) *Limnol. Oceanogr.* 19, 4, pp.591-600, Relation between total quanta and total energy for aquatic photosynthesis.
- Mosher, R.H. and Davis, D.S. Eds. (1968) *Industrial and specialty Papers Vol. I Technology*, pp. 154-162, New York: Chemical Publishing Co. Inc.
- von Munch, W., Gessert, C., Koniger, M.E. (1976) *I.E.E.E. Trans. Electron Devices* ED23, 11, 1203-1207, Photodiodes and junction FET with high US sensitivity.
- Nichiporovich, A.A. (1960) *Soviet Plant Physiology or Plant Physiology (USSR)* 7, pp.617-620. English trans. of *Fiziologiya Rastanii (Pl. Physiol., Wash.)* 7, (Nov/Dec 1960) pp. 744-747, Conference on measurement of visible radiation in plant physiology, agrometeorology and ecology. (April 20-21).
- Norbury, J.R., White, W.J. (1971) *J. Phys. E: Sci. Instrum.* 4, pp. 601-602, A rapid-response rainauge.

- Norman, J.M., Tanner, C.B., Thurtell, G.W. (1969) *Agron. J.* 61, pp. 840-843, Photosynthetic-light sensor for measurements in plant canopies.
- Ogawa, H., Okazaki, R. (1978) *Jap. electron. Eng.* pp. 51-54 (March), Matsushita's Lithium batteries make new miniature devices possible.
- Ouchi, H. et al., (1979) *I.E.E.E. Trans. Electron. Devices.* ED-26, 12, pp. 1965-1969 (Dec), Silicon PN Junction Photodiodes Sensitive to Ultra-violet radiation.
- Palm, A. (1959) extract from *Registriereinstrumente* 2nd edition: Roth, M., Schlosser, E.G. Eds. *Bibliography of chart recorders plus notes on three types (Askania, Lambrecht and AEG/Mix and Genest)* Berlin: Springer Verlag.
- Pereira, H.C. (1959), *Q. Jl. R. met. Soc.* 85, 253-261, Practical field instruments for estimation of radiation and of evaporation.
- Pink, H., Tischer, P. (1981) *Siemens Forsch. u-Entwickl. Ber.* 10, 2, pp. 78-82, Gas detection by metal oxide semiconductors.
- Platt, T., Larsen, E., Vine, R. (1970) *J. Fish. Res. Bd. Can.* 27, pp. 185-191, Integrating radiometer: A self-contained device for measurement of submarine light energy in absolute units.
- Preis, J. (1969) *Wireless Wld.* 75, 484-486 (Oct), High performance low cost "active zener" regulators.
- Prevost, S.E. et al., (1971) *J. appl. Ecol.* 9, 1, pp. 51-55, A system for logging light interception in crop stands.
- Prieur, L., (1970) *Cah. Océanogr.* 22, pp. 493-501, Photometre marin mesurant un flux des photons.
- Prince, M.B., Wolf, M. (1958) *J. Br. Instn. Radio Engrs.* 583-595, New developments in silicon photovoltaic devices.
- Raps, A. (1897), *Elektrotech. Z.* 17, Heft 13, April., pp. 196-197, Vereins nachrichten: Angelegenheiten des Elektrotechnische Vereins III - Vortrage und Besprechungen. Ueber ein Universalregistririnstrument etc. von Siemens and Halske.
- Rauch, K., Voss, E., Ness, P., Rieder, E. (1966) *Elektrochemische Schaltzellen, Aktuelle Batterieforschung, Varta-Buchreihe.*
- Rauschenbach, H.S., Maiden, E.E. (1972) 9th I.E.E.E. Photovoltaic Specialists Conference, Silver Spring, Maryland, USA, pp. 217-225, Breakdown phenomena in reverse biased silicon solar cells.
- RCA (1974) *Electro-optics Handbook Technical Series EOH-11*, Harrison, New Jersey: RCA Inc.
- Rehak, P.H. (1980) *Electron. Engng.* 52, p. 19, (June), Micropower voltage regulator with very low V_{in} - V_{out}

- Rentschler, H.C. (1930) *Trans. Amer. Inst. electr. Eng.* 49, 576-578, An ultraviolet light meter.
- Richards, E.R. (1975) in *Power Sources 5*, Collins, D.H. Ed. pp. 617-635, *Solar cells in the Trinity House Lighthouse Service*, London: Academic Press.
- Richards, J.C. (1970) *Electron. Engng.* 42, p. 48 (March), Simple battery voltage stabiliser.
- Robinson, N. ed. (1966) *Standard short-wave pyranometers*. In *Solar Radiation*, Amsterdam: Elsevier.
- Robitzsch, M. (1932) *Gerlands. Beitr. Geophys.* 35, 37, Über den bimetall-aktiniograph Fuess-Robitzsch.
- Ross, P.J. (1973) *J. Phys. E: Sci. Instrum.* 6, pp. 969-970, A low power voltage regulator for field instrumentation.
- Roth, L., Weiner, J. (1965) "Thermographic Papers" Bibliographic Series No. 221, Appleton, Wisconsin: Institute of Paper Chemistry, Sponsored by the Sensitised Papers Section, TAPPI Coating Committee. 276 references.
- Ruachev, V.P., Berdnikov, V.F., Vashchenko, V.I., (1963/4) *Plant Physiology (USSR) or Soviet Plant Physiology (Washington USA)* 10, pp. 503-507, *Fiziologiya Rastenii (Pl. Physiol. Wash.)* 10, 5, (Sept/Oct 1963) pp. 598-602, Physical basis of measurements of the energy of photosynthetically active radiation by selective detectors.
- Ruff, H.R. (1970) *Light. Res. and Technol.* 2, 1, pp. 43-46, A portable Finsen meter for photobiological studies.
- Salter, G.C., Thomas, R.E. (1977) *Solid-St. Electron.* 20, 95-104, Silicon solar cells using natural inversion layers found in thermally oxidised p-silicon.
- Saffell, R.A., Campbell, G.S., Campbell, E.C. (1979) *Agric. Meteorol.* 20, pp. 393-396, An improved micropower counting integrator.
- Sauberer, F. (1962) *Mitt. Int. Verein. theor. angew. Limnol.* 11, 1-76, Empfehlungen für die Durchführung von Strahlungsmessungen an und in Gewässern.
- Scroggie, M.G. (1981) *Radio and Electronic Laboratory Handbook* 8th edition 1971, London: Butterworth.
- Schnegg, K. (1977) *Bull. Schweiz. elektrotech. Ver.* 68, No. 22 1175-1177, La charge des Accumulateurs nickel-cadmium etanches.
- Schroder, D.K. (1978) *I.E.E.E. Trans. Electron. Devices*, ED 25, 2, 90-97, Transparent-gate silicon photodetectors.
- SCOR (1965) *Unesco Technical Papers in Marine Sciences*, 2, p.5 Report of the first meeting of the joint group of experts in photosynthetic radiant energy.

- Selcuk, K., Yellott, J. (1962) *Sol. Energy* 6, 4, 155-163,
Measurement of direct, diffuse, and total solar radiation
with silicon photovoltaic cells.
- Shannon, C.E., (1949) *Bell System Tech. J.* 27, 379-423 and 625-656,
A mathematical theory of communication.
- Shaw, R.H., McComb, A.L. (1959) *For. Sci.* 5, 234-236, A
comparison of the Gunn-Bellani radiation integrator and the
Eppley pyrheliometer.
- Siemens Ltd (1971/2) Design Examples of semiconductor circuits,
DEAC recharger circuit for NiCd cells p. 182, Munich: Siemens Ltd.
- Sinclair, T.R., Lemon, E.R. (1973) *Sol. Energy* 15, pp. 89-97,
The distribution of 660 and 730 nm radiation in corn canopies
- Sinclair, T.R., Lemon, E.R. (1974) *Agron. J.* 66, pp. 201-205,
Penetration of photosynthetically active radiation in corn
canopies.
- Smith, E.E. (1962) *Proc. Instn. elect. Engrs.* 109, Part B
+ 545-546 + part, Reliability of tantalum foil type
electrolytic capacitors.
- Smith, H. (ed.) (1976) *Light and Plant development*
London : Butterworth
- Smith, H., Holmes, M.G. (1977), *Photochem. and Photobiol.* 25,
pp. 547-550, The function of phytochrome in the natural
environment-III - The measurement and calculation of
phytochrome equilibria.
- Smith, I.R. (1972/3) *Proc. R. Soc. Edinb. (B)* 74, 6, pp. 81-100,
The structure and physical environment of Loch Leven, Scotland.
- Smith, I.R. (1975) Unpublished records, Edinburgh: Institute of
Terrestrial Ecology.
- Smith, R.C., Tyler, J.E., (1967) *J. opt. Soc. Am.* 57, 5, pp. 589-595,
Optical properties of clear natural water.
- Smith, R.C. (1969) *J. mar. Res.* 27, pp. 341-357, An underwater spectral
irradiance collector.
- Smith, R.G., (1975) Building Research Establishment Current paper
CP15/75, Solar ultraviolet radiation in Southern England,
Garston: Building Research Establishment.
- Sommer, G.F., Hammer, K.C. (1951), *Plant Physiol.* 26, (2)
318-330, A simplified integrating light recorder for field
use.
- Spence, D.H.N., Campbell, R.M., Chrystal, J. (1971) *Freshwater
Biol.* 1, pp. 321-337, Spectral intensity in some Scottish
Freshwater lochs.
- Spence, D.H.N. () *Light Quality and Plant response underwater.*
in *British Photobiology Society International symposium
PLants and the Daylight Spectrum* 5th-8th January 1981,
Smith, H. Ed. London: Academic Press to be published.

- Spitzer, D., Wernand, M.R. (1978) *Appl. Opt.* 17, 1, pp. 12-13, Photon irradiance sensor.
- Spencer, H.C. (1961) *Wireless Wld.* 67, pp. 502-503 (Oct), Unattended battery operation.
- Spencer, H.C. (1963) in: *Batteries: Proc. 3rd., Int. Symp., Unattended battery charging from solar cells*, Oxford: Pergamon Press.
- Sprague, V.G., Williams, E.G. (1943), *Pl. Physiol., Wash.* 18, 131-133, A simplified integrating light recorder for field use.
- Sprague, V.G., Williams, E.G. (1941) *Pl. Physiol. Wash.* 16, 629-635, An inexpensive integrating light recorder.
- Stanhill, G., Fuchs, M., (1977) *J. appl. Ecol.* 14 , 317-322 The relative flux density of photosynthetically active radiation
- Stanton, M.G., (1973) *New Phytol.* 72, 1375-1379, Digital light integrator for ecology.
- Steeman Nielsen, E. (1975) *Marine Photosynthesis*, Elsevier Oceanography Series 3, Amsterdam: Elsevier.
- Stiles, W. (1970) *J. appl. Ecol.* 7, pp. 617-622, A diffusive resistance porometer for field use.
- Stimson, A. (1974) *Photometry and Radiometry for engineers*, Wiley Interscience.
- Stirn, R.J., Yeh, Y.C.M. (1977) *I.E.E.E. trans. Electron. Devices* ED24, 4, 476-483, Technology of GaAs Metal oxide semiconductor Solar Ce-ls.
- Strickland, J.D.H. (1958) *J. Fish. Res. Bd. Can.* 15, 453-493, Solar radiation penetrating the ocean. A review of requirements, data, and methods of measurement, with particular reference to photosynthetic productivity.
- Sumner, C.J. (1959) *J. scient. Instrum.* 36, 475-477, Single pen strip chart recorder for unattended long period operation.
- Sumner, C.J. (1964) *J. scient. Instrum.* 46, 638-639, A new robust standard cup anemometer.
- Sumner, C.J. (1965) *A. Jl. Roy. met. Soc.* 91, 364-367, A long-period recorder for wind speed and direction.
- Sutton, F., Rorison, I.H. (1970) *J. Appl. Ecol.* 7, 321-329, The modification of a data-logger for the recording of temperatures in the field.
- Sutton, F., Rorison, I.H. (1972) *J. Appl. Ecol.* 9, 121-126, An automatic data translation system using a simple adaptation to link a D-Mac portable translator and a solartron data logger.
- Suzuki, H., Nakamura, T., Kiyohashi, K., (1977) *Nippon Denki Giho*, 119, 85-90, (Technical Bulletin of the Nippon Electric Co. Ltd), GaAsP photodiodes for cameras. (in Japanese).

- Suzuki, S., Yamamoto, K. (1976) Journal of electronic engineering (Japan) Jan, pp. 20-23, Photodetectors for UV and IR spectral region (Hamamatsu).
- Sydenham, P.H. (1979) Measuring instruments - Tools of knowledge and control pp. , London: Peter Peregrinus / Science Museum
- Szeicz, G. (1966) Field measurements of energy in the 0.4-0.7 μm Range in: Light as an Ecological Factor I, Bainbridge, R., Evans, G.C., Rackham, O Eds. Oxford: Blackwell Scientific Publications.
- Szeicz, G. (1974) J. appl. Ecol. 11, pp. 617-636, Solar radiation for plant growth.
- Tang, P.A., McNaughton, K.G., Black, T.A. (1976) Trans. Am. Soc. agric. Engrs. 550-552, Precision electronic integrator for environmental measurement.
- Taylor, A.H. (1941) J. Opt. Soc. Am. 31, 105-106, A footcandle-hour integrator for daylight.
- Taylor, A.H., Kerr, G.P. (1941) J. opt. Soc. Am. 31, pp. 3-8, The distribution of energy in the visible spectrum of daylight.
- Thaller, M. (1970) Met. Monogr. 11, 33, 211-226, Practical considerations in instrument design.
- Thomas, V.B. (1963) in Batteries (Collins, D.H. ed.) Proc. 3rd Int. Symp., Kinetic basis for the operating characteristics of sealed nickel-cadmium cells. Oxford: Pergamon Press.
- Thurtell, G.W., Tanner, C.B. (1964) J. appl. Meteorol. 3, pp. 198-202, Electronic integrator for micrometeorological data.
- Timko, M.P. (1976) I.E.E.E. Jnl. Solid-State Circuits (USA), SC-11, 6, 784-788, A two-terminal IC temperature transducer.
- Trebbble, F.C. (1980) Proc. I.E.E. Series A 127, 8, 505-527, Solar Cells.
- Trickett, E.S., Mouldsley, L.J. (1956) J. agric. Engng. Res. 1, 1, pp. 1-11, An integrating photometer.
- Tsuji, T (1976) Jap. electron. Eng. June, pp. 43-46, Japan's solar cell technology is moving rapidly ahead.
- Tukey, L.D., Fluck, M.F., Marsh, C.R. (1960) Proc. Am. Soc. Hort. Sci. 75, 804-810, An illumination totalizer for integrating light from either natural or artificial sources.
- Tye, F.L. (1980) Primary batteries for civilian use, pp. 50-150 in Electrochemical Power Sources, Barak, M. Ed. Stevenage, UK: Peter Peregrinus.
- Tyler, J.E. (1973) Limnol. Oceanogr. 18, 5, p. 810, Lux vs. Quanta.
- Tyler, J.E. (1965) J. opt. Soc. Am. 5, 7, pp. 800-805, In situ spectroscopy of Ocean and Lake water.

- Tyler, J.E. (1973) *Oceanogr. and Mar. Biol.* 11, pp. 11-25, Applied radiometry.
- Tyler, J.E., Smith, R.C. (1966) *J. Opt. Soc. Amer.* 56, 10, pp.1390-1396, Submersible spectroradiometer.
- Uchijima, Z. (1968) *Japan agricultural research quarterly* 3, 20-22, A newly devised solarimeter for measuring photosynthetically active radiation.
- Valverde, N. (1981) *J. appl. Electrochem.* 11, pp.305-312, 313-317 Analogue storage cells based on a coulometer with solid electrolyte and stoichiometric variation of the storage phase.
- Vollenweider, R.A. (1961) *IBP Handbook No. 12 (A manual of methods for measuring) Primary Production in Aquatic Environments* Edinburgh and Oxford: Blackwell Scientific Publications.
- Weihofen, U., Woehl, R. (1981) *Agricultural Meteorology* 24, pp. 116-117, A low-cost, multipurpose data acquisition device based on a microprocessor.
- Weinberg, S. *Neth. J. Sea Res.* 8, 4, pp.354-360, A relative irradiance meter for submarine ecological measurements.
- Westlake, D.F. (1965) *Photochem. and Photobiol.* 4, 849-868, Some problems in the measurement of radiation under water: a review.
- Weston, E.T. (1960) *J. Scient. Instrum.* 37, pp.359-360, Cosine correction of a waterproofed photovoltaic cell.
- Whillier, A., Tout, D. (1965) 9, pp. 208-212, A new integrating instrument for measuring daily values of total solar radiation.
- Whiting, E.E. (1968) *Appl. Opt.* 7, 10, pp. 2141-2142, Improved ultra-violet response of a PIN photodiode.
- Wiggins Teape Ltd. (1972/6) *British Patent No. 1,438,765* pp 1-3 Improvements relating to heat-sensitive recording materials
- Williams, C.B. (1936) *Proc. R. Soc.* 226, 357-389, The influence of moonlight on the activity of certain nocturnal insects, particularly of the family noctuidae, as indicated by a light trap.
- Williams, P. (1967) 73, 318-322, A ring-of-two reference, in *Wireless World*.
- Williams, P. (1968) *Electron. Engng.* 40, pp. 517-519, Low-voltage level sensing circuit.
- Williams, P., Carruthers, J., Evans, J.H., Kinsler, J. (1974) *Circuit Designs - Collected Circards I Series 2 Comparators and Schmitts, Series 10, Micropower circuits*, London: *Wireless World*.
- Williams, R.L. (1962) *J. opt. Soc. Am.* 52, 11, 1237-1244, Fast, High sensitivity silicon photodiodes.

- Wetherell, P.G., Faulhaber, M.E. (1970) *Appl. Opt.* 9, 1, pp. 73-78, The silicon solar cell as a photometric detector.
- Wolf, M., Rauschenbach, H. (1963) *Advanced Energy Conversion* 3, 455-479, Series resistance effects on solar cell measurements.
- Woodward, F.I., Yaqub, M. (1979) *J. appl. Ecol.* 16, 545-552, Integrators and sensors for measuring photosynthetically active radiation and temperature in the field.
- Worner, H. (1955) *Z. Met.* 9, 8, 248-250, Die Konstanz von Selenphotoelementen.
- Wigglesworth V.B. (1964), *The Life of Insects*, London: Weidenfeld and Nicolson.
- Yeh, Y.C., Ernest, F.P., Stirn, R.J. (1976) *J. appl. Phys.* 47, 9, pp. 4107-4112, Practical anti-reflection coatings for metal-semiconductor solar cells.

POSTSCRIPT

Value of linearising resistor, R1 (p.47,48, Fig.18)

The following analytical solution for the value of R1 has been provided by my supervisor, Dr. M.G.Stanton. Since $Q = CV$ for a capacitor, it follows that the charge integrated between V_2 , the upper threshold voltage which triggers discharge of the capacitor and registers a count, and V_1 , the lower level to which C_{intg} is discharged after V_2 is reached by the ancillary circuitry is given by

$$\Delta Q = C_{intg}(V_2 - V_1).$$

However, as already observed, p.47, at high currents to be integrated, it is necessary to add in a correction resistor, R1, which has the effect of decreasing the charge that is integrated before the discharge circuitry is triggered, since a small voltage, caused by the current being integrated, appears across R1, and the upper threshold voltage, V_2 , is detected from the upper terminal of R1.

Let us therefore observe what happens with a current being integrated, I_{intg} , which we will assume remains sensibly constant during an integration cycle. The charge change accumulated on the capacitor before triggering the discharge circuitry is now given by :

$$\Delta Q = C_{intg}(V_2 - V_{R1} - V_1)$$

which is, of course, $I_{intg} \times t$, where t is the time taken to charge C_{intg} from V_1 to the point when the ancillary circuitry detects V_2 as the sum of the voltages across C_{intg} and R1. But, Ohm's Law gives

that $V_{R1} = I_{\text{intg}} R1$. Therefore :

$$I_{\text{intg}} t = C_{\text{intg}} (V_2 - V_1) - C_{\text{intg}} I_{\text{intg}} R1 ,$$

or, the charge-up time is given by :

$$t = \frac{C_{\text{intg}}}{I_{\text{intg}}} (V_2 - V_1) - C_{\text{intg}} R1 .$$

The ancillary circuitry takes a time t_{dead} to discharge C_{intg} to V_1 . Therefore the total cycle time will be $t + t_{\text{dead}}$. For perfectly linear integration

$I_{\text{intg}} (t + t_{\text{dead}})$ should be constant for any value of I_{intg} . We thus want :

$$I_{\text{intg}} \left\{ \frac{C_{\text{intg}}}{I_{\text{intg}}} (V_2 - V_1) - C_{\text{intg}} R1 + t_{\text{dead}} \right\} \text{ to be constant.}$$

By inspection, it is obvious that for given values of C_{intg} , V_2 and V_1 it is constant if

$$\underline{\underline{C_{\text{intg}} R1 = t_{\text{dead}}}}$$

and this is therefore the required condition allowing us to select the value of $R1$ (but see later for a slight adjustment to this).

The above condition however is not necessarily complete* because it was tacitly assumed above that t_{dead} was invariant for given ancillary circuitry. No doubt this would be true if this circuitry were discharging C_{intg} always between V_2 and V_1 , but, of course, at high I_{intg} , V_2 is reached across $R1$ and C_{intg} together, but the voltage across C_{intg} is less than V_2 , as is

* but see p.311.

deliberately intended by the introduction of R_1 . Let us refer to this modified voltage across C_{intg} as V_{2C} .^{*} We now need to examine the effect of V_{2C} upon the system. Unfortunately there is no obvious law relating V_{2C} and t_{dead} because the form of it will depend on the behaviour of the discharge circuitry, but as a first approximation it is fair to assume that t_{dead} will be proportional to $V_{2C} - V_1$ provided that V_{2C} is not much less than V_2 and that V_1 is non-zero and is a significant fraction of V_2 . (This may be seen if one examines a CR discharge curve of voltage v. time, and this condition is fulfilled in the embodiment described in this thesis.) Now :

$$V_{2C} = V_2 - V_{R1} = V_2 - R_1 \cdot I_{intg}.$$

* Footnote. In the circuit described in this thesis, the capacitor is first charged up by the ancillary electronics, and then the current to be integrated is used to discharge the capacitor to a threshold value (V_1 actually) which triggers resetting, but in the mathematics here only the difference ($V_2 - V_1$) is involved and so the conclusions drawn apply to both modes of using C_{intg} . The action of R_1 in the embodiment described in this thesis is to present to the trigger point detection circuitry a voltage slightly lower than the actual value on C_{intg} due to the current, I_{intg} , flowing through R_1 , which follows from the sense of the current relative to the polarity of the charge on C_{intg} . During the rapid charge-up reset phase, in the embodiment presented, R_1 takes no part because a diode has been placed across it, directed in the appropriate sense. Although the current being integrated continues to flow during reset, this need not be considered because the reset circuitry easily sinks it, if t_{dead} is a small fraction of the total cycle time.

Let us therefore adopt the assumption stated above and say that :

$$\begin{aligned} t_{\text{dead}} &= k (V_2 - R_1 I_{\text{intg}} - V_1) = k (V_2 - V_1) - k R_1 I_{\text{intg}} \\ &= t_{\text{dead},0} - k R_1 I_{\text{intg}} \end{aligned}$$

where $t_{\text{dead},0}$ and k are constants characteristic of the discharge circuitry, and $t_{\text{dead},0}$ applies when $I_{\text{intg}} = 0$, i.e. $t_{\text{dead},0} = k (V_2 - V_1)$.

If we now rework the condition for adequate correction, we require, as before, the total cycle time $t + t_{\text{dead}}$ to be inversely proportional to I_{intg} , or in other words that $I_{\text{intg}}(t + t_{\text{dead}})$ must be constant. Substituting for t and t_{dead} , we now have that

$$\begin{aligned} C_{\text{intg}}(V_2 - V_1) - C_{\text{intg}}I_{\text{intg}}R_1 + I_{\text{intg}}t_{\text{dead},0} - kR_1I_{\text{intg}}^2 \\ (1) \qquad \qquad (2) \qquad \qquad (3) \qquad \qquad (4) \end{aligned}$$

must be constant. (Terms (1), (2) & (3) were used in the first calculation for R_1 above).

Term (1) is constant for a given setup anyway, so we do not need to consider it. Terms (2), (3) & (4) give the following, if we drop unnecessary suffixes for simplicity and remember later what they were :

$$- CIR + It_{\text{do}} - kRI^2$$

which must be constant, so its first differential/dI must be 0, i.e. :

$$- CR + t_{\text{do}} - 2kI = 0 .$$

Collecting terms in R and re-introducing suffixes gives

$$t_{\text{dead},0} = R I (C_{\text{intg}} + 2k I_{\text{intg}})$$

and it is now clear that it is impossible to achieve perfect correction by including R I since the effect of the value of the integrated current cannot be eliminated.

We can however say that if $t_{\text{dead},0} = C_{\text{intg}} R I$ (the condition worked out on p. 304) then good linearisation prevails so long as $2k I_{\text{intg}}$ is small compared to C_{intg} , but this is a bit vague. It should be observed that the value of k is given by re-arranging $t_{\text{dead},0} = k(V_2 - V_1)$ thus $k = t_{\text{dead},0} / (V_2 - V_1)$.

So, how large is the error in cycle time introduced by this second order effect, and where does it appear, if we set R I equal to $t_{\text{dead},0} / C_{\text{intg}}$? The actual cycle time is $t + t_{\text{dead}}$, which, using what we have above, is :

$$\frac{C_{\text{intg}}}{I_{\text{intg}}} (V_2 - V_1) - C_{\text{intg}} R I + t_{\text{dead},0} - R I \cdot I_{\text{intg}} \frac{t_{\text{dead},0}}{V_2 - V_1} \quad (1)$$

whereas, on the assumption that t_{dead} is invariant, it is

$$\frac{C_{\text{intg}}}{I_{\text{intg}}} (V_2 - V_1) - C_{\text{intg}} R I + t_{\text{dead},0} \quad (2)$$

The ratio of (1) to (2) gives the error. If we, say, allow the error to be acceptable up to 5 %, the ratio of (1) to (2) would be 0.95. Thus, dropping unnecessary suffixes and observing that $R I = t_{\text{do}} / C$ as the set condition :

$$\frac{\left\{ \frac{C}{I} (V_2 - V_1) - C \frac{t_{do}}{C} + t_{do} \right\} - \frac{t_{do}}{C} I \frac{t_{do}}{V_2 - V_1}}{\left\{ \frac{C}{I} (V_2 - V_1) - C \frac{t_{do}}{C} + t_{do} \right\}} = 0.95$$

This has the form

$$0.95 = \frac{A - B}{A} = 1 - \frac{B}{A}, \quad \text{so} \quad \frac{B}{A} = 0.05,$$

whence we see that :

$$\frac{t_{do}^2}{C} \cdot \frac{I}{V_2 - V_1} = 0.05 \frac{C}{I} (V_2 - V_1)$$

if we note that $-\frac{Ct_{do}}{C} + t_{do}$ cancel, as we expect for the set condition. We now have that

$$t_{do}^2 = 0.05 \frac{C^2}{I^2} (V_2 - V_1)^2$$

which indicates that

$$I_{\text{intg(max)}} = 0.22 \frac{C_{\text{intg}}}{t_{\text{dead},0}} (V_2 - V_1)$$

for 5 % error, and it is clear that the figure 0.22 (= $\sqrt{0.05}$) should be replaced by

$$(\text{acceptable percentage error}/100)^{\frac{1}{2}}$$

for any other error. Note that all the quantities in the relation above are accessible on any given system, but perhaps the shortest usable cycle time would be a more useful quantity, since cycle time is immediately available on the readout device of the system. This may be found by substituting the expression for $I_{\text{intg(max)}}$ in that for $t + t_{\text{dead}}$, which is, again dropping unnecessary suffixes temporarily, and using

\sqrt{E} for the numerical factor (acceptable % error/100) $^{\frac{1}{2}}$:

$$\frac{C}{I_{\max}} (V_2 - V_1) - C \frac{t_{\text{do}}}{C} + t_{\text{do}} - \frac{t_{\text{do}}^2}{C} \frac{I_{\max}}{V_2 - V_1}$$

from which, after observing that the two middle terms cancel and substituting for I_{\max} , we see that :

$$\frac{C}{\sqrt{E}} \frac{t_{\text{do}}}{C} \frac{V_2 - V_1}{V_2 - V_1} - \frac{t_{\text{do}}^2}{C} \frac{\sqrt{E} C (V_2 - V_1)}{(V_2 - V_1) t_{\text{do}}}$$

is the minimum allowable cycle time, when further cancellations yield :

$$\underline{\underline{t_{\text{cycle}} (\text{min}) = t_{\text{dead},0} \left\{ \frac{1}{\sqrt{E}} - \sqrt{E} \right\}}}$$

This function indicates that :

1 %	allowable error is achieved when the cycle time has fallen to	9.9 x $t_{\text{dead},0}$
5 %	"	4.3 "
10 %	"	2.8 "

The inclusion of R1 of correctly chosen value thus achieves a marked extension of the sensibly linear dynamic range since, for example, without R1, 1% error would be reached when the total cycle time was about $100 \times t_{\text{dead},0}$. In this case then a further decade (i.e. $100/9.9$) of sensibly linear response has been achieved. However if 10% error is acceptable, then the improvement in dynamic range is not so impressive, being $10/2.8$ or just less than 4 x, but remember that

already 10% extends the uncorrected range further than 1%, but of course at the expense of accuracy. It is also worth observing that further improvement of dynamic range is achieved if R1 is made somewhat larger than the criterion $t_{\text{dead},0}/C_{\text{intg}}$ indicates for its value. The basis of this is that if, say, 1% error can be tolerated, then 1% overcorrection at the onset of dead time error can be accepted and so 1% undercorrection will occur even further on than before. The response curve thus becomes slightly sigmoidal at the high I_{intg} end under optimum correction. Since $t_{\text{dead},0}$ requires to be measured anyway, it is probably wise to set the value of R1 empirically somewhat above $t_{\text{dead},0}/C_{\text{intg}}$ by trial-and-error with the target level of acceptable error in mind. The criterion $t_{\text{dead},0}/C_{\text{intg}}$ thus serves as a guide to the value of R1, and a slightly larger preset adjustable resistor should be incorporated in the unit and trimmed for optimum correction. In the work set out in this thesis, this was the approach adopted.

It is important to realise that good accuracy is necessary for this correction since the integral of any quantity is more affected by high levels than by lower ones. This means that the use of overcorrection for range extension should be used very sparingly, since it acts at the top end, and only a low error figure is here acceptable - say 1%.

Although the value of the integrating capacitor does not appear in the expression for $t_{\text{cycle}(\text{min})}$, it nevertheless assumes that the criterion for calculating $R1$ has been applied and this does of course involve the value of C_{intg} . However the value of C_{intg} almost certainly will affect the reset time, $t_{\text{dead},0}$, probably more or less in proportion to C_{intg} , so that it may well be that the one effect compensates the other (see the criterion equation for $R1$), and no change in $R1$ may be required, but this should not be assumed in any given system without verification. See next section.

Embodiment in this thesis.

Pages 304-310 explain how to estimate the second order effect of variations in the reset time as a result of change in the charge on the integrating capacitor, C_{intg} , resulting from current through $R1$ (Fig.18). However this secondary effect can be avoided if the dead time is both invariant and longer than the maximum time taken to reset the capacitor.

In the embodiment described in this thesis the dead time is effectively invariant because it is set by the time constant of $R16-C10$ (see Fig. 28) which controls the turn-around time of the integrator - which is, of course, an oscillator. This means that the dead time correction (by $R12$ in Fig.28) should be largely free of this second order effect, although it should be observed that no correction could ever

be expected to extend the range indefinitely because the integration oscillator has a minimum integration cycle time determined by its turn-around time. When dead time is controlled by components other than C_{intg} and its reset pathway, it is the turn-around dead time of the whole circuit which is the appropriate value to insert in the criterion equation for the correction resistor, p.304, and not the immediate reset time of the capacitor itself - on the assumption of course that the current being integrated has no effect on the voltage across C_{intg} during the turn-around dead time - which is the case for the circuit described in this thesis.

It should also be observed that only one correction resistor (R12 in Fig.28) has been used. The rationale for this is that it functions for the high level end of the high range (when C_{intg} is large; C6) but that switching to the high range should occur (set to do so) before the low range runs into dead time error. For the low range, the value of R12 has little effect since C_{intg} is so much smaller; C7 (see criterion, p.304). Some further extension of dynamic range could be achieved however by incorporation of two values* for R12, also switched at range change, of appropriate values to correct dead time error for their respective integrating capacitors, C6 or C7. However their incorporation

* Note that an invariant dead time does require different values of correction resistor with different values of integrating capacitor; cf. section on "Range changing", p.311.

into the circuit is not quite straightforward because of the diodes D9 and ZD2 (Fig.28). ZD2 must be hard across C_{intg} to perform its function of setting accurately the voltage on C_{intg} at reset. However assuming a suitable arrangement were devised then it would be desirable to set the ratio of C6 to C7 higher, to make full use of the extra range available with the low level capacitor. For optimum dynamic range, C6:C7 should be of the order of the dynamic range for one value of capacitor with correction resistor, downgraded to the extent of hysteresis deliberately built into the range-changing circuitry - see p. 137.